Applied Optics

April
1963

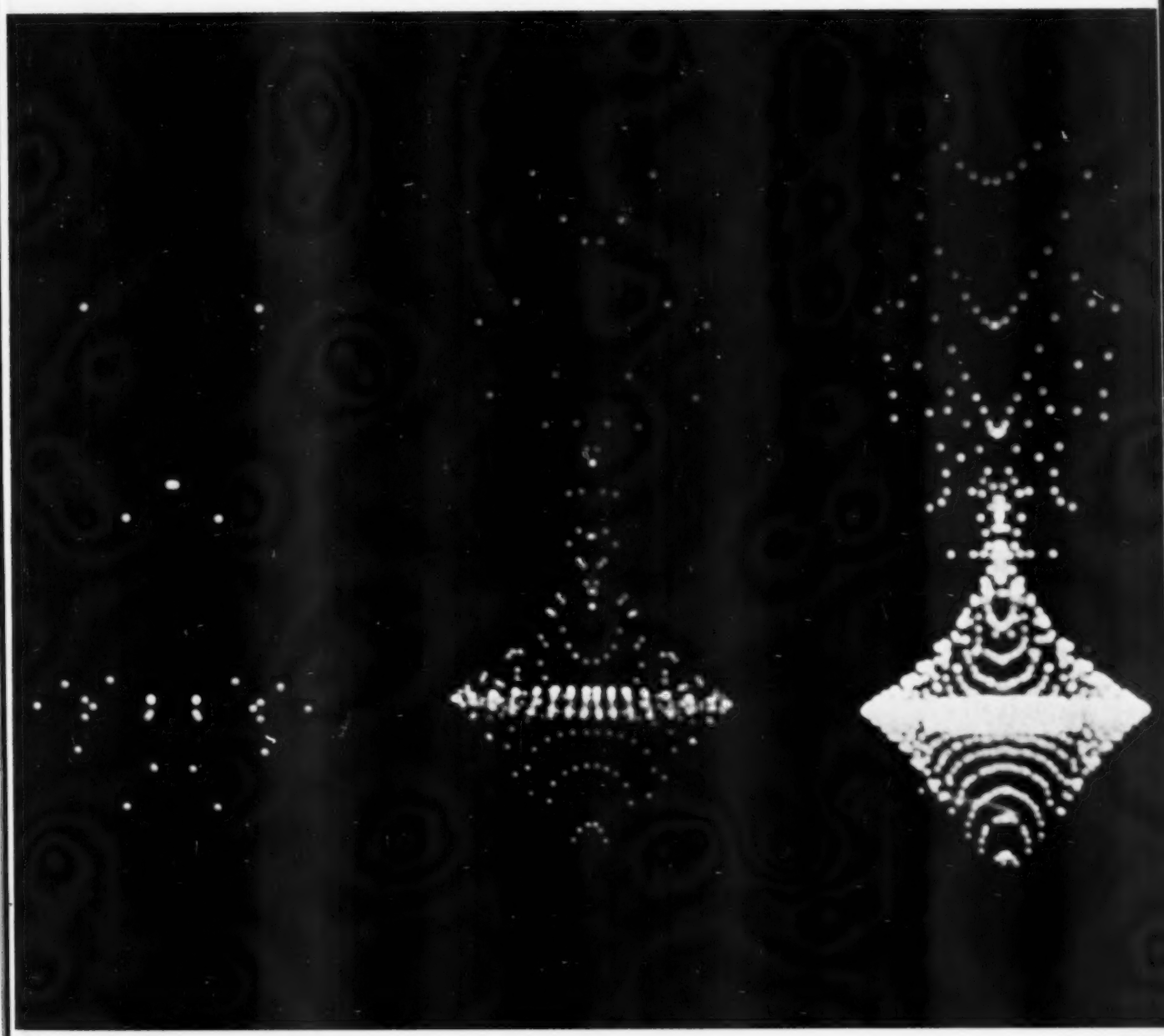

IMAGE EVALUATION

Effective Jan. 1, 1965. All back issues and single copies are sold at $3.00 per copy.

LIGHT SLICED A MILLION WAYS...

BAUSCH & LOMB CERTIFIED-PRECISION DIFFRACTION GRATINGS let you slice light just exactly the way you want it! Choose from the world's widest range of diffraction gratings—over 2000 different gratings available for use, from x-rays to microwaves. This grating selection chart tells the story:

BAUSCH & LOMB GRATING SELECTION CHART

Spectral Region and Wavelength Range	Sizes and Types of Gratings	Grooves/mm	Blaze	Remarks
Soft x-ray 10A to 500A	Concave used in high vacuum at grazing incidence; sizes and types with radii from 400 to 6650mm.	600-3600/mm	1° to 6°	Coating unimportant.
Far Vacuum Ultraviolet 500A to 1000A	Concave gratings used near normal incidence; usually in first order.	600-3600/mm	1° to 10°	Special coating.
Vacuum Ultraviolet 1000A to 2000A	Large variety of concave and plane gratings. Used in first or higher orders.	600-3600/mm	2° to 22°	MgF_2 coating for work below 1600A enhances efficiency.
Ultraviolet and Visible 2000A to 7000A	Over 500 sizes of plane or concave gratings used in first or higher orders. Also a selection of plane transmission gratings.	300-2160/mm	3° to 64°	Plane for photoelectric spectrometers; concave for photographic recording of spectra.
Infrared 0.7 to 75 microns	Complete range of sizes and types of plane gratings. First order.	20-600/mm	5° to 30°	Plane gratings with aluminum coating.
Far Infrared 40 to 1,000 microns	Plane gratings ruled to order in magnesium metal. Any desired size up to 330 x 360mm.	0.8 to 12/mm	15° to 31°	SiO coated . . . used with plane filter gratings.

SAVE FOR FUTURE REFERENCE

MAIL COUPON for details on the theory and mechanics of diffraction grating use in light dispersion plus complete data on all B&L Certified-Precision Gratings.

BAUSCH & LOMB

BAUSCH & LOMB INCORPORATED
77140 BAUSCH ST.
ROCHESTER 2, N. Y.

Please send Catalog D-261.

Name .....

Company .....

Address .....

City ..... *Zone* ..... *State* .....

Applied Optics

VOLUME 2
NUMBER 4
APRIL
1963

A monthly publication of the Optical Society of America

John N. Howard, Editor

F. Dow Smith, Feature Editor

Patricia R. Wakeling, Managing Editor

COVER: These spot diagram photographs, produced on a flicker-free computer display in the course of optical design at Itek Corporation, represent a method of examining the geometrical light distribution in an image. The complexity of these patterns illustrates the basic nature of the image evaluation problem, that of finding a realistic useful measure of the manner in which such a lens will perform in actual use. The visual estimate of the complex shape is itself worth the computation of such diagrams which takes less than one minute on a high-speed computer. Each point represents the intersection of a single ray in the image plane. The photographs illustrate clearly the effect (left to right) of increasing the number of rays which are traced.

Published monthly by the Optical Society of America, Inc., in cooperation with the American Institute of Physics, at 20th and Northampton Streets, Easton, Pa. Editorial and advertising offices: 1155 16th St. N.W., Washington 6, D.C. 202-Di7-6177 Supported in part by a grant from the National Science Foundation. Subscription rates: $6.00 to OSA members, $8.00 other AIP Societies' members; nonmembers and libraries: $10.00 per year. Single copies $2.00. Second class postage paid at Easton, Pa.

© Copyright 1963 by the Optical Society of America.

335 **Optical Image Evaluation and the Transfer Function**—F. Dow Smith

351 **Information Capacity of Radiation Detectors and of Light**—R. Clark Jones

359 **Calculation of Optical Transfer Function from Lens-Design Data**—Erich Marchand and Richard Phillips

365 **An Instrument for Measurement of the Optical Transfer Function**—R. R. Shannon and A. H. Newman

371 **A New Type of Shearing Interferometer for the Measurement of Transfer Functions of the Microscope Objective**—Tadao Tsuruta

379 **Experimental Transfer Characteristics of Image Motion and Air Conditions in Aerial Photography**—L. O. Hendeberg and W. E. Welander

387 **A New Optical Method of Storing and Retrieving Information**—P. J. van Heerden

393 **Theory of Optical Information Storage in Solids**—P. J. van Heerden

401 **One- and Two-Dimensional Processing in Line Scanning Systems**—L. G. Callahan and W. M. Brown

409 **Three-Dimensional Wavefront Reconstruction**—Jurgen R. Meyer-Arendt

411 **Faraday Rotation in FeNi Films**—H. H. Wieder and D. A. Collins

421 **Photographic Emulsions as Computer Storage Media—Especially with CRT Readout**—Leo Levi

425 **Photorefractometer I. Extension of Sensitivity and Range**—N. S. Kapany and D. A. Pontarelli

431 **High-Index-of-Refraction Spherical Sheath Composite-Rod Optical Masers**—O. Svelto and M. Di Domenico, Jr.

441 **Exploding Wire Blast Shutter**—W. G. Chace and C. V. Fish

445 **Multilayer Reflection Coatings on a Metal Mirror**—Leo Young

DEPARTMENTS

448 **Letters to the Editor**

Appearance Criteria for Uncolored Anodized Aluminum Surfaces—Roger L. Saur

Interferometer Laser Mode Selector—S. A. Collins and G. R. White

Use of Platinum or Gold Grating Surface at Grazing Incidence—D. O. Landon

Construction and Calibration of a Bass-Kessler Grating Spectrograph—Theodore Baurer

Optical Pumping of Lasers Using Exploding Wires—Charles H. Church, R. D. Haun, Jr., T. A. Osial, and E. V. Somers

358 **Books**

408 **Optical Activities in Industry**

410 **Meeting Reports**

420 **From the Editor**

453 **Of Optics and Opticists**

infrared specialist

Outstanding Infrared Specialist sought for lead and/or research position in a research and development orientated organization.

Work covers optics, detection, radiometry, information processing, systems electronics, simulation techniques and instrumentation development. Applied work primarily directed toward weapons guidance, sparo seeker systems and surveillance systems. Liberal funds available for more basic research. A complete laboratory is at the disposal of the IR personnel (optics, radiometry, spectrophotometry, electronics, cryogenics and detector analysis). An excellent solid-state laboratory is also available for materials and device research. Candidates should hold a doctorate and possess recognized qualifications, based on demonstrated achievements in one or more of the applicable fields. Professional status will be considered in lieu of doctorate requirement.

The excellent Southern California location of General Dynamics | Pomona offers unsurpassed living conditions. Suburban Pomona is only thirty minutes from Los Angeles and Hollywood and in close proximity to many recreational centers; the mountains, the desert, the ocean and is within America's finest year-round living climate.

Please address your resume to:
Mr. O. C. Byrd, Engineering Personnel Administrator
General Dynamics | Pomona, P.O. Box 1011
Pomona, California

U. S. Citizenship Required

An Equal Opportunity Employer

GENERAL DYNAMICS | POMONA GD

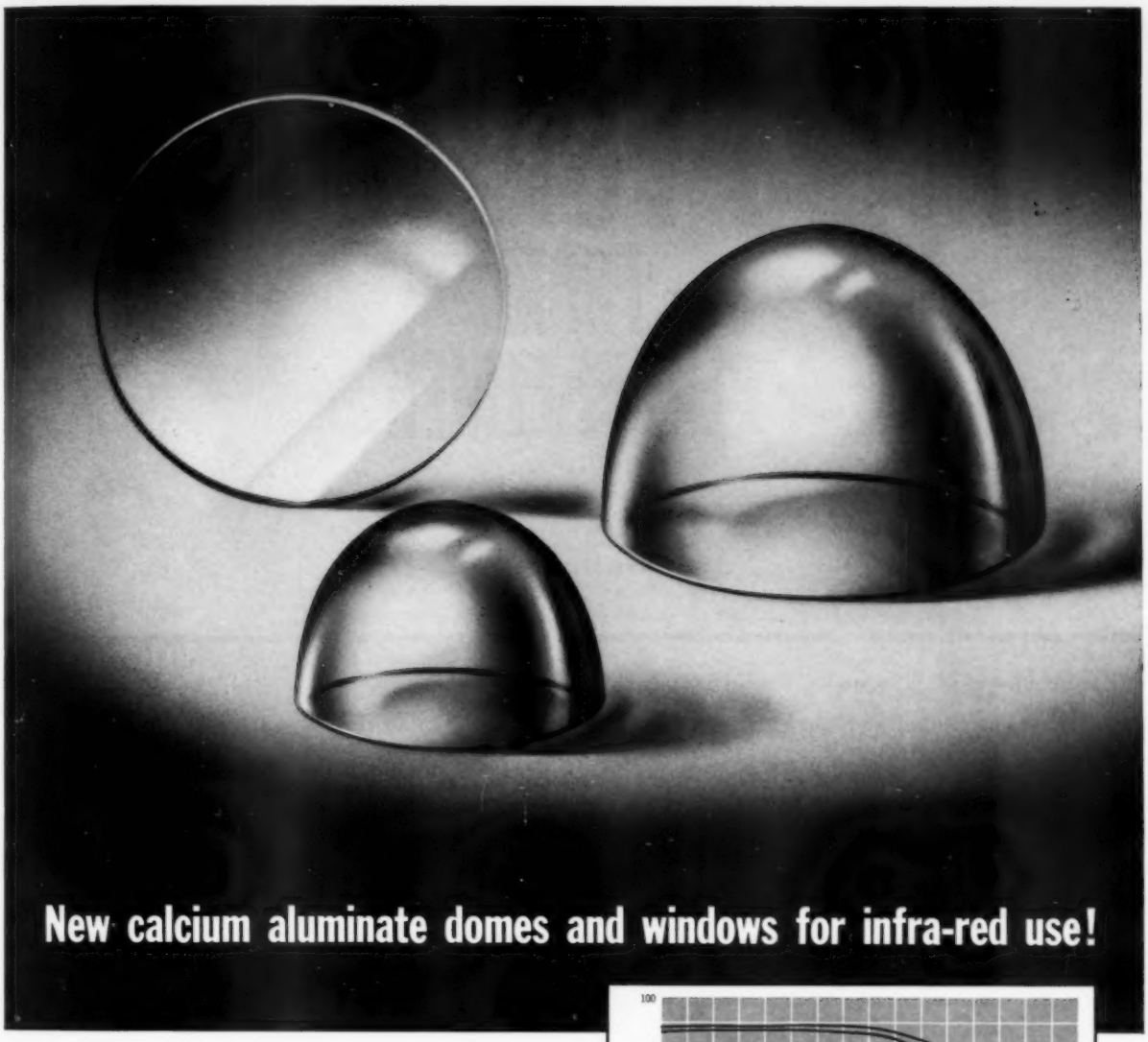

New calcium aluminate domes and windows for infra-red use!

Barr & Stroud Infra-Red Transmitting glasses combine superior optical and mechanical properties!

In the 0.4 to 6.0 micron wavelength range, no other infra-red transmitting material can match the performance of Barr & Stroud Calcium Aluminate glasses (B. S. 37A and B. S. 39B)... at such a low cost.

Excellent optical characteristics! The accompanying graph shows uniformly high transmission level through the visible spectrum up to 4.0 microns wavelength. Type B. S. 37A, 2 mm thick, shows useful 50% transmission to 4.9 microns; type B. S. 39B to 5.5 microns. Cutoff (10% transmission) occurs at 5.4 and 5.9 microns respectively. Transparency of these glasses in near ultra-violet and visible light simplifies alignment.

Outstanding mechanical properties! Barr & Stroud Calcium Aluminate glasses are very hard (6 on Moh's scale) and highly resistant to abrasion and thermal shock. They can be used at temperatures up to 800°C. A specially developed protective coating not only guards the glass against attack of water but also increases its transmission by reducing reflection.

Recommended uses include windows and IR domes on missiles and aircraft, meteorological applications, missile, rocket and satellite detection, weather observation, space navigation and satellite reconnaissance.

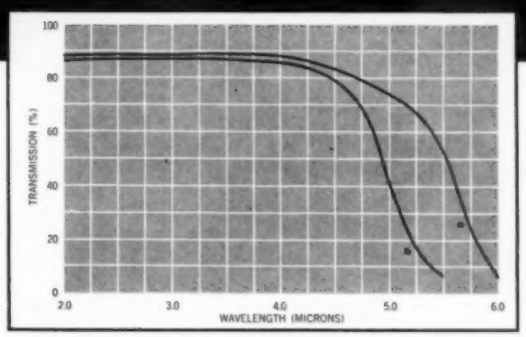

A new bulletin contains complete specifications on Barr & Stroud Infra-Red Transmission glasses... distributed in the U. S. by Kollmorgen Corporation. Write for your copy and current prices today... 347 King Street, Northampton, Mass.

K C **KOLLMORGEN**
CORPORATION
NORTHAMPTON, MASSACHUSETTS

OPTICS FOR LASERS
FROM
PERKIN-ELMER

Perkin-Elmer is a convenient, reliable source of precision optics for lasers, in quantities for research or production programs. All are of unexcelled quality. All reflect Perkin-Elmer's years of experience in the design and development of precision optics and optical instrumentation.

INTERFEROMETER FLATS
1.0", 1.5" and 2.0" diameter
Surface: $\frac{\lambda}{10}$ to $\frac{\lambda}{200}$
BK-7 and Quartz

SPHERICAL MIRRORS
1.0", 1.5" and 2.0" diameter
1M, 2M, 3M, 10M, 25M, 50M
radius of curvature
BK-7 and Quartz

WINDOWS
1.0", 1.5", 2.0" and 2.5" diameter
Standard or Brewster's angle
BK-7 and Quartz

DIELECTRIC COATINGS
Durable, minimum loss,
specified reflectivities
for the full spectrum of laser
research and development

SINGLE CRYSTALS
Tungstate, Molybdate, Sapphire,
Garnet, Emerald

SPECIAL OPTICS
Trihedral and 90° prisms with
deviation within 2 seconds

Perkin-Elmer—a single-source, total capability in optical maser technologies including research, design, material development, fabrication and performance testing, plus development engineering of optical maser systems and applications.

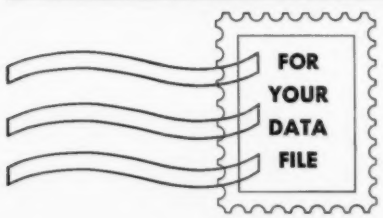

Send today for "Perkin-Elmer Price and Specification Catalog—Optics for Lasers." Write or phone Perkin-Elmer, Optical Maser Marketing, Norwalk, Conn. Area Code 203—847-0411

PERKIN-ELMER

LOCATE LINES TO 1μ OVER 200 mm WITH THIS HI-PRECISION MICROPHOTOMETER

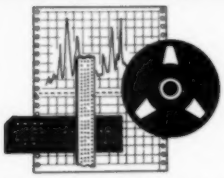

WIDE SELECTION OF READOUT DEVICES AVAILABLE

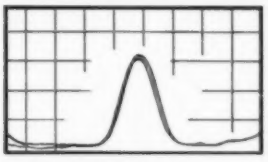

TRACE TAKEN FROM OPTIONAL PHOTOELECTRIC SETTING DEVICE

Sensitive Model 23-500 Microphotometer measures densities over a 0 to 3.5 range.

RESOLUTION . . . two lines, 5μ apart, can be resolved at a transmission level of 50%, at 10x magnification.

SLITS . . . width continuously adjustable 0-100μ; length in .1, .2, .5, 1.0, 1.5, 2.0 and 2.5 mm steps. Circular apertures optional.

ROTARY PLATEHOLDER . . . can be adjusted through ±90° with vernier to 0.1°. Vernier cross motion to 200 mm.

FILM, PLATE VERSATILITY . . . takes films and plates up to 5" x 10". Plates to 8" x 10" optional.

DIGITAL READOUT . . . can be supplied with automatic punched card, paper or magnetic tape readout for three or more parameters to meet critical requirements.

PHOTOELECTRIC SETTING . . . can be provided for quick, manual setting and reading to better than 1μ between two points.

Ask for Catalog 23-500.

Jarrell—Ash

Dedicated to excellence in the research, development and manufacture of precision analytical instrumentation.

For further information . . . clip the coupon, attach to your company letterhead and mail.

JARRELL-ASH COMPANY
26 Farwell Street, Newtonville 60, Mass.

Name _____

R. M.

OPTICAL GAS LASER SYSTEMS AND COMPONENTS

Continuous Beam of Coherent Radiation in Both Infrared and Optical Wavelengths

MODEL MK I
Basic unit for research needs with sealed off optical tube containing confocal mirrors—output at 6,328Å or 11,530Å
$995.00

MODEL MK KIT
Complete gas laser discharge tube
$495.00

COMPONENTS

Brewster Gas Laser Discharge Tube	**$250.00**
Confocal Mirrors Dielectrically Coated—pair	**$245.00**
R. F. Excitor modified	**$250.00**
R. F. Coupling	**$ 40.00**
Mirror Mounts—pair	**$150.00**

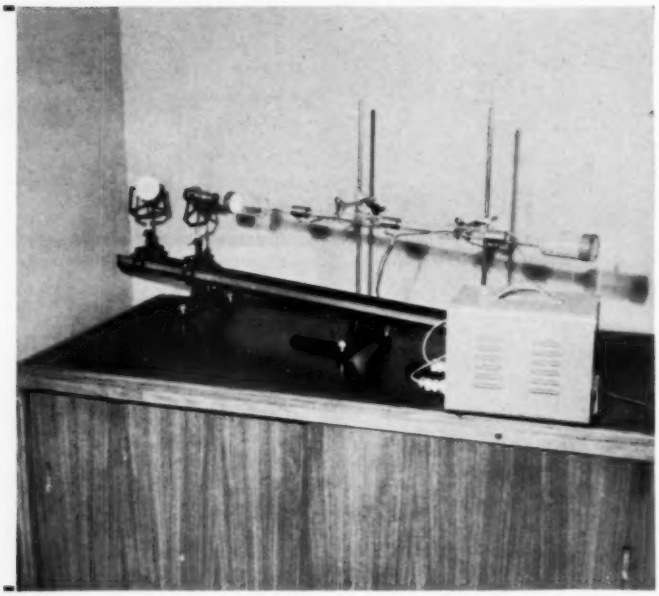

LASER MATERIALS

- **Calcium Tungstate with Neodymium** • **Sodium Terbium Borate**
- **Calcium Fluoride doped with Uranium** • **Ruby** • **Garnets**
- **Cuprous Chloride:** Clear, Colorless Single Crystals For Use in Laser Modulation
- **Ammonium Dihydrogen Phosphate** • **Potassium Dihydrogen Phosphate**

Watch for
OPTICAL COATING CHEMICALS
With all volatile impurities removed

Emissions:

Ruby	6,950 angstroms
Sodium Terbium Borate	5,460 angs.
Calcium Tungstate with Neodymium	10,600 angs.
Calcium Fluoride doped with Uranium	24,900 angs.

The Worlds Largest Supplier of Single Crystals

Semi-elements, inc.
Saxonburg Boulevard, Saxonburg, Pa.
Phone: 412-352-1548

Optical Image Evaluation and the Transfer Function

F. Dow Smith

Evaluation of photographic optical systems through use of the optical transfer function or sine wave response has become commonplace. The fundamental physical concepts which lie behind the theory are not, however, widely known and are outlined for use by the optical engineer. The significance, limitations, and advantages of this tool for image evaluation are discussed along with some suggestions of direction along which future work may be carried. The discussion is from the point of view of an individual interested in the design, fabrication, evaluation, and use of large systems of very high precision.

Introduction

While the use of the optical transfer function (or sine wave response) for test and evaluation of photographic optical systems has received widespread attention both theoretically and experimentally for some years, the methods are still in relatively limited use as practical tools. This is not necessarily a reflection of a lack in the utility of the methods, but perhaps is due to the difficulties inherent in computation and in the scarcity of reliable, yet flexible, test equipment which can be used in a routine fashion. The slowness in application of these ideas to applied testing may be related to the fact that the physical basis of the theory has not been obvious and the relationship between some of the results of the theory and traditional physical optics has not been widely understood. This review will, therefore, be largely devoted to a description of the results in physical terms as a guide to optical engineers and physicists who have had limited contact with these ideas.

The evaluation of optical system performance has been an activity of importance ever since functionally useful optical systems came into use. As these uses have become more specialized, so have test and evaluation methods developed in variety and complexity. The user, the fabricator, the designer, and the planner each has his own problem in specifying or evaluating the quality of the image and each through a difference in outlook has contributed in a different way to the vast array of techniques now available. Indeed, much of the controversy between proponents of various testing methods could have been avoided had there been better recognition of these differences. Thus, for example, scientists in a laboratory concerned with methods of evaluating the final system in terms of use to the customer or user will select a different emphasis from those in a laboratory whose problems center around methods of actually fabricating high quality systems. Each will differ from the emphasis in a laboratory concerned mainly with conceptional and optical design. Even within the few organizations where scientific competence encompasses a majority of the problem areas, individuals will speak with varying emphasis depending on personal interest.

One can roughly separate evaluation methods into two broad classes. The first of these deals with the response of a system to a small source of light (point or line) and consists either of calculations, measurements, or observations which describe the distribution of energy near the image plane (e.g., star test with real star or collimator, encircled energy measurement, Hartmann diaphragm test) or with a determination of the shape of the wavefront as it emerges from the exit pupil (e.g., interferometer, Foucault knife edge). There is no one best method. If, for example, the system is an astronomical telescope for visual use, one cannot better subjective judgments of experienced observers by looking at actual star images. If the same telescope is being tested at the last stages of fabrication, a test is needed which not only assesses over-all quality but which gives a picture of the wavefront to guide the optician in the final figuring operation. When rotational symmetry can be relied upon, the Foucault knife-edge test is preferred by many opticians, but when other irregularities occur, it is more useful to use a shearing or scatter-plate interferometer. For detailed analytical purposes or for correlation with optical design data, the Hartmann diaphragm test may be

The author is with the Itek Corporation, Lexington, Massachusetts.

Received 20 January 1963.

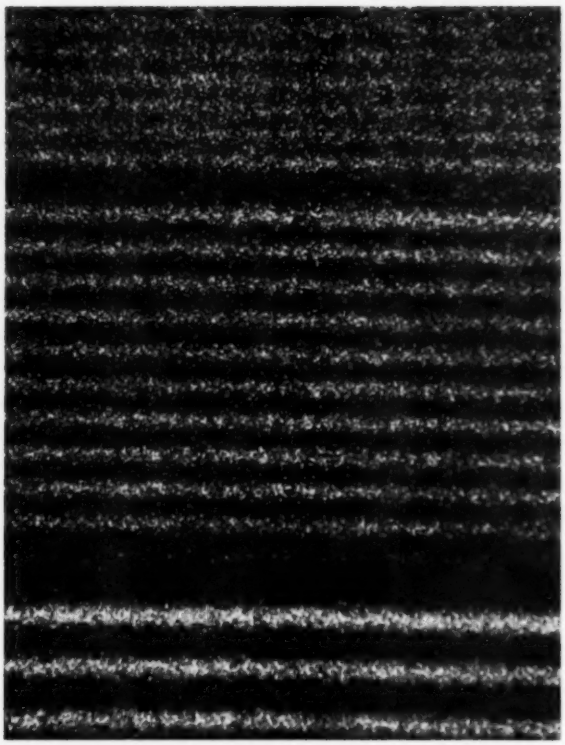

Fig. 1. A sine wave imaged on a moderately fine grained film. The apparent contrast as a function of line length depends both on granularity and the inherent behavior of the visual system.

desirable. If the telescope has a large aperture obscuration, then analysis using the transfer function can provide a rapid insight on the effect of this on performance as we shall see below. Then, too, if the telescope is to be used outside the visual spectrum or with a specialized detector, these and other tests will be combined according to the taste and ingenuity of the observer.

The second class of tests makes use of extended test objects such as the familiar bar target. A common rationale for such testing as used, for example, for photographic cameras, is that such targets resemble, more nearly than a star, the scenes the camera will encounter in actual use. When it is desired to include the photographic film in the test, this argument becomes even stronger because of the highly nonlinear response of the emulsion. For aerial photographic uses, for example, the desire to "simulate" real objects has led to increasing emphasis on low contrast targets of a compact nature, photographed on the actual film to be used. Short lines have been generally selected, since for detail approaching the grain size it has been considered that long lines would produce an unrealistic smoothing of the results. Such a trend shows a strong influence on the part of the user to demand tests that simulate the final use of the system. For reproducibility in testing, however, this smoothing from long lines is often useful and, moreover, if microdensitometry is to be used, long lines become essential to permit the use of a sufficiently narrow slit. In Fig. 1, which illustrates this, the reader will find it interesting to observe the apparent contrast of the pattern as he masks off the line to reduce its length. In addition, for repeatability and accuracy in testing, it is generally more useful to use high contrast targets perhaps even on very high resolution film. On the other hand, if the performance differs from design predictions, all such data, regardless of the detailed character of the target, are of little use to the optical designer as a quantitative guide in modifying the design. The question of selecting an appropriate array of lines can be used to emphasize the importance of point of view. Thus, the camera user might argue that natural objects are random and that the traditional targets made up of sets of mutually perpendicular lines are useless. Such an argument led, for example, to the Howlett[1] annular targets. In any event, the measured resolution in the two directions of the more common bar target is commonly averaged before final analysis of the data or averaging across the field of view. On the other hand, a difference between vertical and horizontal resolution on the axis of a supposedly centered optical system can be a useful guide to the lens assembler in his work. The same difference is meaningless to the lens designer, but a consistently measured difference, particularly a focal shift at a field point, can be a useful check against design data.

A third and often highly useful method which lies between these two involves the use of an illuminated edge.

The complexity of use to which optical systems are put, plus the nonlinear properties of the detectors, make it clear that no universal test or evaluation technique is likely to meet all requirements. It is equally clear from operational arguments alone that it will never be possible to describe usefully the performance of a photo-optical system by a single number any more than the performance of an airplane or other complex device can be so described. On the other hand, the state of affairs outlined above has long been recognized as unsatisfactory and the need for theoretical and experimental tools to bridge better across the full range of the problem is well established. Many readers will find it strange that the problem justifies comment at all when the limitations just outlined have been understood for so many years. However, solutions in principle have not been widely converted to practice.

For photographic systems in particular, a bridge is needed to tie together the point source performance so useful in design and in the laboratory, with extended target performance so necessary for over-all evaluation

of performance. The method of testing based on determining the image formed by an optical system of a pattern of lines with sinusoidal intensity distribution provides such a self-consistent bridge. It is for this reason that the sine wave response or transfer functions which result have received such persistent attention over recent years.

For a useful review of general image evaluation procedures, including use of the transfer function, the reader is directed to a recent two-part article by Perrin.[2]

Early History

Interest in the application of Fourier methods to optics and to what is now known as the transfer function became widespread in the late forties and early fifties. There was, however, an early foundation in the literature going back some years. The earliest suggestion for the use of a periodic target was by Rayleigh[3] in 1896 in a paper dealing with the formation of an image of uniformly spaced lines by a rectangular aperture. A description of the image of such a target as a function of line spacing is closely related to the transfer function. Frieser[4] in 1935 applied the notion to film and refers to the amplitude reduction of sine wave targets by an emulsion. Selwyn[5,6] developed this concept during World War II and separately applied it to lens and film. Luneberg[7] in a limited publication in 1944 gave a detailed theoretical discussion of the resolution of objects of periodic structure. Duffieux[8] in a series of papers beginning in 1935 applied Fourier methods to optics. His book, *L'Integral de Fourier et ses Applications à L'Optique*, published in 1946, unfortunately not available in English, became a source book of great value particularly to European workers in the field. Duffieux introduced a transmission factor equivalent to the transfer function and showed how to compute this from a knowledge of the wavefront in the pupil.* In the United States the main impetus came from a different direction. Schade,[6,9] as an electrical engineer, faced with the problem of evaluating lenses for television systems, applied the notions of communication theory to develop all the essential concepts of contrast reduction through a sequence of cascaded system elements. This work is described in a series of papers beginning in 1948. In Schade's work, as in an important paper by Elias *et al.*[10] in 1952, the ideas are discussed in the framework of system input and output without any reference to the physical optics of the system itself. It is, perhaps, of basic significance, and a measure of the fundamental nature of the whole approach, that related results were being generated simultaneously, though quite independently, from quite different origins. The published proceedings[6] of a symposium at the National Bureau of Standards in 1951 provide an excellent summary of views at that time. A subsequent symposium at the University of Rochester in 1955 provided an additional useful review. Proceedings were not published, but a number of the papers appeared in the *Journal of the Optical Society of America* in September 1956.

The theoretical work of Hopkins[11,12] is comprehensive and provides a complete discussion from the basis of physical optics. The summaries of O'Neill,[13] and particularly the impact of his teaching on graduate students and others, represent a major contribution. O'Neill's approach, moreover, is in a mathematical form which makes the optical ideas particularly accessible to engineers and others with a background in communication theory as applied in electronics.

Early work on the measurement of the transfer function will be discussed later in the paper.

Fourier Transforms and Reversibility

The Fourier relationship between light distribution patterns in different parts of an optical system has been known for many years. It lies, of course, at the center of the Abbe theory of microscope imagery, the basis of most fascinating demonstrations by Porter[14] and was used both implicitly and explicitly by Michelson.[15] However, the statement that these amplitude distributions in the aperture and in the Fraunhofer plane make a Fourier transform pair is made more often than it is understood. The following conceptual discussion provides an interesting physical interpretation.

Consider the simple case of a rectangular aperture in parallel light using an elementary application of Huygens principle (Fig. 2). The model is one-dimensional, i.e., all quantities are considered constant in the η-direction perpendicular to the page. The notation ξ, η is used for coordinate axes in the aperture since we wish to reserve x, y for coordinates in an object plane conjugate to x' y'. We will omit the usual brief analysis which justifies explicit omission of diffraction in skew directions. Our object is to compute the

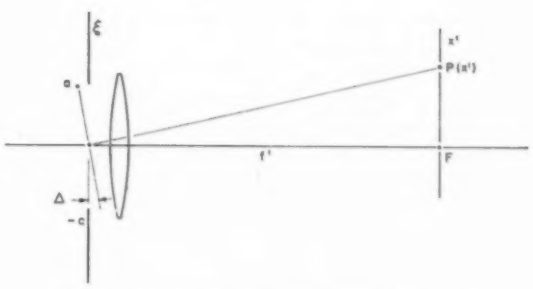

Fig. 2. Image formation from a plane wave.

* Indeed the derivation of Eq. (11) for the convolution of the pupil function is a simplified version of a derivation given by A. Marechal in an unpublished lecture at Boston University in 1952, which, in turn, was stimulated by the derivation of Duffieux.

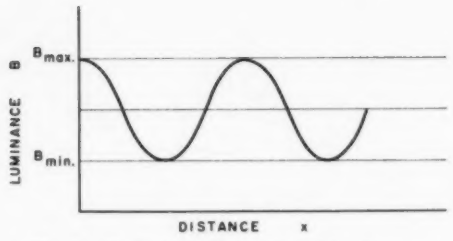

Fig. 3. Sinusoidal distribution of luminance.

amplitude of diffracted light at P, an arbitrary point near a point F of good imagery, as a sum of contributions from elements of width $d\xi$ of the incident wavefront. A surface in the aperture can be constructed such that the optical path is constant from any point on the surface to the point P. Let the path difference measured in wavelengths between this surface and the incident wave be Δ, then the phase difference is $2\pi\Delta$. Each element of width $d\xi$ contributes a vector at P which may be represented by $(d\xi)\cos 2\pi\Delta$. More conveniently, we write $(d\xi)e^{2\pi i\Delta}$. We may regard this as a mathematical convenience of which the real part is of physical interest or alternatively as a way of using the complex plane to represent the plotting of vectors.

From Fig. 1

$$\Delta/\xi = x'/f'.$$

If we express ξ in wavelengths and for convenience take f' equal to one, the phase difference becomes $2\pi\xi x'$. Thus, the amplitude distribution in the image, $A'(x')$ can be written

$$A'(x') = \int_{-\infty}^{\infty} A(\xi)e^{2\pi i\xi x'}\,d\xi, \qquad (1)$$

where $A(\xi)$ is the amplitude distribution in the aperture.

Aberrations if present can be described by an additional phase shift corresponding to the wave aberration (deviation of the wavefront from reference surface). This phase shift is included in $A(\xi)$ by regarding it as a complex quantity.

Since the system is assumed linear and the light is considered to be propagated without absorption, we can, according to the classical principle of reversibility, imagine the system reversed in time and it will retrace all its previous history. Suppose that after reversal we set ourselves the problem of computing the amplitude in the original aperture from the amplitude in the original image plane. That is, we hypothesize an aperture distribution identical with the image distribution just computed. Following the previous procedure in analog we shall obtain

$$A(\xi) = \int_{-\infty}^{\infty} A'(x')e^{-2\pi i\xi x'}\,dx'. \qquad (2)$$

The integrals have the form of a Fourier transform pair. Had we persisted in representing the contribution vectors at the image by the cosine (or sine) we would have a similar result but with cosine (or sine) transforms instead. We have demonstrated that the amplitude distribution in the aperture of an optical system is the Fourier transform of the amplitude in the image plane and vice versa. Armed with this knowledge and with access to tables of Fourier transforms, it now becomes a trivial matter to "compute" a wide variety of Fraunhofer diffraction integrals. The reciprocal character of the integrals is simply a mathematical expression of the possibility of considering the system as reversible in the classical sense.

Theory of the Transfer Function

Definition

The approach we are pursuing represents the application to optical system analysis of the Fourier methods so powerful in other areas of physics. We wish to proceed, however, without explicit appeal to Fourier mathematics. The input to the system is considered to be a system of parallel lines whose intensity across a direction perpendicular to the lines varies sinusoidally. The variable spacing is usually described by the spatial frequency, i.e., reciprocal of the element width, in lines or cycles per millimeter exactly analogous to the familiar lines per millimeter in conventional bar targets.

This object or target may be illuminated coherently or incoherently, the degree of coherence referring to the extent that there is a significant phase relationship between the light at separated points in the object. We shall, however, deal initially and primarily with incoherent illumination.

An important parameter of such a sinusoidal distribution, Fig. 3, is the modulation, i.e., ratio of amplitude (this is the amplitude of an intensity pattern in space and is unrelated to the amplitude A of electromagnetic disturbance of the previous section) to mean background luminance. The mean value is taken high enough to provide a "bias" so that the luminance is always positive. This parameter, equivalent to the classic Michelson visibility, describes the visual contrast

$$C = \frac{B_{max} - B_{min}}{B_{max} + B_{min}}. \qquad (3)$$

If the spatial period of the target is p we can now define the spatial frequency

$$\omega = 2\pi/p.$$

The transfer function T can then be defined as the ratio of the contrast in the image to that in the object

$$T(\omega) = \frac{\text{Contrast of the image at frequency } \omega}{\text{Contrast of the object at frequency } \omega}. \qquad (4)$$

Since the above definition of contrast is not in universal

use, especially in the photographic field, it may be better to refer to (C) as the modulation. This definition of $T(\omega)$ provides, however, a sound conceptual base for the theory.

The utility of the definition depends on the important fact demonstrated below that a sine wave object is always imaged as a sine wave. Moreover, this definition implies the absolute contrast of the object to be unimportant, and we are freed from all questions concerning the proper contrast for the test object itself. In other words, the addition of unmodulated background luminance has an equal effect on numerator and denominator in Eq. (4) and so cancels out. This is an important result which if overlooked can lead to considerable confusion in the interpretation of normalized transfer function curves. There may, however, be a spatial phase shift or translation of the pattern as a whole which varies with the spatial frequency. It can obviously only occur where the point image is asymmetric. Thus, in a centered optical system, spatial phase shifts will occur only off-axis and for tangentially oriented lines. Radially oriented lines will have no phase shift. Phase shifts of π can occur, however, even with a symmetrical image (defocusing provides a common example), but in this case the contrast falls to zero between regions of sign change, giving rise to pseudo-resolution. Both phenomena are quite consistent with physical intuition. In the off-axis case consider the point-by-point construction of the line image by a typically comatic image. In the case of defocusing, consider the alternate bright and dark centers to the on-axis diffraction pattern as the system goes through focus.

Dependence on Spread Function

If the point source image distribution or spread function of the optical system is known we can integrate point by point across the object plane and so compute in direct fashion the distribution in the image. The intensity distribution $O(x)$ in the sinusoidal object can be written

$$O(x) = 1 + C_0 \cos\omega x,$$

where $\omega = 2\pi/p$, p being the period of the spatial sine wave.

The intensity in the image, $i'(x)$ can be computed by adding incoherently the image blur (spread function) from each point in the object. The spread function must be expressed as a function of X, a distance measured from the Gaussian image point x', as in Fig. 4. Assume unit magnification, $X = x' - x$, and the result of this so-called convolution is

$$i(x') = \int_{-\infty}^{\infty} |A'(x' - x)|^2(1 + C_0 \cos\omega x)\, dx. \qquad (5)$$

To simplify the discussion we omit a constant factor needed properly to express the result in absolute light level. Actually, of course, the convolution takes place in two dimensions over the object, and both variables should be included. In the integral as written, we may alternatively consider an integration in the direction of the lines to have already taken place so that $|A(x')|^2$ is the line spread function rather than the point spread function. The infinite limits on the integration need not concern us. In practice, good results will be obtained as long as the integration is carried out over a region large compared to the line spacing p,
setting

$$x' - x = X,$$

$$\begin{aligned} i(x') &= \int_{-\infty}^{\infty} |A'(x)|^2[1 + C_0 \cos\omega(x' - X)]\, dX \\ &= \int_{-\infty}^{\infty} |A'(X)|^2\, dX \\ &+ C_0 \cos\omega x' \int_{-\infty}^{\infty} |A'(x)|^2 \cos\omega X\, dX \\ &+ C_0 \sin\omega x' \int_{-\infty}^{\infty} |A'(x)|^2 \sin\omega X\, dX. \end{aligned} \qquad (6)$$

Since the integrals all have numerical values, say a_0, a_1, and a_2, we can write

$$i(x') = a_0 + a_1 C_0 \cos\theta \cos\omega x' + a_1 C_0 \sin\theta \sin\omega x'.$$

The image is clearly sinusoidal and can be rewritten in the form

$$i(x') = a_0\left[1 + \frac{a_1 C_0}{a_0} \cos(\omega x' - \theta)\right], \qquad (7)$$

where $a_1 C_0/a_0$ is the contrast or modulation in the image as previously defined.

Consider for simplicity the case where the image is symmetrical. Then the spread function $|A'(x')|^2$ is an even function, i.e., with identical values at (x) and $(-x)$ so that the phase shift, θ, will be zero.

$$i(x') = a_0\left[1 + \frac{a_1 C_0}{a_0} \cos\omega x'\right]$$

$$T(\omega) = \frac{a_1 C_0}{a_0} \Big/ C_0,$$

and we see that the contrast of the object drops out as we anticipated.

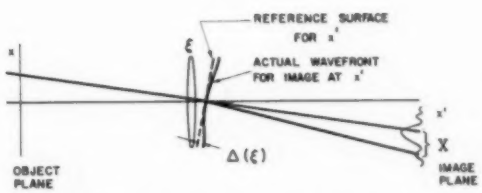

Fig. 4. Notation for image formation.

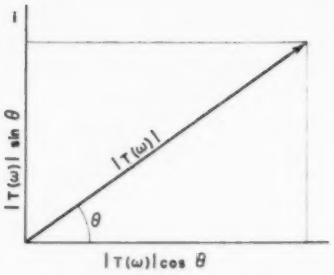

Fig. 5. Graphical representation of the real and imaginary portions of $T(\omega)$.

$$T(\omega) = \int_{-\infty}^{\infty} |A'(X)|^2 \cos\omega x \, dX. \tag{8a}$$

This result is the real part of the more general case for an asymmetrical image in which $T(\omega)$ is regarded as complex.

$$T(\omega) = K \int_{-\infty}^{\infty} |A'(X)|^2 e^{i\omega X} \, dX, \tag{8b}$$

where K is a normalizing constant equal to the first integral in Eq. (6).

In many situations it is useful to compute both the real (cosine integral) and imaginary (sine integral) parts of the complex transfer function. This is shown schematically in Fig. 5. The phase shift θ is most conveniently obtained by a separate measurement of the real and imaginary parts. In many practical cases only the modulus is measured even though there may be some asymmetry. In this case the function should be referred to, following the recommendation of the ICO Subcommittee on Image Assessment, as the modulation transfer function.[16]

Lamberts[17] describes an explicit method for carrying this process in reverse and computing the line spread function from the transfer function T.

Dependence on Wavefront

We can now compute the transfer function from the amplitude in the aperture.

Figure 4 summarizes the notation including the wave aberration $\Delta(\xi)$. We can omit explicit reference to the aberration by including it in the complex amplitude

$$A(\xi) = |A(\xi)| e^{2\pi i \Delta(\xi)}.$$

Since we are interested in the spread function about the central ray joining x and x', we rewrite Eqs. (1) and (2) with variable X

$$A'(X) = \int_{-\infty}^{\infty} A(\xi) e^{2\pi i \xi X} \, d\xi, \tag{9}$$

$$A(\xi) = \int_{-\infty}^{\infty} A'(X) e^{-2\pi i \xi X} \, dX, \tag{10}$$

substituting in Eq. (8) and replacing $|A'(X)|^2$ by the mathematical equivalent, $A'(X)A'^*(X)$, where the asterisk indicates complex conjugate, we have,

$$\begin{aligned} T(\omega) &= K \int_{-\infty}^{\infty} A'(X) A'^*(X) e^{i\omega X} \, dX \\ &= \int_{-\infty}^{\infty} A'(X) \left[\int_{-\infty}^{\infty} A(\xi) e^{-2\pi i \xi X} \, d\xi \right] e^{i\omega X} \, dX \\ &= \int_{-\infty}^{\infty} A(\xi) \left[\int_{-\infty}^{\infty} A'(X) e^{2\pi i (\xi - \omega/2\pi) X} \, dX \right] d\xi, \end{aligned}$$

but the bracketed integral (separated for clarity) is $A^*(\xi - \omega/2\pi)$

$$\therefore \; T(\omega) = K \int_{-\infty}^{\infty} A(\xi) A^*(\xi - \xi_0) d\xi, \tag{11}$$

where

$$\xi_0 = \frac{\omega}{2\pi} = \frac{1}{p}.$$

This relationship is of the greatest importance and shows that the transfer function can be computed solely from a knowledge of the wavefront in the pupil produced by a small source. While the above derivations are one dimensional, the extension to two dimensions is easy. If the pupil coordinate in the perpendicular direction is η, then we can obtain

$$T(\omega_x \omega_y) = K \int_{-\infty}^{\infty} \int_{-\infty}^{\infty} A(\xi,\eta) A^*(\xi - \xi_0, \eta - \eta_0) d\xi \, d\eta. \tag{11a}$$

It is now necessary to interpret the result. The integrals are formed in effect by multiplying the wavefront with the wavefront at a second set of coordinates displaced linearly from the first by an amount ξ_0. Consider the case of an aberration-free system with circular aperture; then A is a real number. Assume the hypothetical sine-wave target to be horizontal. At a given spatial frequency ω, the value of the integral becomes the area of the overlapping portion of the aperture transposed over itself as shown in Fig. 6. The response drops to zero when the shift ξ_0 is equal to the diameter of the aperture. If the diameter of the aperture is d,

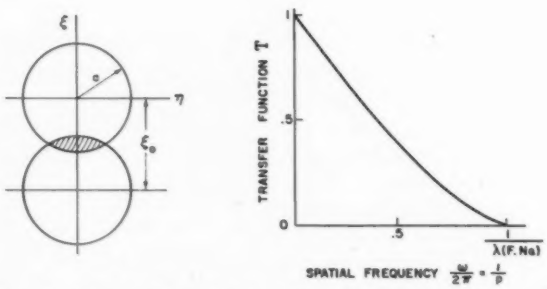

Fig. 6. Transfer function for aberration-free optical system with circular aperture.

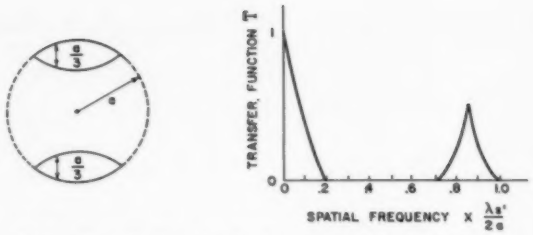

Fig. 7. Transfer function for hypothetical divided aperture.

then, since the image distance is unity, the maximum shift

$$\xi_0 = \frac{d}{\lambda} = \frac{1}{\lambda(\text{F.No.})}.$$

The period of the sine wave at the cutoff is therefore equal to λ(F.No.) corresponding exactly to the semi-width of the central maximum in the diffraction image of a point source with a rectangular aperture of width d (Rayleigh criterion).

The reason for this abrupt cutoff can readily be understood on physical grounds as can the peculiar result that at a period ω the transfer function is completely determined by the behavior of the lens over two regions at each edge of the aperture identical to the shaded "zweieck"* in Fig. 6.

It should be emphasized that for a diffraction-limited system the transfer function will be given by the convolved area of the aperture regardless of the aperture shape. The example of Fig. 7, while of no obvious practical significance, will help in understanding the phenomena. An aperture of the shape shown will have a transfer function with two peaks. The shapes of each of the three segments are identical and the same as that for the last one-sixth of the curve of Fig. 6. Of two parts to the curve, one corresponds to the transfer function of the individual zweieck and the other is related to the transfer function for an aperture corresponding to the separation.

A physical argument may be developed to assist in understanding this. Consider an aperture for which we wish to determine the transfer function. It is well known (e.g., Rayleigh refractometer) that a system with two narrow slits placed across the aperture will image a narrow line source as a sinusoidal interference pattern with a fringe spacing (period) given by $\lambda f/d$. It is intuitively clear that, if the line source is replaced by a sinusoidal target with spacing of its geometrical image corresponding to the spacing of the interference pattern, the distribution will remain sinusoidal. We can now ask what additional regions of the aperture can contribute to the image of this selected spatial frequency. We proceed by mapping out regions of the aperture which can provide "slit" pairs of the selected spacing and equal height. The latter requirement is necessary as the unbalanced flux from equally wide slits of different length will simply appear as background light. Beginning at the extreme left edge of the aperture (Fig. 8) we select elemental "slits" (a,b,c, . . ., etc.) dedicating other parts of the aperture ($a'b'c'$, . . ., etc.) at the appropriate distance ξ_0 to provide the second slit of each pair. When the points (m,n,o, . . ., etc.) are reached, it is the height of strips ($m'n'o'$, . . ., etc.) which determine the integration zone. The region resulting is clearly that which would have been obtained by convolution. Pursuing the method to the case of a system with aberrations demands breaking each vertical strip into elements (since the phase will vary vertically along each strip). This leads immediately to a heuristic derivation of Eq. (11).

While the previous discussion has concentrated on diffraction theory, it is important to recognize that the basic definition Eq. (3) we have chosen for the transfer function in no way limits us to any special kind of image formation. Diffraction in a lens may be considered to govern the formation of the point image, but once that image or spread function is known we can compute the transfer function directly from Eq. (8). Images in fiber bundles, on film or cathode ray tubes, may all be handled although precautions are needed when nonlinearities are involved. Equation (11) simply provides a useful short cut for situations where the diffraction is important.

Fourier Transform Relationships

In the reversibility example discussed above, the transforms describe two aspects of the same physical situation, a system of waves of light. The comparison is, however, at two physically different points and the reciprocity between the two descriptions can be understood on physical grounds.

In the case we are about to consider, however, Fourier transforms are used to provide two different mathe-

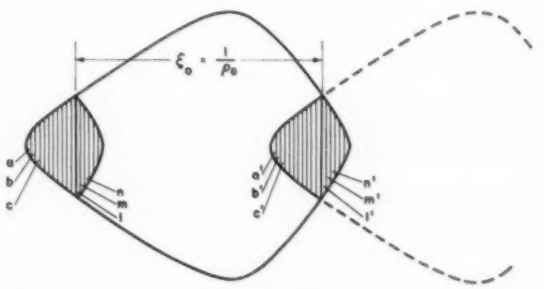

Fig. 8. Region of integration for diffraction calculation of T.

* The author knows of no English word corresponding to this useful German term, although "biangle" in analogy with the German *dreieck* for "triangle" is a possibility. The word "lens" commonly used in mathematics for this figure is less suitable for optics.

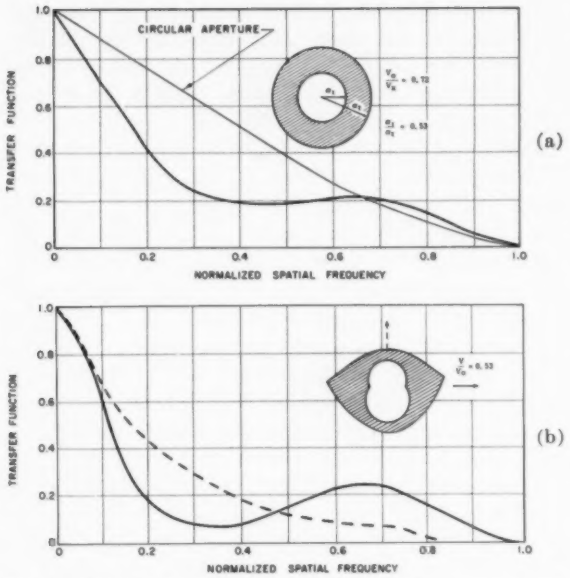

Fig. 9. Transfer function from a given annular aperture (a) for symmetrical case (b) off-axis with vignetting.

matical descriptions of a physical situation in one given place. Indeed this is the fundamental and traditional role of Fourier analysis. The Fourier integral results in a natural way from an extension to continuous nonperiodic functions of the methods of analysis used in decomposing a given periodic function into harmonic components of different frequencies.

Consider, for example, a one-dimensional distribution of luminance $o(x)$ describing an extended object to be viewed by an optical system. We can regard this distribution as a superposition (assumed linear) of an infinite number of periodic spatial components with frequencies from zero to infinity. The distribution, call it $O(\omega)$, giving the relative strengths of these frequencies may be regarded as the spectrum and is given by the Fourier transform

$$O(\omega) = \int_{-\infty}^{\infty} o(x)\, e^{i\omega x}\, dx$$

$$= \int_{-\infty}^{\infty} o(x)\, \cos\omega x\, dx + i\int_{-\infty}^{\infty} o(x)\, \sin\omega x\, dx. \quad (12)$$

For certain functions the cosine integral (or the sine) may provide a complete description, but the more general and mathematically more convenient exponential is almost universally used in theoretical work. Consider now the case where the integration of Eq. (6) is carried out over a general object of intensity distribution $o(x)$

$$i(x') = \int_{-\infty}^{\infty} |A'(X)|^2 o(x)\, dx. \quad (13)$$

We multiply through by $e^{i\omega x'}$ and integrate with respect to x'

$$\int_{-\infty}^{\infty} i(x')\, e^{i\omega x'}\, dx' = \int_{-\infty}^{\infty}\left[\int_{-\infty}^{\infty} |A'(X)|^2 o(x)\, dx\right] e^{i\omega x'}\, dx'$$

$$= \int_{-\infty}^{\infty} |A'(x)|^2\, e^{i\omega X}\, dX \int_{-\infty}^{\infty} o(x)\, e^{i\omega x}\, dx.$$

The three integrals are the Fourier transforms of $i(x')$, $|A(X)|^2$, and $o(x)$, respectively. Using the customary capital letters we have

$$I(\omega) = T(\omega)O(\omega). \quad (14a)$$

This fundamental equation is often derived directly from (13) as the definition of $T(\omega)$ and used as the starting point for development of transfer function theory. The conceptually simpler approach of considering one frequency at a time and relating this to target contrast is less elegant but quite equivalent. Of course, in practice, the integrals are two dimensional and

$$I(\omega_x,\omega_y) = T(\omega_x,\omega_y)O(\omega_x,\omega_y). \quad (14b)$$

It should be noted following this approach that, by a change of notation in the Fraunhofer diffraction case first discussed, the image coordinate x' can be replaced with ω, a frequency component in the aperture distribution. Thus, the amplitude in the image diffraction pattern can be shown to be the spatial frequency spectrum of the amplitude distribution in the aperture, and vice versa.

Computational Procedures

Analog Methods

We have seen that for a focused, aberration-free system, the transfer function is given by the overlapping area of the aperture shifted against itself. The transfer functions due to vignetted apertures such as occur, for example, in occulted reflecting systems, can be easily and usefully determined by a direct measurement of this area. It is only necessary to place suitable masks in a uniformly illuminated aperture and measure the total transmitted flux as one is shifted past the other. Figure 9 shows an example. The drop in T is rather dramatic. The method can be used for any shape aperture including supports and spiders.

In the case of nonuniform transmission over the aperture as in the case of a nonphase shifting anti-

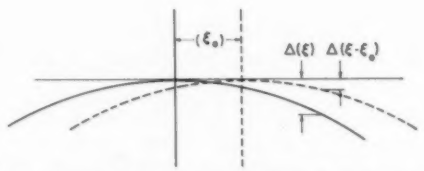

Fig. 10. Phase shift between wavefronts in a shearing interferometer for a relative displacement ξ_0.

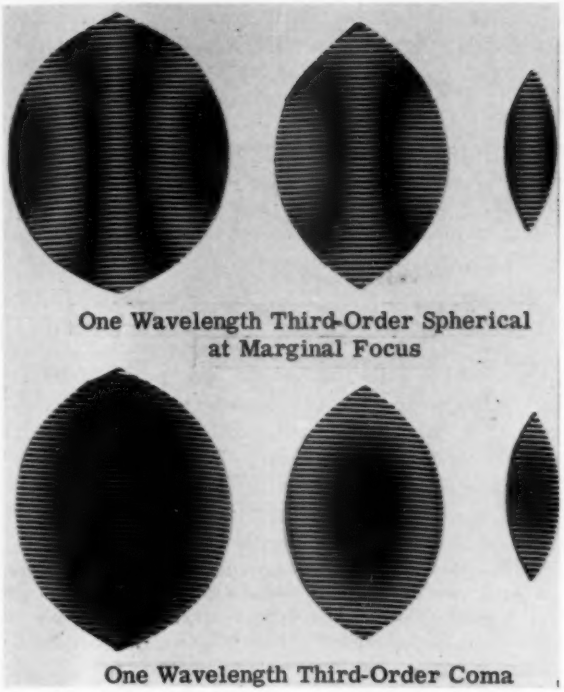

Fig. 11. Simulated shearing interferograms obtained by moiré interference between grids for a circular aperture at shifts of 0.25, 0.5, and 0.75 the diameter of the aperture.

vignetting filter, it would be necessary to construct masks whose intensity transmission corresponds to the amplitude distribution of the aperture. Fortunately, situations requiring such treatment are rare.

Further examination of Eq. (11) suggests an elaboration of this method when the wavefront deviates from the reference surface because of defocusing or aberration. Consider the result of using a shearing interferometer (e.g., Bates,[18] Françon[19]) to shift one wavefront across an identical wavefront produced by amplitude division. From Fig. 10 the path difference at a point (ξ,η) is, for a shift in the ξ direction,

$$\Delta(\xi,\eta) - \Delta(\xi-\xi_0, \eta).$$

If the corresponding phase difference is $\delta_1 - \delta_2$, the intensity of the interference pattern at that point will be proportional to

$$\cos\frac{(\delta_1 - \delta_2)}{2} = \frac{1}{2}[\cos(\delta_1 - \delta_2) - 1]. \qquad (15)$$

Assuming unit amplitude the integral (11) becomes

$$T(\omega) = \int e^{i\delta_1} e^{-i\delta_2}\, d\xi\, d\eta = \int \cos(\delta_1 - \delta_2) d\xi\, d\eta + i \int \sin(\delta_1 - \delta_2) d\xi\, d\eta. \qquad (16)$$

Let us integrate both sides of (15) over the aperture. The left-hand side will describe the total flux in the interference pattern (measurable by a photocell collecting all light in the pattern). The right-hand side gives the cosine integral needed for (16) except for a constant term which is the area of the overlapping region of integration (i.e., the known transfer function for the aberration-free case). The sine integral or imaginary part may be found by introducing a deliberate separation of the wavefronts in the interferometer of one quarter wave. The new phase difference will be

$$\delta_1 - \delta_2 - \frac{1}{2}\pi,$$

giving a new interference pattern,

$$\frac{1}{2}[\cos(\delta_1 - \delta_2 - \pi) - 1] = \frac{1}{2}[\sin(\delta_1 - \delta_2) - 1].$$

This method was described as a measurement technique by Hopkins.[20]

The same procedure but using moiré fringes was described by Smith[21] as an analog computing device. In the latter case the fringes are obtained between identical transmitting grids in which the grid lines are displaced at each point by an amount proportional to the aberration at that point. For accuracy, the aberration should change slowly over regions comparable in size with the line element width, and the line element width should be small compared with the aperture. Figure 11 shows sample moiré patterns for third-order spherical aberration and coma. The sine integral needed for determining spatial phase shift is obtained by sliding one plate relative to the other transversely one quarter cycle of the grid pattern. Two identical square waves used in this way give triangular rather than sinusoidal fringes. By making one pattern rectangular rather than square it is possible to obtain trapezoidal fringes which are a good approximation to a sine wave.

The grid patterns were made by laying strips of 6-mm wide masking tape across a 61-cm diam circle for subsequent photo reduction to glass plates about 5 cm in diameter. Routine use of the method

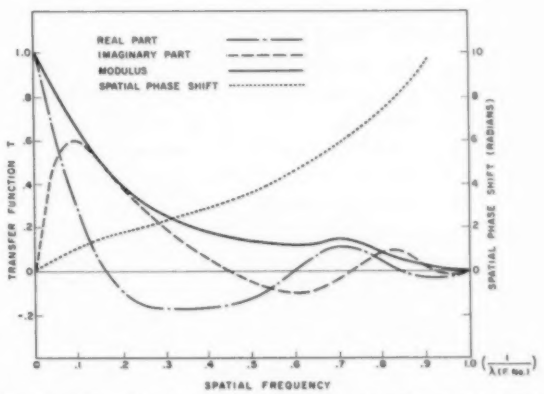

Fig. 12. Transfer function for one wavelength of third-order coma obtained from patterns like those in Fig. 11.

would require a more convenient method for preparing the plate, perhaps by electronic display or by foreshortened viewing at an angle, of lines projected on a three-dimensional model of a wavefront. The method would be particularly suitable for computing the transfer function from a highly irregular wavefront, (e.g., studying the effect of instantaneous air turbulence as recorded in a regular interferogram).

Geometrical Calculations

The performance of most high-quality lenses cannot be completely described by geometrical optics. Nevertheless, the use of geometrical optics as a practical lens design tool needs no justification to the optical engineer. It was natural, therefore, for attempts to be made to develop geometrical approximations to the transfer function. Hopkins[22] and his colleagues, De,[23] and Bromilow,[24] gave examples to show that good agreement could be obtained at low frequencies for aberrations larger than 2 λ. Miyamoto[25] and Hopkins[22] obtained a general expression for T_g, the geometric transfer function. The basis of the calculation is the transformation of the equivalent point spread function obtained by tracing a large number of rays through the system. This is equivalent to expanding the integrand of Eq. (8) in a Taylor's series and discarding terms which approach zero as λ approaches zero.

$$T_g(\omega_x,\omega_y) = \lim_{\lambda\to 0} T(\omega_x\omega_y) = K \int_{-\infty}^{\infty}\int_{-\infty}^{\infty} |A(\xi,\eta)|^2 \times \exp\left[2\pi i\left(\omega_x \frac{\partial\Delta}{\partial\xi} + \omega_y \frac{\partial\Delta}{\partial\eta}\right)_{d\xi\, d\eta}\right] \quad (17)$$

The expansion converges very slowly, however, and additional approximations are often needed to get good results. The method gives good results for very large aberrations, poor results for very small aberrations. In the intermediate area of one or two wavelengths, a mixed method of multiplying the geometrical transfer by the transfer function of the aberration-free system often gives good results. Linfoot[26] in a recent publication has shown, however, that the mixed method may sometimes give worse results than the geometrical method alone in the region of one to two wavelengths of aberration. Miyamoto,[27] in *Progress in Optics*, discusses the subject in detail. He shows that the geometrical method is also applicable to the case of partial coherence in certain special cases.

Hopkins[28] and Shannon and Perry[29] at the Institute of Optics in Rochester have developed a technique of computing an averaged frequency response from the encircled energy. In this procedure, the intensity distribution in an asymmetric off-axis image of a point source is averaged over azimuth. The resulting encircled energy function is Bessel-transformed to produce a transfer function averaged over azimuth. Computational comparisons with experimental work have shown that this gives a prediction of resolution which is approximately equal to the root-mean square of the resolutions in the sagittal and tangential directions.

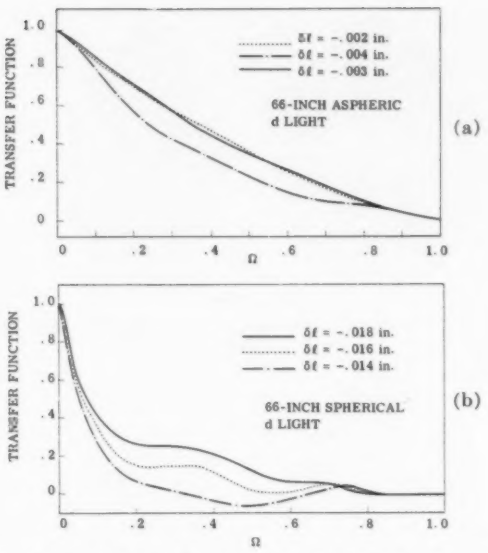

Fig. 13. Computed modulation transfer function for the axial image of a well-corrected doublet lens of focal length 66 in. (168 cm) at several focal settings with (a) all spherical surfaces and (b) one aspheric surface (after Barakat).

Diffraction Calculations

The most exact method for computing the transfer function during optical design involves the direct computation of Eq. (11). Yet, while the integral is simple in principle, the computation in practice is complex, particularly in the case of an asymmetrical wavefront because of the large number of elements $d\xi d\eta$ in the aperture at which the phase and amplitude must be known, and the resulting large number of arithmetical steps which must be carried out for each point on the curve. For aberrations which can be described analytically, the computation is, however, relatively straightforward, and curves showing the transfer functions for the Seidel aberrations and for fifth-order spherical aberration have been published, for example, by O'Neill,[13] Black and Linfoot,[30] De,[23] Parrent and Drane,[31] Steel,[32] and Barakat and Lev.[33]

Barakat and Lev[34] have described a method for smoothly fitting a rotationally symmetric wavefront in a mathematically economical way from ray trace data using Chebyschev polynomials. Figure 13 shows an example of the results obtained. A high degree of accuracy is maintained. These programs are in routine use on both a small low-speed computer and a moderate sized computer of very high speed and are being extended to handle off-axis aberrations. Others have felt that such high accuracy is not needed and have, there-

fore, sought the use of approximate methods. A paper by Marchand in this issue of *Applied Optics* is an example.

White Light

In all the above cases the computation is carried out at a given wavelength. A transfer function describing the behavior of the system over the wavelength interval of actual use may be calculated by simply adding together appropriately weighted (according to light source, filter, and detector) transfer functions at selected wavelengths. This procedure is valid since the radiation at separate wavelengths is incoherent.

Analytical approximations are often of use. Shannon, for example, by approximating the residual color curve of a monochromatically good lens, was able to compute and display rapidly on a cathode-ray tube families of curves showing the transfer function as a function of wavelength and focal position. The data can then be rapidly integrated to show the resulting over-all transfer function. Photographs of the display are shown in Fig. 14.

Measurement

Lens Testing

The most direct approach to measuring the transfer function of an actual lens is to use a series of targets with sinusoidal intensity distribution and varying frequency, the image of the target being scanned by a moving slit to obtain the image contrast. Herriott[35] described such a measurement in which the scanning slit was mounted on the armature from a small loudspeaker. This appears to be the first direct measurement of spatial frequency in an optical image. A square wave was used which gives good results in the higher frequencies in exact agreement, of course, with a sine wave when all frequency components of the square wave but the fundamental lie beyond the cutoff. Schade[6] also made use of sinusoidal intensity targets, for example, by the use in the object plane of a sinusoidal pattern recorded in the fashion of a sound track on a long strip of moving film. The output was recorded at a slit in the image plane. The use of intensity sine wave targets has not become general, however, because of the difficulty in producing the targets. While the actual contrast of the target is unimportant, most measurement schemes require the contrast to be constant over the full frequency range. This is more difficult to achieve. In this kind of testing, T is determined from the ratio of the contrast in the image at frequency ω to the contrast in the image at zero frequency. This follows from Eq. (4) when the system is linear. The denominator cannot as a rule be determined directly, but is approached asymptotically as ω decreases. The method is therefore convenient but of questionable accuracy. The early devices had no provision, in most cases, for measurement of the phase shift, but this is not a fundamental limitation (e.g., Herriott[36]).

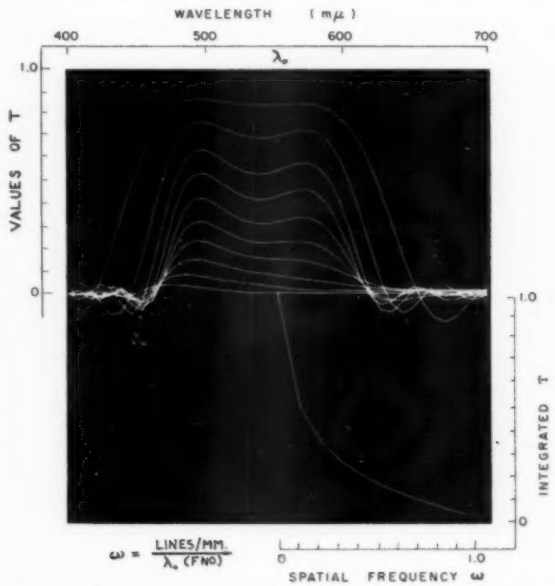

Fig. 14. Transfer function analysis of system with secondary spectrum as displayed on computer cathode-ray tube by R. R. Shannon. Upper portion shows the transfer function vs wavelength for spatial frequencies (beginning at the top curve) of 0.1, 0.2, 0.3, . . ., 1.0. The lower portion shows the over-all transfer function which results from integrating over all wavelengths.

Lindberg,[37] in Ingelstam's laboratory proposed a method which uses a sinusoidal area mask in place of a sinusoidal intensity distribution. He pointed out that the integral of Eq. (8) could be evaluated experimentally by superimposing two transmission masks, one with transmission corresponding to the line spread function, the other to the sinusoidal object distribution. The total transmission as one mask is transported past the other is a complete analog of the mathematical convolution, and will give the image intensity distribution. More importantly, he pointed out that the sinusoidal object mask can be an area mask. The experimental arrangement, therefore, involves a narrow line source, the image of which is scanned by an area with sinusoidal aperture moving linearly across the line image. Lindberg also described a more convenient method which permitted the use of a tuned ac amplifier. A point source was used, the image of which was scanned by a star sector wheel in the image plane. As the center of the wheel is displaced toward the pinhole, an increasing spatial frequency is obtained. The sector wheel gives a square wave, but by tuning the amplifier to the fundamental frequency, it is quite equivalent to a sine wave. It is difficult, however, with the method to obtain a wide frequency range.

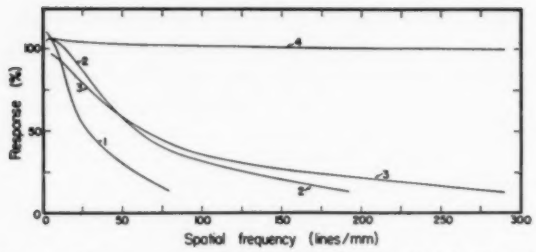

Fig. 15. Sine-wave response of the following Kodak films developed in the following Kodak developers: (1) Tri-X, DK-50, 5 min; (2) Panatomic-X, D-19, 3 min; (3) Micro-File, D-11, 4 min; (4) Experimental document-recording, DK-50 (1:10), 10 min. Exposed through Kodak Wratten No. 61 filter (after Lamberts). *Figure reproduced by permission of the Editor J. Opt. Soc. Am.*

A similar method was used by Lamberts,[17] except that the moving area mask is in the object plane and scanning slit at the image. Two masks scanning in opposite directions permit measurement of the phase shift. The method has the important advantage that the equipment can be easily adapted, through use of a cylindrical lens, to determining the modulation transfer function of film.

A variation of the first method of Lindberg is described by Shannon in the present issue of *Applied Optics*. Since it is known that the image of a sine wave will be a sine wave, it is not necessary to scan the entire image but only to know the modulation. The modulation can, in fact, be obtained from a single measurement in which the line image is symmetrically placed at the peak of the sinusoidal mask (more accurately a cosine so that the value is unity at the origin), combined with a measurement which gives the mean transmission of the mask. A second mask displaced a quarter period will permit determination of the phase shift. There is no scanning in the Lindberg sense, although a rotating drum is used to index new masks into position. The alignment of masks on the drum must be carried out with extreme precision.

A quite different approach to measuring the transfer function has been used by Hopkins[20] using the shearing interferometer technique described above. Some of the early experimental results are outlined in papers by Baker[38] and Kelsall.[39] Tsuruta, in the present issue, describes an application of the method to testing microscope objectives. The theoretical analysis of Menzel[40] is used by Tsuruta to give results for both coherent and partially coherent illumination.

Transfer Function for Film

The transfer function for film can be obtained by exposing on the straight line portion of the characteristic curve to a sinusoidal distribution of light. Lamberts,[41] using a modification of his lens test apparatus described above, was the first to provide data for a variety of materials. The exposed image is scanned with a microdensitometer and the density values so obtained are converted to exposure values E through the use of the characteristic curve. The image modulation

$$\frac{E_{max} - E_{min}}{E_{max} + E_{min}}$$

can therefore be computed, and the ratio of this to the known modulation of the illuminating sine wave gives the transfer function. Since the film is assumed to have a symmetrical spread function, the function is real and corresponds, therefore, to the modulus of the complex transfer function. It may, therefore, be referred to alternatively as the modulation transfer function (MTF). For a direct positive emulsion at gamma unity (or for the over-all response of a negative positive pair) it would be practical to define MTF following Eq. (4) as the ratio of output transmittance to input illumination. For a negative emulsion the output will not be sinusoidal and so the artifice described above must be used. This in effect compares the actual illuminating modulation with the illuminating modulation needed to give, with an ideal film, a result identical to that on the actual test film.

Precautions must be taken to account for adjacency effects, but it appears that, apart from this, the type of developer has little effect on the MTF, nor does the level of exposure. Figure 15 (from Lamberts' paper) shows the character of these functions. Transfer function curves are now available from the manufacturer for a wide variety of films.[42]

Linearizing the photographic system by determining MTF for the straight-line portion of the curve sidesteps, however, a rather significant problem. In many photographic situations, for example, in aerial photography, the shape of the highly nonlinear toe of the characteristic curve governs the rendition of important shadow detail. Methods have yet to be developed for dealing with this problem.

Hempenius, in a paper at the 1962 ICO Conference on Vision and Image Formation, described a convenient graphic method for carrying out system analysis using the MTF. More importantly, he incorporated a method based on the work of Selwyn[5] for including the effect of grain, and showed that a system analysis based on MTF alone could, in at least some cases, be significantly in error. More data on the role of grain are needed here as well.

Kelly[43] has described a model for the photographic process which can be used for photographic system analysis. He provides in addition a detailed description of methods for measuring and working with the transfer function.

Coherent Illumination

In the previous discussion we have applied the notion of transfer function to incoherently illuminated objects.

In the case of coherence, a quite analogous approach is possible except that now both the amplitude and phase of light in the object distribution must be considered. Such systems, as shown schematically in Fig. 16, are linear in the transmission of amplitude distribution but not of intensity. Coherence theory, as the term is used here, stems from work by Zernicke[44] and Hopkins.[11] A useful summary and interpretation has been given by Linfoot.[45] Of fundamental importance is the phase relationship between two nearby points in the object plane since light from two such points will interfere in the image plane and modify the resultant distribution of light. This phase clearly depends on the geometry of the source. Imagine pinholes at the two object points of interest. If the source is a point, fully modulated, Young's interference fringes will be produced in the aperture plane. As the source becomes very large, the contrast or modulation of the fringes will approach zero. This provides a basis for a scale of coherence and is the essence of the partial coherence factor γ introduced by Hopkins. If the two points are separated a distance $\delta(x)$, then, one-dimensionally

$$\gamma(\delta x) = \int_{-\infty}^{\infty} \Gamma(\mu) e^{i\mu\delta x}\, d\mu,$$

where $\Gamma(\mu)$ is the intensity distribution of the source.

In Fig. 16 assume the object to be a sinsusoidal amplitude distribution and that γ is unity, i.e., that we have a point source and complete coherence. The object can now be regarded as a grating which will form a diffraction pattern in the plane of the lens with the light distributed between the zero and first orders (one on each side). Since the pattern is sinusoidal, no energy goes to higher orders. If all three points of light strike within the lens aperture the image will be constructed with full modulation. As soon as the spatial frequency reaches a point where the diffracted orders lie outside the lens, the transfer function drops abruptly to zero. Since reconstruction of the image involves interference between the zero order and each first order separated by *half* the diameter of the aperture, the cutoff spatial frequency will be half that of the incoherent case. The transfer function is therefore unity out to this cutoff and zero beyond. The similarity between this function and the pupil function (unity over the aperture and zero beyond) is no accident. Indeed, simple physical arguments predicting the modulation in the imaged sine wave as the first-order diffraction spot "scans" the aperture with increasing ω will verify that the coherent transfer function is identical with the aperture distribution $A(\xi,\eta)$. If the direction of illumination is made oblique so that the zero order is moved to one edge of the aperture, then the separation between first and zero orders can double, and response will be maintained out to the original limit.

Caution must be used in defining the transfer function. In the incoherent case the system is linear in intensity, and the definition of T given by Eq. (4) is completely consistent with that based on Eq. (14). In the coherent case the system is linear in amplitude. If Eq. (13) is written with amplitudes instead of intensities, we can take Fourier transforms as in Eq. (14) and derive a transfer function. This transfer function has a definition equivalent to (2) only if defined as the ratio of the modulation of the image *amplitude* distribution $|A'(x')|$ to the modulation of the object *amplitude* distribution $|A(x)|$.

If the system is partially coherent, an analogous linear transfer function does not exist but an approximate computation is sometimes possible. This involves the integral in Eq. (11) but with a change in the limits of integration. The origin of the new limit of integration can be understood by an extension of the heuristic argument relating to Fig. 8. Since the source is considered imaged in the aperture, we proceed with the selection of slit pairs only over those parts of the aperture which are actually illuminated by the source.

Many important practical cases involve sources of finite size which may or may not be accurately imaged in the aperture plane. Each of these must be computed as a special case, and it is not possible to generalize about the effect of aberrations. Relatively little work has been done in this area and it is to be hoped that it will receive more emphasis in the future.

Linearity in the limiting cases of complete coherence or incoherence permits the cascading of a sequence of the appropriate transfer functions. Thus, for example, in an aerial camera, given lens design data on a lens, one may compute the incoherent transfer function over the wavelength band of use, multiply by the transfer function resulting from image motion (one would also like to include the transfer function of the atmosphere but data are limited), multiply by the modulation transfer for the film and taking into account the transfer function of the eye, as given, for example, by DePalma and Lowry,[46] and determine the modulation in the final visual image. There is, however, a catch. With respect to the atmosphere in the above example, the multiplication of the corresponding transfer function is valid only if the imagery is bad enough to be described adequately by a geometrical blur contribution from the atmosphere. If the imagery is better, so that over the aperture in use the amosphere is deforming the wavefront by only a few wavelengths (although perhaps in a highly irregular pattern) then the procedure is invalid, and the wavefront aberrations of atmosphere and lens must be added to give a combined pupil function from which an over-all optical transfer function may be computed. The reader can easily demonstrate to himself that combinations of "perfect" thin lenses do not have over-all incoherent transfer functions which can be derived by cascading the incoherent transfer functions

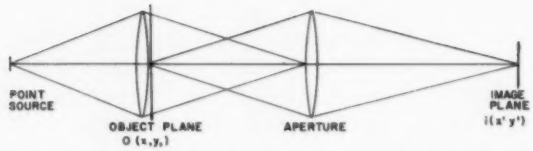

Fig. 16. Schematic layout for a coherent optical system with point source.

of the separate elements. The coherent transfer functions can, however, be so cascaded in a procedure that corresponds to multiplying the corresponding aperture functions $A(\xi,\eta)$ or in other words, adding the wavefront aberrations Δ which appear with the exponents.

This points up a major problem area, namely, that associated with optical design. The final stages of optical design involve a continuous evaluation of the performance of the lens as various parameters change by small amounts. The criteria used for this evaluation (ray intercept curves, for example) can be physically interpreted in terms that relate to the geometry of the system. Transfer function curves are at present of limited use as a guide to the designer (or to his automatic computer program) at least in terms of telling him what to do next, although, they are, of course, of great value in letting him decide if the lens will be capable of performing in some way previously specified by the user. The first (design) evaluation could be done with wavefront aberrations, i.e., the coherent transfer functions. The second (user) evaluation must use an incoherent transfer function if the system is to be used for incoherently illuminated objects. Methods of linking the two kinds of transfer function would, therefore, be of great value. The preceding remarks indicate that there is certainly no direct correlation between the two transfer functions, even for a rotational symmetry, since the portions of the aperture which contribute to the function for a given ω are quite different.

Some hybrid nonlinear function could conceivably be of use. Consider, for example, that in Fig. 16 the point source is replaced by a vertical line source parallel to the lines (also assumed vertical) in the amplitude sine wave target. Then the aperture will be illuminated by a zero-order line along a full diameter and by first-order lines on each side whose distance from the central diameter depends on ω. The source is assumed to be incoherent along its length so that each element of length may be considered to contribute in the image plane a separate incoherent image of the target. The frequency cutoff of this image contribution will correspond to half the aperture diameter for the element at the axis and will decrease according to a semi-chord of the aperture as the source element moves away from the axis. The cutoff becomes zero when zero-order image of the source reaches the edge of the aperture. The intensity distributions corresponding to each source element may now be added to compute the modulation. A "transfer function" can be defined from Eq. (4) in spite of the nonlinearity. The method is interesting since the resulting function will depend on the aperture function in a way more closely resembling the pure incoherent case than the pure coherent case. Success with the method would depend on (1) this resemblance being an adequate basis for inference of the incoherent transfer function, and (2) that the computations needed to propagate the coherent elements of the function through the system surface by surface, would not become too formidable.

Quality Assessment

It is perhaps remarkable that the transfer function proves so useful in practice when so little is known about how to interpret the curves. There is no accepted procedure, for example, by which one may compare the quality of two lenses which have generally similar curves but which differ in detail. It is possible, however, to predict in advance through a cascaded system the contrast level that can be achieved in a given case, or to determine thresholds. Thus, for example, in cascading the elements of the aerial camera system described in the last section, one can determine the spacing of a target on the ground of given contrast (both inherently and as affected by haze) which will at a selected viewing magnification be just detectable. Hempenius in the paper mentioned previously described a technique in which transfer functions plotted logarithmically on large plastic sheets may be superimposed against a ruled-off plotting board. The multiplication may be carried out quite simply.

Curves plotted logarithmically are, it should be stated, of great practical use and, moreover, have the advantage that constant error corresponds to a given curve displacement. Most data in the literature have been given in linear form, but it is to be hoped that the volume of that is not sufficient to dictate tradition. (See, however, Scott.[47])

While this kind of application to system analysis is useful and important for cases in which important detail lies near the threshold, it becomes less and less of use as one must deal with lower frequencies. Several criteria based on the over-all shape of the curve have been proposed, but little appears to have been done in putting these to experimental test.

Fellgett and Linfoot[48] introduced three such quality factors. The first of these, called the relative structure content F, measures the ratio of mean-square intensity fluctuations in the image to those in the object. It may be obtained by integrating the product of the power spectrum of the object and the squared modulus of the transform function. When the object spectrum is flat, F is given by a normalization factor times the integral of the transfer function (modulus) squared. This latter

integral corresponds to the equivalent bandpass N_e introduced much earlier by Schade.

A second factor, the fidelity factor θ, compares the degree to which maxima and minima appear in the image in their appropriate Gaussian image positions. The quantity $T(\omega_x\omega_y)^2$ which appears in the integrand of F replaced by $1\text{-}T(\omega_x\omega_y)^2$. Thus, since negative nature of the transfer function now plays a role, spatial phase shifts and spurious resolution are taken into account as was not the case with F.

A third factor, the correlation quality Q, is obtained by integrating in the same way over the product of the object power spectrum and the transfer function itself. This factor can be shown to be an arithmetical average of the first two. In the case of a flat object spectrum, it is simply the normalized area under the transfer function curve. It is interesting that this last integral is equivalent to quite a different quality factor, the Strehl criterion, which is defined for the case of a point source image as the ratio of the on-axis intensity in the actual diffraction pattern to the corresponding intensity for an aberration-free objective.

Study is needed, as well, of methods for averaging the performance for different directions of the sine wave target. Possibly a single measurement or calculation for lines midway between the tangential and radial directions would be adequate. It is conceivable that a rotationally symmetric target based on a sinusoidal distribution could be of value. The rotation of a sine wave gives a zero-order Bessel function such as shown in Fig. 17. Kelly[49] has used such targets as stimuli for visual testing. This target or a modification along similar lines might provide a rotationally symmetric discrete target for photographic testing that would be more amenable to computation than bar targets.

An understanding of the role of spatial phase shift is needed. Possibly a way can be found of including the phase in a multiplicative factor to be used with the transfer function modulus to produce a single curve lower than the modulus by an amount dependent on the phase shift. Such understanding can only come out of extensive analysis of empirical data.

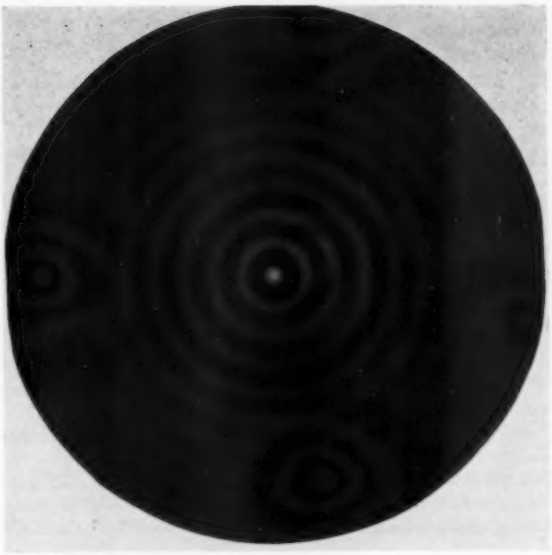

Fig. 17. Bessel function. Appearance of J_0 spatial pattern proposed as a stimulus for visual research (after Kelly).

Summary

The practical utility of the transfer function is based on the following concepts most of which have been implicitly or explicitly discussed in the preceding paragraphs.

1. A sine wave is imaged as a sine wave. This result of linearity is important because it simplifies the readout problem in testing.

2. The transfer function of a serial combination of components (assumed linear) is the simple product of the transfer functions of the separate components.

3. The transfer function provides a way of mathematically smoothing the detailed irregularities in the diffraction pattern of a point source, putting the interpretation of diffraction calculations on a more manageable basis.

4. The transfer function can be used to predict the image of line or of an edge and it may be computed from ray trace data, wavefront data, or from the known energy distribution in the image of a point, a line, or an edge.

5. It deals with an extended target (this is relevant only for systems designed for use with continuous objects) and offers the possibility of system optimization for an object of known spatial frequency content.

The concept cannot be fully used, however, until a great deal more work is carried out to improve the basis for the interpretation of results. Now that calculations are being carried out routinely and actual sine wave testing is becoming more general, much more empirical data will become available. It is to be hoped that as such data, including the effects of granularity, become available, it will be reported in the literature. Theoretical work is needed to link more closely the theory to optical design needs. Data are needed, too, on the transfer functions of optical fibers, image tubes, and projection screen materials.

While the early pioneering work is well identified in the bibliography, no attempt has been made to provide a complete listing of the many publications in this field.

The writer wishes to express his thanks to a number of his colleagues, but particularly R. Barakat, G. C. Harvey, and R. R. Shannon for helpful discussion and criticism during the preparation of this paper.

References

1. L. E. Howlett, Can. J. Res. **A24,** 15 (1946).
2. F. H. Perrin, J. Soc. Motion Picture Television Engrs. **69,** 151, 239 (1960).
3. Lord Rayleigh, Phil. Mag. **42,** 167 (1896).
4. H. Frieser, Compt. Rend. Proc. IX, Congr. Intern., Phot. Paris (1935).
5. E. W. H. Selwyn, Phot. J. **75,** 571 (1935).
6. *Symposium on the Evaluation of Optical Imagery 1951,* NBS Circular 526 (1954).
7. R. K. Luneberg, *Mathematical Theory of Optics* (Brown University, Providence, R.I.).
8. P. M. Duffieux, *L'Integrale de Fourier et Ses Applications à L'Optique* (Besancon, 1946).
9. O. Schade, RCA Rev. **9** (1948); also, J. Soc. Motion Picture Television Engrs. **56,** 137 (1951); **58,** 182 (1952); **61,** 98 (1953); **64,** 593 (1955).
10. P. Elias, D. S. Grey, and D. Z. Robinson, J. Opt. Soc. Am. **42,** 127 (1952).
11. H. H. Hopkins, Proc. Roy. Soc. (London), Ser. A **208,** 263 (1951).
12. H. H. Hopkins, Proc. Roy. Soc. (London) Ser. A **217,** 408 (1953).
13. E. L. O'Neill, *Selected Topics in Optics and Communication Theory* (Itek Corporation, Lexington, Mass., 1958).
14. A. B. Porter, Phil. Mag. **11,** 154 (1906).
15. A. A. Michelson, *Studies in Optics* (Univ. of Chicago Press, Chicago, Ill., 1927).
16. Recommendation on Nomenclature by ICO Subcommittee for Image Evaluation, Opt. Acta **8,** 359 (1961).
17. R. L. Lamberts, J. Opt. Soc. Am. **49,** 425 (1959).
18. W. J. Bates, Proc. Phys. Soc. (London) **59,** 940 (1947).
19. M. Françon, Opt. Acta **1,** 50 (1954).
20. H. H. Hopkins, Opt. Acta **2,** 23 (1955).
21. F. D. Smith, J. Opt. Soc. Am. **45,** 408 (1955).
22. H. H. Hopkins, Proc. Roy. Soc. (London) Ser. A **231,** 81 (1955).
23. M. De, Proc. Roy. Soc. (London) Ser. A **233,** 91 (1955).
24. N. S. Bromilow, Proc. Phys. Soc. (London) Ser. B **71,** 231 (1958).
25. K. Miyamoto, J. Opt. Soc. Am. **48,** 57 (1958).
26. E. H. Linfoot, Opt. Acta **9,** 82 (1962).
27. K. Miyamoto, *Progress in Optics* (North-Holland, Amsterdam, 1961).
28. R. E. Hopkins, *Notes for Summer Course in Applied Optics* (Institute of Optics, Rochester, N.Y., 1962).
29. R. R. Shannon and S. Perry, J. Opt. Soc. Am. **49,** 506 (1959).
30. G. Black and E. H. Linfoot, Proc. Roy. Soc. (London), Ser. A **239,** 522 (1957).
31. G. Parrent and C. Drane, Opt. Acta **3,** 195 (1956).
32. W. Steel, Rev. Opt. **32,** 4, 143, 269 (1953).
33. R. Barakat and D. Lev, J. Opt. Soc. Am. **53,** 324 (1963).
34. R. Barakat and D. Lev, J. Opt. Soc. Am. **52,** 264, 276 (1962).
35. W. Herriott, J. Opt. Soc. Am. **37,** 472 (1947).
36. D. R. Herriott, J. Opt. Soc. Am. **48,** 968 (1958).
37. P. Lindberg, Opt. Acta **1,** 69 (1954).
38. L. R. Baker, Proc. Phys. Soc. (London) Ser. B **68,** 871 (1955).
39. D. Kelsall, Proc. Phys. Soc. (London) Ser. B **66,** 145 (1953).
40. E. Menzel, Optik **15,** 460 (1958).
41. R. L. Lamberts, J. Opt. Soc. Am. **49,** 425 (1959).
42. Modulation Transfer Data for Kodak Films, Kodak Pamphlet No. P-49.
43. D. H. Kelly, J. Opt. Soc. Am. **50,** 269 (1960); **51,** 319 (1961).
44. F. Zernicke, Physica **9,** 974 (1942).
45. E. H. Linfoot, *Recent Advances in Optics* (Oxford Univ. Press, Oxford, 1955).
46. J. J. DePalma and E. M. Lowry, J. Opt. Soc. Am. **52,** 328 (1962).
47. R. M. Scott, Phot. Sci. Eng. **3,** 201 (1959).
48. P. B. Fellgett and E. H. Linfoot, Phil. Trans. Roy. Soc. London Ser. A **247,** 369 (1955).
49. D. H. Kelly, J. Opt. Soc. Am. **50,** 1115 (1960).

UNIVERSITY OF MINNESOTA

Summer Courses in Infrared Spectroscopy, Molecular Spectroscopy Laboratory, July 30 through August 9, 1963

The University of Minnesota will offer two courses in Infrared Spectroscopy, under the direction of Bryce Crawford, Jr., Stuart W. Fenton and John Overend, all of the University of Minnesota, and W. J. Potts, of the Dow Chemical Company. The first course on "Techniques of Infrared Spectroscopy" will run Tuesday, July 30 through Saturday, August 3, and will be followed by the second course "Chemical Interpretation of Infrared Spectra" running Monday, August 5 through Friday, August 9. The courses are related, but operate independently and participants may register for either or both. The lecture courses begin with the fundamentals and carry through to include recent developments; discussion seminars provide opportunity for treatment of advanced topics. Participants should have at least basic training in chemistry and physics, but not necessarily experience in spectroscopy.

The Techniques Course will include lectures on basic optics and instrument theory, on instrument design, on sample preparation, and on laboratory techniques exploiting the capabilities of modern instruments and accessories. Laboratory work will provide experience in these techniques, acquainting participants with prism and grating infrared spectrometers, both single and double beam, and with gaseous, liquid, solid, and plastic samples. Experience will be provided with all of the most modern commercially available spectrometers.

The Interpretation Course will include lectures and guidance from two leading spectroscopists of wide experience, Drs. Foil S. Miller of the Mellon Institute, and Clara D. Smith of Cranbury, New Jersey. The lectures will provide systematic coverage of the group frequencies useful in chemical diagnosis and structure determination, as well as lectures on the factors giving rise to these group frequencies and their variations, and the practical use of infrared in day-to-day chemical work. In the afternoon sessions, individual practice will be provided in the interpretation of a graded set of typical spectra of "unknowns" with appropriate guidance and counsel. Standard catalogs of spectra will be available and their use will be explained.

Enrollment for each course is limited; those interested should write to the Director, Center for Continuation Study, University of Minnesota, Minneapolis 14, Minnesota; or to Professor Crawford.

Information Capacity of Radiation Detectors and of Light

R. Clark Jones

Data are presented on the information capacity and on the information efficiency of a beam of light and of several kinds of detectors including heat detectors, a multiplier phototube, an image orthicon, four photographic films, and human vision. The information efficiency is the information capacity divided by the number of photons that are needed to achieve the capacity, and is measured in bits per photon. The photographic films are discussed in separate sections from two points of view: that of maximizing the information capacity in bits/cm², and that of maximizing the information efficiency. The other detectors and the beam of light are discussed only from the point of view of maximizing the information efficiency, because there is no upper bound to the information capacity that is related to practical use. The paper is primarily a review of the results of four previously published papers, but some new material is included: The results in Tables I and II on the information capacity of a beam of light are more extensive and more accurate than those previously published, and an explicit proof is given for the fact that it is not necessary to employ a radiation signal having spatial structure to obtain the greatest information efficiency with an image-transducing detector; a time varying radiation signal incident at a single point of the responsive surface is sufficient to achieve the maximum possible information efficiency.

I. Introduction

This is a review of four publications (refs. 3–6) on the information capacity of radiation detectors and of light. As explained in the next section on the concept of information capacity, a more interesting concept is the information efficiency. Except for photographic films, the emphasis of this paper is on the information efficiency.

Section III is on the information efficiency of light; the results presented in Tables I and II are new. Section IV is a brief review of the concepts needed for the discussion of radiation detectors: the energy detectivity and the detective quantum efficiency. Section V shows how the information efficiency of unitary radiation detectors may be described in terms of these two concepts, and presents results for five different kinds of radiation detectors.

Section VI considers the information capacity of photographic films, and is the only part of this review in which the information capacity *per se* plays the major role.

The author is with the Research Laboratory of the Polaroid Corporation, Cambridge, Massachusetts.

Received 4 January 1963.

This research was supported by the Geophysics Research Directorate, AFCRL.

II. Information Capacity and Information Efficiency

In the English language there are at least two good books on information theory, one by Shannon[1] and one by Goldman.[2] If one takes a broad look at these books, one might say that the first important point is that information, defined in a suitable way, can be measured quantitatively; and that the unit of measurement is called the *bit*. Before a coin is flipped, a head and a tail are equally probable results. If you actually flip a coin and find that the result is for example a head, this result carries exactly one bit of information. If you spin a roulette wheel with 32 different and equally spaced pins, and if you find that the result of one spin of the wheel is 17, this result carried five bits of information, because one must make five equiprobable binary decisions to determine one result from 32 equally probably alternatives. One way of deriving the number 5 is that 32 is the *fifth* power of 2. Another way is to note that the digits from zero to 31 (32 digits) require a *five* digit binary number; in particular 17 has the binary representation 10001.

The second important point in these books is that one can define the information capacity of a noisy continuous channel. It is not all obvious that the simple consideration of the preceding paragraph can

be extended to include an ordinary telephone or telegraph channel, but in fact they can be. The enormous contribution that Professor Shannon made to information theory is his demonstration that one can precisely state the maximum possible information capacity of a channel. If one tries to send more than the maximum capacity, transmission errors are inevitable. The famous formula that Shannon developed is

$$C_{\text{bit/sec}} = W_{\text{cps}} \log_2 (1 + P_s/P_n). \tag{2.1}$$

This formula gives the capacity in bits per second of a communication channel with a bandwidth W_{cps} in cycles per second when the average signal power is P_s and the average noise power is P_n.

The above equation for C should not be stated without also stating the many conditions on its validity. In particular, the powers P_s and P_n are each supposed to be proportional to the squares of voltages. The two voltages must be additive, must individually have a Gaussian distribution, and the two distributions must be statistically independent. There are also other conditions.

The theorem represented by the above formula has a rather peculiar status. No one has ever found a way by which one can actually transmit as much information as this formula indicates. There is a good deal of literature about this, and in recent years methods have been found that permit one to transmit perhaps half as much information as this formula indicates. Nevertheless, the formula is important as an upper limit; it tells us the maximum possible amount of information that we shall ever be able to transmit without error.

The author is responsible for a number of recent articles on the information capacity of radiation detectors[3–5] and of a beam of light.[6] The information capacity C is not precisely the subject that is studied in these articles, because (except for photographic films) the information capacity has no upper bound that is relevant to the way that detectors are actually used. The information capacity increases without limit as the amount of signal radiation increases, until the amount of radiation gets so large that it injures the detector in some way: either decreased response or increased intrinsic noise or both. There is a related concept, however, that is of more interest: this is the information efficiency I defined as the ratio of the information capacity C to the signal power P

$$I = C/P. \tag{2.2}$$

If the information efficiency C is measured in bits per second, and the power in photons per second, then the information efficiency is measured in bits per photon. All radiation detectors have an information efficiency that reaches an upper bound for quite moderate amounts of the signal power.

Fig. 1. The physical situation used for the calculation of the information efficiency of a beam of light. The source of the light is at the left, and the receiver at the right. In between is the shutter, which is supposed either to be fully open or fully closed during each of a sequence of time intervals of equal duration. The result of the calculation is independent of the length of the time intervals.

In refs. 3–5, the information efficiency is formulated in terms of a unitary detector, by which we mean a detector like a bolometer of a phototube that does not transduce an image. But the concept of information efficiency is also relevant for image-transducing detectors like image orthicons, photographic films, and human vision. I have not previously elucidated the reason why the information efficiency is so particularly useful for image-transducing detectors.

Consider an image-transducing detector; for example, an image orthicon. Let the radiation signal be incident at a point on the responsive surface, and let the power of the signal be adjusted so that the information efficiency is maximized. Now let a second radiation signal fall on another point of the responsive surface (which is well separated from the first, so that there is no crosstalk), and let the power of this signal also be adjusted so that the information efficiency of the second channel is maximized. If the responsive surface is uniform, the two powers will be identical and the two information efficiencies will be identical. Now consider the two channels as one grand channel. The grand channel has twice the information capacity and involves twice the radiation power. The information efficiency of the grand channel is thus equal to the information capacity of either of the single channels.

Thus whether we have one, two, or more radiation signals incident on the responsive surface, we obtain the same information efficiency, so long as there is no crosstalk. Furthermore, there is no way to achieve a greater information efficiency; thus the information efficiency obtained for radiation incident on a point of the responsive surface is *the* information efficiency of the image-transducing detector.

If, however, in the effort to make the information capacity as large as possible, we crowd so many channels on the responsive surface that crosstalk occurs between the channels, then *the* information efficiency is decreased. This decrease may be seen in the data in Sections V and VI, where the information efficiency of Royal-X film is found in Section V to be 12.7 ×

10^{-4} bit/photon, and where the information efficiency found in Section VI (where the information capacity is maximized) is only 1.22×10^{-4} bit/photon—a decrease by a factor of 10.

III. Information Efficiency of a Beam of Light

In this section we consider the information efficiency of a beam of light. Figure 1 shows the physical situation. On the left is a steady source of light, an incandescent lamp operated on direct current, for example. In front of the source is a shutter that is either fully open or fully closed. On the right is the receiver. The receiver is supposed to be an ideal photon detector.

We suppose the time scale is divided into a large number of time intervals, each of equal duration. When the shutter is closed during any time interval, we say that a "zero" is transmitted; and when the shutter is open, we say that a "one" is transmitted. The receiver decides that a "one" is received if any photons at all are received and otherwise that a "zero" is received. Now so far as the "zero" digit is concerned, this is a perfect communication channel, because, when the shutter is closed, there are no photons and the receiver always decides that a "zero" is received.

But there is noise in the channel when a "one" is transmitted, because even when the shutter is open, there is always a finite probability that no photons are received. In ref. 6 it is shown that this probability is e^{-M}, where M is the mean number of photons received when the gate is open.

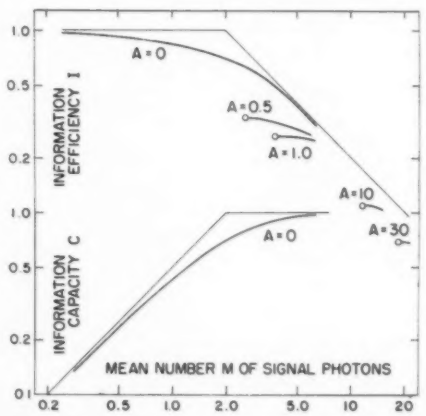

Fig. 2. All of the data in the plot are for symmetrical on-off modulation: $p = 0.5$. The upper plot shows the information efficiency I in bits per photon plotted against the mean number of signal photons. The curve $A = 0$ is based on Eq. (3.1). The short curves labeled $A = 0.5$, $A = 1.0$, $A = 10$, and $A = 30$ show the behavior for the indicated values of the number of ambient photons A. The open circles show the maximum of these curves, and correspond to the data in Table I. The lower curve shows that the information capacity C increases linearly with the number of signal photons M for small values of M, and approaches the value of one bit per digit as M becomes infinite.

Besides M, the mean number of photons when the gate is open, we must also get firmly in mind the parameter p, which is the *a priori* probability of sending a "one." If p is one-half, this means that over a long period of time there are just as many "ones" as "zeros." If p is one-tenth, it means that on the average there are nine "zeros" sent for every "one."

In summary, M is the mean number of photons received per gate period when a "one" is sent, and p is the probability of sending a "one."

The standard formulas[7] for the information capacity of a discrete channel permit us to calculate the information capacity per digit. One finds

$$C = pN \log_2 p^{-1} + (1 - pN)\log_2(1 - pN)^{-1} - (\log_2 e)pMe^{-M}, \quad (3.1$$

where N is the abbreviation

$$N \equiv 1 - e^{-M}. \quad (3.2$$

This equation gives the information capacity C in bits per digit for any values of M and p. It is not a very transparent equation.

The information efficiency I, in bits per photon, is obtained from C in bits per digit by dividing by the mean number of photons per digit, which is p times M. Thus

$$I = C/pM. \quad (3.3)$$

If one puts some numbers into these equations and gets a feel for them, one soon finds out that the information efficiency I has its maximum value in the limit where M gets very small. In this limit, I becomes very simple:

$$I = \log_2 p^{-1}. \quad (3.4)$$

When the probability of "ones" and "zeros" are equal, p is one-half and the maximum information efficiency is just one bit per photon. If p is equal to a thousandth, then the maximum information efficiency is about ten bits per photon.

The upper curve in Fig. 2 shows the information efficiency I plotted against the mean number of photons M per gate period. The plot is for the special case $p = 1/2$. One notes that the information efficiency does not drop rapidly as M increases. Even when the mean number of photons per open gate period is 2, the information efficiency has dropped from unity only to 0.7.

The lower curve in Fig. 2 shows the information capacity C, in bits per digit, also for the special case $p = 1/2$. One notes that C rises linearly with M, and then levels off at just one bit per digit.

Now we add a further complication to the physical situation. So far it has been supposed that there is

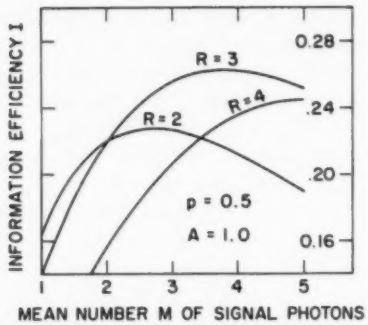

Fig. 3. Showing the dependence of the information efficiency I on the mean number M of signal photons per gate period, for the special case in which, on the average, the gate is open half the time ($p = 0.5$), and in which the mean number A of ambient photons per gate period is 1.0. The three curves show the results for three different receiver thresholds. The curve for a threshold of 3 photons is the highest, and reference to Table I shows that the exact value of the maximum is $I = 0.26324$ bit per photon, and that the maximum is achieved when the mean number of signal photons is $M = 3.790$.

no light at all except that which arrives from the modulated source. Now we make the contrary assumption. We suppose that steady ambient light does reach the receiver, to the amount of, on the average, A photons per period.

When there is ambient light, there is another complication. It is no longer necessarily true that the receiver should decide a "one" is received if one or more photons arrive. The receiver adopts the criterion that a "zero" is received if less than R photons are received, and otherwise that a "one" is received. R is an integer. Thus the problem involves four parameters: p, M, A, and R.

The expression for the information efficiency in this more complicated situation is given by Eq. (4.5) in ref. 6. The expression itself is complicated. The results obtained with the aid of an IBM 1620 computer are summarized in ref. 6, and Fig. 3 shows a sample of these results.

Since the work reported in ref. 6 was completed, Polaroid has acquired an IBM 1401 computer, and further results have been obtained as follows:

In the 1401 calculations, the values of p and A were first chosen. The computer then calculated a 9 by 9 array of values of I in which the value of R differed by one in adjacent columns and in which the value of M differed by a selected amount in adjacent rows. The largest value in the array was then noted by inspection, and third-order curves were fitted to the data in the noted column and in the two adjacent columns.

From the third-order fitted curves it was easy to find the maximum value of I for the given values of p, A, and R, and then to find the value of R for which the maximum of I is largest. Thus one finds the upper bound of the

Table I. Information Efficiency of Light[a]

A/p	0.5	0.1	10^{-2}	10^{-3}	10^{-5}	10^{-10}
	1.0000	3.32193	6.64386	9.96578	16.60964	33.21928
0	0	0	0	0	0	0
	1	1	1	1	1	1
	0.33074	0.73321	1.06774	1.28783	1.60529	2.09314
0.5	2.666	3.517	4.753	6.084	7.502	12.76
	2	3	4	5	6	10
	0.26324	0.58772	0.86714	1.05595	1.32207	1.75723
1.0	3.790	4.508	5.702	7.008	9.638	16.04
	3	4	5	6	8	13
	0.17772	0.39356	0.59156	0.73172	0.93653	1.27277
3.0	6.149	6.621	8.893	11.35	15.12	22.58
	6	7	9	11	14	20
	0.11059	0.24608	0.37168	0.46554	0.60540	0.84745
10.0	11.81	12.96	15.06	18.59	24.585	35.35
	16	18	20	23	28	37
	0.069316	0.1502	0.23456	0.29560	0.39005	0.55610
30.0	18.62	21.31	25.48	30.03	38.18	54.40
	39	43	47	51	58	72
	0.029015	0.064486	0.099014	0.12589	0.16858	0.24659
200.0	48.17	52.82	62.76	73.68	91.46	127.1
	224	232	242	252	268	300

[a] In each group of three entries, the top number is the absolute maximum of the information efficiency I in bits per photon, for the value of the probability p of an open gate that is shown at the top of the table, and for the mean number A of ambient photons that is shown in the left-hand column. To achieve this absolute maximum value of I, the mean number M of signal photons must have the value shown by the middle number, and the detector threshold R (smallest number of received photons for the decision "one") must have the value shown by the integer at the bottom of each group of three entries.

information efficiency I for each set of the values of p and A. Furthermore, the calculation gives as a by-product the values of M and R that achieve the upper bound of I. Thus for each chosen set of values of p and A, the calculation gives the upper bound of I along with the value of A and R that achieve this upper bound.

The results are shown in Table I, which includes the 42 sets of values of p and A obtained by giving the probability p the values 0.5, 0.1, 10^{-2}, 10^{-3}, 10^{-5}, and 10^{-10}, and by giving A the values 0, 0.5, 1.0, 3.0, 10.0, 30.0, and 200. Underneath each value of the information efficiency I is shown the value of the mean number of signal photons M, and the value of the threshold R.

An auxiliary calculation gave the results shown in Table II, which is for $p = 0.5$, and for $A = 0$, 10^{-5}, 10^{-4}, 10^{-3}, 10^{-2}, 0.1, 0.2, and 0.3.

IV. Description of Detector Performance

The detecting ability of radiation detectors is usually described in terms of the power detectivities D and D^*. It will shorten the presentation here, however, if we define at once the energy detectivity.[8]

We imagine that a short burst of radiation is incident on the detector. This radiation produces in the electrical output of the detector an electrical pulse that we naturally call the signal pulse. Also in the output of the detector is a certain amount of electrical noise. The amplitude of the signal is measured by the peak voltage of the pulse, and the amplitude of the noise is measured by the root-mean-square deviation of the voltage from its mean value. The ratio of these two voltages is the signal-to-noise ratio S/N, and the energy detectivity Δ is defined by S/N divided by the total energy E of the radiation pulse that is intercepted by the responsive area of the detector:

$$\Delta \equiv (S/N)/E. \tag{4.1}$$

The amount of energy E that makes the signal-to-noise ratio equal to unity is by definition the noise equivalent energy E_N, and thus we see that the energy detectivity is equal to the reciprocal of the noise equivalent energy:

$$\Delta = 1/E_N. \tag{4.2}$$

When the duration of the radiation pulse is made sufficiently short, and when the electrical circuit employs optimal filtering, then the energy detectivity reaches its upper bound which is denoted by Δ_m; see ref. 8 for details. Finally, if the energy detectivity Δ_m is measured under conditions where only the internally generated noise is effective (radiation noise is negligible), then the energy detectivity is denoted by Δ_{mi}.

It is also useful to compare the detecting ability of a radiation detector with the detecting ability of a suitably defined ideal detector. The ideal detector is here defined on a detector that has no internally generated noise, and that gives equal weight in its output to every incident photon. If the ideal detector is exposed to steady background radiation one can show that its energy detectivity is given by

$$\Delta_{m,\ \text{ideal}} = 1/(\varepsilon E_a)^{1/2}, \tag{4.3}$$

where ε is the energy of a photon, and E_a is the energy of the steady background radiation that is incident on the detector during the detector's integration time.

The detective quantum efficiency is then defined by

$$Q_D = [\Delta_{m,\ \text{meas}}/\Delta_{m,\ \text{ideal}}]^2. \tag{4.4}$$

Since the detectivity of the actual detector cannot be greater than that of the ideal detector, it is clear that the detective quantum efficiency has an upper bound of unity. The author has written a monograph[9] on the subject of the detective quantum efficiency, to which the reader is referred for further details.

In all of this author's other writings, except in ref. 5, the detective quantum efficiency has been defined as above. In this article, as also in ref. 5, we wish to define the detective quantum efficiency somewhat differently. Specifically, we wish to use in the defining equation, not the actual measured detectivity, but rather the detectivity increased by a compensation for the in-

Table II. An Extension of Table I for $p = 0.5$ and for Values of A Lying between 0 and 0.5

A	
	1.0000
0	0.0
	1
	0.99222
10^{-5}	0.0258
	1
	0.97746
10^{-4}	0.0729
	1
	0.93588
10^{-3}	0.198
	1
	0.82289
10^{-2}	0.4987
	1
	0.54736
0.1	1.100
	1
	0.42224
0.2	1.340
	1
	0.37544
0.3	2.654
	2

Table III. Information Efficiency of Five Kinds of Radiation Detectors.[a]

Detector	Area (cm^2)	Q_{Dc}	Δ_{mi} (photon^{-1})	I_{max} (bit/photon)
1P21 phototube	1.0	0.1	25	0.1
Human vision	—	0.03	0.02	7.2×10^{-3}
Royal-X film	$\sim 10^{-4}$	0.009	0.003	1.3×10^{-3}
6849 image orthicon	1.0	0.044	2.0×10^{-5}	2.0×10^{-5}
Heat detector	1.0	1.0	3.3×10^{-8}	1.6×10^{-8}

[a] All of the results are calculated for a wavelength near 0.045 μ. This figure is reproduced by permission of the Editor of *J. Opt. Soc. Am.*

ternal noise of the detector. What we wish to obtain is the detectivity the actual detector would have if it had no internal noise. When this compensation has been made in the measured detectivity, then the corresponding value of the detective quantum efficiency is denoted Q_{Dc}. This compensated value will be used through the remainder of this paper.

Then the energy detectivity with any given value of the ambient energy E_a may be written

$$\Delta_m = \left(\frac{1}{\Delta_{mi}^2} + \frac{\varepsilon E_a}{Q_{Dc}} \right)^{-1/2}. \tag{4.5}$$

This equation for the energy detectivity Δ_m shows explicitly the dependence of Δ_m on Δ_{mi}, which is the energy detectivity when the radiation noise is negligible, and on the compensated detective quantum efficiency Q_{Dc}. The first term inside the parenthesis represents the effect of the internal noise, and the second terms the effect of the radiation noise.

For a more complete discussion of the energy detectivity and the detective quantum efficiency see refs. 8 and 9.

V. Information Efficiency

If one sets up the general expression for the information efficiency, it is found to depend on the detector parameters introduced in the last section and also on the amount, spectrum, and modulation factor of the radiation that is the signal. The procedure used in ref. 5 is to choose the spectrum and modulation factor of the signal so that the information efficiency is maximized. When one carries through this maximization, it is found to be desirable and convenient to introduce a number of mathematical and physical approximations, some of which are made to make the calculation feasible and others of which are made to make the result as simple as possible.

The final result obtained by this procedure is that the upper bound of the information efficiency may be written in the following rather simple form:

$$\frac{1}{I_{max}} = \frac{1}{Q_{Dc}} + \frac{2}{\Delta_{mi}}, \tag{5.1}$$

where the energy detectivity must be expressed in reciprocal photons. If Δ_{mi} is to be expressed in energy units, then $2/\Delta_{mi}$ must be replaced in the above formula by $2/(\varepsilon\Delta_{mi})$.

From this expression we see at once that if the energy detectivity Δ_{mi} is much greater than the detectivity Q_{Dc}, then one has

$$I_{max} = Q_{Dc}. \tag{5.2}$$

On the other hand, if Δ_{mi} is much less than Q_{Dc}, then one has

$$I_{max} = {}^1/_2\Delta_{mi}. \tag{5.3}$$

In other words, when ${}^1/_2\Delta_{mi}$ and Q_{Dc} are widely different in magnitude, then the maximum value of the information efficiency is equal to the smaller of these two quantities.

Table III shows the values of the energy detectivity Δ_{mi} and the detective quantum efficiency Q_{Dc} for five different kinds of detectors. The last column shows the energy efficiency I_{max} in bits per photon calculated by Eq. (5.1). Inspection of the table shows that the values of the information efficiency vary from 0.1 bit/photon for the 1P21 multiplier phototube, down to 1.6×10^{-8} for the best thermocouples and bolometers. The information in Table III is taken from ref. 5.

Three of the five kinds of detectors in Table III are image-transducers. Two of these (photographic films and human vision) are analyzed in accordance with Section 2 by having the radiation incident at a point on the responsive surface. The corresponding experimental data for the image orthicon were not available; accordingly, the information efficiency for the image orthicon is calculated for the radiation signal incident upon a 1-cm^2 area. The information efficiency of the two unitary detectors is also calculated for a responsive area of 1 cm^2.

VI. Information Capacity of Photographic Films

The photographic film to some extent contradicts the statements made at the beginning of Section II. A film is easily overloaded, and for this reason one has

Table IV. Identification and Developing Conditions for the Four Kodak Films

		Time	Developer	Gamma
I	Kodak Royal-X Pan film, code 6128	5 min	DK-50	0.65
II	Eastman Tri-X Panchromatic negative film, type 5233	6.5 min	SD-28	0.54
III	Eastman Plus-X Panchromatic negative film, type 4231	6.5 min	SD-28	0.79
IV	Kodak Panatomic-X film, code 5240	6 min	D-76	0.67

Table V. Various Ways of Expressing the Information Capacity of the Four Films

Film	C_1 bits/cm²	$\mathfrak{a} = C_1^{-1}$ microns²/bit	$r = (\mathfrak{a}/\pi)^{1/2}$ microns	C_1/E_{av} bits/erg	$h\nu C_1/E_{av}$ bits/photon	T_{HF} sec/cm²	$\mathfrak{a}_{TVF}$ cm²/frame
Royal-X	0.449×10^6	200	7.98	26.5×10^6	1.22×10^{-4}	3.01	2.98
Tri-X	0.845×10^6	118.4	6.14	7.35×10^6	0.339×10^{-4}	5.1	1.76
Plus-X	1.86×10^6	53.8	4.14	6.45×10^6	0.298×10^{-4}	11.2	0.80
Pan-X	2.85×10^6	35.0	3.34	7.45×10^6	0.344×10^{-4}	17.2	0.52

a legitimate interest in the information capacity of a photographic film, whereas with most other detectors the information efficiency is the concept of greater interest.

Of all the detectors that have been involved in studying information capacity, the photographic film has required the most recondite analysis.[6] There are several reasons for the difficulty of the analysis. One is the nonlinear character of photographic films: the density is not a linear function of the exposure, nor is the granularity (the noise of photographic films) independent of the amount of the exposure. Furthermore, the film is essentially an image-recording device—the only image-recording detector that I have so far analyzed.

In the determination of the maximum possible information capacity of an image-forming detector, one must determine not only the optimum level of the signal, but also the spectrum of the signal, where by spectrum is meant the spectrum in terms of the two spatial frequencies of the messages. The only available tool for this maximization is the calculus of variations, and the use of this tool requires that all of the relevant physical relations be introduced as analytic functions.

It is not possible in this short review to indicate the course of the calculation used in ref. 6. It must suffice to say that the ingredients of the calculation are the relation between the density and exposure, the modulation transfer function (sine-wave response function), and the Wiener spectrum[10] of the granularity of the film.

The four films for which the information was calculated in ref. 6 are identified in Table IV. This table shows also the developing conditions and the gamma of the developed films.

The chief result of ref. 6 is the set of values of the information capacity C_1 of the four films; C_1, measured in bits/cm², is shown in the second column of Table V. The four values lie in the range from one-half to three million bits/cm².

These numerical results are transformed and interpreted in a variety of ways in the last six columns of Table V.

The reciprocal of C_1 in cm²/bit is the film area required to record one bit. This area $\mathfrak{a}$ is shown in the third column of Table V in μ^2; the areas lie between 35 and 200 μ^2. The fourth column shows r, the radius in microns of a circle that has the area $\mathfrak{a}$; the radii lie between 3 and 8 μ.

The fifth column of Table V shows the information capacity C_1 divided by the exposure E_{av} (in ergs/cm²) that produces a density halfway between the maximum and minimum density of the film. It may be noted that the values for three of the films are nearly the same. The next column shows the information efficiency in bits per photon of the mean exposure; this ratio is calculated with the help of the fact that the energy $h\nu$ of a 430-m photon is 4.61×10^{-12} erg. The values lie between 0.3×10^{-4} and 1.3×10^{-4} bit/photon.

So much for transformation of the results. We shall now compare the information capacity of photographic films with that of some other channels. Consider a high-fidelity speech and music channel with a bandwidth W of 10,000 cps and a signal-to-noise ratio of 50 dB ($P_s/P_n = 10^5$). Equation (2.1) then indicates an information capacity of 166,000 bits/sec. The seventh column of Table V shows the duration T_{HF} of this channel that has the same information capacity as one square centimeter of the film. The results lie between 3 and 20 sec.

A standard television channel in the United States has a bandwidth of 4.5×10^6 cps, provides 30 frames/sec, and under average conditions has a signal-to-noise ratio of about 30 dB in the transmitted signal. The information capacity per second is then 44.9×10^6 bits/sec, on 1.49×10^6 bits/frame. (This is the information capacity of the electrical channel, not the over-all optical channel; the limited resolution of the image orthicon and the kinescope will make the over-all optical channel have a smaller capacity per frame.) The last column of Table V shows the area $\mathfrak{a}_{TVF}$ of the film that has the same information capacity as one television frame. The film area lies between 0.5 and 3 cm².

At the May 1962 meeting of the Society of Photographic Scientists and Engineers in Boston, H. J. Zweig and J. H. Altman reported means to store information on these films with a packing density equal to about one-tenth of the values shown in Table V. They also reported an information storage of 160×10^6 bits/cm² on Type 649 film.

VII. Discussion

I wish to thank the Feature Editor of this issue, F. Dow Smith, for the opportunity to present the above summary of the results obtained in my four publications.[2–6] In these papers the results tended to be swamped by the rather large number of restricting conditions and simplifications and by the mathematical development. It is a pleasure to present the results freed of most of the mathematics.

In some of the original four publications, I was rather emphatic in expressing the opinion that I knew of no applications of the results. I still do not know of any application, but it is undeniable that the results are interesting and intellectually stimulating. And no one will be more delighted than I if someone does find some use for the results!

I have also emphasized that the information theoretic approach has failed to reveal a wholly new way of evaluating the performance of radiation detectors. I may have overemphasized this negative aspect; in any event, one reader was sufficiently motivated to prepare a rebuttal.[11]

In conclusion, I hope that the readers of this paper have found the results to be as interesting as I have found them to be.

References

1. C. E. Shannon, *The Mathematical Theory of Communication* (University of Illinois Press, Urbana, Ill., 1949).
2. S. Goldman, *Information Theory* (Prentice-Hall, Inc., Englewood Cliffs, N. J., 1953).
3. R. Clark Jones, J. Opt. Soc. Am. **50,** 1166 (1960).
4. R. Clark Jones, J. Opt. Soc. Am. **51,** 1159 (1961).
5. R. Clark Jones, J. Opt. Soc. Am. **52,** 1193 (1962).
6. R. Clark Jones, J. Opt. Soc. Am. **52,** 493 (1962).
7. Ref. 2, pp. 47–49.
8. R. Clark Jones, J. Opt. Soc. Am. **50,** 883 (1960).
9. R. Clark Jones, Adv. Electron. Electron Phys. **11,** 88 (1959).
10. R. Clark Jones, J. Opt. Soc. Am. **45,** 799 (1955).
11. R. I. Ścibor-Marchoki, J. Opt. Soc. Am. **51,** 1029 (1961).

Applied Optics BOOKS

Books for review should be submitted to the Managing Editor, APPLIED OPTICS, 1155 16th St., N.W., Washington 6, D.C.

Elements of Infrared Technology: Generation, Transmission and Detection. By PAUL W. KRUSE, LAURENCE D. McGLAUCHLIN, AND RICHMOND B. McQUISTON. John Wiley & Sons, Inc., New York, 1962. 448 pp. $10.75.

This is one of several texts which have recently appeared that treat infrared physics (for a general discussion of such texts see Stanley Ballard's column in the September 1962 issue of *Applied Optics*). As in the case of Smith, Jones, and Chasmar's book, this one is written by authors whose primary interest and background appear to be in solid-state physics and infrared detectors. About one half of the text is devoted to the physics of semiconductors and a discussion of infrared detectors, and the remainder covers sources and transmission through various media including the atmosphere. However, the authors promise a second volume which will treat optical, electronic, and cooling systems and applications, both commercial and military.

Kruse and his colleagues have included considerable mathematical discussion and have attempted to present logical but simplified developments of many of the laws and principles of radiation physics. Thus in the chapter on Infrared Sources they include a derivation of the Planck function rather than just giving a statement of it. Included also are derivations of formulas for radiation from various sources, an elemental discussion of coherence and photon noise, and an introduction to line and band sources. Similarly, starting with Maxwell's equations, the next chapter develops the theory of the infrared optical characteristics of media, while the following chapter briefly discusses optical properties of solids and liquids and gives abbreviated data on specific materials for use as windows, domes, and filters. Chapter 5 is a short chapter on absorption and scattering in the atmosphere including some theory on molecular absorption and Mie scattering and a small amount of the experimental data available. The authors then take up infrared detectors with an introductory chapter on the physics of semiconductors and a chapter on sources of noise including Johnson noise, noise in electron tubes (shot, partition, and flicker noise and microphonics) and in semiconductor materials including transistors and diodes. The last three chapters discuss infrared detectors more specifically beginning with purely phenomenological descriptions of detection mechanisms of thermal and photon detectors including photocells, photomultipliers, image converters, image orthicons, photoconductors and the IR vidicon, photovoltaic and PEM effects, phosphors, various bolometers, thermopiles, the Golay cell, and the evaporagraph. The penultimate chapter goes, in some mathematical detail, into the theories of the photovoltaic, PEM, photoconductive, and bolometer effects, and the final chapter considers the actual performance of various available elemental detectors.

As mentioned above, it is the reviewer's impression, that the book leans heavily on the detector part of the picture though the promised second volume may tend to correct this. The emphasis on detector theory will be most useful to those in the infrared field whose background or training has included little or no training in solid-state or semiconductor physics. The authors suggest that the book may provide a suitable text for a senior-level course in infrared radiation physics, a course not to be found in too many colleges. For those who wish or need to delve deeper into the subject, the original or more comprehensive texts in the various subjects covered will be necessary to appreciate fully the material. In fact, since there are now several of the survey-type texts available, perhaps what is needed, for more comprehensive study or for more detailed reference or data, is a series of volumes on the various subjects such as optical materials or atmospheric transmission.

J. S. GARING

Books *continued on page 36A*

Calculation of Optical Transfer Function from Lens-Design Data

Erich Marchand and Richard Phillips

A description is given of a calculation procedure for obtaining the optical transfer function of an optical system from its design data for both axial and extra-axial object points. The first part of the calculation involves determining the wave aberration of the system to the fifth order (in the classical sense), with vignetting taken into account. The second part involves calculating the optical transfer function from this aberration by the methods of physical optics (diffraction theory). A high-speed computer is required but the particular program to be written from the equations depends upon the kind of computer to be used.

It has been well established in recent years that the appraisal of an optical system can be facilitated by investigating its spread function or its Fourier transform, the optical transfer function. Although these functions are equivalent and can be interconverted to serve the occasion, it is considerably easier to calculate the transfer function from the design data of the lens than to compute the spread function.

The mathematical analysis of the transfer function has been explored by several authors.[1] Methods of calculating this function for practical optical systems have been outlined,[2] and methods for determining it experimentally from the finished lens have been devised.[3,4]

The numerical work involved is so extensive, especially for extra-axial objects, as to require high-speed computing equipment. Some workers[5] have investigated a simplified approximate formula giving the so-called geometrical-optical transfer function. This formula appears to give fairly good results with a considerable saving in time and expense, but it was felt in our laboratories that a more accurate method of obtaining the transfer function should be available, both as a control for the approximate method being studied and for comparison with measurements made on finished lenses. This work describes a procedure that can be developed into a program for a high-speed computer.

The authors are with the Eastman Kodak Company, Rochester, New York.

Received 7 December 1962.

Communication No. 2333 from the Kodak Research Laboratories.

Notation and Theory

No attempt will be made here to derive the basic formulas connected with the transfer function and its use, this subject being adequately treated in the literature.[6] We shall mention, however, a few of the important formulas with a view to clarifying the present notation and explaining the method of computation.

Figure 1 indicates a typical rotationally symmetrical optical system, with P_0 a monochromatic point source and P_0' its ideal image point.

The wave aberration ϕ for a typical ray is indicated by the distance $\bar{Q}Q$ measured along the ray, the refractive index in the image space being assumed to be unity. Thus the wave aberration represents the deviation of the wavefront from the spherical form, the deviation being measured along the ray in question and defined relative to a reference sphere centered at the ideal image point P_0'. We shall choose the radius of the reference sphere so that this sphere passes through the axial point O of the exit pupil and choose the wavefront so that it also passes through the point O.

The aberration ϕ may be considered to be a function of the lateral coordinates (x', y') of the point M where the ray intersects the plane of the exit pupil. However, it is more convenient to introduce modified coordinates u and y defined by

$$y = y'/a, \quad u = (x'^2 + y'^2)/a^2, \tag{1}$$

where a is the radius of the exit pupil, or the maximum radial distance if vignetting is present.

Owing to the symmetry of the optical system, P_0 can be assumed to lie on the plane $x' = 0$ and the aberration can be assumed to be an even function of x'.

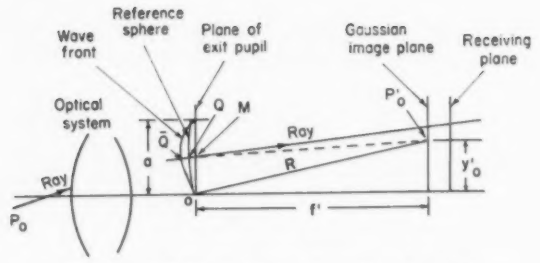

Fig. 1. Definition of wave aberration $\phi = \bar{Q}Q$.

The aberration ϕ will then be a function of u and y, the coordinates defined in Eq. (1). Furthermore, in view of the way ϕ enters the basic formula, it is convenient to replace it by $-k\phi = f$, where $k = 2\pi/\lambda$, λ being the wavelength of the light in the image space.

If one approximates the function f by a polynomial of the form

$$f = -k\phi = f_1 y + f_2 u + f_3 y^2 + f_4 yu + f_5 u^2 + f_6 y^3 + f_7 y^2 u + f_8 y u^2 + f_9 u^3, \quad (2)$$

the coefficients f_i may be interpreted as various aberrations of the lens for the object point P_0 being considered. The form and degree of the polynomial were chosen so as to account for aberrations of third and fifth order (in classical terminology).

The nine coefficients f_i in Eq. (2) can be determined from the lens formula by least-square methods based on the tracing of a number of typical rays through the system. It is well known that the two-dimensional optical transfer function can be obtained by the convolution of the so-called "aperture function" with itself. The aperture function has the form τe^{if}, where f is the function represented in Eq. (2) and τ is a real factor indicating the variation of amplitude in the pupil and having the value zero outside the pupil.

Hopkins[7] has shown that in practical optical systems very little error arises if τ is assumed constant in the aperture. With this assumption and a suitable choice of the variables of integration, the transfer function can be written in a form well suited to numerical computation. Let A be the area of the aperture and S the region obtained by shifting the aperture A in the x and y directions first by amounts of $s/2$ and $t/2$ and then by amounts of $-s/2$ and $-t/2$ and then constructing the overlapping portion of the resulting two regions. With this notation, the formula for the transfer function can be written

$$D(s,t) = \frac{1}{A}\iint_S \exp\left[if(x+\frac{s}{2}, y+\frac{t}{2}) - if(x-\frac{s}{2}, y-\frac{t}{2})\right]dxdy. \quad (3)$$

The quantities s and t prove to be normalized spatial frequencies of the line structures being considered. To obtain line frequencies in ordinary units (lines/mm), we can use the relation

$$s = \frac{\lambda R'}{n' \sin\alpha'}, \quad (4)$$

with a similar formula for t. Here R' is given in lines per millimeter if λ is in millimeters, and $n' \sin\alpha'$ represents the numerical aperture of the system, which can usually be taken as a/f' in the notation of Fig. 1. Conversely, when, as is usually the case, an evaluation is to be made for a certain spatial frequency R', this equation and its analog for t can be used to compute the corresponding values of the parameters s and t.

The variables x and y used in Eq. (3) are normalized coordinates in the exit pupil defined by

$$x = x'/a, \quad y = y'/a, \quad (5)$$

where a is the same normalizing constant as in Eqs. (1). The division by A in Eq. (3) ensures that the transfer function, $D(s,t)$, is normalized to unity when s and t become zero, i.e.,

$$D(0,0) = \frac{1}{A}\iint_A dxdy = 1, \quad (6)$$

since the overlap area S in this case coincides with A.

Equation (3) can be used to obtain the frequency response for line structures at any orientation with the meridional plane. However, since the calculation is lengthy in any case, it was decided to restrict the present program to the two extreme cases, *viz.*, $t = 0$, for lines parallel to the meridional plane, and $s = 0$, for lines perpendicular to the meridional plane. The program, as written, automatically calculates these response values for any specified set of frequency values equally spaced so that the meridional and tangential response curves can be plotted.

Owing to the symmetry of the corresponding spread function across the meridional plane, it follows that the meridional response $D(s,0)$ is real, and in this case there is no phase shift of the line structure except for occasional jumps of π when $D(s,0)$ changes sign.

In the tangential case, we can separate the real and imaginary parts and write

$$D(0,t) = D_1 + iD_2, \quad (7)$$

$$D = (D_1^2 + D_2^2)^{1/2}, \quad \theta = \tan^{-1}(D_2/D_1),$$

where D is the modulation transfer function for the given frequency and θ is the phase-transfer function.

The reason for the difficulty of the calculation becomes clear when one considers that for each choice of frequency one must compute three double integrals representing $D(s,0)$, D_1, and D_2, each extended over the overlap area S, and this area has a different form for each frequency. The basic area A used to obtain S is, in general, the area common to three intersecting circles as obtained from an approximate vignetting

calculation. Furthermore, the exponential integral exhibits a considerable amount of fluctuation, requiring care in the numerical integration. However, a quadrature scheme suggested by Hopkins has proved very helpful in reducing the amount of computation required. The details involved in the numerical evaluation are described in the Appendix.

Determination of the Aberration Coefficients

In theory two methods are available for determining the wave aberration by tracing rays through the system. One method is based on the well-known relations between the partial derivatives of the characteristic function and the arrangement of the rays in the image space. The alternative method involves the evaluation of the light paths directly. It has the advantage of theoretical simplicity and consists essentially of three steps: (1) obtaining the vignetting figure in the exit pupil, (2) tracing rays and computing the light path and wave aberration for each, and (3) fitting each of these aberrations to a polynomial of the form of Eq. (2). This method was adopted. The Fortran program system was used (with a switch to Autocoder language in part for high precision) to do the three steps automatically on the IBM 7080 Computer, starting with the construction data of the lens.

In step 1 the vignetted aperture in the exit pupil can be approximated by the area common to the three circles F, D, and L in Fig. 2. Circle F indicates the region reached by rays from the given object point and passing through the first element of the lens, assuming that these rays pass through the rest of the system. Circles D and L represent the corresponding clearance of rays at the diaphragm stop and the last element, respectively. After the figure is scaled by dividing all radii and center distances by a (the radius of circle D), the resulting common area serves as the region A of the double integral in Eq. (3).

Actually it is necessary for the machine also to compute the corresponding vignetting figure in the first vertex plane. Then it automatically selects a number of rays evenly distributed over this vignetted aperture for use in step 2. Experience to date indicates that about 50 rays are needed to determine the aberration function sufficiently well.

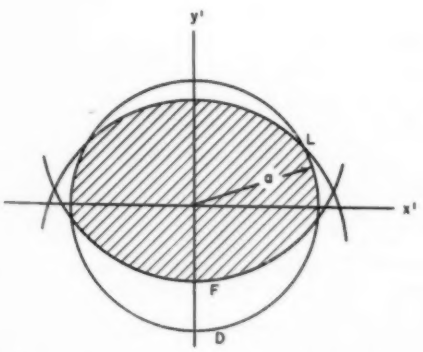

Fig. 2. Typical vignetted aperture in exit pupil.

In step 2 each of the chosen rays is traced up to the exit-pupil plane and at the same time the light path is accumulated to give the total path from the object point to the exit pupil. Apart from a constant this is the distance $\bar{Q}M$ in Fig. 1, since the surface through $\bar{Q}$ and Q is a wave surface. The value of the constant is obtained by performing the same calculation for the principal ray (the ray through the axial point of the exit pupil).

To determine QM in Fig. 1, we may assume with a high degree of accuracy that this distance can be measured along the radial line QP_0' instead of along the ray. If the coordinates of M are (x', y'), this leads to

$$QM = R - [x'^2 + (y' - y_0')^2 + f'^2]^{1/2} \tag{8}$$

with

$$f'^2 = R^2 - y_0'^2.$$

Then the wave aberration for the given ray is given by

$$\phi = \bar{Q}Q = \bar{Q}M - QM \tag{9}$$

and

$$f = -k\phi = -2\pi\phi/\lambda.$$

The selection of the "ideal" image point P_0' has not yet been considered. It might be taken as the Gaussian image point, but this introduces a slight discrepancy when distortion is present. It is therefore better taken as the intersection of the principal ray with the Gaussian image plane. Moreover, this selection simplifies the computations because the coefficient f_1 in Eq. (2) is then strictly zero and only eight coefficients need to be found by least squares.

Step 3 consists in a regression calculation to give the least-square fit of each value of f to a polynomial of the form of Eq. (2), the exit-pupil coordinates being normalized as indicated in Eq. (1). The output of step 3 consists of the nine coefficients f_i of Eq. (2).

The theory underlying Hopkins' formula, Eq. (3), indicates that it yields the response in a "principal" plane through P_0' and perpendicular to the principal ray. When the response in a plane parallel to this one is desired, it is only necessary to adjust the coefficients f_2 and f_3 in the aberration polynomial. A shift of amount z_p away from the lens along the principal ray can be accounted for by adding an amount

$$p = (\pi/\lambda)(a/R)^2 z_p \tag{10}$$

to the coefficient f_2 and subtracting from f_3 the value

$$p(y_c'/R)^2.$$

The quantity p corresponds to a defocusing parameter,

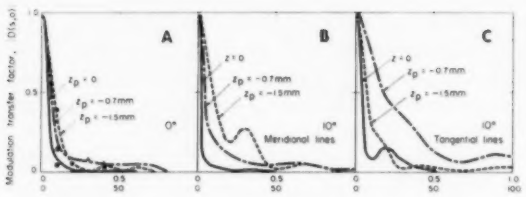

Fig. 3. Modulation transfer curves of a certain 30 cm, $f/5$ lens for three image planes at different distances from the principal plane ($z_p = 0$) and for an object point (A) on the axis and (B and C) 10° away. Values computed by the method of stationary phase are indicated in A by $O(z_p = 0)$, $\Delta(z_p = -0.7$ mm), and $\square(z_p = -1.5$ mm). Upper scale of abscissas' frequency in terms of s; lower scale in terms of R'.

Eq. (1) having been obtained by considering the usual normalized longitudinal diffraction variable p.

In practice one often requires the transfer function in a receiving plane perpendicular to the optical axis (as indicated in Fig. 1). If the inclination angle of the principal ray is small, the desired result is essentially the same as that for a plane perpendicular to the principal ray. For the case of larger angles of inclination, however, an adjustment must be made for the tilt of the receiving plane. Hopkins[8] indicates that a suitable adjustment of the frequency scale will usually compensate with sufficient accuracy.

Examples

The program based on the procedure outlined here has been used to analyze the behavior of a number of lenses. In most cases, several object positions (axial and extra-axial) were studied and the corresponding transfer curves obtained for each of several receiving planes. In each case, both the meridional and the tangential transfer curves were found.

Figure 3(A) shows the curves obtained for a 30 cm, $f/5$ lens for an axial object point and three receiving planes. A comparison is shown with the results computed by an independent method, namely, by calculating the actual spread function by the method of stationary phase and then taking its Fourier transform. The agreement is seen to be satisfactory. The curves for a point 10° from the axis are shown at B and C for the same image planes. Similar curves for a diffraction-limited lens are shown in Fig. 4, where for comparison the curve for a perfect lens, computed from the relation

$$I = (2/\pi)\left\{\cos^{-1} s/2 - s/2[1 - (1/28)^2]^{1/2}\right\},$$

is also shown.

To make a comparison with experiment, curves for an available lens whose constructional data were known were computed for two field angles (Fig. 5). The lens itself was then measured by Lamberts,[3] and the resulting values are shown as circles and triangles in the figure. Some interpolation from the measured data was required because of the difficulty of locating the image plane that had been assumed for the computations, but the agreement with the theoretical curves is nevertheless good.

The primary aim of this project was originally accuracy rather than economy. However, modern computers are so very fast that the procedure described here may not be excessively costly for the routine analysis of lens behavior. A recent run of the second part (calculating the transfer function) with the IBM 7080 Computer took only $2^1/_2$ min to produce meridional, tangential, and phase values for ten frequencies. The time required for the first part of the procedure (calculating the wave aberration) is even less.

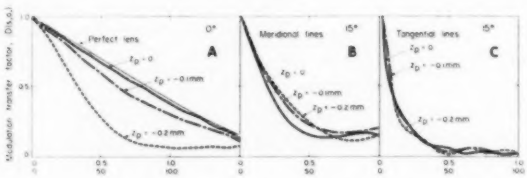

Fig. 4. Modulation transfer curves of a certain diffraction-limited lens for three image planes at different distances from the principal plane ($z_p = 0$) and for an object point (A) on the axis and (B and C) 15° away. Upper scale of abscissas' frequency in terms of s; lower scale in terms of R'.

Appendix. Calculation of the Transfer Function

The numerical evaluation of Eq. (3) with s or t equal to zero was done by the following quadrature scheme suggested by Hopkins. The procedure applies to double integrals of the form

$$I = \iint_S e^{iF(x,y)}dxdy. \qquad (11)$$

Consider the region S to be divided approximately into squares A_p, each of side 2ϵ. The integral over S can then be expressed as the sum of the integrals over the squares. Within one of the squares centered at a point (x_p, y_p), the function F can be approximated by the first three terms of its Taylor series:

$$F(x,y) = F_p + (x - x_p)(F_x)_p + (y - y_p)(F_y)_p, \qquad (12)$$

the subscript p indicating the evaluation of F and its partial derivatives at the center of the square. The value of the integral I_p over a single square can then be obtained readily as follows (we now omit the subscript p on F_x and F_y):

$$
\begin{aligned}
I_p &= \int_{A_p}\int \exp\{i[F_p + (x - x_p)F_x + (y - y_p)F_y]\}\,dx\,dy \\
&= \exp(iF_p)\int_{-\epsilon}^{\epsilon}\int_{-\epsilon}^{\epsilon} \exp[i(F_x\bar{x} + F_y\bar{y})]\,d\bar{x}\,d\bar{y} \\
&= \exp(iF_p)\left[\int_{-\epsilon}^{\epsilon} \exp(iF_x x)\,dx\right]\left[\int_{-\epsilon}^{\epsilon} \exp(iF_y y)\,dy\right] \\
&= \exp(iF_p)\left[2\int_0^{\epsilon} \cos(F_x x)\,dx\right]\left[2\int_0^{\epsilon} \cos(F_y y)\,dy\right] \qquad (13) \\
&= 4\exp(iF_p)\,\frac{\sin(\epsilon F_x)}{F_x}\,\frac{\sin(\epsilon F_y)}{F_y} \\
&= 4\,\epsilon^2 \exp(iF_p)\,\mathrm{sinc}(\epsilon F_x)\,\mathrm{sinc}(\epsilon F_y),
\end{aligned}
$$

where

$$\mathrm{sinc}\,\chi = (\sin\chi)/\chi.$$

The evaluation of Eq. (11) is done by summing the results for each of the squares with centers in the region S. Thus

$$I = 4\epsilon^2 \sum_p \exp(iF_p)\,\mathrm{sinc}\,(\epsilon F_x)_p\,\mathrm{sinc}\,(\epsilon F y)_p. \qquad (14)$$

A second approximation (also suggested by Hopkins) is based on a Taylor expansion relative to s or t of the bracket appearing in Eq. (3). Thus for the case $t = 0$,

$$f(x + s/2,y) = f(x,y) + \frac{(s/2)}{1!}f_x + \frac{(s/2)^2}{2!}f_{xx} + \frac{(s/2)^3}{3!}f_{xxx} + \ldots \qquad (15)$$

$$f(x - s/2,y) = f(x,y) - \frac{(s/2)}{1!}f_x + \frac{(s/2)^2}{2!}f_{xx} - \frac{(s/2)^3}{3!}f_{xxx} + \ldots$$

with derivatives evaluated at (x, y). This leads to

$$f(x + s/2,y) - f(x - s/2,y) = s\left[f_x + \frac{(s/2)^2}{3!}f_{xxx} + \frac{(s/2)^4}{5!}f_{xxxxx}\right], \qquad (16)$$

if we stop at the fifth-degree term in s.

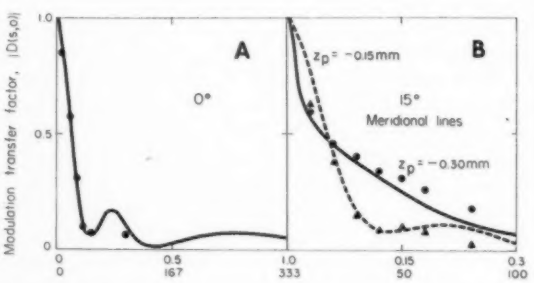

Fig. 5. Modulation transfer curves of a certain lens compared with experimental values (circles and triangles). A, object on axis, one image plane; B, object 15° from axis, image planes 0.15 and 0.30 mm from "principal" plane, meridional lines only. Upper scale of abscissas' frequency in terms of s; lower scale in terms of R'.

We associate this quantity with the function F in Eq. (11) but indicate its value at the center of a typical square by Z. The values of ϵF_x and ϵF_y at the center are denoted by Y and Z. Thus

$$
\begin{aligned}
F_p \quad &= Z = s\left[f_x + \frac{(s/2)^2}{3!}f_{xxx} + \frac{(s/2)^4}{5!}f_{xxxxx}\right] \\
(\epsilon F_x)_p &= X = \epsilon s\left[f_{xx} + \frac{(s/2)^2}{3!}f_{xxxx} + \frac{(s/2)^4}{5!}f_{xxxxxx}\right] \qquad (17) \\
(\epsilon F_y)_p &= Y = \epsilon s\left[f_{xy} + \frac{(s/2)^2}{3!}f_{xxxy} + \frac{(s/2)^4}{5!}f_{xxxxxy}\right]
\end{aligned}
$$

and from Eq. (14) we have

$$I = 4\epsilon^2 \sum_p e^{iZ}\,\mathrm{sinc}\,X\,\mathrm{sinc}\,Y. \qquad (18)$$

Now f is an even function of x by symmetry and hence Z is an odd function of x, while sinc X and sinc Y are even functions of x. Consequently, the imaginary part of Eq. (18) vanishes. Moreover, I is an even function of x so the work can be reduced by integrating for positive values of x alone and then doubling the result. The final formula can thus be written

$$D(s,0) = \frac{8\epsilon^2}{A}\sum_p \cos Z\,\mathrm{sinc}\,X\,\mathrm{sinc}\,Y, \qquad (19)$$

the sum being done on only one half of the region S.

The formulas for the various derivatives needed in Eq. (17) are easily found from Eq. (2). Values for F and its derivatives are computed numerically for many points of the vignetted aperture A, and these values are stored in the computer memory since they are used a number of times later when various values of s are being considered.

For dealing with $D(0,t)$, equations somewhat similar to Eqs. (15–19) are used except that $D(0,t)$ is complex and hence requires twice as much computation to obtain its real and imaginary parts.

It must be kept in mind that each new value of s (or t) yields a new shape for the region S(as was pointed out earlier).

In the program as written by us, the value of ϵ was chosen as 0.05. According to Hopkins this produces accuracy within at least 5% in the final values of the transfer factors. Our experience is in agreement with this conclusion. Verification was obtained by comparison with accurate results computed by various workers using other methods applied to cases of isolated aberrations.

Mention should be made of the elegant procedures used by Barakat[9,10] for the case of spherical aberration. However, he has not treated extra-axial object points.

It is a pleasure to acknowledge the help of Emil Wolf for valuable advice and of Nancy McClure in connection with the vignetting and ray-tracing procedures.

References

1. E. O'Neill, *Selected Topics in Optics and Communication Theory* (Itek Corp., Boston, 1958).
2. H. H. Hopkins, Proc. Roy. Soc. (London) Ser. A **231,** 91 (1955).
3. R. L. Lamberts, J. Opt. Soc. Am. **48,** 490 (1958).
4. F. H. Perrin, J. Soc. Motion Picture Television Engrs. **69,** 239 (1960). This paper contains an extensive bibliography.
5. K. Miyamoto, J. Opt. Soc. Am. **48,** 57, 567 (1958).
6. M. Born and E. Wolf, *Principles of Optics* (Pergamon, New York, 1959), pp. 483–489.
7. H. H. Hopkins, Proc. Phys. Soc. (London) Ser. B **62,** 22 (1949).
8. H. H. Hopkins, Proc. Phys. Soc. (London) Ser. B **69,** 562 (1956).
9. R. Barakat, J. Opt. Soc. Am. **52,** 985 (1962).
10. R. Barakat and M. Morello, J. Opt. Soc. Am. **52,** 992 (1962).

Books *continued from page 358*

Fundamentals of Infrared Technology. By MARVIN R. HOLTER, SOL NUDELMAN, GWYNN H. SUITS, WILLIAM L. WOLFE, GEORGE J. ZISSIS. The Macmillan Company, New York, 1962. 442 pp. $12.50.

Prior to World War II the infrared portion of the electromagnetic spectrum attracted little attention outside university research laboratories. This was the "wax and string" era of infrared instrumentation and technology; equipment was built in university shops for research purposes, and looked the part. During the war, intensive development was undertaken in Germany, and to a lesser extent in England and the United States, seeking to make use of invisible infrared radiation for the detection of troops and military equipment. Since the war, use of infrared radiation for commercial, scientific, and military purposes has expanded tremendously, and at the present time several thousand people in the United States are engaged in the development, manufacture, sale, and use of infrared devices.

It is only during the last five years that infrared engineers have had available moderately comprehensive, readily available reference literature. Since most of the advances in the field were carried out under military sponsorship of limited, specific developments, the literature consisted mainly of reports on such work and was, therefore, highly fragmented and mostly classified. In 1957 the first comprehensive treatment of the subject to appear in book form since the early 1930's (*The Detection and Measurement of Infra-Red Radiation* by R. A. Smith, F. E. Jones, and R. P. Chasmar) was published in England. The September 1959 issue of the *Proceedings of the Institute of Radio Engineers* was a special infrared edition containing a useful series of review articles by United States' authors. The first book on the subject to be published in the United States (*Infrared Radiation* by Henry L. Hackforth) appeared in 1960. Until this year these three publications have constituted the bulk of the open literature available in the field of infrared technology.

Fundamentals of Infrared Technology by Holter, Nudelman, Suits, Wolfe, and Zissis is one of two books* published in the United States in 1962 providing general treatment of the subject. The book has grown out of classroom notes used by the authors in recent years for teaching purposes at University of Michigan accelerated summer courses. It is written at the level of a senior student in the physical sciences. The fact that five authors have collaborated in the writing reflects the scope of the material covered. The general content of the book is best described by a direct quotation from the authors' preface:

> The book is made up of four major sections. The first section, Chapters 1 through 4, covers basic radiation concepts: sources and the nature of the radiation processes, radiation measurements, and transmission through various media with particular emphasis on the earth's atmosphere. Chapter 1 also discusses commonly accepted nomenclature for radiation quantities recommended by the Working Group on Infrared Backgrounds; this nomenclature has usually been followed throughout the book. Chapters 5 through 7, which comprise the second part, are devoted to optics, optical materials, and optical instruments. The next section, Chapters 8 through 12, includes that part of solid-state physics appropriate to detectors, physical mechanisms suitable for detection, and interaction of radiation and matter, noise processes in semiconductors, and detector measurements. Finally, Chapters 13 and 14 deal with applications; design procedures are discussed and applied to typical problems. One Appendix describes the major sources of infrared information; another contains atmospheric spectra.

Fundamentals of Infrared Technology is a chatty book which should prove useful for teaching purposes and for the indoctrination of workers with no prior experience in the field. The inclusion of copious references in most of the chapters will make it useful to the more advanced worker as well as to the beginner. The orientation of the book is toward the design of the kind of equipment used in military infrared systems. The last two chapters and the first two appendices help to integrate the material presented in the earlier chapters by discussing specific examples of system design problems and approaches. A new worker who has mastered this material will be ready for action the moment his security clearance arrives. In reading through *Fundamentals of Infrared Technology,* those who have been working on military infrared developments for some time will undoubtedly find much that is reminiscent of reports they have used for reference purposes. The argot of such material clings tenaciously to its pages. This is understandable because in a sense the book is a product of many of the elder statesmen in this relatively young field. It is dedicated to one of them, and most of the others appear to have influenced it through their writings and participation in summer course activities at the University of Michigan. Those who have known these people and have read their reports will certainly detect the flavor of their talk and writing in this useful volume.

WILLIAM G. LANGTON

Books *continued on page 378*

* The other book, *Elements of Infrared Technology* by P. W. Kruse, L. D. McGlauchlin, and R. B. McQuistan, is the first of a projected two-volume set. The authors have reserved treatment of system applications for the second volume. (It is reviewed on page 358. M/Ed.)

NEW SUBSCRIPTION ORDER

APPLIED OPTICS

Please enter my/our subscription* and continue until countermanded:

- ☐ OSA member rate $6.00 per year
- ☐ Other AIP Societies' rate $8.00 per year
- ☐ Regular rate $10.00 per year
- ☐ Please send OSA membership information
- ☐ check enclosed ☐ bill me
- ☐ Single copy of issue $2.00
- ☐ **MASERS Supplement** published December 1962 .. $5.00

Name ..... Membership No. .....

Address .....

.....

*Subscriptions entered for calendar year only.

NEW SUBSCRIPTION ORDER

APPLIED OPTICS

Please enter my/our subscription* and continue until countermanded:

- ☐ OSA member rate $6.00 per year
- ☐ Other AIP Societies' rate $8.00 per year
- ☐ Regular rate $10.00 per year
- ☐ Please send OSA membership information
- ☐ check enclosed ☐ bill me
- ☐ Single copy of issue $2.00
- ☐ **MASERS Supplement** published December 1962 .. $5.00

Name ..... Membership No. .....

Address .....

.....

*Subscriptions entered for calendar year only.

FIRST CLASS
Permit No. 18297
New York, N. Y.

BUSINESS REPLY MAIL
No postage stamp necessary if mailed in the U. S. A.

POSTAGE WILL BE PAID BY

APPLIED OPTICS
American Institute of Physics
335 E. 45th Street
New York 17, N. Y.

Attention Miss J. Raimondi, Circulation

FIRST CLASS
Permit No. 18297
New York, N. Y.

BUSINESS REPLY MAIL
No postage stamp necessary if mailed in the U. S. A.

POSTAGE WILL BE PAID BY

APPLIED OPTICS
American Institute of Physics
335 E. 45th Street
New York 17, N. Y.

Attention Miss J. Raimondi, Circulation

An Instrument for Measurement of the Optical Transfer Function

R. R. Shannon and A. H. Newman

An experimental method is described for determining the optical transfer function as a function of spatial frequency. The method has a frequency range of 1.79 lines/mm to 730 lines/mm, is self-normalizing, reasonably compact, and usable over a wide wavelength region. The precision and reliability is good to within 0.02. Sample results are given for a Tessar $f/2.8$, 50 mm photographic lens at various focal settings. The same lens at $f/8$, $f/16$ is compared with that of a theoretically diffraction-limited perfect system. It takes approximately one minute to obtain a trace of the transfer function of an optical system for any given focal setting.

Theory

The principle of the device to be described is based upon the construction of an optical analog computer or incoherent spatial filter. Similar techniques have been described, see refs. 1–4. The advantage of the technique to be described here is that it determines phase shifts through a separate measure of the real and imaginary (cosine and sine) transforms.

Presume that an infinitesimal slit is imaged by a lens. The image will be uniform along the slit axis, but will be spread laterally into a spread function $f(y)$. The modulation transfer function derived from this spread function is determined mathematically for a spatial frequency N by[1]

$$F(\omega) = \frac{\int_{-\infty}^{\infty} f(y)e^{i\omega y}\,dy}{\int_{-\infty}^{\infty} f(y)\,dy} = \frac{1}{A}\int_{-\infty}^{\infty} f(y)e^{i\omega y}\,dy. \qquad (1)$$

Here ω is $2\pi N$ and the denominator is a normalization which ensures that $F(0) = 1$. There are many alternate forms for this complex expression, but one of the simplest is

$$F(\omega) = \mathrm{Re}(\omega) + i\,\mathrm{Im}(\omega), \qquad (2)$$

where Re and Im represent the real and imaginary parts, respectively. Examination of (1) shows that

$$\mathrm{Re}(\omega) = \frac{1}{A}\int_{-\infty}^{\infty} f(y)\cos\omega y dy,$$
$$\mathrm{Im}(\omega) = \frac{1}{A}\int_{-\infty}^{\infty} f(y)\sin\omega y dy. \qquad (3)$$

This may be rearranged for convenience later as

$$\mathrm{Re}(\omega) = \frac{1}{A}\left[\int_{-\infty}^{\infty} f(y)(1 + \cos\omega y)dy - \int_{-\infty}^{\infty} f(y)dy\right],$$
$$\mathrm{Im}(\omega) = \frac{1}{A}\left[\int_{-\infty}^{\infty} f(y)(1 + \sin\omega y)dy - \int_{-\infty}^{\infty} f(y)dy\right]. \qquad (4)$$

By making the substitution

$$C = \int_{-\infty}^{\infty} f(y)(1 + \cos\omega y)dy,$$
$$S = \int_{-\infty}^{\infty} f(y)(1 + \sin\omega y)dy,$$

we get

$$\mathrm{Re}(\omega) = (C - A/A),$$
$$\mathrm{Im}(\omega) = (S - A/A), \qquad (5)$$

where C and S stand for the cosine and sine integrations and A is the average of the line-spread function.

Now Eqs. (5) are in a form which are very useful for a measurement device. The physical spread function is allowed to fall upon a target having an average transmission we call unity, and no spatial modulation. Collection of all of the light passing through this target, integration (by a light bar or ground glass), and measurement of this quantity (by a photomultiplier) yields A.

If the above spatially unmodulated target is replaced by one having a transmission $(1 + \cos\omega y)$, the quantity C is obtained. The use of a target $(1 + \sin\omega y)$ yields S. Thus one normalization measurement (A) at zero spatial frequency and two measurements at a stated frequency permit the obtaining of the properly normalized modulation transfer function.

In principle this is exact. In practice the targets used

The authors are in the Optics Department, Itek Corporation, Lexington, Massachusetts.

Received 14 December 1963.

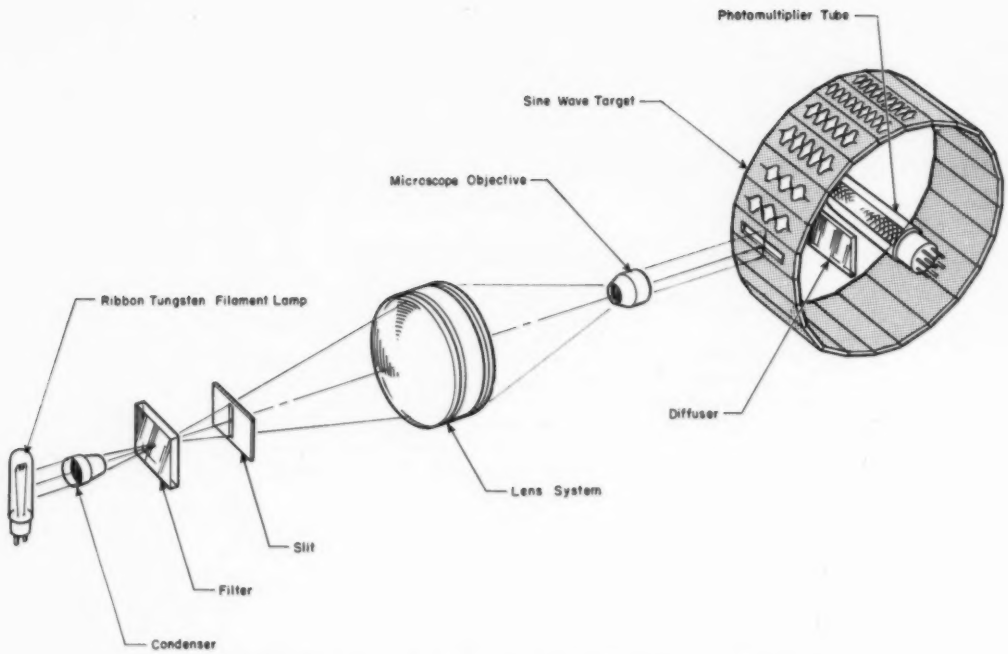

Fig. 1. Schematic diagram of the transfer function measurement apparatus.

may have an average transmission t_ω that varies from target to target or will have a modulation k_ω which is not the same for targets at different frequencies. In this event the result is

$$\mathrm{Re}(\omega) = \frac{1}{k_\omega}\left[\frac{C^*\dfrac{t_0}{t_\omega} - A^*}{A^*}\right],$$
$$\mathrm{Im}\,(\omega) = \frac{1}{k_\omega}\left[\frac{S^*\dfrac{t_0}{t_\omega} - A^*}{A^*}\right], \tag{6}$$

where A^*, C^*, and S^*, are experimentally determined quantities. Equations (6) may be used for precise data reduction when required.

From Eqs. (6) is it obvious that maximum accuracy will be obtained when $t_0 = t_\omega$ and $k_\omega = 1.0$. It is presumed that the sine and cosine targets are identical, only laterally shifted by one-fourth period. It now remains to describe a method of making these measurements.

Description of Apparatus

A stabilized tungsten ribbon filament lamp serves as a source (Fig. 1), the filtered light passing through a condenser system uniformly illuminates a fine slit. The slit then serves as a self-luminous incoherent object. The lens under test forms an image of the slit in the front focal plane of a microscope objective. The microscope objective then presents the image to sinusoidally varying masks of fixed spatial frequency and amplitude which are mounted in frequency pairs on a rotating drum. The image transmitted by the sinusoids is integrated by a 931-A RCA photomulitplier tube. The diffuser in front of the phototube uniformly illuminates the photo cathode elements. The output of the photomultiplier tube is then presented to a potentiometer pen recorder.

The area masks are arranged in frequency pairs, where one area mask is stepped 90° out of phase with the other. In this way ten spatial frequency pairs are arranged, all the peaks of the cosine area masks are in

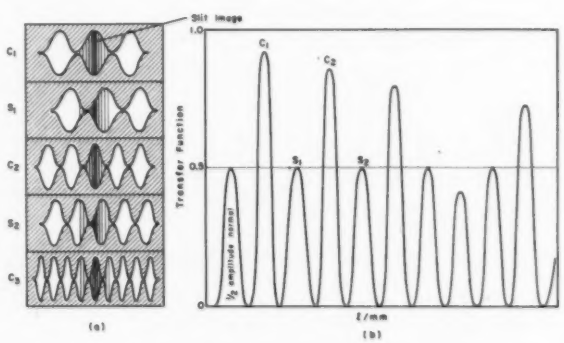

Fig. 2. (a) Cosinusoidal and sinusoidal area masks making up frequency pair. In actual use, each target passes the image separately. (b) Peaks on the potentiometer recorder corresponding to each of the targets in (a).

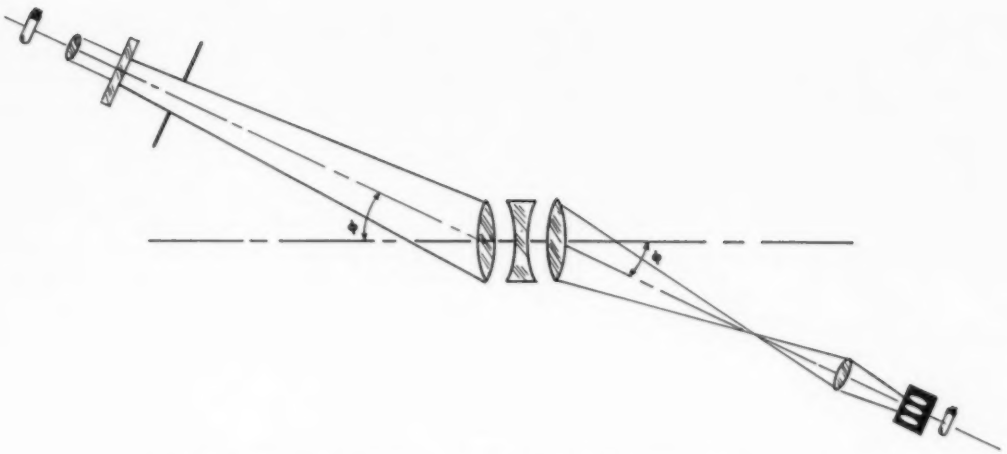

Fig. 3. Schematic diagram of an off-axis transfer function measurement.

line with one another on the drum, then automatically the area masks representing the sine component would be in line. Thus when a slit image is presented to the area masks and its transmission measured and recorded, the peaks on the chart recording would then represent the real and imaginary parts of the transfer function for each spatial frequency available on the drum.

For an image which shows no phase shift effect, all the peaks on the chart recording corresponding to the transmission of the sinusoids (imaginary part) will be equal to each other and equal to the half amplitude zero spatial frequency area mask which in turn is equal to the average transmission of the area masks. These peaks represent the baseline for the measurement, and is the self-normalization constant for the measurement. The half-amplitude normalization target has an area transmittance equal to the average chart transmittance but is a zero frequency target, and is illustrated in Fig. 1 as the first target on the drum. Thus at some frequency, when the image suffers a shift in phase a peak appears below the normalization curve; this phenomenon, most common when the system suffers from defect of focus, is called "spurious resolution." This is illustrated in the fourth pair of cosine and sine targets on Fig. 2. A curve connecting all the maxima of the cosines is then the real part of the transfer function of the system relative to the half-amplitude or average transmittance. A curve connecting all the sine terms is a plot of the imaginary part vs frequency.

The drum carries ten frequency pairs, ranging from 0.201 lines/mm for the lowest to 8.20 lines/mm for the highest frequency. The apparatus is equipped with three microscope objectives which magnify the frequencies such that it is possible to obtain a range from 1.79 lines/mm to 730 lines/mm. The drum rotates at two speeds. At the high speed the transfer function can be seen on an oscilloscope where rapid adjustments can be made for proper position and normalization. When the drum is switched to low speed, which is approximately 1 rpm, a permanent record can be made on the recorder. Thus it can be seen that after proper normalization, it takes only minutes to record directly the transfer function of an optical system. For an experienced operator a complete characteristic can be measured for a lens system for at least twenty positions through focus in one-half hour.

The sine wave bench essentially consists of three basic elements, the source and slit, lens mount, and sine wave target assembly all mounted on sliding carriages. It is thus possible to make off-axis measurements as illustrated in Fig. 3, with the reference focal position determined by mechanical cross slides on the carriages. Also, it is possible to measure systems in cascade where the net transfer function thus measured is the product of the transfer functions of the individual systems. The system illustrated here is that of a lens alone, but measurements can be made for systems using various focusing screens, such as diffuser plates and fiber bundle face plates. Figure 4 is a plot of the transfer function vs normalized spatial frequency for a Tessar

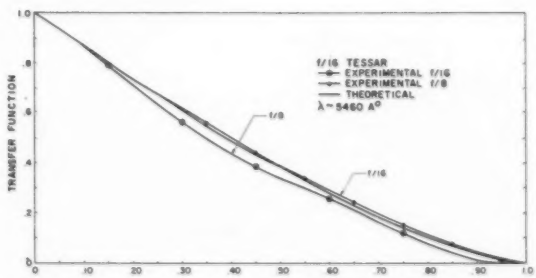

Fig. 4. Transfer function vs normalized spatial frequency of a Tessar lens system stopped down to $f/8$ and $f/16$.

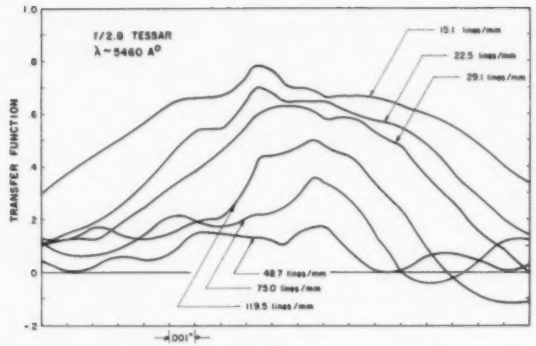

Fig. 5. Transfer function vs focal setting of a Tessar lens stopped to $f/2.8$.

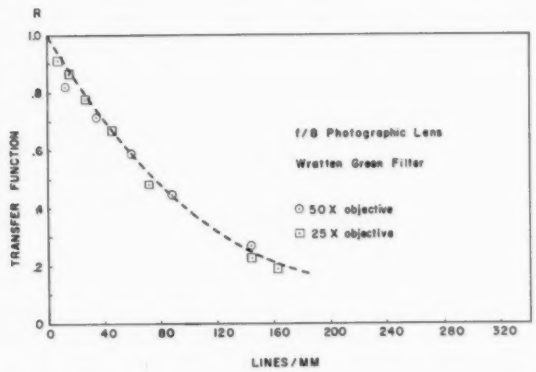

Fig. 6. Transfer function vs spatial frequency of a simple lens stopped to $f/8$. Scanning is accomplished with a 50× objective and a 25× objective.

lens stopped down to $f/8$ and $f/16$ at best visual focus. Figure 5 is a plot of the transfer function through focus of Tessar lens stopped to $f/2.8$. Figure 6 is a plot of an $f/8$ lens vs normalized spatial frequency at best visual focus. In Fig. 6 the range of frequencies is illustrated when scanning is accomplished with two different microscope objectives.

Phase-Shift Discussion

By this method it is also possible to obtain information on the phase shift of the image. This can be computed from the same chart recording for those spatial frequencies available to the instrument.

Figures 7(a) and (b) show two recordings of a Tessar lens ($f/8$) at the same focal setting. In Fig. 7(a) the image is presented to the maxima of the cosinusoidal masks (ideal position) and in (b) the image was shifted laterally from the maxima position. The phase shift (ϕ) is then

$$\phi = \tan^{-1} \frac{l}{R}$$

and can be computed directly from the chart recordings of Fig. 7(a) and (b). A phase shift of constant slope is measured when the image is deliberately shifted from its ideal position; however, the transfer function remains fixed.

Since the chart recording can only be read to an accuracy of 1% the phase shift of the lowest frequency can only be determined to within ±3.0°, while that of the higher frequencies, 142 lines/mm, is ±11.0°. To this must be added the accuracy to which the target themselves are aligned. However, as seen in Fig. 7(c) the phase shift can accurately be determined for small amounts of lateral shift of the image.

Comments

The heart of this apparatus is the cosinusoidal and sinusoidal area masks. Difficulties encountered in building the apparatus included the production of area masks of precisely equal transmission and the subsequent alignment of the masks on the drum.

Making area masks of high quality proved to be the most difficult task in accomplishing this method. In order to do this, sine curves were carefully plotted and inked on large cardboard plates. The plates were then reduced by photographic means to a transparency where the sine curves were clear and the background opaque. The transparencies were then further reduced to the desired size on a fine grain photographic film and

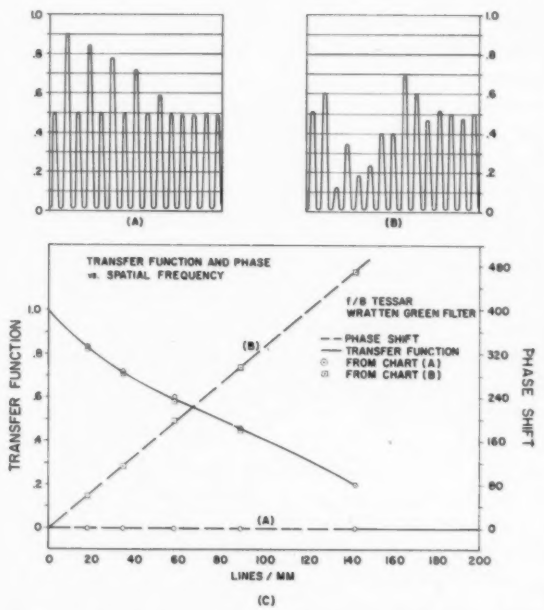

Fig. 7. (a) Chart recording of ideal position of the slit image. (b) Chart recording when the slit image is shifted laterally from its ideal position. (c) Transfer function and phase shift vs spatial frequency of a Tessar lens stopped to $f/8.0$ as taken from chart recording (a) and chart recording (b).

developed by a reversal process. Thus, flare usually troublesome from large white areas was kept down to a minimum.

All the frequency pairs were made in this way. The transmission of each chart was measured on a microdensitometer. Difficulty was encountered in achieving uniform transmission coefficients for all transparencies. It took many trials finally to obtain a set of area masks of desired quality. Still, the apparatus is not entirely free from error. Although frequencies up to 730 lines/mm are available on this instrument, we have found that reliability is good at present only to 322 lines/mm.

Figures 8 and 9 are photographs of the sine wave bench and drum carrying the sinusoidal and cosinusoidal area masks. As can be seen, the modular construction of the scanning equipment permits ready modification to other types of scanning, such as energy distribution and knife-edge scanning.

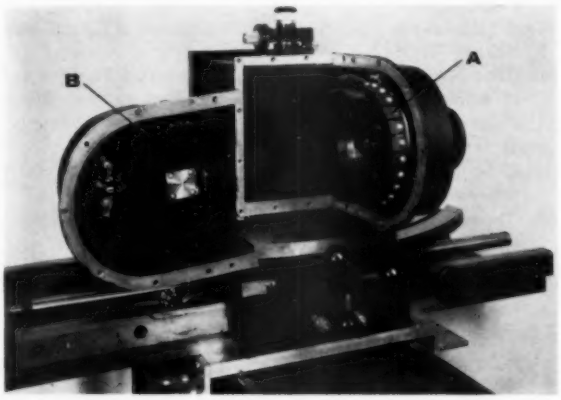

Fig. 8. Photograph of the transfer function measurement apparatus. A. Drum carrying targets; B. photomultiplier tube.

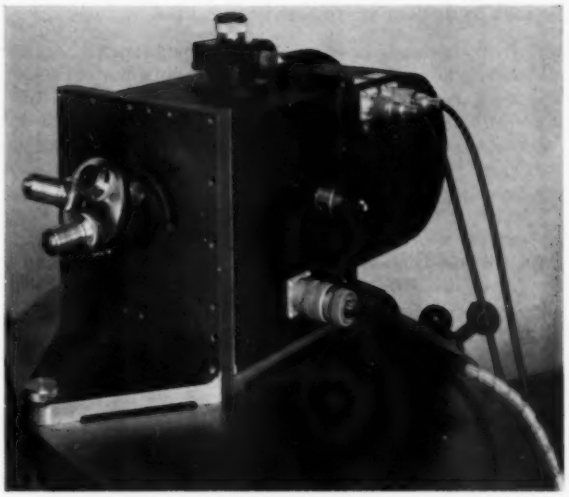

Fig. 9. Front view of the transfer function measurement apparatus.

We are greatly indebted to W. Drumm, R. van Ligten, G. C. Harvey, R. Charpentier, and R. Barakat for their help and continued encouragement.

References

1. P. Lindberg, Opt. Acta **1**, 80 (1954).
2. E. Ingelstam, E. Djurle, and B. Sjögren, J. Opt. Soc. Am. **46**, 707 (1955).
3. R. L. Lamberts, J. Opt. Soc. Am. **48**, 490 (1958).
4. D. R. Herriott, J. Opt. Soc. Am. **48**, 968 (1958).

R. R. Shannon *Itek*, R. J. Potter *IBM*, R. Pole *IBM* and friend during the OSA Rochester Meeting.

F. Dow Smith *Itek*, R. E. Hopkins *Rochester*, and E. Snitzer *American Optical* on one of the tours arranged during the ICO Munich Meeting last year. Dr. Smith is feature editor for this April issue on Image Evaluation.

Papers to appear in subsequent issues

We have had so many papers submitted for publication during the past eighteen months that we have already built up a backlog which is as embarrassing for a new publication as it is a demonstration of the need for this journal. We have done our best to publish papers as quickly as we can by bringing out bigger issues than had originally been intended last year, **becoming a monthly in 1963** and by occasionally dropping some of the "filler" departments. The Editors wish to express their sincere appreciation to all contributors who have thus demonstrated their faith in *Applied Optics*.

Overhauser and Jeffries-Abragam Effect in a Four-Level System—*Narchal and Barker*

Spurious Harmonic Generation in Optical Heterodyning—*Cummins, Knable, and Yeh*

Interferometric Measurement of Vibration Amplitudes—*Bowie*

International Length Standard—*Baird and Howlett*

Infrared Transmission through the Atmosphere—*Green and Griggs*

Practical Aspects of Aerial Photographic Targets—*Rosenau*

Infrared Transmission through Fogged Salt Windows—*Morrow and Turk*

Method of Inferring Single-Path Band Transmission Factors from Double-Path Measurements—*McKiernan and Wessely*

Total Absorptance of Water Vapor in the Near Infrared—*Burch et al.*

A Simple Grating Calibrator for the Visible and Vacuum Ultraviolet—*Hammer, Arakawa, and Birkhoff*

Photorefractometer II. Measurement of N and K—*Kapany and Pontarelli*

Lighting Parameters and Generalized Characteristics of Xenon Lamps—*Marshak*

Design of Superachromatic Lenses—*Herzberger and McClure*

Reflection and Transmission of Infrared Materials—*McCarthy*

The Use of Polarized Infrared Radiation in Magneto-optical Studies of Semiconductors—*Palik*

A Multicolor Photoelectric Photometer for Artificial Satellite Observations—*Moore and Elliott*

An 8–14 μ IR Astronomical Photometer—*Westphal and Murray*

An Optical Null Double-Beam Double-Pass IR Spectrophotometer—*Minami*

A Photomultiplier Circuit for Precision Spectrophotometry—*Budde*

Large-Scale Photoelectric Planimeter for Leaves—*Carman*

Spectral Band Absorptance for Atmospheric Slant Paths—*Plass*

A New Method for High-Speed Motion Picture Photography of Transparent Drops—*Pfeiffer*

Photometric Accuracy of Infrared Spectrophotometers—*Stewart*

Absorption by Ozone in the 4.75-μ Region of the Solar Spectrum—*McCaa and Shaw*

The 15–26 μ Sky Emission Spectrum at Jungfraujoch (3570 m)—*Bolle*

Infrared Dispersion of Some Oxide Glasses—*Malitson et al.*

Study of the Fabrication of Aspherical Surface—*Sakurai and Shishido*

Transmission of Isotropic Radiation Across An Interface Between Two Dielectrics—*Stern*

Electric Chopper for Spectral Lamps—*Mackey and Pollack*

Helium Continuum Light Source for Photoelectric Scanning in the 600–1100 Å Region—*Huffman, Tanaka, and Larabee*

Asymmetry of an Integrating Sphere—*Olson and Pontarelli*

Isosceles Total Internal Reflectors as Optical Elements—*Rothstein*

Direct Recording of Integrated Band Intensities from a Linear Wavelength Spectrometer—*Schurin, Williamson, and Clough*

Jet Controlled Arc I—Excitation of Second Spectra—*Thygesen and Moore*

Men and Milestones in Optics II—Thomas Young—*Barr*

Test of Theoretical Absorption Band Model Approximations—*Burch and Williams*

Interferometric Method of Velocity of Light Measurements—*Stroke*

Brighter Spectrographic Images by the Use of Anamorphic Optics—*Eisner*

Optics in Norway—*Hisdal and Omholt*

Mesure de la Dispersion dans les Rais d'Absorption Infrarouge des gaz. Appareillage et Corrections Instrumentales—*Alamichel, Assous, and Legay*

Dichroic Multiple-Beam Interferometer Microscope—*Irland and Schermer*

Quantum Limit to Precision of Wavelength Determination—*Hanes*

Improved Silver Films for Multiple-Beam Interferometry—*Bradley*

Rapid Measurement of Photographic Records of Interference Fringes—*Dyson*

Empirical Methods for Computing the Integrated Absorptances of Infrared Bands of Atmospheric Gases at Nonuniform Pressures—*Shaw*

Interference Comparators for Line Standards—*Baird*

Use of an Analog Computer in Side-on Arc Spectroscopy—*Shumaker and Yokley*

An Analysis of Radiation Transfer by Means of Elliptical Cylinder Reflectors—*Schuldt and Aagard*

The Evaporation Rate of Filament Material from Alternating Current Heated Filaments—*A. D. Wilson*

On the Correction Phase Errors in Interferograms—*Loewenstein*

A New Condenser for a Sun-Powered Continuous Laser—*Keck Redmann, White, and DeKinder*

Performance of a cw Neodymium Laser—*Keck et al.*

Attenuation by Ozone and the Earth's Albedo in the Middle Ultraviolet—*Green*

Tilted Plate Interferometry with Large Plate Separations—*Moos et al.*

Double Monochromator System—*Christensen and Potter*

Experiments with the Optical Excitation of Mercury Vapor for the Production of Isolated Fluorescence—*Zito and Schraeder*

Application of the Senarmont Polariscope to Analysis of Optical Light—*Hellerstein*

Observation of Ionization of Gases by a Ruby Laser—*Damon and Tomlinson*

Hole Burning Model of Oscillation of Ruby Laser—*DeMaria and Gagosz*

Angular Distribution of Light Rays from a Gas Discharge Source—*Aagard, Dufault, and Schuldt*

An Alignment Interferometer—*Saunders*

Electro-Optic Light Modulation with Cubic Crystals—*Buhrer, Bloom, and Baird*

Observations of Near Infrared Radiation from the Solar Atmosphere—*Taylor and MacQueen*

Simple Method for Photographic Photometry—*MacAdam and Altman*

Irradiance on a Flat Object Underwater—*Tyler and Shaules*

The Detectivity of Cryogenic Bolometers—*Low and Hoffman*

Kirchhoff Diffraction Pattern Calculations—*Moore*

Electro-Optic Effect of Gallium Arsenide—*Ho and Buhrer*

A New Type of Shearing Interferometer for the Measurement of Transfer Functions of the Microscope Objective

Tadao Tsuruta

A shearing interferometer using polarized light has been devised for the measurement of transfer functions of microscope objectives. In this device, a birefringent system of calcite is employed for obtaining the variable amounts of shear of the aperture. The interferometer is easy to adjust and permits relative lateral shear up to $s = 2$ corresponding to the resolution limit of a perfect lens, with a great amount of light available in the measurement. Experiments were carried out on an aberration-free 4.3-mm objective, with a numerical aperture of 0.60 under partially coherent illumination, and on an objective having primary spherical aberration of 1.0 λ under incoherent illumination. The experimental results showed fairly good agreement with those of calculation.

Fourier analysis treatment of an optical system[1,2] has been successful in evaluating image-formation properties of lenses under partially coherent illumination. Menzel[3] showed that the optical transfer function can be defined with respect to the illumination alone when the object structure causes only small changes in the phase and amplitude of the transmitted light. (The device to be described carries out a measurement of the transfer function for this case.) The function has great effects on the image properties in the microscope under partially coherent illumination. In spite of the fact that the measurement of transfer functions is expected to provide useful data even in designing, testing, and evaluating of microscope objectives, studies have not been conducted on the microscope. The main reason is that the direct measurement of transfer functions of microscope objectives has hitherto been prevented due to difficulties inherent in the interferometric method proposed by Hopkins[4] as well as in the direct scanning made on the intensity distribution of a point image. The interferometric method has the considerable advantage of high photometric efficiency over the direct scanning one. However, the former requires more delicate adjustment, and its photometric efficiency decreases as the line frequency approaches the resolution limit of the objective.

To overcome these disadvantages, the author of the present article has devised an interferometer using polarized light, in which a birefringent lens of calcite is used to give a continuous lateral shear of the aperture of the test lens.

Experiments were carried out on an aberration-free 4.3-mm objective with a numerical aperture (N.A.) of 0.60 under incoherent and partially coherent illumination, and on the same type of a lens having primary spherical aberration of amount 1.0 λ under incoherent illumination.

Optical Transfer Function

When the object is self-luminous or incoherently illuminated, the lens is considered as a linear filter in regard to the intensity, and the relation between the inverse Fourier transform of the object $i_o(s, t)$ and that of the image $i(s, t)$ is given by

$$i(s, t) = r(s, t) i_o(s, t), \tag{1}$$

where the normalized transfer function $r(s, t)$ is the inverse Fourier transform of the intensity distribution in the image of a point source, and where (s, t) are the normalized spatial frequencies defined by

$$\begin{aligned} s &= \lambda R_x / n \sin\alpha & t &= \lambda R_y / n \sin\alpha \\ &= \lambda R_x' / n' \sin\alpha', & &= \lambda R_y' / n' \sin\alpha'. \end{aligned} \tag{2}$$

Here, n is a refractive index; (R_x, R_y) denote the corresponding number of lines per unit length on the object plane; and α is the angular inclination to the axis of rays from the margin of the pupil of the lens. The primes denote the corresponding quantities in the image plane. Equation (1) is not, however, valid in the strict sense if the object is under partially coherent illumination.

The author is with Nippon Kogaku K.K. (Japan Optical Industry Company Ltd.), Shinagawa-ku, Tokyo, Japan.

Received 26 October 1962.

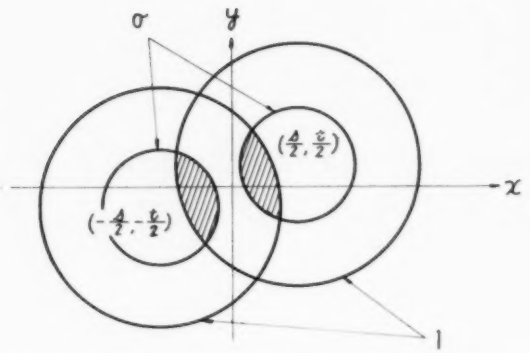

Fig. 1. Region of integration of $A(s, t)$ and $B(s, t)$ for the frequency pair (s, t).

Residual aberrations of a microscope objective are so well corrected that the Strehl intensity ratio attains a value as high as 0.8, equivalent to the Rayleigh limit of $\lambda/4$. Therefore, microscope objectives have a significant value of response for all the spatial frequencies up to the resolution limit of a perfect lens. The interval of the neighboring lines on the object space corresponding to the finer part of line frequencies becomes comparable with the coherence patch due to the illumination from behind. Thus, we must take into account the illumination condition for treating the image properties of microscope objectives.

Menzel showed that transfer functions on the amplitude and phase could be defined as well for a partially coherent object of low contrast. Following Maréchal and Françon,[5] we assume

$$D(u, v) = 1 + D'(u, v), \qquad D'(u, v) \ll 1, \tag{3}$$

where $D\ (u, v)$ is the amplitude distribution of the object, and (u, v) are normalized coordinates on the object plane. Then the transform of the image function $i\ (s, t)$ is given by

$$i(s, t) = A(s, t)[\delta(s, t) + d'(s, t) + d'^*(-s, -t)] + B(s, t)[d'(s, t) - d'^*(-s, -t)]/2, \tag{4}$$

where $d'\ (s, t)$ is the inverse Fourier transform of $D'\ (u, v)$, * denotes the complex conjugate, and $\delta\ (s, t)$ is the Dirac delta function. $A\ (s, t)$ and $B\ (s, t)$ are

$$A(s, t) = \int_{S_o} [\epsilon(x - s/2, y - t/2) + \epsilon(x + s/2, y + t/2)] \times F(x + s/2, y + t/2)F^*(x - s/2, y - t/2)dxdy, \tag{5}$$

$$B(s, t) = \int_{S_o} [\epsilon(x - s/2, y - t/2) - \epsilon(x + s/s, y + t/2)] \times F(x + s/2, y + t/2)F^*(x - s/2, y - t/2)dxdy,$$

where $F\ (x, y)$ is the pupil function being not zero inside the circle $x^2 + y^2 = 1$, and where $\epsilon\ (x, y)$ is the intensity in an effective source. For a microscope using transillumination through a condenser, which is bounded by a radius having a numerical aperture σ times that of the objective, $\epsilon\ (x, y) = 1$ is obtained inside the circle $x^2 + y^2 = \sigma^2$, and zero on the outside. Then the region S_o over which the integration has to extend is the shaded area shown in Fig. 1.

By separating $D'\ (u, v)$ into real and imaginary parts, the following relations are obtained:

$$\begin{aligned} D'(u, v) &= a(u, v) + ib(u, v) \\ 1 + D'(u, v) + D'^*(u, v) &= 1 + 2a(u, v) \\ D'(u, v) - D'^*(u, v) &= 2ib(u, v). \end{aligned} \tag{6}$$

This implies that $A\ (s, t)$ and $B\ (s, t)$ are the filtering coefficients as to the amplitude and phase, respectively. For characterizing the image formation properties of an ordinary microscope objective, except the one for the phase contrast method, it would be reasonable to suppose that the phase variations on the specimen tend to zero. Hence, the second term in Eq. (4) vanishes, and the lens can be regarded as a linear filter as to the intensity. In the case of $\sigma \gtrsim 1$, the two integrands coincide, and $A\ (s, t)$ agrees with the transfer function in the case of a self-luminous object. $B\ (s, t)$ is a transfer function if small changes of phase are converted into those of intensity and will play an important role in the discussion of phase contrast objectives. $B\ (s, t)$ is defined and named the phase contrast function according to Menzel.

Adoption of a shearing interferometer was originally proposed by Hopkins for the measurement of transfer functions of lenses. Baker[6] constructed an interferometer of this kind and used it to measure the influence of defects of the focus on the response of an aberration-free lens. Kelsall[7] succeeded in the measurement of lenses having several amounts of spherical aberration.

An interference pattern occurs in the region of overlap of two separate apertures which are laterally sheared with respect to each other. By assuming the path difference between the two beams to be δ, the intensity at some elementary area in the interference pattern is given, apart from a constant factor by

$$|F(x + s/2, y + t/2) + F(x - s/2, y - t/2) \exp(ik\delta)|^2. \tag{7}$$

The total light flux $B\ (\delta)$ in the region where interference takes place is given, apart from a constant factor, by

$$B(\delta) = \int_{so} |F(x + s/2, y + t/2) + F(x - s/2, y - t/2) \exp(ik\delta)|^2 dxdy = 1 + |A(s, t)| \cos(\delta - \beta), \tag{8}$$

where β is the argument of the transfer function and S_o the region of integration which is shaded in Fig. 1. By changing the path difference δ, a variation in the

total light flux in the interference pattern is produced, whose amplitude gives the modulus of the transfer function of the test lens.

Birefringent System

Lateral Shear of the Aperture

The method for obtaining lateral shear of an aperture may be divided into two classes. The principle of the first type is as follows: An aberrant beam to be tested is separated by a beam splitter into two indentical beams, which are reflected back along their incident directions by the two right-angle mirror systems, one of them being laterally displaced to produce the corresponding amount of shear without tilt. Most of the interferometers developed for the measurement of transfer functions of lenses are included in this class.

The second type is essentially a method using interference of polarized light with a double-image system as the shearing element. The principle is as follows: A birefringent double-image prism, such as a Wollaston prism, which is located on the focus of a converging beam, makes a fixed amount of an angle of duplication between ordinary and extraordinary beams, thus producing an interference pattern of laterally sheared aperture by placing it between polarizers. In this case we can obtain only a fixed amount of shear determined by the birefringence of the material and the geometry of the prism. Lohmann[8] proposed interferometers of this type for the measurement of the transfer functions at a fixed spatial frequency. Because the optical path difference is produced by the retardation in the solid birefringent prism, an interferometer of this class is sufficiently rigid and stable against shock and vibration in comparison with the first type.

The author employed a birefringent system of calcite to obtain various amounts of shear. It consists of a plano-convex lens and a plano-concave one, cut parallel to the optic axis and cemented together with the axes crossing at a right angle. In short, the cemented plane surface of a Wollaston prism is replaced by a spherical one. This birefringent system will hereafter be called a Wollaston lens. This is actually the same system as that employed by Girard[9] in the study of spectrometers of high luminosity. It is placed on the focus of the converging beam between crossing polarizers with the optic axis of calcite at 45° to the plane of polarization. By localizing the interference fringes in the exit pupil of the converging beam—the back focal plane of a test objective in a case of a microscope—one obtains a sheared interferogram on the exit pupil. A desired amount of shear of the aperture is obtained by the displacement of the Wollaston lens normal to the incident beam. The reason stems from the fact that the angle of duplication is changeable according to the vertex of the prism determined by the position through which the beam passes. The angle of duplication is given by $2(n_o - n_e)q/a$, where a is the radius of curvature of the cemented surface; q, the distance of the point concerned from the axis of the Wollaston lens; and n_o, n_e, ordinary and extraordinary indices. Therefore, the magnitude of shear of the aperture varies as the Wollaston lens is driven across the converging beam.

Phase Compensation

With the optical system shown in Fig. 2, we can obtain a much greater amount of light than with the one described above. The system is symmetric about the object plane of two identical lenses R and T. The Wollaston lenses B_1 and B_2 are also considered to be identical and placed at a right angle to each other; that is, the axis of the convex lens is parallel to that of the concave lens of the other. The system is placed between crossing polarizers. If the image of B_1 on B_2 is perfectly similar in size to B_2, the retardation introduced by B_2 is fully compensated by that of B_1 over the whole area of B_2. Then a uniform field can be seen on B_2. If the displacement of the image of B_1 with respect to B_2 is introduced, the path difference on a different position of B_2 changes and causes interference fringes localized on B_2. For decreasing the number of interference fringes, a centering adjustment of R is adopted. The adjustment is made by replacing S by a circular aperture which is large enough and by finding the position where the uniform field localized on B_2 can be observed. The decrease in the visibility can be neglected if the image of a pinhole source on B_2 is small as compared to the interval of the interference fringes.

When light once passes through the Wollaston lens, the visibility is given by $\sin k\theta R/k\theta R$, where θ is one-half of an angle of duplication, the maximum value of θ being equal to the angular inclination of a converging beam. This shows that the visibility decreases as the amount of shear increases. Let α' of a microscope objective in the image space be 0.016, then the radius of a pinhole aperture equal to 5 μ can be used, which results in a value of the visibility of 0.80 at the maxi-

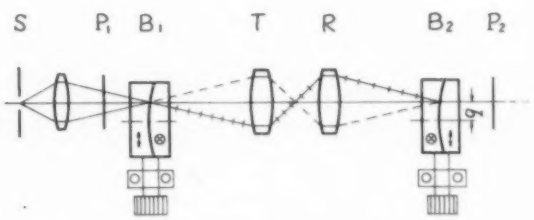

Fig. 2. Phase compensation arrangement. B_1 and B_2—identical Wollaston lenses; T and R—identical lenses; P_1 and P_2—crossing polarizers; S—point source.

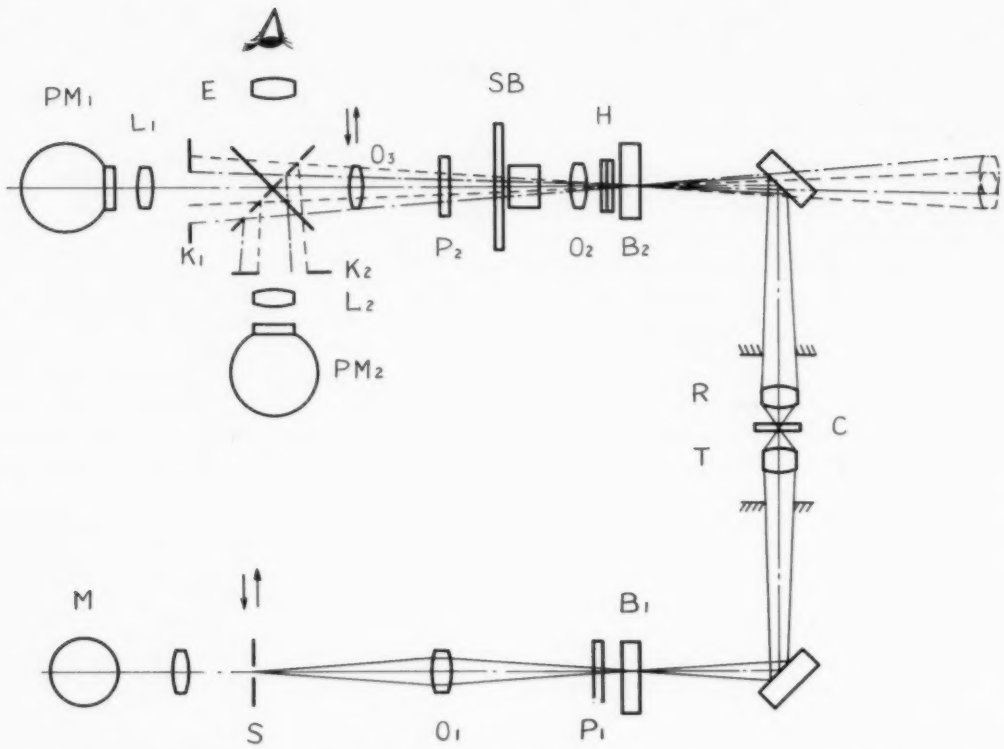

Fig. 3. Schematic diagram of the apparatus for measuring transfer functions of microscope objectives. M—high-pressure mercury lamp; O_1, O_2, and O_3—lenses; B_1 and B_2—identical Wollaston lenses; T—test lens; R—reference lens; C—coverglass of 0.34-mm thickness; P_1 and P_2—crossing polarizers; H—half-wave plate; SB—Soleil-Babinet's compensator; E—eyepiece; K_1 and K_2—aperture diaphragms corresponding to effective source; L_1 and L_2—light collectors; PM_1 and PM_2—photomultipliers.

mum angle of duplication corresponding to the line frequency of the limit of resolution of a perfect lens.

If a pinhole source of 0.1-mm rad is employed in the phase compensation apparatus, the gain of the light flux to be measured becomes as large as 400 times that of the single-passage method.

Angular Aperture Available

It is well known that the Wollaston prism traversed by a converging beam does not give a uniform field but isochromatic lines of equilateral hyperbolas at infinity. The ordinary beam given by the first prism becomes extraordinary in the second prism, thus showing some astigmatism. The extraordinary beam, by becoming ordinary in the second prism, has its astigmatism unchanged. Finally the ordinary and extraordinary beams suffer the same amount of astigmatism oriented at 90° after each other. The resultant wave-front aberration ϕ (r, φ) between the two beams is given by

$$\phi(r, \varphi) = \frac{n_o^2 - n_e^2}{2n_o^2 n_e} \alpha'^2 r^2 d \cos 2\varphi, \qquad (9)$$

where (r, φ) are the normalized polar coordinates on the aperture of the beam, and d is the common thickness of the prism. A vertex of the prism does not appear in Eq. (9), so that it is valid for any radial point of the Wollaston lens, if the thickness difference of the approximate prisms under consideration is neglected.

By imposing the condition that the wave-front aberration caused by the Wollaston lens does not exceed one-eighth of the wavelength (546 mμ) on the

Fig. 4. Photograph of the apparatus.

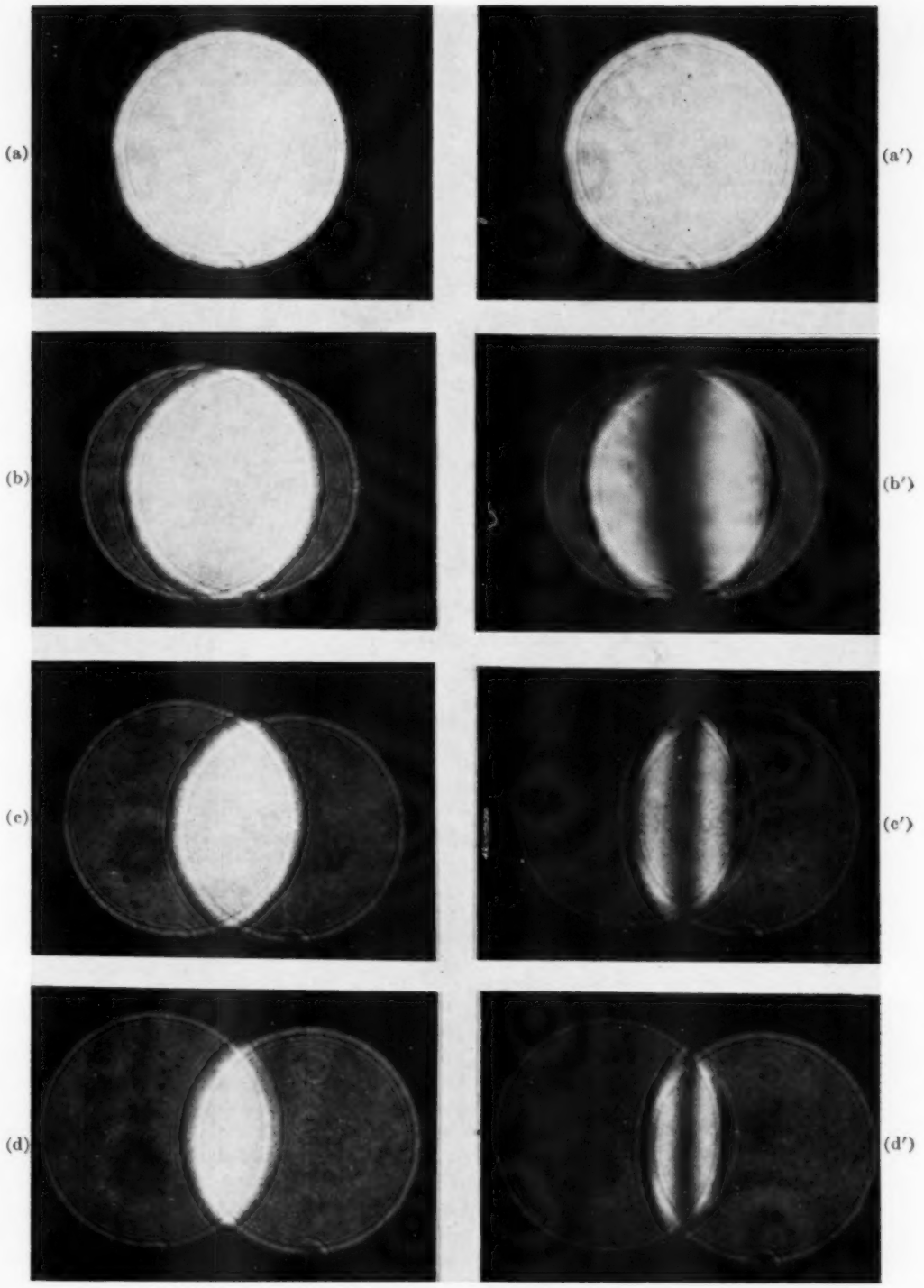

Fig. 5. Sheared interferograms of aberration-free wavefront on a diffraction focus: for (a) $s = 0$, (b) $s = 0.5$, (c) $s = 1.0$, (d) $s = 1.5$, where s is the distance between the centers of sheared circles. Primes denote the corresponding quantities on the defocused-image plane.

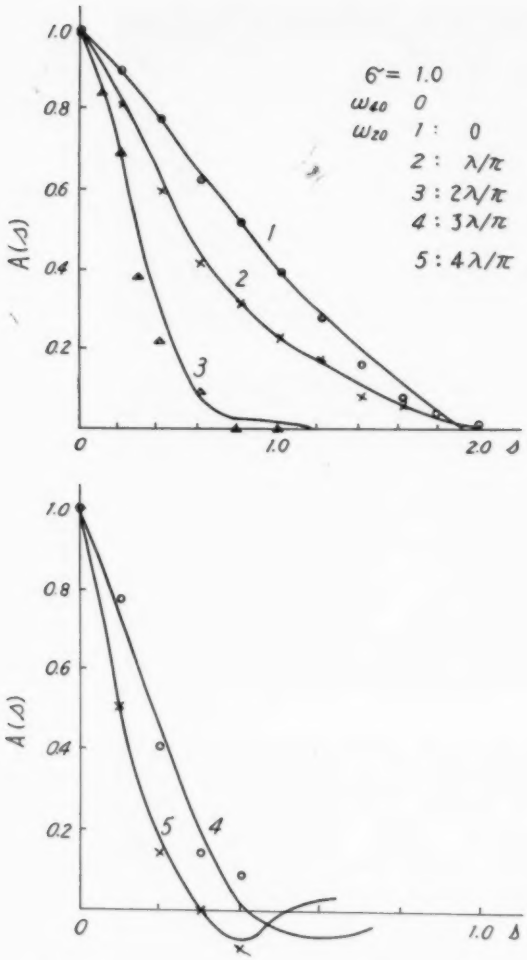

Fig. 6. Transfer functions under incoherent illumination, for a defocused lens without aberration.

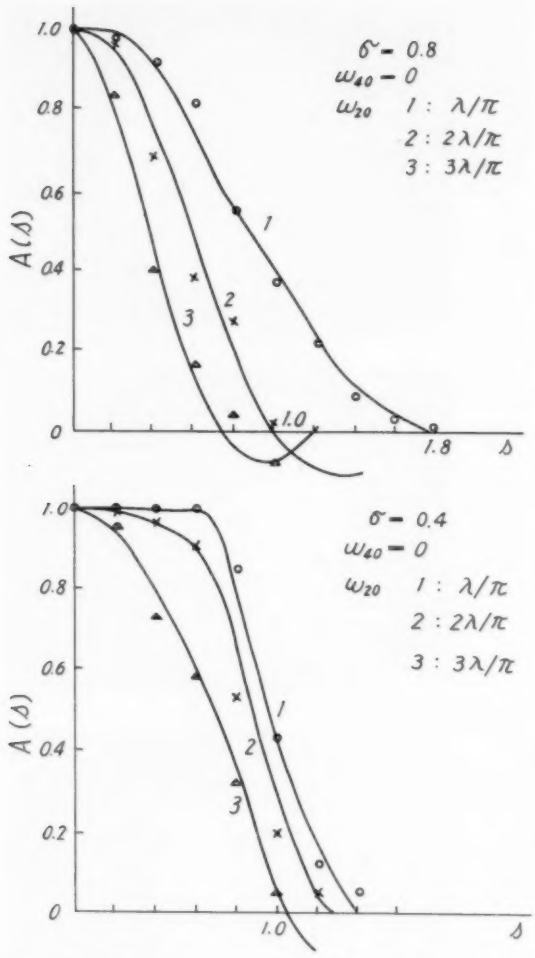

Fig. 7. Transfer functions under partially coherent illumination for a defocused lens without aberration: calculated, o,x,Δ: experimental point.

aperture, the limit of an angular aperture available is given by Eq. (10), with the compensating method taken into account,

$$\alpha' < 2.28 \times 10^{-2}/d^{1/2}. \tag{10}$$

For the Wollaston lens of 4-mm thickness ($d = 2$ mm) of calcite as used in the apparatus

$$\alpha' < 1.62 \times 10^{-2}. \tag{11}$$

For ordinarily used objectives such as 40 X; 0.65 N.A., 60 X; 0.80 N.A., and 100 X; 1.25 N.A., the angular inclination α' in the image space satisfies Eq. (11).

Details of Experiments

The schematic diagram and photograph of the apparatus are shown in Fig. 3 and Fig. 4, respectively. As the device is worked out by the phase-compensating method, the arrangement of P_1, P_2, B_1, B_2, T, and R is the same as that described in the previous section. M is a high-pressure mercury-discharge lamp from a stable 100 V ac power supply, with a filter to isolate 546 mμ line. M is focused on the source pinhole S, whose image S_1 is produced on the Wollaston lens B_1 by the objective O_1. The radius of S_1 is taken to be 0.1 mm. The Wollaston lens used in the apparatus has 10-mm rad, 4-mm thickness, and 70-mm rad of curvature of the cemented surface. Then, an angle of duplication up to 2°40′ is obtained, which is generally sufficient for the measurement of microscope objectives. B_1 and B_2 are placed 150 mm from the bottoms of the objective threads of T and R. This length corresponds to the tube length of the microscope. The test lens T and the reference lens R are the same in focal length and numerical aperture. R is so designed and assembled as to

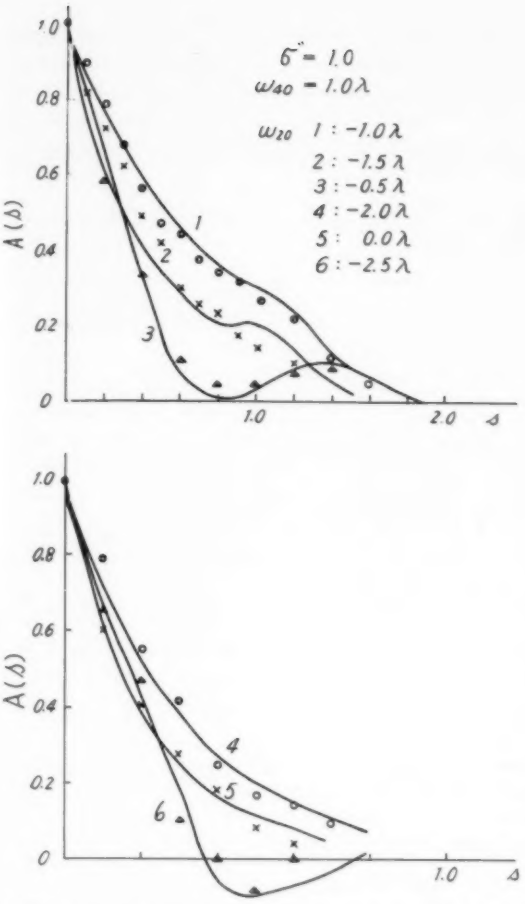

Fig. 8. Transfer functions under incoherent illumination in the presence of primary spherical aberration 1.0 λ in different focal planes.

produce a nearly aberration-free image on the axis. R has been tested by a Twyman-Green lens interferometer.

A parallel glass C of 0.34-mm thickness is inserted between R and T, to compensate the influence of the cover glass, for testing dry objectives. To measure transfer functions of different azimuth, P_1, B_1, and B_2 are rotated to the corresponding angle. A half-wave plate H placed behind B_2 is then rotated to one-half of an angle of their revolution, by leaving the planes of polarization in the analyzer P_2 to the same. A Soleil-Babinet's compensator SB is placed in front of P_2 at an angle of 45° with respect to P_2. It changes the path difference between the two polarized beams by means of lateral traverse of one of the quartz plates of the compensator. The modulus of the transfer function is therefore given by the variation of the total light flux expressed in Eq. (8), as δ is changed by the compensator.

The objective O_2 produces an image of the sheared interferogram on the focus of the eyepiece E, with a 45° mirror inserted in front of it. In the measurement, the beam is divided into two identical ones by a half mirror. They come to the foci at the apertures K_1 and K_2, respectively. An interchangeable mask on K_1 equivalent in size to the effective source is mounted on a carriage which is driven by a rotating screw. The mask on K_1 is moved to the position where its center coincides with that of the sheared image of the aperture. The same mechanism is applied to the other aperture K_2, which corresponds to the other region of integration as shown in Fig. 1.

Light is received by two identical photomultipliers through condenser lenses behind K_1 and K_2, respectively. In the case of incoherent illumination, a single photomultiplier is sufficient for the measurement, because the two shaded regions of integration overlap each other as shown in Fig. 1. Normalization of the sensibility is performed by making the two outputs equal when $s = 0$. The outputs are then added and fed to the ac amplifier tuned with 380 cps, the chopping frequency of light which is supplied into the interferometer. The interferometer is constructed on a rigid plate which is supported on a vibration-free mounting.

Results

The two aberration-free objectives 4.3 mm in focal length and 0.60 in N.A. are employed as the reference and test lenses, respectively. Primary spherical aberration corresponding to wave-front aberration of 1.0 λ at the margin of the beam of the Gaussian focus is produced by replacing C by a plane-parallel glass 0.44 mm in thickness. Figure 5 shows interference patterns of an aberration-free objective. Because the rotational symmetry was being considered, we treated only the case of a line structure with the direction parallel to the x-axis leaving t at zero.

Transfer functions of an aberration-free objective for several different planes of focus under illumination conditions of $\sigma = 1.0$, 0.8, and 0.4 were obtained. They are shown in Figs. 6 and 7. Those suffering from spherical aberration of 1.0 λ under incoherent illumination are shown in Fig. 8. The defects of the focus ω_{20} are found from the formula,

$$\omega_{20} = (\sin\alpha)^2\delta z/2, \tag{12}$$

where δz is the axial displacement of T with respect to R.

Experimental results were compared with those calculations made according to Hopkins,[10] Black and Linfoot,[11] and Goodbody.[12] A good agreement between calculated and measured values was found for all the spatial frequencies up to $s = 2.0$. The measurement of the argument of the transfer function which is not essential for the study of an axial image, is not dealt with in this paper.

Summary

A new type of shearing interferometer of polarized light is applied for the measurement of transfer functions of microscope objectives. Essential features of the interferometer are (1) the birefringent system of calcite, which gives variable amounts of shear of the aperture of the test lens and (2) the phase-compensating method, which supplies a great amount of light without decreasing the visibility of interference fringes.

Measurements were carried out on 4.3-mm objectives of 0.60 N.A. on the optical axis under incoherent and partially coherent illumination. The results showed fairly good agreement with those of calculation. This suggests that the interferometer of polarized light is useful for testing microscope objectives.

Another type of shearing interferometer for the measurement of transfer functions of photographic lenses will be reported at a later date. A shearing device employed in the interferometer is a modified Savart polariscope to obtain a continuous lateral shear of the aperture.

The author is indebted to Y. Fujino and S. Fujiwara of Japan Optical Industry Company Ltd. for their suggestions and encouragement throughout this work and to T. Asakura of the Insititute of Industrial Science, University of Tokyo, for advice in the preparation of this manuscript.

References

1. P. M. Duffieux, *L'Intégrale de Fourier et ses Applications à l'Optique* (Besancon, 1946).
2. H. H. Hopkins, Proc. Phys. Soc. (London) **A217,** 408 (1953).
3. E. Menzel, Optik **15,** 460 (1958).
4. H. H. Hopkins, Optica Acta **2,** 23 (1955).
5. A. Maréchal and M. Françon, *Diffraction: Structure des Images* (ed. Rev. optique, 1960).
6. L. R. Baker, Proc. Phys. Soc. (London) **B68,** 871 (1955).
7. D. Kelsall, Proc. Phys. Soc. (London) **73,** 465 (1959).
8. A. Lohmann, Optik **14,** 510 (1957).
9. A. Girard, Optica Acta **7,** 81 (1960).
10. H. H. Hopkins, Proc. Phys. Soc. (London) **A231,** 91 (1955).
11. G. Black and E. H. Linfoot, Proc. Roy. Soc. (London) **A239,** 522 (1957).
12. A. M. Goodbody, Proc. Phys. Soc. (London) **72,** 411 (1958).

Books *continued from page 364*

Physik und Technik der Ultrarotstrahlung. By WERNER BRÜGEL. Curt R. Vincentz Verlag, Hannover, 1961. 448 pp. DM 48.00.

This is a revised, enlarged second edition of the popular book by Brügel originally published two or three years ago. It is not intended primarily as a text (although it could surely be so used) but rather as an introductory reference volume for working physicists, engineers, and technicians who have no special background or training in infrared physics or spectroscopy. It is interesting to compare this volume with some of the other books on infrared now available to note some similarities and differences.

The chapter on methods of spectral dispersion is vaguely reminiscent of Sawyer's *Experimental Spectroscopy,* with the difference that Sawyer's book was prepared as a text and treats derivations in detail, whereas this book indicates the principal schematics and derivations and refers the reader to the literature for the details. It is not that the author is trying to evade matters; in this way he can concentrate on the essentials and tell the reader where to go for more detail. The section describing available apparatus and accessories is akin to Harrison, Lord, and Loofbourow, but with much more coverage of European equipments. A major difference between this volume and Harrison, Lord, and Loofbourow is the orientation of the latter to applications of spectrochemical analysis and chemical spectroscopy. Brügel devotes only one short chapter to chemical applications, and refers those interested in this topic to Bellamy's *Infrared Spectra of Complex Molecules.* (Brügel is also the author of the 1955 translation of the first edition of Bellamy into German.) Brügel incorporates some material from the monograph *The Detection and Measurement of Infra-red Radiation* by Smith, Jones, and Chasmar, but whereas that book was very strong on radiation detector physics and the newer quantum detectors, Brügel gives these only a brief treatment and devotes most of his attention to thermal detectors.

The chief difference between the present work and the flurry of recent American books on "infrared technology" is that a large part of the applications of these recent books pertains to military uses in reconnaissance, surveillance, homing, seeking, guidance, and so on. Brügel devotes only about a dozen pages to military applications, and these consist primarily of such uses as the detection of camouflage, of night vision devices, and line-of-sight secure communication. The types of applications discussed in this book are infrared photography (as applied to botany, zoology, astronomy, the textile industry, and forensic studies), infrared in medicine, infrared communications, infrared space heating, radiation baking of enamels, and related commercial applications.

The book contains many tables and graphs which the author has condensed from the literature. The most remarkable thing about this edition (and also about the earlier book on molecular spectroscopy by the same author *Einführung in die Ultrarotspektroskopie,* Verlag Steinkopff, Darmstadt, 1957) is the ample evidence that the author has studied and digested a tremendous number of original references. There are more than three hundred references to the recent literature up to 1960, and the author has not simply read these references; he has studied them and has even corrected mistakes in them. In this type of scholarship the author is carrying on a fine tradition in the infrared field; Brügel was a student of M. Czerny, who in turn was a student (I am told the last student) of H. Rubens. This is an excellent reference work for your infrared library.

J. N. HOWARD

Have you read the Russian maser papers in OPTICS AND SPECTROSCOPY?

Experimental Transfer Characteristics of Image Motion and Air Conditions in Aerial Photography

L. O. Hendeberg and E. Welander

Factors that impair the quality of aerial photographs include image movement, air turbulence, and haze. The effects of image movement are treated theoretically and experimentally. In the experimental study, data have been obtained by photographing a pattern on one airplane from another flying above it. The effects of the atmosphere can be separated into two types. One, due to haze, reduces contrast in a manner independent of spatial frequency; the other, attributed to air turbulence, has a spatial-frequency dependence and is treated as an apparent "aberration" of the optical system.

One of the most important of the many factors affecting image quality in aerial photography is movement unsharpness, particularly when photographs are taken at low altitudes. A special investigation of the relations between the effect of the image movement unsharpness and the remaining factors determining the quality of an aerial photograph has therefore been considered justified. This work is a continuation of the experiments begun earlier to develop objective methods of judging the practical usefulness of aerial photographs in photogrammetry.

Earlier Investigations

The effect of image movement unsharpness on the resolution of a photograph has been dealt with earlier by Selwyn and Romer, according to Brock,[1] and others. When an object has been photographed without movement unsharpness at a certain resolution limit, Selwyn found that the same subject could be moved linearly during exposure, a distance of 0.5 times the resolved distance of the corresponding photographs taken with stationary cameras, without the resolution limit being affected noticeably by the movement. This referred to sinusoidal test patterns. Romer found, among other things, that the greatest image movement that could be tolerated was affected by the test contrast. He found that, for objects with low contrast, the value 0.6 times the resolved distance could be accepted without the resolution being noticeably impaired.

The difficulty with this kind of investigation has hitherto been to find a test method that can be used for each of the stages in the image-forming system, in which the aerial photograph is the ultimate result. One can now obtain reliable measurements of the transfer function of lenses $T_{\text{lens}}(N)$ and of photographic emulsions $T_{\text{em}}(N)$. The function $T(N)$ is normalized so that $T(0) = 1$, where N is the spatial frequency expressed in cycles/mm. $T(N)$ is the Fourier transform of the line spread function $\phi(x)$, where x is the linear coordinate in the image plane.

In 1960, Scott[2] reported mathematical expressions for transfer functions in aerial photography. He gave, among other things, the transfer function $\sin\alpha N/\alpha N$ of the linear movement unsharpness for a rectangular shutter function. Paris[3] has also made certain experiments with a test pattern of the Foucault type, which was vibrated at a suitable amplitude and frequency. Laboratory investigations have also been extended to include practical experiments by Wolfe and Tuccio[4] and others.

In 1960 Welander[5] made experimental determinations of the T function in aerial photography. It was shown that the linear movement unsharpness is a dominant factor. At such an altitude as 1500 m, the effect of motion, presented as a T function, is of approximately the same magnitude as the total effect of the lens and film. This gives rise to the question of how the T function for the movement unsharpness alone can be determined experimentally under practical conditions.

Theoretical Deliberations Regarding the Effect of Image Motion

Formerly, the resolving power or resolution limit (R) was used as a criterion of the quality of aerial photographs; but R fails to give a result free from

L. O. Hendeberg is with the Institute of Optical Research, and E. Welander is with the Geographical Survey Office, Stockholm, Sweden.

Received 18 October 1962.

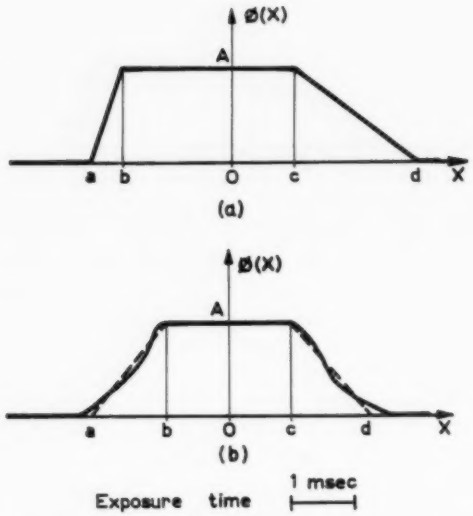

Fig. 1. Shutter function $\phi(x)$. a, b, c, and d are x coordinates; A is a normalizing constant. (a) Asymmetric shutter function; (b) experimental function (———), symmetric function (— — — — — — — —).

subjectivity. Moreover, it is now known that the reduction of contrast at lower frequencies, e.g., $N < 30$ cycles/mm, is also important in many cases. The Fourier transform $T_t(N)$ of the line image describes the image more completely than the resolution limit, which is really a relatively indefinite point of intersection between the threshold curve of the eye and the $|T_t(N)|$ curve. The emphasis in this paper will be on the $|T_t(N)|$ curve as a measure of image quality.

If the problem is approached in this way, every link in the image-forming system may be described by its $T(N)$ function for all frequencies under consideration. A multiplication of these functions gives the transform $T_t(N)$ of the image function. Thus, in laboratory work,

$$T_t(N) = T_o(N) \cdot T_{lens}(N) \cdot T_{em}(N) \cdot T_v(N), \qquad (1)$$

where $T_o(N)$ is the Fourier transform of the object and $T_v(N)$ the function of the influence of the image motion at velocity v.

As is well known, $T_v(N)$ may be largely or wholly eliminated by movement-compensating arrangements. In aerial photography for photogrammetric purposes, however, such arrangements do not yet exist. For that reason we have studied the unsharpness caused by image motion both theoretically and experimentally. In the latter work it has been possible to make comparisons between two aerial negatives, one with and the other without movement unsharpness.

In aerial photography, the speed of the aircraft causes a widening of the details of the photographic image parallel to the direction of flight. This problem will now be discussed theoretically.

The Shutter Function

The opening of the shutter as a function of exposure time may be determined in the laboratory with the help of a combination of a photocell and an oscilloscope. The shutter is found to open and close approximately linearly with the time. The whole shutter action may thus be approximated by a parallel trapezium, as in Fig. 1(a). When the velocity is constant and unidirectional, the line-image profile in linear measure x is the same as the shutter function in time coordinates.

The widening of the image is calculated as a function $\phi_v(x)$ containing the independent factors f, v, r, and t, where f is the focal distance of the lens in m, v is the speed of the aircraft in km/hr, r is the altitude in m, and t is the time in sec.

The variable x is given by the relation

$$x = \frac{f}{r} \cdot v \cdot t \cdot \frac{10^3}{3.6} \text{ mm}, \qquad (2)$$

where f/r is the scale of aerial photography and v/r determines the angular velocity.

The shutter function will be as follows:

$$\begin{aligned}
&\phi_v(x) = 0, && \text{for } x < a,\\
&\phi_v(x) = \frac{A}{b-a}(x-a), && \text{for } a \leqslant x \leqslant b,\\
&\phi_v(x) = A, && \text{for } b < x < c,\\
&\phi_v(x) = \frac{A}{c-d}(x-d), && \text{for } c \leqslant x \leqslant d,\\
&\phi_v(x) = 0, && \text{for } d < x,
\end{aligned}$$

where $a < b < c < d$.

This function $\phi_v(x)$ forms the spread function to be Fourier-transformed in order to obtain the transfer function $T_v(N)$. Special calculations will be required if a "between-the-lens" shutter is not used.

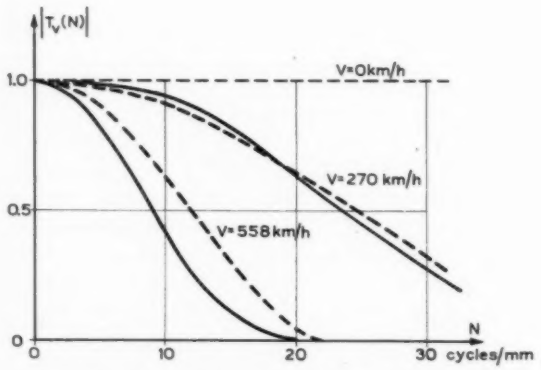

Fig. 2. Movement unsharpness $|T_v(N)|$ as function of frequency N. Velocity, v, is parameter. Experimental curve (———), theoretical curve (— — — — — — — —).

Fig. 3. Airplane, type Siebel NC 701, with two test lines upon the wings.

The Fourier transform of $\phi_v(x)$ can be shown to be

$$T_v(N) = \frac{A}{2\pi N}\left[\frac{e^{i2\pi Na} - e^{i2\pi Nb}}{2\pi N(a-b)} - \frac{e^{i2\pi Nc} - e^{i2\pi Nd}}{2\pi N(c-d)}\right], \quad (3)$$

and the modulus of $T_v(N)$ is

$$|T_v(N)| = \frac{A}{2\pi N}\left\{\left[\frac{\sin\pi N(a-b)}{\pi N(a-b)}\right]^2 + \left[\frac{\sin\pi N(c-d)}{\pi N(c-d)}\right]^2 - 2\cdot\frac{\sin\pi N(a-b)}{\pi N(a-b)}\cdot\frac{\sin\pi N(c-d)}{\pi N(c-d)}\cdot\cos\pi N[(c+d)-(a+b)]\right\}^{1/2}, \quad (4)$$

where $|T_v(N)|$ is normalized by choosing the constant A, so that

$$T_v(0) = \int_{-\infty}^{+\infty}\phi_v(x)dx = 1.$$

Thus,

$$A = \frac{2}{(c+d)-(a+b)}.$$

The modulus shows the effect of the aircraft speed and flight altitude on the transfer function. The coordinate values a, b, c, and d are of course related to f, v, and r as shown by Eq. (2).

In our case, the shutter function may be approximated by assuming that the function is symmetrical, which gives $|T_v(N)|$ with sufficient accuracy.

$$||T_v(N)|_{sym} - |T_v(N)|_{exper.}| < 0.05.$$

Then, according to Fig. 1(b),

$$-a = d, \text{ and } -b = c.$$

The imaginary part of $T_v(N)$ then disappears, so that

$$T_v(N) = \frac{\sin\pi N(d-c)}{\pi N(d-c)}\cdot\frac{\sin\pi N(d+c)}{\pi N(d+c)}. \quad (5)$$

In our measurement the values are

$$b - a = d - c = 12 \text{ msec, and } c - b = 19 \text{ msec.}$$

There is a possibility that the width of the shutter curve increases at the lower temperature at 1500-m flight altitude, but this effect has not been taken into account in our calculations.

The main factor in Eq. (5), $\sin\pi N(d+c)/\pi N(d+c)$, depends on the effective shutter speed, i.e. the rectangular opening process equivalent to the half-width of the shutter function. This function is identical with that published by Scott,[2] which gives a somewhat too high approximate value. The correction factor $\sin\pi N(d-c)/\pi N(d-c)$ must be applied to the aforementioned factor and depends on the slope of the opening ($a < x < b$) and closing ($c < x < d$) phases of the shutter. For our data, the correction factor is 0.87 when $v = 270$ km/h, $r = 1500$ m, and $N = 30$ cycles/mm and is naturally closer to 1 for lower N.

Only when $v = 0$, the transform is $T_{v=0}(N) = 1$ for all N. In all other cases, the function decreases continuously from the value 1 when $N = 0$ to zero, depending on the velocity according to Fig. 2. The theoretical curves are dashed. If the theoretical curve goes below zero, this means physically that spurious resolution exists.[6]

Experimental Arrangements

The investigation methods are based on a comparison of the total T functions for an aerial image with movement unsharpness and another of the same object without movement [see Eq. (6)]. Both these functions may be obtained if two aircraft are employed simultaneously, one photographing test figures on the other. Their speeds and the difference in altitude between the two planes must be known. Photographs are taken when the aircraft are flying in the same and in the opposite directions.

The test figures used consisted of a bright line, 8-cm wide and 3.5-m long, painted on a dark background along the upper sides of both wings (see Fig. 3). Two different test contrasts (ΔD) were used. The density values of the lines when measured in diffuse reflection were 1.0 on one wing and 0.6 on the other, while that of the background was 1.4 in both cases. Thus ΔD is 0.4 and 0.8, respectively.

In the aerial photography carried out in the autumn of 1961, one of the planes flew a certain flight strip at an altitude of 1900 m, while the other plane, with the test line, flew along the same strip at an altitude of 400 m. In this way, the test line was photographed on a scale of 1:10,000 from an altitude of 1500 m. A Wild aerial camera, with a 6-in. (15-cm) Aviogon lens, and Plus-X Aerographic film were used. The nominal exposure was 1/250 sec at $f/6.3$.

Three trial series were made. In the first, both aircraft flew in the same direction twice at a speed of 263 km/hr. There was no movement unsharpness, apart from the vibrations in the airplanes. These

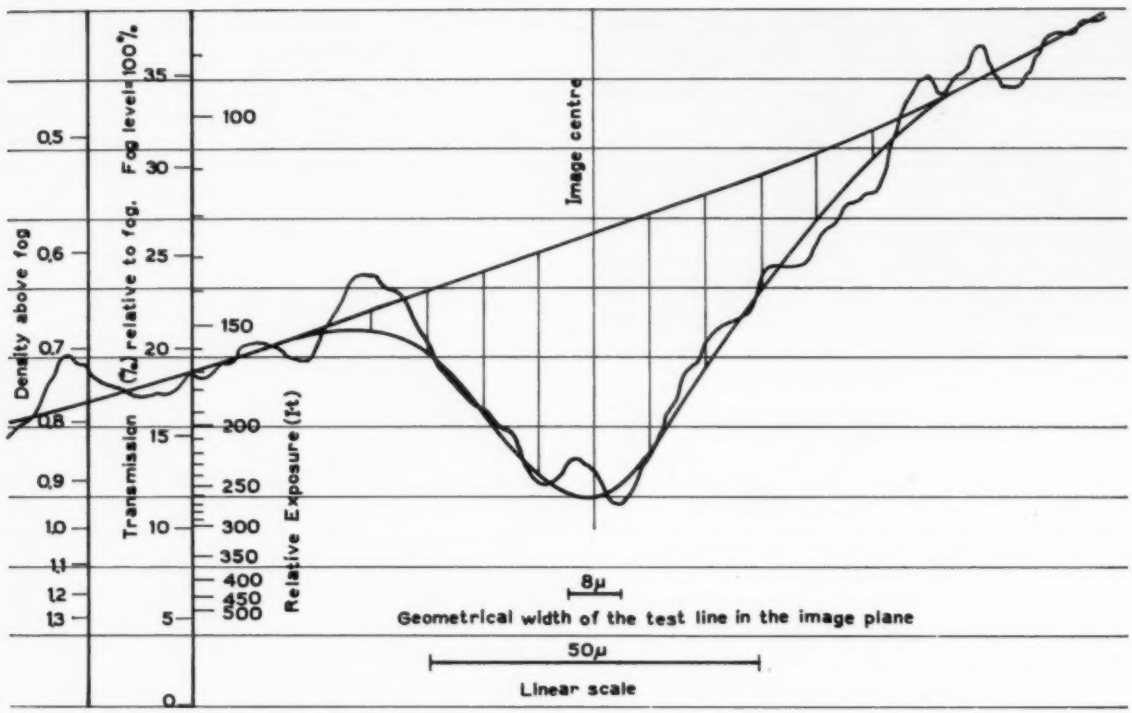

Fig. 4. Microphotometer trace of the object of a test line on a wing of the aircraft. Mean curves of background and superposed test line are marked. The H and D curve determines the relation between transmission and $I \cdot t$ values.

had been tested earlier, and the vibrations were shown to be insignificant compared with other influences. $|T_{vibr}(30)| > 0.98$. In the second series of flights, one-half hour later, both planes had about the same speed but opposite directions. Three exposures were made. The speeds were then 283 km/h for the higher aircraft and 275 km/h for the lower one. At the third and last trial series, two days later, the airplane with the test line was stationary on the ground, while three exposures were made from the other plane at an altitude of 1500 m at speeds of 249 and 292 km/h.

The photographs were taken with two twin-engine aircraft of the types Beechcraft D 18 S and Siebel NC 701. The weather was clear, with no visible haze. All exposures were made on films of the same emulsion number. The films were joined together with plastic tape and processed in a developing tank of the motor-driven type generally used for aerial films. The development time for a gamma of 1.0 was 9 min in DK 50 at 20°C.

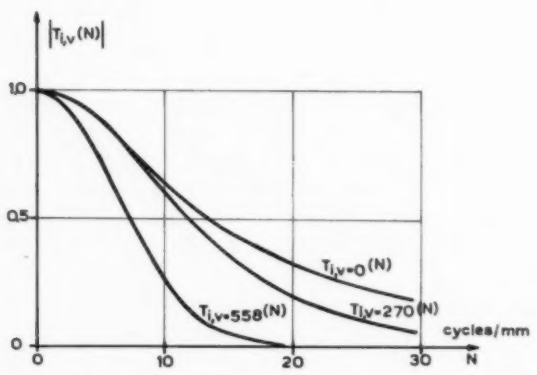

Fig. 5. The Fourier transform of the image $|T_{i,v}(N)|$. The velocity v is 0, 270, and 558 km/h for the upper, middle, and lower curves, respectively.

Functions for the Total Image and Image Motion

The bright test line on the aircraft was clearly visible in the negative when examined in 10× magnification. A distinct difference could be observed in the width of the line when flights had been performed in the opposite or the same direction. The darker test line could also be discerned in the negative, but the density difference relative to the background was in some cases hardly visible.

The negatives were measured with a microphotometer with a rectangular slit 0.8 μ × 400 μ and a speed of 50 μ/min. Both the line and the slit were so long that diffractions in that direction may be ignored. Thus the whole of the experiment may be treated as a one-

dimensional problem. A microphotometer scan gives the transmission values as a function of the x-coordinate, at right angles to the line. In Fig. 4 the fog which is given the transmission value 1.0 is on the 100% level. On the basis of the background density and with the help of the H and D curve of the emulsion, it is possible to convert the observed image to a symmetrical line image $\phi_i(x)$ measured in terms of effective exposure $I \cdot t$. This image is Fourier-transformed to $|T_i(N)|$ by means of a Ferranti Mercury digital computer. This function contains all the factors affecting the image and is shown in Fig. 5. Dividing the functions with and without movement unsharpness gives the function for the movement unsharpness alone. Thus,

$$|T_v(N)| = \frac{|T_{i,v}(N)|}{|T_{i,v=0}(N)|}, \tag{6}$$

when

$$|T_{v=0}(N)| = 1.$$

No systematic asymmetry due to the movements of the aircraft, the illumination of the test line, or the like, has been observed. The line image has been exposed as near to the optical axis as possible to avoid, among other things, phase alterations which spoil the symmetry. The distance of the test image from the center of the field is less than 40 mm. But the values $|T_{\text{lens}}(N)|$ for $N < 30$ cycles/mm differ only by a few percent in the different cases.

The variation of density shows that the luminance on the wings varied owing to the low value, 30 deg, of solar elevation and because of the inclination of the airplane at the moments of exposure. Table I gives the density values measured in the images.

Regarding the effect of the test contrast on the appearance of the T curve, Fig. 6 shows that the spread

Table I. Density Measurements of the Objects and the Images and Half-Width and Tenth-Width of the Image Function

Trial series	$v = 0$ km/h		$v = 270$ km/h		$v = 558$ km/h	
Diffuse density difference of test chart	0.8	0.4	0.8	0.4	0.8	0.4
Distance of image from the optical axis in mm.	6	6	40	40	40	40
Density of the background	1.0	0.8	0.8	0.6	0.9	0.7
Peak value of image in density measure	0.64	0.26	0.35	0.13	0.32	0.13
Half-width of $\phi_i(x)$ in μ.	18	17	28	35	56	67
Tenth-width of $\phi_i(x)$ in μ.	56	50	64	70	96	95

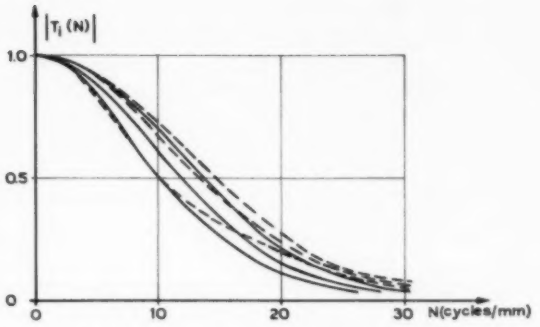

Fig. 6. The Fourier transforms of the images $|T_i(N)|$ of six experiments. $v = 270$ km/h. Diffuse density of the test line of the object = 0.6 (— — — —) and =1.0 (————). Density of the background = 1.4.

of the curves is somewhat greater for the lower test contrast, $\Delta D = 0.4$, and that the higher contrast, $\Delta D = 0.8$, gives a somewhat higher T value. The differences are not significant, however, so both contrasts have been used in calculations of mean curves for each of the flight velocities 0, 270, and 558 km/h. In spite of the variations in the test series, the results show sufficient agreement between the T functions for the experimental and theoretical movement unsharpness, especially with the lower speed of 270 km/h (see Fig. 2).

In an object which gives the spatial frequency $N = 20$ cycles/mm in the image plane, the signal can be distinguished with certainty from the granularity noise of the emulsion[7] only if the velocity, altitude, and air conditions are such that $|T_v(20)| > 0.3$ (see Fig. 7). The linear relation between flight velocity and altitude is shown in Fig. 8, where the movement unsharpness is shown by curves with $|T_{v,r}(20)| =$ constant as

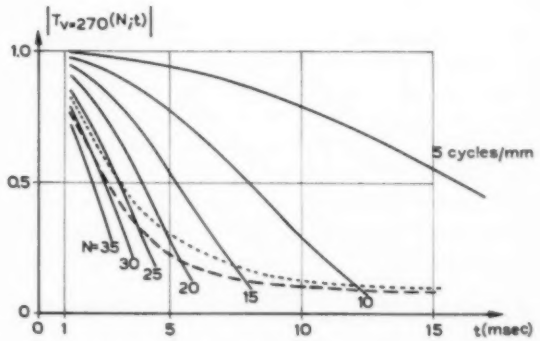

Fig. 7. $|T_{v=270}(N;t)|$ as function of time of exposure t. N is parameter. $v = 270$ km/hr and $r = 1500$ m(————). Resolution limit influenced by lens, photographic emulsion, and image motion (— — — — — —). Resolution limit influenced by turbulence and haze as well (. . . . . .).

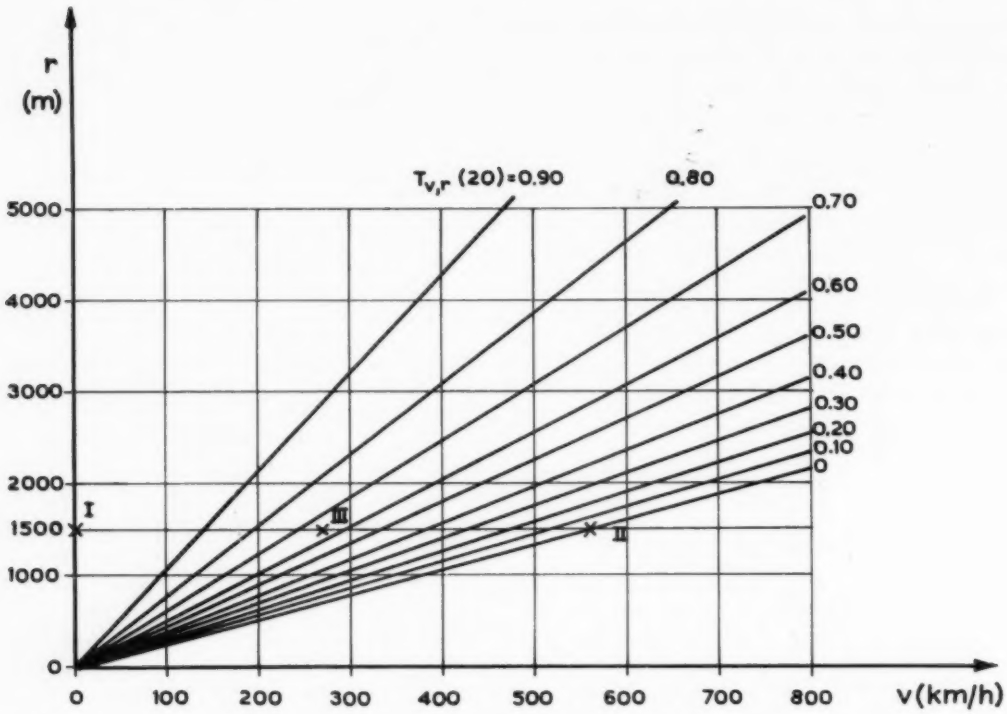

Fig. 8. Linear relation between velocity v and altitude r. No turbulence and haze. The modulation is the parameter. The crosses indicate the conditions of the actual experiments.

parameters. Such factors as turbulence and haze are not included. The positions of the three trial series are marked in the figure. The point corresponding to the velocity 558 km/h lies below the limiting curve for zero modulation. This shows that spatial frequencies higher than 20 cycles/mm must disappear. The air turbulence causes further deterioration.

The Effect of the Atmosphere and the Weather

A necessary prerequisite for the application of the present method is that conditions are exactly the same when all the exposures are made. This means, among other things, that haze and air turbulence are considered to have like effect on all images. No noticeable change took place in the haze conditions during the short interval between the first and second trial series. Nor could variations in the general illumination conditions have affected the result. The third series of photographs, on the other hand, was not taken on the same day, but conditions were judged visually to be identical. Unfortunately, no quantitative measurements were made of the haze and illumination conditions.

The effect of air turbulence on the results is more difficult to estimate. The general turbulence may naturally vary from day to day and from hour to hour, even if weather conditions may seem identical. When both aircraft are in motion, the turbulence in the immediate vicinity of the machines should be of about the same magnitude, regardless of direction of flight. The camera mounting was such that local turbulence in the vicinity of the lens may have been significant. This mount was of a type frequently used for mapping cameras. The camera, with a yellow filter over its lens, was recessed about 5 cm inside a round hole of 30-cm diameter in the skin of the fuselage, and the gap between the filter mount and the skin was sealed to prevent the entrance of air. Obviously, turbulence could develop around this opening, and such local turbulence may exaggerate the modulation degradation attributed to general atmospheric turbulence.

Hitherto, the effect of the weather has been eliminated together with other influencing factors, namely the object, the optics, the air turbulence, the haze, and the emulsion, in order to calculate the transfer function of the shutter function. The $|T_v(N)|$ functions are obtained as a ratio between two T functions [see Eq. (6)]. Because the experimental values have coincided with the theoretical, we have some confirmation that the weather conditions have been unchanged during both exposure series. It now also seems possible to discuss two types of effects of the air: one where the image is degraded in a frequency-dependent manner and the other where the effect

reduces the amplitudes of all frequencies in the same manner.

Evidently, small and large field angle disturbances from air turbulence, shimmer, or the like will decrease the contrast differently for different spatial frequencies. It seems clear from our experimental observations that higher frequencies are destroyed more than lower ones. Abnormalities can, of course, happen and are, in many cases, sporadic and short-lived but not infrequent. In our case, we are more interested in "standard" air conditions that seem to have prevailed during the experiments. The frequency-dependent part, the air turbulence, etc., and the optics are calculated as one transfer function, $|T_{\text{lens+turb}}(N)|$. The air is thus treated as an intrinsic part of the optical system. When the distance between object and image is small, the lens itself dominates. The function is the same as $|T_{\text{lens}}(N)|$, which is experimentally determined in the laboratory. At a large distance, the layer of the air becomes significantly thick, and its effect on $|T_{\text{lens+turb}}(N)|$ is large. One can then say that those "aberrations" resulting from air turbulence will predominate over the aberrations of the lens itself when the layer of air is thick enough. The values of the Fourier transform of the image are reduced, and the resolution limit occurs at a lower frequency. In our favorable experiment with little turbulence and no variable haze, $|T_i(20)| < 0.4$ even when there is no motion.

It is also well known that haze and other similar effects seem not to diffuse an edge of an object. Middleton[8] gave a theoretical explanation. He also gave a typical example of objects viewed from different distances.[9] All silhouettes of the objects, far and near in haze and in fog, have the same sharp contours. But the luminance of an object farther away seems to be more similar to the luminance of the background than to the object near the observer. Duntley[10] measured distant resolution limit targets. His findings were the same. Differences in diffusion have no real influences according to Barber[11] when small angle measurements were made in clear or hazy weather.

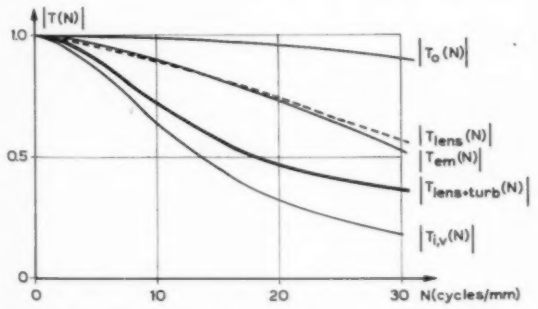

Fig. 9. Transfer functions of lens, emulsion, lens and turbulence, and spectra of the object and the image.

According to these findings, the haze effect should not be frequency dependent. The amplitudes of all spatial frequencies within the range of interest here are multiplied with the same constant c. At the same time, c is a measure of the attenuation and is dependent on the object distance. At short distances and in laboratory measurements, $c = 1$. However, it may be possible to determine the constant if a sufficiently large black and white target is photographed or telephotometered from different distances. Thus, c and $|T_{\text{lens+turb}}(N)|$ should be factors in the Fourier product $|T_i(N)|$ and should be derived from the equation

$$|T_{i,\text{corr}}(N)| = c \cdot |T_o(N)| \cdot |T|_{\text{lens+turb}}(N)| \cdot |T_{\text{em}}(N)|, \qquad (7)$$

where $T(0) = 1$ and $0 < c \leq 1$.

$|T_o(N)|$ has been calculated mathematically. $|T_o(0)| = 1$.

$|T_{\text{lens}}(N)|$ has been determined experimentally with the help of an apparatus described by Ingelstam.[12] $|T_{\text{lens}}(0)| = 1$.

$|T_{\text{em}}(N)|$ on the other hand is uncertain. Available data for Plus-X Aerecon, but under other processing conditions, are taken from Tarkington.[13] Errors arising from this factor may be ignored in view of the large magnitude of $|T_{\text{em}}(N)|$ for $N < 30$ cycles/mm. $|T_{\text{em}}(0)| = 1$.

$|T_{\text{lens+turb}}(N)|$ is the factor that frequently dominates the other factors, according to Fig. 9. At the greatest velocity, $v = 558$ km/h; however, $|T_v(N)|$ has more effect on the image than the transfer function of the lens and the air together. $|T_{\text{lens+turb}}(0)| = 1$.

Djurle and Bäck[14] have shown that great variations may occur in the turbulence. Their experiment is not directly comparable, however, for it was made at night with a horizontal sight-line about 7 miles (11 km) long in an urban area.

The method of determining the image-movement unsharpness applied here has also provided certain possibilities of calculating the effect of haze and turbulence. A necessary condition, however, is knowledge of the T functions of the various image-forming links in the process of photography. Whether $|T_{\text{lens+turb}}(N)|$ satisfies all the necessary conditions for a transfer function, such as linearity, and is also reproducible can by no means be regarded as having been confirmed by this work. On the other hand, it has been possible to treat $|T_{\text{lens+turb}}(N)|$ mathematically as a separate factor in the determination of image-movement unsharpness.

Shutter Function and Effect of Emulsion on the Modulus

The modulus $T_v(N)$, Eq. (5), with N as parameter, falls with the exposure time for all frequencies from an initial value down to the resolution limit of the system. Solid curves in Fig. 7 for different values of

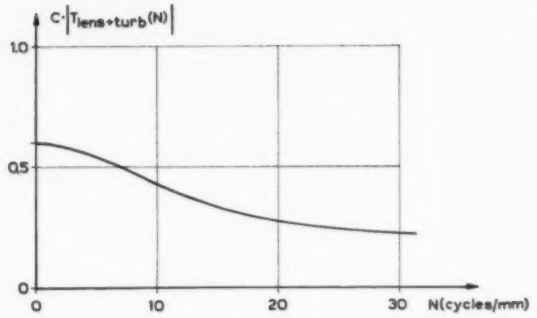

Fig. 10. Transfer function of lens together with air turbulence and haze.

N decrease more rapidly when N increases. The initial value is limited by the construction of the shutter. The calculations are applicable to shutter functions of normal symmetrical appearance with a constant opening phase, a parallel trapezium in profile. The lower limit of the duration of exposure time is, under these circumstances, 1.2 msec when $v = 270$ km/h and $r = 1500$ m.

The upper limit is determined by the resolution limit of the total system. As an example, we put in the limit of the contrast caused by the granularity noise of the emulsion, etc., according to the following: Tarkington[13] published a table about "Maximum Resolving Power" for the contrast ratio 1.26:1. This probably means the ratio between the exposure $(I \cdot t)_{max}$ and $(I \cdot t)_{min}$. The emulsion Plus-X Aerecon is developed 8 min in D-19. However, we have not used the same emulsion batch and the same developer. Nevertheless, Tarkington's result gives an idea about the possibilities of this emulsion. Thus the sinusoidal modulation used here is

$$\frac{(I \cdot t)_{max} - (I \cdot t)_{min}}{(I \cdot t)_{max} + (I \cdot t)_{min}} = 0.115,$$

which gives the maximum resolution limit = 27 cycles/mm. Another frequently used limiting value is 0.04 for small N. Between these two values the curve may be linear, as proposed by Selwyn and Tearle.[7]

Together with the Selwyn curve, the functions of lens and emulsion give an upper limit for the exposure time. In Fig. 7, these limiting values end the drawings of the curves with different N as parameter. The shutter function has no influence here ($v = 0$).

Then, when the shutter function is combined with lens and emulsion, the limit will, in the most favorable situation, be in accordance with the dashed curve. If the effect of the turbulence is also taken into consideration, the limit will be displaced upward as the layer of air increases in thickness. This means that only that part of the curves above the limit marked by the dotted curve can be observed in an experiment. At, for example, $N = 20$ cycles/mm, the emulsion resolves a sinusoidal test object of maximum contrast at an exposure no longer than 4.8 msec. The resolution limit R is lower for longer exposures. However, no matter how short the exposure may be, $N = 30$ cycles/mm cannot be reproduced.

With Plus-X Aerographic Film, speed 80 ASA, an exposure of 3.1 msec has been used. The change to the more finegrained Panatomic-X, speed 25 ASA, requires an exposure time of 9.9 msec. The dotted curve will lie only a few percent lower for the highest frequencies when this emulsion is used. With the same aperture, this means that the resolution is reduced from about 24 to about 12 cycles/mm. A better result is obtained, however, if a larger aperture is used. But another shutter function is then probable. The alteration in the transfer function $|T_{lens}(N)|$ will have little effect if the lens is sufficiently well corrected. During the opening and closing phases of the shutter, $|T_{lens}(N)|$ depends, of course, on the continuously changed relative N.A., but the effect of this is probably small.

A transfer function which represents both the turbulence and the haze at the time is determined by the two factors c and $|T_{lens+turb}(N)|$. We have not measured c, so we can only give an approximately estimated value of $c = 0.6$. The curve in Fig. 10 begins at $c \cdot |T_{lens+turb}(N)| = 0.6$ and ends at the resolution limit. It must be pointed out that a larger atmospheric attenuation leads to a decreasing R value.

This joint work has been initiated by Welander, who gave the idea of this method and whose department, Geographical Survey Office, has carried out the aerial photography and the processing work. Hendeberg has studied the slit images photometrically and theoretically.

Our thanks are due to E. Ingelstam for many valuable discussions and constant encouragement.

References

1. G. C. Brock, *Physical Aspects of Air Photography* (Longmans, London, 1952).
2. R. M. Scott, Phot. Sci. Eng. **3,** 201 (1959).
3. D. P. Paris, Phot. Sci. Eng. **6,** 55 (1962).
4. R. N. Wolfe and S. A. Tuccio, Phot. Sci. Eng. **4,** 330 (1960).
5. E. Welander, "Contrast Transfer Functions in Aerial Photography," Geographical Survey Office, Comm. to IX Int. Congr. for Photogrammetry, Stockholm, August 1960.
6. C. G. Brock, Phot. J. **101,** 165 (1961).
7. E. W. H. Selwyn and J. L. Tearle, Proc. Phys. Soc. (London) **58,** 493 (1946).
8. W. E. K. Middleton, J. Opt. Soc. Am. **32,** 139 (1942).
9. W. E. K. Middleton, *Vision Through the Atmosphere* (Univ. of Toronto Press, Toronto, 1952).
10. S. Q. Duntley, J. Opt. Soc. Am. **38,** 179 (1948).
11. D. R. Barber, Proc. Phys. Soc. (London) **B63,** 364 (1950).
12. E. Ingelstam, Phot. Korr. **3,** Sonderheft (1959).
13. R. Tarkington, Photogrammetric Eng. **25,** 695 (1959).
14. E. Djurle and A. Bäck, J. Opt. Soc. Am. **51,** 1029 (1961).

A New Optical Method of Storing and Retrieving Information

P. J. van Heerden

The analogy between electronic filters or networks and optical filters placed in the focal plane of an imaging arrangement has drawn attention to the potentialities of optical arrangements for information processing. This paper develops the theory of the filter in the focal plane whose transmission at each point is proportional to the intensity of the light from the object. This intensity filter—in imaging arrangements using coherent light sources—has the property of forming a "ghost image" of the whole object, when only a small fragment of the original object is shown. This ghost image can be utilized in principle for recognizing and locating a small fragment in the original object.

I. Introduction

The word "filter" has been in use for a long time in optics and electronics in two meanings which are only loosely related by the English language. In the last fifteen years, however, it has been realized that there is a mathematical analogy between the operation of an electronic filter or network on an electric signal and the operation of an optical filter, provided the latter is placed in the focal plane of the lens in an imaging device (Fig. 1). A good review on this development and its consequences has been written, for instance, by Cutrona *et al.*[1] This analogy, in short, is the following: an electrical signal, which is a voltage or current varying in time, can be analyzed as a Fourier integral into components of the form $A(\omega) \exp(i\omega t)$, where t is the time and ω the frequency. A filter then acts to modify each Fourier component separately in a way described by some function of ω. For an object in an optical imaging arrangement on the other hand, like a slide in a projector, we can also analyze in a Fourier integral the point by point transmission, given as a function $f(xy)$, where x and y are the spatial coordinates in the plane of the slide. This time the Fourier components are of the form $A(k, l) \exp(ikx + ily)$. Provided now that the light illuminating the slide is monochromatic and parallel, the light diffracted by a certain spatial Fourier component, acting like an optical grating, will be parallel and will be focused to a certain point in the focal plane of the imaging lens. When a filter is placed in this focal plane with a transmission varying from point to point, the filter will modify each Fourier component in a specific way, independent of any other Fourier component.

The specific problem this article is concerned with is the one of recognition and location of information. In radar, this problem has led to the concept of the "matched filter." Translated in optical terms, this would be a filter located in the focal plane with a transmission proportional to the amplitude, *with the correct phase angle*, of the light from the original object. This will be discussed in detail in Section II. Although such an optical filter can be realized in principle, the difficulty of making a matched filter for a high resolution object is considerable. On the other hand, making a filter proportional to intensity, not amplitude, is a thing photography can cope with.* It will be shown that this "intensity filter" has properties which make it excellent for search operations.

The main property of an intensity filter is the generation of a "ghost image," which is the following: A photographic plate is exposed in F (Fig. 1) to the light from a slide in O. A positive is made of this plate and put back in F. Now the original slide is removed, and a small fragment of this slide, right side up, but displaced from its original position, is substituted for it. Then there will be visible in the image plane I, besides the real image of this fragment, *a ghost image of the whole slide*, displaced from its original position so much that the image of the fragment coincides with its own ghost image. This ghost image becomes weaker and

The author was at the General Electric Research Laboratory, Schenectady, New York. His present address is: Polaroid Corp., Cambridge 39, Mass.

Received 17 May 1962.

* The specific problem of producing a change in the light intensity by a photographic transparency without at the same time introducing a phase shift has been discussed by Maréchal *et al.*[2]

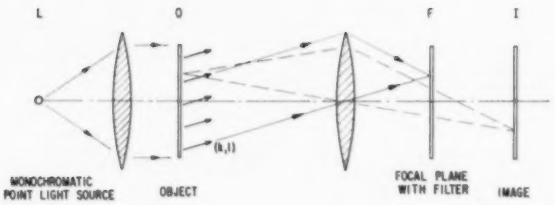

Fig. 1. Optical filter analogous to electronic filter. The filter in F modifies each spatial Fourier component $A(kl)$ independently.

noisier the smaller the size of the fragment. Experimentally, this ghost image has not yet been demonstrated, but the theory is such a straightforward application of the well-known wave properties of light that there can be little doubt about its existence. There is also a close relation of this intensity filter with the imaging method as demonstrated by Gabor in his "new microscopic principle."[3]

II. Formulation of the Search Problem and the Matched Filter

Before describing the properties of the intensity filter, we will discuss the problem to which it can be applied. Suppose somebody enters a library,* shows the librarian the fragment of a page of a book and asks whether this is in the library and if so, where? Unless the librarian recognizes the page, the only way to answer the question is to search through the whole library, page by page, until the passage is found. When the library and the fragment both are in a standard letter type, this search could also be carried out by a machine, simply by comparing the blackness of the fragment, point by point, with that of each possible position in the library.

Imagine the library reproduced on one large transparent sheet and the fragment on a similar small one. Then one photocell could measure the light transmission through both sheets superimposed. The light transmission will vary from one position to another in some random fashion. But for one position, where the fragment coincides with its copy in the library, there will be a sharp peak in transmitted light. This will be the recognition signal and it will at the same time locate the position of the fragment.

Mathematically, this operation is described by the correlation function $C(xy)$. Let the light transmission in a point (xy) of the library sheet be given by $f(xy)$. Let further the fragment be given by a similar function $g(xy)$. The total amount of light received by the photocell is now proportional to a function $C(xy)$ given by:

$$C(xy) = \int\int f(x'y')g(x + x', y + y')dx'dy'$$

when the fragment coincides with the library for $f(x, y) = g(x + x_0, y + y_0)$, then $C(xy)$ will show the coincidence peak for (x_0y_0).

The insight given us by the electronic engineers is to look upon this operation as a filtering operation, by considering the Fourier transform:

$$f(xy) = \frac{1}{2\pi}\int_{-\infty}^{+\infty} A(kl)\exp\,[i(kx + ly)]dkdl.$$

(A single integral sign will be used for multiple integrals to save space without loss of clarity.)

It is well known that $A(kl)$ is given by:

$$A(kl) = \frac{1}{2\pi}\int_{-\infty}^{+\infty} f(xy)\exp\,[-i(kx + ly)]dxdy,$$

and this also leads to a useful identity, applied throughout this paper:

$$f(x_0y_0) = \left(\frac{1}{2\pi}\right)^2\int_{-\infty}^{+\infty} f(xy)\exp\,[ik(x_0 - x) + il(y_0 - y)]dkdldxdy. \quad (1)$$

When further

$$g(xy) = \frac{1}{2\pi}\int_{-\infty}^{+\infty} B(kl)\exp\,[i(kx + ly)]dkdl,$$

then we find for $C(xy)$ by substitution:

$$C(xy) = \left(\frac{1}{2\pi}\right)^2\int_{-\infty}^{+\infty} A(k'l')B(k''l'')\exp\,[i(k'x' + l'y') + ik''(x' + x) + il''(y' + y)]dx'dy'dk'dl'dk''dl''$$

By taking advantage of a useful identity similar to the one given above, this is reduced to:

$$C(xy) = \frac{1}{2\pi}\int_{-\infty}^{+\infty} A(-k'', -l'')B(k''l'')\exp\,[i(k''x + l''y)]dx''dl''.$$

The correlation function $C(xy)$ is obtained by multiplying every Fourier component $B(kl)$ of $g(xy)$ with $A(-k, -l)$, which for real $f(xy)$ is the same as $A^*(k, l)$, the complex conjugate of $A(k, l)$. Without going into the details, which will be given in the discussion of the intensity filter, this means that in the image plane I (Fig. 1) is obtained the correlation $C(xy)$, when the fragment $g(xy)$ is put in the object plane and an optical filter proportional to $A^*(kl)$ in the filter plane. This is the filter which in the electronic literature is often called a matched filter, although sometimes this term is used in a more general meaning. In our discussion, however, it will only be used in this narrow sense. The production of $C(xy)$ by a filter operation is a wonderful result, because it shows how a complete and cumbersome search operation through the library can be carried out, at least in principle, in one single step with the aid of a matched filter. The image plane would show noise with one bright spot, and the displacement (x_0y_0) of this spot from the origin would indicate the correct position of the fragment.

* The example given here does not necessarily mean that the method is actually practical in this case. It illustrates in general the problem of search, in a large amount of stored information, for a specific item without the benefit of a catalog.

While the making of a matched filter for a highly detailed object, giving both the correct amplitude and phase shift in each point of F, is so difficult as to make it somewhat academic, a filter proportional simply to the light intensity in F is quite feasible in optics. This intensity filter, as we will see, can perform the same essential function of search as the matched filter.

III. The Theory of the Intensity Filter

Consider Fig. 2. The optical arrangement given here is equivalent with the one in Fig. 1, except that the imaging lens has been split in two to make the arrangement more symmetric. The light amplitude illuminating the slide containing the library, in O, is given by $U = U_0 \exp(im_0 z - i\omega_0 t)$. When $S(xy)$ is the amplitude transmission of the slide in a point (xy), then $US(xy)$ is the light amplitude immediately behind the slide. We write $US(xy) - {}^1/_2U = f(xy)$, and the total amplitude behind the slide is now given by

$$f(xy)\exp(im_0 z - i\omega_0 t) + {}^1/_2U_0\exp(im_0 z - i\omega_0 t).$$

This allows $f(xy)$ to be both positive and negative. The second term ${}^1/_2U$ represents light that remains parallel and is focused in F_0, the focal point of the lens.

To find the amplitude $A(klm)$ of a wave emerging from the object at $z = 0$ through diffraction, we must match the amplitudes of incoming and outgoing waves at that point. In writing

$$f(xy) = \frac{1}{2\pi}\int_{-\infty}^{+\infty} A(k, l)\exp i(kx + ly)dkdl,$$

then, $A(k, l) = A(k, l, m)$, since m is determined by the relation $k^2 + l^2 + m^2 = \omega_0^2/C_0^2$ (C_0 is the velocity of light). A wave $A(klm)$, describing the parallel light emerging from the slide in the direction $(k - m)$, will be focused by the first imaging lens in its focal plane $z_1 = 0$, such that $k = cx_1$; $l = cy_1$, where c is a constant which can be taken to be unity by a proper choice of the unit of length (because c has the dimension cm^{-2}). The formation of the image in I, with or without filter in F, can now be obtained by

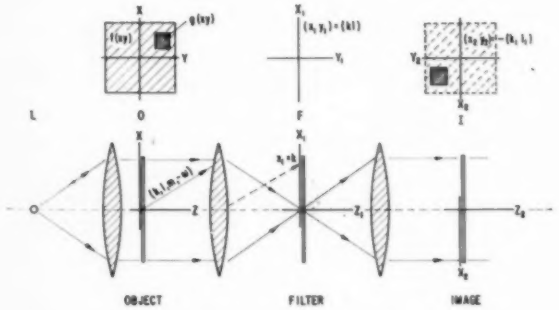

Fig. 2. Optical filter equivalent to Fig. 1, but symmetrical. Notice the reversal of the coordinate axes in the (x_2y_2) plane to simplify the computation.

again matching incoming and outgoing waves at the boundary F and noticing that every outgoing plane wave is focused in a point $k_1 = -cx_2$, $l_1 = -cy_2$ in I. For instance, without a filter, this will reproduce in I the original amplitude $f(xy)$ both in amplitude and phase, for $(xy) = +(x_2y_2)$, that is, we obtain a reversed image. (Notice that for the convenience of the calculation in the x_2y_2 plane + and − signs have been reversed; see Fig. 2.) We can now discuss the intensity filter in F. This filter has a transmission in each point $(kl) = (x_1, y_1)$ given by $A(kl)A^*(kl)$. Suppose now that the library fragment or test object $g(xy)$, when put in the object plane, has a Fourier spectrum $B(kl)$, then the amplitude immediately behind the filter in F, from this fragment, is given by $A(x_1y_1)A^*(x_1y_1)B(x_1y_1)$. The resulting amplitude $D(x_2y_2)$ in the point (x_2y_2) of I is obtained by computing the Fourier component (k_1l_1) of the amplitude in F, such that $(k_1l_1) = -(x_2y_2)$. This is given by the integral:

$$D(x_2y_2) = \frac{1}{2\pi}\int_{-\infty}^{+\infty} A(kl)A^*(kl)B(kl)\exp[i(kx_2 + ly_2)]dkdl.$$

To obtain an insight into the meaning of the function D, we remember that $A(kl)$ and $B(kl)$ are given by Fourier integrals. By substituting these integrals we obtain:

$$D(x_2y_2) = \left(\frac{1}{2\pi}\right)^2\int_{-\infty}^{+\infty} f(x'y')f^*(x''y'')g(x''', y''')\exp[ik(x_2 - x' + x'' - x''') + il(y_2 - y' + y'' - y''')]dkdldx'dy'dx''dy''dx'''dy'''.$$

We now apply again the useful identity (1) in integrating over k, l, x''', *and* y''' and obtain:

$$D(x_2y_2) = \left(\frac{1}{2\pi}\right)^2\int_{-\infty}^{+\infty} f(x'y')f^*(x''y'')g(x_2 - x' + x'', y_2 - y' + y'')dx'dy'dx''dy''.$$

Comparing this expression of $D(xy)$ to the correlation function $C(xy)$ we see that there is a certain resemblance. But what is the actual meaning of $D(xy)$? We will show now that $D(xy)$ consists of three parts. The first part is the normal image of $g(xy)$ that would also be obtained when the filter in F was not present. The second part is the ghost image of the whole object $f(xy)$ and the third part is noise.

There can be an argument about calling this last part "noise," since it arises in a purely causal, predictable way from two known functions $f(xy)$ and $g(xy)$. However, this can be justified by considering the analogy with the correlation function C. In determining this function in a search operation for the proper position of $g(xy)$, we are looking for one peak in a fluctuating function which from the point of view of the searcher is unpredictable, and therefore can be called noise.

The presence of these three parts of $D(xy)$ can best be demonstrated by approximating the integral by a sum:

$$D(x_2y_2) = \left(\frac{1}{2\pi}\right)^2 \sum_{-\infty}^{+\infty} f(x'y')f(x''y'')g(x_2 - x' + x'', y_2 - y' + y'')\Delta x'\Delta y'\Delta x''\Delta y''.$$

Here, while the sum is taken for the limits $-\infty$ and $+\infty$, we must remember that $f(xy)$ is defined in a square with sides l, and identical zero outside that square, while $g(xy)$ is different from zero only in a small square with sides d. $f(xy)$ is assumed to be completely uncorrelated in two different intervals $\Delta x\Delta y$. Now first consider all terms in which $x' = x''$, which result in a function $D_1(x_2y_2)$ given by:

$$D_1(x_2y_2) = \left(\frac{1}{2\pi}\right)^2 \sum_{-\infty}^{+\infty} f^2(x'y')g(x_2)(\Delta x')^2(\Delta y')^2,$$

or

$$D_1(x_2y_2) = C_1 g(x_2y_2),$$

where C_1 is a constant independent of (x_2y_2) given by

$$C_1 = \left(\frac{1}{2\pi}\right)^2 \sum_{-\infty}^{+\infty} f^2(x'y')\Delta x'\Delta y'.$$

It follows that $D_1(x_2y_2)$ is the image of $g(xy)$. Next consider those terms for which $(x'y') = (x_2 - x_0, y_2 - y_0)$. This leads to a function $D_2(x_2y_2)$:

$$D_2(x_2y_2) = \left(\frac{1}{2\pi}\right)^2 \sum_{-\infty}^{+\infty} f(x_2 - x_0, y_2 - y_0)f(x''y'')g(x'' + x_0, y'' + y_0)\Delta x''\Delta y''.$$

Now in the small square that $g(xy)$ is not zero, we have the relation $f(x''y'') = g(x'' + x_0, y'' + y_0)$, and therefore:

$$D_2(x_2y_2) = C_2 f(x_2 - x_0, y_2 - y_0),$$

in which C_2 is a constant independent of (x_2y_2):

$$C_2 = \left(\frac{1}{2\pi}\right)^2 \sum_{-\infty}^{+\infty} g^2(x'' + x_0, y'' + y_0)(\Delta x'')^2(\Delta y'')^2.$$

$D_2(x_2y_2)$ is the ghost image of the whole slide $f(xy)$, displaced over a distance (x_0y_0).

All other terms in the expression for $D(x_2y_2)$ are noise, from the searcher's point of view as discussed above. It is easy to make an estimate of the magnitude of this noise and the signal to noise ratio in the ghost image for certain specific assumptions. Let the rms value of $f(xy)$ in the square with sides l be f_0. Let further the value of $f(xy)$ in a "picture element" $\Delta x\Delta y$ be statistically independent of the value in an adjacent picture element. The total number of terms contributing to the function $D(x_2y_2)$ in a specific point is now of the order of $l^2d^2/(\Delta x\Delta y)^2$, and since all these terms are statistically independent, the rms value will be $[l^2d^2/(\Delta x\Delta y)^2]^{\frac{1}{2}} = ld/\Delta x\Delta y$ times the value of a single term. The rms noise N in the value of $D(x_2y_2)$ in a picture element is therefore: $N = (1/2\pi)^2 f_0{}^2 ld\Delta x\Delta y$. On the other hand, the rms value of the ghost image will be $S = (1/2\pi)^2 f_0 d^2\Delta x\Delta y$. Therefore, the signal-to-noise ratio $S/N \cong d/l$.

With special assumptions, a computation of the signal-to-noise ratio can also be given in the case of continuous functions. In that case we assume $f(xy)$ to be a sample of an ensemble which has certain properties on the average. A computation requires a specific analytical form of the autocorrelation function, and the simplest form for computations, without loss of general validity of the results, is the Gaussian:

$$\langle f(x - \delta, y - \epsilon)f(x + \delta, y + \epsilon)\rangle = f_0{}^2 \exp\left[-\frac{1}{\alpha_0{}^2}(\delta^2 + \epsilon^2)\right],$$

where the brackets $\langle\ \rangle$ signify the ensemble average. Any other analytical form of the autocorrelation function will lead to a numerically different result, but not by a large amount, as long as this function expresses the fact that there is little correlation between two values of $f(xy)$ at a distance α_0.

Since $D(x_2y_2)$ represents the function $f(x_2 - x_0, y_2 - y_0)$ with noise, we will compute:

$$\langle K^2\rangle = \langle [D(x_2y_2) - d_2 f(x_2 - x_0, y_2 - y_0)]^2\rangle,$$

and determine the constant d_2 such that this expression is a minimum. This will give us d_2 and the noise. It should be pointed out that in $D(x_2y_2)$ is also present a contribution of the direct image of $g(xy)$. However, this can be ignored as long as we deal with points outside this image, as will be the case in our calculation. Substitution of the integral expression for $D(x_2y_2)$ gives us:

$$K^2 = \left(\frac{1}{2\pi}\right)^4 \int_{-\infty}^{+\infty} f(x'y')f(x''y'')g(x_2 - x' + x'', y_2 - y' + y'')$$
$$\times f(x''', y''')f(x'''', y'''')g(x_2 - x''' + x'''', y_2 - y''' + y'''')$$
$$\times dx'dy'dx''dy''dx'''dy'''dx''''dy'''' - 2d_2\left(\frac{1}{2\pi}\right)^2 \int_{-\infty}^{+\infty}$$
$$\times f(x'y')f(x''y'')g(x_2 - x' + x'', y_2 - y' + y'')f(x_2 - x_0, y_2 - y_0)dx'dy'dx''dy'' + d_2{}^2 f^2(x_2 - x_0, y_2 - y_0).$$

These expressions now have to be averaged over the ensemble, which can be done by averaging the integrands before integration. The result is:

$$\langle K^2\rangle = \left(\frac{1}{2\pi}\right)^4 f_0{}^6 \frac{\pi^2}{3}\alpha_0{}^4 d^2l^2 - \left(\frac{1}{2\pi}\right)^2 2d_2 f_0{}^4 2\pi\alpha_0{}^2 d^2 + d_2{}^2 f_0{}^2.$$

Minimizing this expression for d_2 gives us:

$$(d_2)_{\min} = \left(\frac{1}{2\pi}\right)^2 2\pi f_0{}^2\alpha_0{}^2 d^2.$$

Therefore, the signal S is given by:

$$S = \left(\frac{1}{2\pi}\right)^2 2\pi f_0{}^2\alpha_0{}^2 d^2.$$

Since $d<<1$, the rms noise N turns out to be:

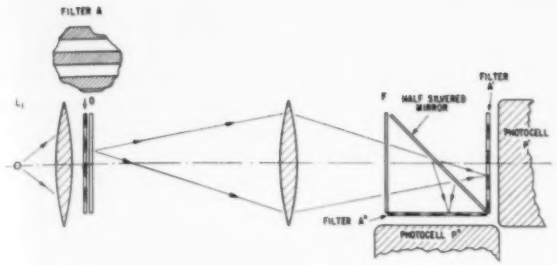

Fig. 3. Redundant information (filter A) for recognizing and partly locating the test object. The difference in photocurrents in P′ and P″ determines the phase of the square wave generated by the ghost image of A.

$$N = \left(\frac{1}{2\pi}\right) f_0^2 \frac{\pi}{\sqrt{3}} \alpha_0^2 dl,$$

and so:

$$\frac{S}{N} = \frac{2}{\sqrt{3}} \frac{d}{l}.$$

This result is satisfactorily close to the estimate made in the case of a discrete function f.

IV. Application of the Ghost Image for Search

When the test object is small, the signal-to-noise ratio in a picture element is also very small. It is equal to the square root of the ratio of the areas of the small fragment and the whole library. It is therefore impossible to read out the ghost image of the library in detail. Only when there are some redundant features present, which allow recognition by averaging over many picture elements, can the ghost image be made useful. To use the ghost image to recognize and locate the test object, there must be present in the original library picture $f(xy)$ redundant information, like a regular structure of lines or points. This structure then serves the same purpose as the racks, shelves, book covers, pages, lines, and letter spacings of an ordinary library.

One system* for recognizing and partially locating a fragment is illustrated in Fig. 3. The intensity filter of the library is formed by illuminating $f(xy)$ at O through a filter A consisting of a number of alternating gray and white stripes. The light to the image plane is split in two by a half-silvered mirror, to give two identical images I′ and I″. In I′ is placed a filter A′ with stripes coinciding with the image of A, while in I″ a similar filter, A″, is present, but displaced one-half stripe width. Two photocells P′ and P″, placed behind these filters, complete the arrangement. A test object in O now will give a displaced image of A in I′ and I″, and this will lead to different currents in P′ and P″. The difference, when large enough, will be a recognition signal, indicating that the test object is in the library, and the ratio of the currents gives the approximate position within a stripe, but it is not yet known which stripe. More elaborate systems can be worked out to give a more exact location.

Another recognition system is to use as a redundant object a strong point source of light in the center of O, which source is coherent with the original light source. The test object now will result in a ghost image of one displaced bright spot in the image plane. To locate such a single spot automatically in a manner which is most advantageous, it would require a television camera tube in the image plane. At this point it is of interest to point out the close relation of this method with the actual matched filter. There is a method* of making a matched filter in an optical arrangement by considering only symmetric objects such that $f(xy) = f(-x, -y)$. In that case the Fourier components $A(kl)$ are real: $A(kl) = A^*(kl)$. However, $A(kl)$ can still be positive or negative. To detect the sign of the amplitude, one can add light in the focal plane F as a constant amplitude A_0. Now the intensity in F is given by $[A_0 + A(kl)]^2 = A_0^2 + 2A_0A(kl) + A^2(kl)$. When $A(kl) << A_0$, then the variable part of this intensity is $2A_0A(kl)$, which is proportional to $A(kl)$. Therefore, by making an intensity filter† we really obtain a matched filter. The constant amplitude A_0, however, must necessarily originate from a point source in the center of O. It follows, therefore, that this method to obtain a matched filter for the special case of symmetric $f(xy)$ is really identical with the case of an intensity filter which uses as a redundant image a point source in the center of O. The light point which will appear when a test object is shown can therefore be looked upon, either as the coincidence peak produced by a matched filter or as the ghost image of the point source produced by an intensity filter.

V. Physical Components of an Optical Search Arrangement

It is quite clear that a workable optical setup for search requires a laser light source of sufficient intensity and stability. It can be shown, for instance, that the number of picture elements cannot be larger than $(\lambda/\Delta\lambda)^2$, when λ is the wavelength of the light and $\Delta\lambda$

* The examples of two systems of locating information given here are not intended to be necessarily practical in detail, but they give the essence of the two methods which can be used. The first one, with a periodic filter, requires a narrow band output detection of a few photocells, the second one, a wide band detector like a television camera tube.

* G. D. Watkins, unpublished, 1954.

† H. Hurwitz suggested as an alternative the use of a photographic plate with a square root blackening curve.

the line-width. However, lasers are in such an active state of development that it is difficult to speak of a physical limit. For the time being, it seems that the limiting element in an optical arrangement will be the resolution of the imaging lens. Imaging lenses which resolve 25,000 lines in an image have been made. This leads to 6×10^8 separate picture elements. Let us assume an average of four picture elements required for one letter in coded form, and 2500 letters per page, then the total library can contain 300 books of 200 pages each.

What size of library fragment could still be recognized? Let us assume the redundant ghost image to be that of a single point in the center of O, and let this be a laser light source of the same strength as the one illuminating the whole picture in O and therefore 6×10^8 times the intensity, or $\sqrt{6 \times 10^8} = 2.5 \times 10^4$ in amplitude, of the light in one picture element. Assuming that a signal-to-noise ratio of 20 is required for recognition, this results in $2.5 \times 10^4\ d/l = 20$, or $d/l = 8 \times 10^{-4}$. Therefore, a fragment of 0.03 pages or about one single line could immediately be recognized and located. It must be remembered that this theoretical figure ignores the physical limitations of light sources and lenses. Only experimental work can determine whether this limit can actually be approached. Like previous work[1] it does point out, however, that optical filters form a promising field of research in information processing.

Something more should be said about the physical form of an intensity filter. Photographic plates can be used in principle, but it may turn out to be very difficult indeed to expose a plate, make a positive, and put it back in exact registry. A much more natural choice for filters are materials which can be bleached while they are left in position. The color centers in alkali halides[4] offer the possibility of bleaching with high quantum efficiency. Alkali halides, therefore, look promising for optical memory filters when visible light lasers can be used. For infrared lasers, so-called deep impurity levels in germanium or silicon[5] can be bleached and therefore these materials may turn out very valuable for this kind of application. It should be pointed out that the optical filters as discussed here must be thin; that is, of the order of one wavelength. The very thought of the above-mentioned materials, however, makes it attractive to investigate the optical storage and the appearance of a ghost image in filters which are no longer thin, but essentially three dimensional. This problem, however, will be discussed in another paper.

The author would like to thank G. D. Watkins and H. Hurwitz for illuminating discussions and useful suggestions made regarding this paper.

References

1. L. J. Cutrona, E. N. Leith, C. J. Palermo, and L. J. Porcello, I.R.E. Trans. **IT-6,** 386 (1960).
2. A. Maréchal, P. Croce, and K. Dietsch, Opt. Acta **5,** 25 (1958).
3. D. Gabor, Nature **161,** 777 (1948); Proc. Roy. Soc. **A197,** 454 (1949); Proc. Phys. Soc. **B64,** 449 (1951).
4. F. Seitz, Revs. Modern Phys. **26,** 7 (1954).
5. R. Newman and W. W. Tyler, Solid State Phys. **8,** 49 (1959).

REFEREES

The following people referee papers submitted to APPLIED OPTICS from time to time, and the Editors wish to acknowledge with gratitude this service:

H. H. Allen, Jr., W. Arnold, G. F. Aroyan, J. G. Atwood, A. V. Baez, J. G. Baker, S. S. Ballard, R. Barakat, R. B. Barnes, E. Barr, E. S. Barr, A. M. Bass, J. R. Benford, L. E. Bergstein, B. H. Billings, L. S. Birks, H. H. Blau, W. S. Boyle, E. Burstein, F. F. Byrne, H. Cary, R. M. Chapman, L. H. Chasson, C. B. Childs, C. H. Church, K. C. Clark, G. W. Cleek, V. J. Coates, R. J. Collins, W. A. Craven, Jr., A. Danti, H. A. Daw, E. S. Dayhoff, J. A. Dobrowolski, K. Dressler, M. Dreyfus, W. G. Driscoll, S. Q. Duntley, D. Dutton, H. Edgerton, A. T. Forester, D. F. Eggers, Jr., R. S. Estey, E. Evtuhov, W. Fastie, D. P. Feder, P. A. Franken, J. S. Garing, N. Ginsburg, J. P. Gordon, G. E. Gross, F. F. Hall, Jr., G. B. Harrison, L. W. Herscher, M. Herzberger, I. C. Hisatsune, R. E. Hopkins, G. A. Hornbeck, E. O. Hulburt, R. S. Hunter, W. L. Hyde, J. A. Hynek, S. S. Impiombato, J. S. Johnson, R. C. Jones, R. N. Jones, K. Innes, J. A. Jamieson, L. D. Kaplan, S. Katz, J. W. Kemp, K. G. Kessler, J. I. F. King, R. Kingslake, W. F. Koehler, N. Kreidl, E. W. Kutzscher, J. Lambe, E. Leith, E. V. Lowenstein, D. J. Lovell, C. F. Luck, T. K. McCubbin, R. K. McDonald, R. H. McFee, J. R. McNally, Jr., R. W. McQuaid, R. P. Madden, A. D. May, A. B. Meinel, P. E. Mengers, L. H. Meuser, D. F. Nelson, L. S. Nelson, P. Nolan, L. J. Nugent, J. Parsons, P. S. Pershan, F. H. Perrin, G. N. Plass, E. K. Plyler, H. D. Polster, R. Potter, R. W. Powell, D. Richardson, D. W. Robinson, D. Z. Robinson, N. Rosenberg, J. A. Sanderson, J. B. Saunders, A. L. Schawlow, B. F. Scribner, J. H. Shaw, W. A. Shurcliffe, E. H. Siegler, W. Sinton, F. D. Smith, E. Snitzer, P. P. Sorokin, I. Spiro, V. J. Stakutis, O. N. Stavroudis, S. Sternberg, H. S. Stewart, B. Stoicheff, G. W. Stroke, R. E. Stroup, F. J. Studer, R. Tabeling, R. M. Talley, Y. Tanaka, R. W. Terhune, R. Tousey, A. F. Turner, G. Turrell, J. Valasek, G. A. Vanasse, M. E. Warga, J. U. White, B. W. Wild, P. G. Wilkinson, P. A. Wilks, Jr., V. Z. Williams, D. E. Williamson, M. K. Wilson, W. Wolfe, E. M. Wormser, N. Wright, H. W. Yates, M. Zelikoff, and G. J. Zissis.

Theory of Optical Information Storage in Solids

P. J. van Heerden

In photography, information is stored in a medium which is essentially two-dimensional. Three-dimensional optical storage is possible in semitransparent colored materials, like alkali halides with color centers. With the use of coherent light sources, like lasers, large amounts of information can be stored in the volume, and retrieved with little interference. The storage of information is accomplished by the formation of interference patterns between each two plane parallel waves. This paper develops the theory of this form of storage. It turns out that the information storage capacity is as if every little cube with sides equal to the wavelength of light acts as an independent information storage cell, and the essential noise in recovering this information is only the statistical fluctuation in the number of color centers in such a cube. The storage capacity is therefore of the order of 10^{12}–10^{13} bits per cm^3. The main property of this way of information storage is the appearance of a "ghost image," partly but not completely analogous to the one described previously. This property makes three-dimensional storage very suitable for associative memories. The theory lends support to Beurle's proposed mechanism of information storage in the brain.

I. Introduction

The usual way of storing information optically, as in photography, is in a thin layer that is essentially two-dimensional. This paper will discuss optical information storage in thick, three-dimensional media. The method of storage can be, for instance, by the bleaching of color centers[1] in alkali halides. Three-dimensional optical information storage becomes possible only because of the development of sufficiently bright coherent light sources in the form of lasers. With coherent light sources, as will be shown, information can be stored "in bulk" and recovered with little error.

The physical principle of three-dimensional information storage described here is the formation of interference patterns by plane waves of the same frequency but of different directions. However, interference patterns formed by light of other frequencies can be stored in the same space without confusion. The basic idea is not new. It was first demonstrated by Seebeck[2] in 1810. He showed the reproduction of colors in silver chloride after exposure to light. Lippman, in 1891, demonstrated color photographies based on this principle, which he called "interference heliography."

A different and more obvious way of storing information optically in three dimensions is as is actually done in a nuclear track plate. Here every small volume element—instead of the interference pattern extending through the whole volume—contains a specific amount of information. In this method, since the resolution of optical instruments is limited to a volume with a diameter equal to the wavelength of light λ, every cube with side λ could act as an independent information storage element. With a wavelength $\lambda = 1\ \mu$, this would lead to a storage capacity of the order of 10^{12} bits per cm^3. It will be shown that the information storage with interference patterns has essentially the same capacity.

The importance of storage by interference patterns is that it allows simultaneous, and therefore fast, search for a specific piece of information through the whole memory. It is similar in this respect to the two-dimensional optical memory already described by the author.[3] It is similar to this also in its operation, in that recovery of information is based on the generation of a ghost image. There are differences, however, which will be brought out in the discussion.

Beurle[4] has proposed essentially the same mechanism of information storage in the human brain, based on interaction of waves propagated by neuron networks. The theory of three-dimensional optical storage given in this paper lends support to his hypothesis.

II. The Principle of Three-Dimensional Storage

The recovery of information stored by bleaching is accomplished by the diffracted light that accompanies every nonuniform absorption in the medium. Consider

The author is with the Polaroid Corporation, Cambridge 39 Mass.

Received 23 July 1962.

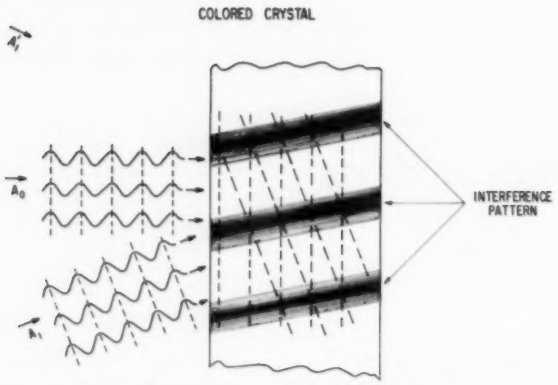

Fig. 1. Bleached interference pattern of two waves $\mathbf{A}_0$ and $\mathbf{A}_1$. The pattern consists of planes such that the reflection of the direction of propagation of $\mathbf{A}_0$ is that of $\mathbf{A}_1$, and vice versa.

as a medium an alkali halide crystal which has been discolored by well-known methods[1] to add so-called color centers or F-centers. Let the total absorption of light in crystal, for this color band, be of the order of 10%. When the color centers are distributed homogeneously in the crystal, no more diffraction of light will take place in the crystal than would be caused by a simple aperture of the same dimensions. This means that the diffraction pattern has an angular width around the direction of incidence of a beam of light of λ_0/a, when λ_0 is the wavelength and a the side of the crystal.

Now let us assume that the crystal is bleached in a way which is not homogeneous through the volume. Bleaching of color centers can take place by irradiation with light in the color band. This bleaching, for low intensities, is proportional to the light absorbed and takes place with rather high quantum efficiency. In particular it will be assumed (Fig. 1) that the crystal is bleached simultaneously by two beams of light, represented by the amplitude vectors $\mathbf{A}_0$ and $\mathbf{A}_1$, respectively. The two light beams have different directions but the same frequency λ_0. After bleaching, the color centers will no longer be distributed homogeneously in the crystal, because of the interference pattern formed by the amplitudes $\mathbf{A}_0$ and $\mathbf{A}_1$. It will be shown in the next section that this bleaching pattern consists of alternating lighter and darker planes, at equal distances from each other. These planes are such that the direction of propagation of $\mathbf{A}_1$ is the reflection in this plane of $\mathbf{A}_0$, and vice versa.

Suppose that next this bleached crystal is illuminated with $\mathbf{A}_0$ only, and let us assume that in this second illumination the bleaching effect can be neglected. (This is possible by using only a short illumination time, or by fixing the bleaching, which in alkali halides can be achieved by lowering the temperature.[1]) Now the bleached crystal will show, besides the direct beam, one single strong diffracted plane wave in the original direction of $\mathbf{A}_1$. This phenomenon is analogous to the reflection of an x-ray beam in a crystal by crystallographic planes. The condition, that the amplitudes of waves diffracted from different parallel planes add up in phase (Bragg relation), is automatically satisfied in the interference pattern.

Assuming this to be true for the moment, we can then understand how all information which can be stored in a black and white transparent slide can also be stored in a colored crystal. Consider (Fig. 2) such a slide in the object plane of an imaging arrangement. The slide is illuminated by a coherent parallel light beam of amplitude $\mathbf{A}_0$. The light will be diffracted by the slide to give parallel light beams of different directions, with amplitudes $\mathbf{A}_1, \mathbf{A}_2, \ldots, \mathbf{A}_n$, respectively. Assume these amplitudes to be weak with respect to $\mathbf{A}_0$, then the bleaching patterns in the colored crystal placed behind the slide will mainly consist of the interference patterns $(\mathbf{A}_0, \mathbf{A}_1)$ through $(\mathbf{A}_0, \mathbf{A}_n)$. When now after bleaching the slide is removed, and the bleached

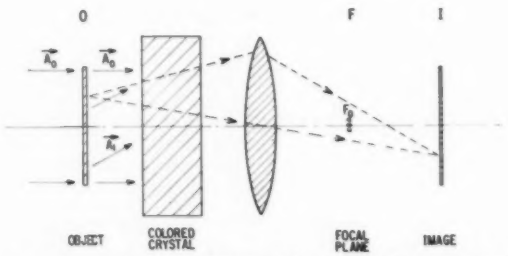

Fig. 2. Storage in the crystal, by bleaching, of the image of a picture in O. It can be reproduced by illuminating with $\mathbf{A}_0$.

crystal is illuminated directly with $\mathbf{A}_0$, then there will be regenerated in the crystal all waves $\mathbf{A}_1$ to $\mathbf{A}_n$, in the same amplitude and phase relations as they originated in the original slide, with very little distortion. Therefore an image of the original slide will be formed in the image plane I of the imaging arrangement.

Actually, this arrangement is very similar to the one already given by Gabor[5], who used a (two-dimensional) photographic plate at the position of the colored crystal. In the bleached crystal, however, an ambiguity is removed which is still present in Gabor's method of imaging. As is clear in Fig. 1, a pattern produced by the interference of $\mathbf{A}_1$ with $\mathbf{A}_0$ can also be produced by a second beam $\mathbf{A}_1'$ with $\mathbf{A}_0$ when the pattern is stored only in a two-dimensional slice.

III. Quantitative Description

The amplitude vector $\mathbf{A}$ of any light wave in space can be described by a sum of plane waves of complex amplitude $\mathbf{A}_i = A_{i0} \exp[i(k_i x + l_i y + m_i z - \omega_i t)]$, in which (xyz) are the spatial coordinates and t is the time.

k_i, l_i, m_i, and ω_i obey the relation $k_i^2 + l_i^2 + m_i^2 = \omega_i^2/c_0^2$, where c_0 is the velocity of light. **A** will stand for the electrical vector in the wave only, since it is responsible for the interaction with the color centers.

Consider the bleaching in the case that **A** is the sum of two plane waves only, of different directions, but of the same frequency ω_0: $\mathbf{A} = \mathbf{A}_0 + \mathbf{A}_1$. The intensity of this light wave is equal to the scalar product $(\mathbf{A},\mathbf{A}^*)$, in which $\mathbf{A}^*$ is the complex conjugate of **A**. The bleaching in the colored crystal, that is, the change in the initial absorption coefficient α_0 due to exposure to light during a time t_1, may be called β, and is proportional to the intensity: $\beta = bt_1(\mathbf{A},\mathbf{A}^*)$.

After bleaching, the crystal is illuminated with $\mathbf{A}_0$ only, and we have to evaluate the light diffracted in the different directions. The application of Huygens principle leads to the conclusion that every volume element $\Delta V = \Delta x \Delta y \Delta z$ that absorbs part of the light will also emit a diffracted spherical wave of amplitude $\Delta B(x_2y_2z_2)$ such that:

$$\Delta B(x_2y_2z_2) = -A_0(xyz)\frac{2\alpha}{\lambda_0 r'}\cos\varphi_{01}\Delta V \exp[i(k'x' + l'y' + m'z' - \omega_0 t)].$$

In this expression, we have introduced the scalar amplitude ΔB and A_0 (in italics), which represents the total length of the vector, but still with the complex phase factor. $\alpha = \alpha_0 - \beta$ is the absorption coefficient in the volume ΔV, and φ is the angle between the vector $\mathbf{A}_0$ and its projection on the plane perpendicular to the distance vector $\mathbf{r}' = (x', y', z') = (x_2 - x, y_2 - y, z_2 - z)$. $(k', l', m') = (2\pi/r'\lambda_0)(x', y', z')$ (Fig. 3).

The factor of proportionality $(2\alpha/\lambda_0 r')\Delta V$ can be derived from the consideration that the spherical wave at large distances interferes destructively with $\mathbf{A}_0$, leading to an energy loss in the illuminating beam, and to conserve energy this must be equal to the energy actually absorbed in the volume element ΔV. It is derived in Appendix I. The factor $\cos\varphi$ originates in the fact that the electrical vector represented by ΔB must fall in the plane formed by $\mathbf{A}_0$ and $\mathbf{r}'$, and also must be perpendicular to $\mathbf{r}'$.

A crystal with an absorption coefficient α which is uniform throughout the crystal will not give any substantial diffraction. Therefore we only have to consider the interference pattern in the bleaching term, given by: $bt_1[(\mathbf{A}_0, \mathbf{A}_1^*) + (\mathbf{A}_0^*, \mathbf{A}_1)]$. Considering only the second term $(\mathbf{A}_0^*, \mathbf{A}_1)$, and writing $(\mathbf{A}_0^*, \mathbf{A}_1) = A_0^* A_1 \cos\theta_{01}$, where θ_{01} is the angle between the vectors $\mathbf{A}_0$ and $\mathbf{A}_1$, then this term will lead to a diffracted wave with amplitude:

$$\Delta B = \frac{2bt_1}{\lambda_0 r'}\cos\varphi_{01}\cos\theta_{01}A_0 A_0^* A_1 \Delta V \exp \times [i(k'x' + l'y + m'z' - \omega_0 t)].$$

For r' large with respect to the dimensions of the crystal, (k', l', m') becomes practically independent of (xyz), and we can write: $(k', l', m') \rightarrow (k_2, l_2, m_2) = (2\pi/r_2\lambda_0)(x_2, y_2, z_2)$ and $r' \rightarrow r_2 = \sqrt{x_2^2 + y_2^2 + z_2^2}$. In substituting this in the expression for ΔB, and also the value for (x', y', z') and $A_i = A_{i0}\exp[i(k_1x + l_1y + m_1z - \omega_0 t)]$, we obtain:

$$\Delta B = \frac{2bt_1}{\lambda_0 r_2}\cos\varphi_{01}\cos\theta_{01}A_{00}A_{00}^*A_{10} \times \exp[i(k_2x_2 + l_2y_2 + m_2z_2 - \omega_0 t)] \times \exp\{i[(k_1 - k_2)x + (l_1 - l_2)y + (m_1 - m_2)z]\}\Delta x\Delta y\Delta z.$$

To find the total amplitude B of the diffracted wave, we must integrate this over all volume elements $\Delta x \Delta y \Delta z$ of the crystal. This leads to the integral I:

$$I = \int_v \exp[i\{(k_1 - k_2)x + (l_1 - l_2)y + (m_1 - m_2)z\}]dx\,dy\,dz = \frac{i}{(k_1 - k_2)(l_1 - l_2)(m_1 - m_2)}\{\exp[i(k_1 - k_2)a] - 1\} \times \{\exp[i(l_1 - l_2)a] - 1\} \times \{\exp[i(m_1 - m_2)d] - 1\}.$$

Since k, l, and m are of the order of $1/\lambda_0$, I is small of the order λ_0^3 when $(k_1l_1m_1)$ and $(k_2l_2m_2)$ are widely apart. However, when $(k_2l_2m_2)$ approaches $(k_1l_1m_1)$ then, in the limit: $I \rightarrow a^2d = V$. *The conclusion is therefore that the bleaching term* $(\mathbf{A}_0^*, \mathbf{A}_1)$ *gives rise to a diffracted wave with a negligible amplitude in all directions except in the original direction of propagation of* $\mathbf{A}_1$, in which case the amplitude is given by:

$$B_1(x_2y_2z_2) = \frac{2bt_1a^2d}{\lambda_0 r_2}\cos\varphi_{01}\cos\theta_{01}A_{00}A_{00}^*A_{10} \times \exp[i(k_1x_2 + l_1y_2 + m_1z_2 - \omega_0 t)].$$

This amplitude at distance r_2 can be reduced to the amplitude of the wave at the position of the crystal with the factor derived in the Appendix I:

$$B_1(k_1l_1m_1) = 2bt_1d\cos\varphi_{01}\cos\theta_{01}A_{00}A_{00}^*A_{10} \times \exp[i(k_1x_2 + l_1y_2 + m_1z_2 - \omega_0 t)].$$

When we now consider again Fig. 2, where $\mathbf{A}_1$ originates in a slide illuminated by $\mathbf{A}_0$, then $\cos\varphi_{01} = \cos\theta_{01}$. Therefore, it is clear that all waves $\mathbf{A}_1, \ldots, \mathbf{A}_n$ originally generated in the object slide will be regenerated by the illumination of the bleached crystal by $\mathbf{A}_0$ with the proper amplitude and phase, since all

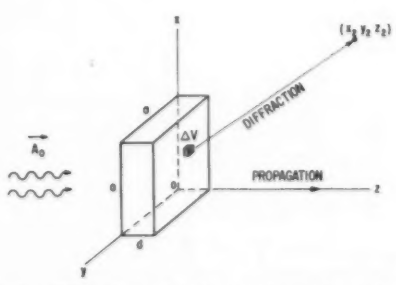

Fig. 3. Diffraction of $\mathbf{A}_0$ by a volume element ΔV.

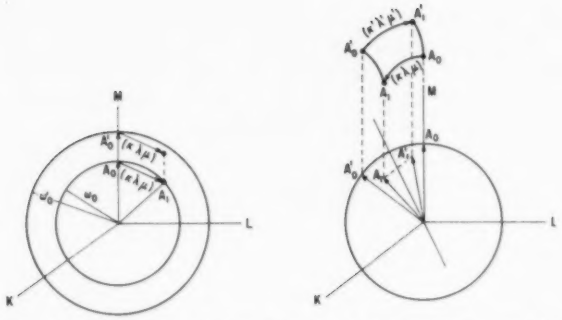

Fig. 4. Illuminating vectors A_0 and A_0' of different frequencies and directions. For different frequencies, A_0' is not diffracted by the bleaching plane (k,λ,μ). For different directions A_0' is diffracted by (k,λ,μ) only in a special case.

amplitudes are multiplied with the positive factor: $2bt \cos^2 \theta_{0f} A_{00} A_{00}^*$. The only distortion in the reproduction is the term $\cos^2\theta_{0f}$ which tends to reduce resolution in the reproduction of details of the order λ_0.

IV. Simultaneous Storage of Several Pictures

The fact that a two-dimensional picture is stored in a three-dimensional medium suggests that the storage space is not used to full capacity. This is actually the case. Many pictures can be stored simultaneously in a crystal, either by illuminating these pictures with light beams of different wavelengths or of different directions. This is most easily seen by representing an interference pattern like ($\mathbf{A}_0^*$, $\mathbf{A}_1$) as a vector (κ, λ, μ) = ($k_1 - k_0$, $l_1 - l_0$, $m_1 - m_0$) in momentum space (Fig. 4). This vector, added to ($k_0 l_0 m_0$) representing the direction of A_0, gives the vector ($k_1 l_1 m_1$) of the diffracted wave A_1. When one would illuminate the bleached crystal with light presented by ($k_0' l_0' m_0'$) in the same direction but of different frequency ω_0', no diffracted wave results, because the vector ($k_0' + \kappa$, $l_0' + \lambda$, $m_0' + \mu$) must satisfy the condition that the total length is equal to ω_0'/c_0, meaning that the diffracted wave has the same frequency as the illuminating wave. It can be seen from Fig. 4 that this condition cannot be satisfied. Said in different terms, it means that, although a bleaching plane (Fig. 1) in the crystal will show a reflected wave, the reflected waves from different planes will not add up in phase, since Bragg's relation is not satisfied. Many pictures of different frequencies can be stored, therefore, simultaneously without confusion. The disadvantage is, of course, that the bleaching for every picture becomes weaker, since the total bleaching cannot exceed the original coloring of the crystal.

In a similar way, different pictures can be stored by illuminating with light beams A_0 and A_0' of the same frequency ω_0 but of different directions [Fig. 4(b)]. It is impossible to draw vectors (κ, λ, μ) and (κ', λ', μ') from the end of A_0 and A_0' which are parallel, of equal length, and such that their end point lies on the sphere of radius ω_0, except for a special case. This is the situation that the end points of these vectors fall in the plane which reflects A_0 into A_0'. Therefore, there is an ambiguity in regenerating the pictures only as far as the e special vectors A_1 and A_1' are concerned. The over all disturbance in the pictures is minor however, and so many can be stored with different directions A_0' without causing excessive noise.

In principle it is possible to store time-dependent signals in the three-dimensional medium. The requirement is that the time duration of the signal is less than it takes the light to traverse the crystal. This means that it would be necessary to modulate coherent light sources with frequencies comparable to the frequency of light itself. No physical principle is available, nor is any in sight, by which this could be accomplished. It is still of some interest to discuss this case, because of the storage of slower wave phenomena, which will be mentioned in Section VIII. Imagine, therefore, (Fig. 5) that in O every picture element varies its transmission in time independent of every other picture element, resulting in a movie of some very fast phenomenon. To be able to reproduce this movie from the bleaching in the storing crystal, there is only one restriction, which is the following: Consider the transmission $D_i(t)$ as a function of time in a picture element i, and write $D_i(t)$ as a Fourier sum:

$$D_i(t) = \sum_{-n}^{+n} C_{in} \exp[in\omega t].$$

The restriction is now that, in comparing C_{in} and C_{jn} in any two picture elements i and j, the ratio C_{in}/C_{jn} must be a real positive number. This reduces the possible information content of the movie by about 50%. When this is satisfied, since a Fourier component D_{in} gives rise to a light wave with frequency $\omega_0 + n\omega$, by the modulation of $\mathbf{A}_0$, all wavelets emanating from different picture elements of that frequency will be exactly in phase. It is now the strong wave of frequency $\omega_0 + n\omega$, parallel to the optical axis, which forms the main interference pattern with all diffracted

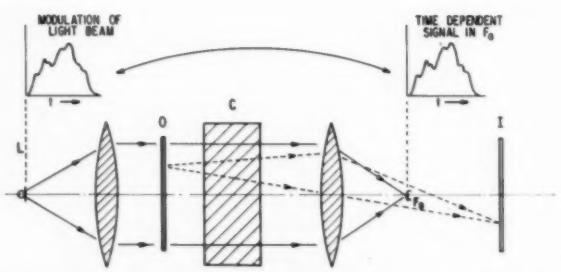

Fig. 5. Reproduction of time dependent signals. Amplitude modulating of L with a pulse of a specific shape will reproduce the movie.

waves of the same frequency but of different directions. To regenerate the movie from the bleached crystal, it is only necessary to reproduce simultaneously all these waves, of different frequencies but parallel to the optical axis, with the proper phase relations. In principle, this can be done as follows. All these waves are focused in the focal point F_0 of the imaging lens. They will add to the amplitude of the original frequency ω_0 to give a time-dependent signal in F_0. Amplitude modulation of the original illuminating beam of frequency ω_0 with this signal is therefore identical with generating these different frequencies $\omega_0 + n\omega$ in the proper amplitude- and phase relations. This can be accomplished in principle by an amplitude varying element close to L_0. By merely illuminating the bleached crystal with this pulse of light, the whole movie would be regenerated.

V. The Information Storage Capacity

The general considerations determining the storage capacity by bleaching can be given in a simple way. This will lead to an order of magnitude number for this capacity. Let us first consider the number of independent information cells present in a crystal of dimensions $a \times a \times d$ cm³ (Fig. 2). A wave in a direction $(k_1 l_1 m_1)$ emerging from a $a \times a$ cm² aperture will show, as is well known, a narrow diffraction pattern of a solid angle $\sim\lambda^2/a^2$. Therefore, about a^2/λ^2 independent directions can be recognized. In the same way, the number of independent wavelengths λ that can be stored in the crystal depends on the thickness d. It is known, for instance from the resolving power of echelon gratings, that the number of separately resolved wavelengths is given by $\sim d/\lambda_0$, where λ_0 is the average wavelength. The total number n of independent storage cells is therefore given by $n_0 \cong a^2 d/\lambda_0^3 = V/\lambda_0^3$. This number is the same as when the information would be stored in specific small volumes, like in the nuclear track plate, instead of in interference patterns.

To know the storage capacity, it is necessary to know, besides the number of independent storage cells, the signal-to-noise ratio in each cell. It was shown already in Section III that the noise introduced in the regeneration of the vector A_1 by the other bleaching pattern $A_0 A_j$ is very small, since it is of the order $\lambda_0^3/V = 1/n_0$. The noise introduced in A_0 by all n_0 vectors A_j will only increase this by a factor $\sqrt{n_0}$. The total noise in A_j caused by the other bleaching terms is therefore of the order $1/\sqrt{n_0}$, which is still small.

The main fundamental source of noise is the random distribution of color centers in the crystal, in the same way as the random distribution of electrons in a beam gives rise to shot noise. Let there be N_0 color centers per cm³ in the crystal. In a bleaching pattern $(\kappa_1 \lambda_1 \mu_1)$ in the crystal, there will be, according to the laws of probability, about $\sqrt{N_0 V}$ more color centers in the positive part of this pattern than in the negative part,

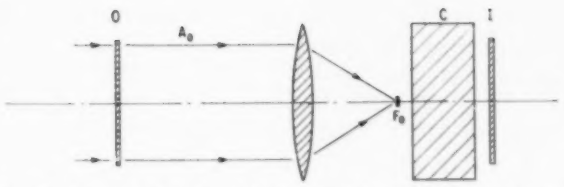

Fig. 6. Storage of an image in the crystal with the center beam A_0 cut off.

or vice versa. This constitutes the noise N_p in the amplitude. To estimate the signal, there are n independent bleaching patterns, and in a certain point these patterns can be positive or negative; therefore the total bleaching amplitude will be $\sim\sqrt{n}$ times the average bleaching amplitude A_p of a single pattern. Since there are $N_0 V$ color centers available for bleaching, $A_p \cong N_0 V/\sqrt{n}$. The signal-to-noise ratio S_p/N_p is therefore given by: $S_p/N_p = \sqrt{N_0 V/n}$. When the storage space is filled to capacity, $n = n_0 = V\ \lambda_0^3$, and $S_p/N_p = \sqrt{N_0 \lambda_0^3}$.

This result is again as if every cube with side λ_0 acts as a separate storage cell. The signal is then equal to the number $N_0 \lambda_0^3$ of color centers in that cube, and the noise is the root mean square fluctuation in that number, which is $\sqrt{N_0 \lambda_0^3}$.

The storage capacity C in bits is equal to the number of independent storage cells times the logarithm to the base two of the signal-to-noise ratio: $C \cong n_0 \log_2 S_p/N_p$. As an example, take a crystal of $1 \times 1 \times 1$ cm³, with $N_0 = 10^{15}$ color centers per cm³, which would give about 25% absorption. Let λ_0 be 1 μ. In that case: $C \cong 10^{12}$ $\log_2 10^3 \cong 10^{13}$ bits.

VI. The Appearance of a Ghost Image

In the previous paper[2] describing two-dimensional information storage, it was shown that a ghost image of the whole object will appear in the image plane, when only a small fragment is illuminated in the object plane. The same is true for three-dimensional storage. The important difference is that when the fragment is displaced from its original position, no ghost image will appear.

To demonstrate this ghost image, let us consider Fig. 6. To avoid the effect of the central light beam A_0, the parallel light illuminating the transparency is now focused in a point and blocked off. Only the waves diffracted by the object will bleach the crystal. Let these parallel waves originating in O again be called $A_1, A_2, \ldots, A_n$. The bleaching is again described as proportional to

$$\sum_1^n ij[A_i A_j^* + A_i^* A_j].$$

Let, further, the wave amplitude in the ith direction as generated by the small fragment be called A_i', and

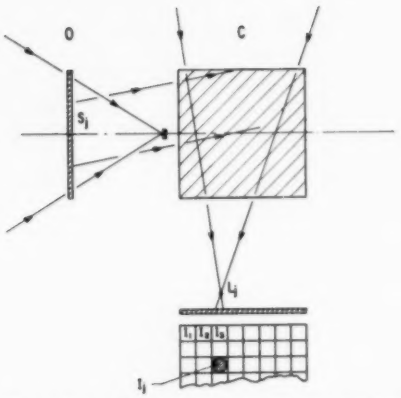

Fig. 7. Three-dimensional storage as an associative memory. Exposure of S_j in O after bleaching will reproduce a ghost image of L_j, which in turn will illuminate I_j.

the wave in the same direction be generated by the rest of the object A_i''. So $A_i = A_i' + A_i''$. Now let the crystal be illuminated by the light from the fragment only, that is, by $A_1', A_2', \ldots A_n'$. The amplitude of the wave generated in the direction i will now be proportional to $\sum j[A_iA_j^* + A_i^*A_j]A_j'$. But since $A_j = A_j' + A_j''$, $A_j^* = A_j'^* + A_j''^*$, this sum contains the part:

$$\sum jA_i[A_j'A_j'^*].$$

Since $[A_j'A_j'^*]$ is positive, all these terms add up in phase, and the intensity with which A_i is generated is simply proportional to $\sum j[A_j'A_j'^*]$, which means proportional to the energy of the light emitted by the picture fragment. All components of the original object are therefore regenerated in the proper magnitude and phase, and a ghost image will appear in I. This ghost image is therefore analogous to the one in the two-dimensional case,[3] and will require no further discussion. In particular, this is true for the other terms in the bleaching which can be considered as noise.

On the other hand, suppose that the fragment is displaced by an amount $(x_0y_0z_0)$ from its original position. Every wave A_i', in the second illumination, will have acquired an extra phase factor $\exp[i\varphi_i] = \exp[i(k_ix_0 + l_iy_0 + m_iz_0)]$, when $(k_il_im_i)$ is the direction of the wave. The contribution to A_i, instead of being the sum of positive quantities: $\sum j[A_j'A_j'^*]$, will now be $\sum jA_j'A_j'^* \exp[i\varphi_j]$. Since the factor $\exp[i\varphi_j]$ is different for every j, and distributed randomly over the phase circle, the terms will sometimes add, sometimes subtract, and the sum will be negligibly small for large n. The ghost image therefore will have disappeared.

VII. The Use of Three-Dimensional Storage as an Associative Memory

In this section will be shown how three-dimensional storage can be used as what is called an associative memory. Suppose we want to build a machine which can face many situations in each of which it has to carry out a different instruction. Suppose, moreover, that both the situation and the instruction can be coded as information in a black and white transparency. An example is a translating machine, in which the situation is an English sentence in a standard type, while the instruction is the translation of this sentence into a foreign language. In this particular example, it is possible to arrange all situations $S_1, S_2, \ldots, S_n$ in an alphabetical order, with the instructions $I_1, I_2, \ldots, I_n$ written behind them. This is called a catalog memory, not an associative memory, because a fast systematic search for a specific situation S_i and its instruction I_i is possible. In many cases an alphabetical ordering of instructions may not be possible or desirable. In that case a memory is useful which allows a fast search for a situation-instruction pair regardless of its ordering. This is an associative memory.

Consider Fig. 7. The situation S_i is coded as a transparency S_i in 0. The transparency is illuminated by a converging light beam L_0 in F, where the direct light of the beam is blocked off. The diffracted light containing the black and white information will illuminate the crystal. A second converging light beam L_i, coherent with L_0, is made to illuminate the crystal simultaneously. L_i is focused in a point just above a transparency I, divided into n squares, in each of which an instruction, I_i, is written. And, of course, L_i is focused in such a position that it illuminates I_i. Suppose now that all situations S_i are stored subsequently, each with its own light source L_i illuminating I_i. When now an arbitrary situation S_j is put in the object plane, a ghost image of L_j will appear. A television camera tube focused on the whole plane I can locate L_j and move a second camera tube over to this spot to read out the instruction I_j.

It might be said that a simpler arrangement of the memory is possible (Fig. 8), in which S_i and I_i are stored simultaneously by illumination in O. When in a search S_j is put in the object plane, the instruction I_j will appear as a ghost image in the image plane. However, this arrangement has a serious disadvantage, in that two different situations S_j and S_k may have parts which are identical. In that case the appearance of S_j in O will cause the ghost images I_j and I_k to appear simultaneously in I, giving rise to confusion. It

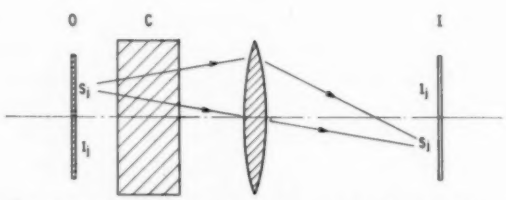

Fig. 8 A simplified associative memory subject to noise.

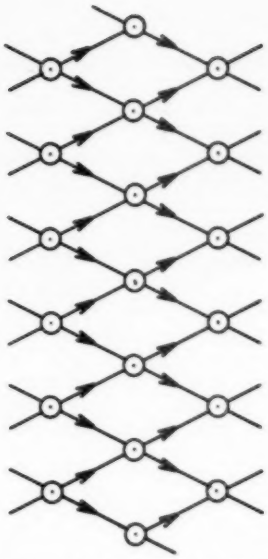

Fig. 9. Simple neuron network obeying Huygens principle.

seems desirable, therefore, to have in an optical associative memory always two separate storage spaces. One where all information is mixed together, which allows a quick search, and one area where different items of information are kept separate, to maintain a noise-free readout.

VIII. A Possible Analogy with Information Storage in the Brain

Beurle[4] proposed an information storage mechanism for the brain by the interaction of propagating waves. There is a rather complete analogy between Beurle's principle of storage of information by brain waves, which are propagated by brain cells and which modify the properties of these cells in a permanent way, and the principle of bleaching by coherent light waves developed in this paper. Actually, since our theory is more quantitative, it may add some details to Beurle's hypothesis.

Clearly, our theory of three-dimensional storage of information holds for any wave phenomenon that obeys Huygens principle and in which a permanent change in the propagation is brought about by the energy of the waves (sound waves, spin waves or microwaves may be considered). Without going into details about any model, any regular neuron network (Fig. 9) can be imagined to satisfy this principle, in that every cell in a layer passes an impulse, in the form of an electrical potential, on to several cells in the next layer. What supports Beurle's hypothesis in our theory is that it shows the very large amount of information that could be stored in the brain in this manner. When the frequencies in the waves are sufficiently high, or, in other words, when the pulse times are shorter than the time of propagation between two cells, then the amount of information that can be stored is of the same order as the number of brain cells. On the other hand, the quantitative theory points out the necessity of maintaining exact phase relations in the waves over large distances. Any change in the speed of propagation in one part of the neuron network compared to the speed in another part would scramble the information in a hopeless way. It seems therefore necessary to assume a calibrating system of pulses in the brain, which at all times checks this and compensates, if necessary, the speed of propagation. The detailed model of an optical associative memory in the previous section also points out the desirability of two different regions of storage. One region where all information of passed experience is mixed to make fast search and recognition possible; and a second region where the information about different situations is stored separately.

IX. Conclusions

The mathematical theory of three-dimensional optical information storage by bleaching shows how very large amounts of information can be stored. The manner of storage by interference patterns of waves make it particularly suitable for associative memories, in which a fast search for a specific piece of information is possible. The theory is applicable to any other wave phenomenon in solids which can effect a permanent or temporary change in the propagation properties. The detailed theory lends support to Beurle's hypothesis, that information in the human brain is stored in this manner.

The author would like to thank G. D. Watkins for a valuable discussion of this paper.

Appendix I

With the direction of the light beam $\mathbf{A}_0$ along the Z-axis, the decrease of A_0 over a thickness Δz will be $A_0\alpha\Delta z$. This means there is an energy loss ΔE in the volume element ΔV given by $\Delta E = A_0A_0^*[1 - (1 - \alpha\Delta z)^2]\Delta x\Delta y$, or $\Delta E = 2A_0A_0^*\alpha\Delta V$.

Let the amplitude of the diffracted spherical wave be represented by $\Delta B/r$. The parallel wave $\mathbf{A}_0$ will be diffracted by the aperture, formed by the crystal with sides a, into a narrow cone of angle λ_0/a. At large distances r from the crystal, this amplitude will be decreased therefore by a factor inversely proportional to the square root of the area over which it has spread. This amplitude therefore will be A_0a^2/λ_0r. The spherical wave $\Delta B/r$ will interfere destructively with the wave in the forward direction, to give an energy loss

$$\Delta E_1 = \left(A_0\frac{a^2}{\lambda_0 r} - \frac{\Delta B}{r}\right)^2 \frac{\lambda_0^2}{a^2} r^2 = -2A_0\Delta B\lambda_0.$$

Conservation of energy requires that $\Delta E_1 = \Delta E$, and therefore:

$$\Delta B = A_0 \frac{2\alpha}{\lambda_0} \Delta V.$$

It is true that the spherical wave $\Delta B/r$ represents an additional amount of energy in directions other than the forward one, but this contains the factor $[(2\alpha/\lambda_0)\Delta V]^2$, and therefore may be neglected in this computation, since $(2\alpha/\lambda_0)\Delta V \ll 1$.

References

1. R. W. Pohl, Physik. Z. **39,** 36 (1938); F. Seitz, Rev. Modern Phys. **26,** 7 (1954).
2. *Encyclopædia Britannica,* Photography, Colour (U. of Chicago Press, Chicago, 1947), Vol. 17, p. 816.
3. P. J. van Heerden, Appl. Opt. **2,** 387 (1963).
4. R. L. Beurle, Phil. Trans. Roy. Soc. London, Ser. B, **240,** 55 (1956).
5. D. Gabor, Nature **161,** 777 (1948); Proc. Roy. Soc. **A197,** 454 (1949); Proc. Phys. Soc. **B64,** 449 (1951).

SUMMER COURSE IN MODERN OPTICS

Institute of Optics, University of Rochester

The Institute of Optics will offer a special noncredit course in Modern Optics during 8–27 July 1963. The first week will be devoted to an intensive presentation of fundamentals: basic properties of sources, optical systems, and detectors. The second and third weeks will discuss the design of optical imaging systems and multilayer filters; this portion of the course is an expanded and updated version of "Modern Methods in Optical Design" (first presented in Summer 1962). A tentative outline of course organization follows:

General Principles of Optics (8–13 July 1963)

Topics: Generation of electromagnetic radiation with wavelength in the range 100Å–50 μ (including conventional and laser sources), basic properties and types of imaging systems, dispersing instruments and filtering systems, properties of optical image detectors.
Staff: Professors Hopkins, Givens, Boynton, Baumeister, Eyer, and Murty
Invited lecturers include:
Eli Snitzer (American Optical) "Optical Masers"
David Richardson (Bausch & Lomb) "Gratings"
R. Bolling Barnes (Barnes Engineering) "Infrared Detectors"

Optical Imaging Systems and Multilayer Filter Design (15–20 July 1963)

Topics: Fundamentals of optical design: ray tracing on computers, aberration theory, interpolation polynomials, automatic correction procedures, image evaluation, lens testing; multilayer filters: methods of computation and production, antireflection coatings for the visible and infrared, multilayers with period structure.
Staff: Professors Hopkins, Givens, Baumeister, Murty, Spencer, and Eyer
Invited lecturers include:
Adriaan Walthers (Diffraction Ltd.) "Diffraction Theory"
Emil Wolf (University of Rochester) "Coherence Theory"
J. A. Dobrowolski (National Research Council, Ottawa) "Automatic Methods of Multilayer Design"

A special seminar, "Optical Shop Practices," will be held on 20 July 1963. Participants: F. Cooke, W. Klinkert, N. Hochgraf

Optical Imaging Systems and Multilayer Filter Design (22–27 July 1963)

Topics: Design of refracting and reflecting systems—telescope optics, Petzval types, telephotos, triplets, eyepieces, immersion systems, special systems; multilayer filters—quarter-wave stacks, bandpass filters, the Herpin equivalent index, beam splitters and dichroic mirrors, laser coatings, narrow band interference filters, inhomogeneous coatings.
Staff: Same as for second week
Invited Lecturers include:
W. Lewis Hyde (American Optical) "Space Optics"
Roderic Scott (Perkin-Elmer) "Space Optics"
J. W. Hicks (Mosaic Fabrications) "Fiber Optics"
Rudolph Kingslake (Eastman Kodak) "Lens Types"

Tuition

The tuition fee of $200/week includes extensive course notes. Students are permitted to register for the first week only, for the first and second weeks, for the second and third weeks, or for the complete three week sequence. Persons with limited formal training in optics are advised to consider the first week as a prerequisite to the more advanced discussions of the following weeks.

Correspondence

A formal brochure and enrollment application will be available shortly. Correspondence concerning this course should be sent to: Institute of Optics Summer Course, University of Rochester, River Campus Station, Rochester 20, New York.

One- and Two-Dimensional Processing in Line Scanning Systems

L. G. Callahan and W. M. Brown

The performance of line scanning systems is analyzed in this paper. The results apply to systems such as infrared scanners, TV systems, and radar systems. The main objective of the analysis is to compare the performance obtainable when optimum two-dimensional processing of the data is used and the performance obtainable when only one-dimensional (along the lines) processing is used. Optimization under the constraint that only processing along the lines is available is a new and interesting problem in optimum filter theory, and the results are of practical importance since in most systems this constraint is imposed. Since it is possible to modify the systems to accommodate arbitrary two-dimensional processing at the expense of some system complexity, it is important to determine the corresponding performance improvement. The emphasis is on the general theory, and many special cases deserve quantitative treatment. In this paper quantitative comparisons are made for two cases; specifically, top hat and cone-shaped frequency responses of the aperture are considered. These characteristics occur in coherent and incoherent scanners in which the "resolution" is limited by the optical aperture of the scanner. Three performance criteria are used: least-squares error, maximum-peak signal to rms noise ratio, and minimum system resolution. Table I shows the improvement of arbitrary two-dimensional filtering over one-dimensional filtering along the lines.

Introduction

Many optical processes of image formation, image transfer, and image analysis may be represented as one or a succession of linear transformations of a two-dimensional signal from an object plane into a two-dimensional response in an image plane. This representation is the spatial equivalent of one-dimensional time transformations performed by electrical networks. Therefore, many of the concepts and techniques normally associated only with linear electrical systems can be extended to problems involved in the analysis and synthesis of optical imaging systems. For example, a radiation pattern in the object plane can be represented by two-dimensional Fourier components just as a voltage input to an electric circuit is commonly represented by one-dimensional Fourier frequency components. Further, imperfect lens, grain on photographic film, and other imperfections in optical components which tend to degrade the performance of optical systems can be considered in the same perspective as electrical noise.

In recent years, these and other equivalences have been noted and used by a number of investigators in the solution of various types of optical problems.[1-22] However, aside from the work of Elias, Jones, O'Neill, and Wessley, relatively little attention has been directed at the optimization of line scan imaging systems.[10,11,13,15,22] Although both Mertz and Schade used two-dimensional electrical techniques for the analysis of line scan systems, they did not concern themselves with the optimization problem.[14,21]

Line scan imaging systems denote the class of imaging systems such as television, facsimile, and airborne infrared mapping devices which record input spatial signals as sequences of parallel lines in accordance with a specified scanning pattern. Interest in this class of systems has been largely motivated by the desire to reduce two-dimensional spatial data to one-dimensional electrical data to facilitate recording or transmission over electrical communication channels. Consequently, the notion of an aperture moving with a constant velocity along the scan lines, and producing a continuous one-dimensional, modulated signal at the output of the system, has generally been accepted as a model of the scanning system by previous investigators. Influenced by this model, most processing of data produced by existing physical scanning systems is effected in only one dimension even though it is intuitively apparent that processing in two dimensions should result in improved performance. The

L. G. Callahan is the Executive Officer at the U.S. Army Research Office, Durham, North Carolina. W. M. Brown is in the Electrical Engineering Department and Institute of Science and Technology of The University of Michigan.

Received 30 April 1962.

Table I. Improvement Factors Afforded by Optimum Two-Dimensional Processing over Optimum One-Dimensional Processing

Criteria	Pre-filter frequency response	
	Top hat	Cone
Least-squares error low noise level (white spectra)	$\pi/4$	$\pi^2\sqrt{\left(\frac{\text{Noise power den.}}{\text{Signal power den.}}\right)}$
$\frac{\lvert\text{Peak signal}\rvert^2}{\text{Mean square noise}}$	$\frac{3\pi}{8}$	1.3
Resolution	1	2/3

purpose of this paper is to present a new model for the analysis of line scan imaging systems which permits the quantitative comparison of optimum one- and two-dimensional linear filtering operations. Optimum filters are derived which are optimum under three different criteria, least-squares error, spatial resolution, and noise-to-signal ratio.

Line Scan Filter Model

The basic model adopted in this paper is indicated in Fig. 1. A single scanning aperture, or possibly an aggregate of electro-optical collection devices which record a signal for processing, is represented as a pre-filter. Thus, if $f_1(x,y)$ represents a spatial signal in an object plane, and $a_1(x,y)$ represents the over-all spatial impulse response of the pre-filter, then the output for a linear system is

$$f_2(x,y) = \iint_{-\infty}^{\infty} a_1(x-u,\, y-v) f_1(u,v)\,du\,dv$$

or

$$= a_1 * f_1. \tag{1}$$

The sampler in Fig. 1 represents the scanning pattern which limits the observed data to a set of parallel lines. Thus, if the scan pattern permits continuous observation in the x coordinate, but at discrete positions in the y coordinate with spacing Δy, the output of the sampler on any line may be expressed as

$$\tilde{f}_2(x, m\Delta y) = \iint_{-\infty}^{\infty} a_1(x-u,\, m\Delta y - v) f_1(u,v)\,du\,dv, \tag{2}$$

where m indicates the integer index of the sample line

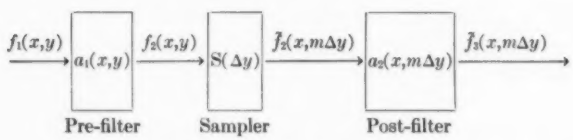

Fig. 1. Line scan filter model.

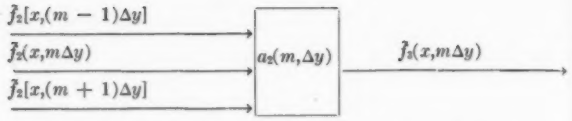

Fig. 2. Two-dimensional semidiscrete linear filter.

along the y spatial coordinate, and the tilde denotes sampled functions which will be termed semidiscrete functions.

The post-filter is considered a two-dimensional semidiscrete, linear operator which has available sets of parallel data lines for simultaneous processing, and is depicted in Fig. 2. The input–output relationships of the post-filter are defined in terms of a two-dimensional semidiscrete convolution operation as

$$\tilde{f}_3(x, m\Delta y) = \int_{-\infty}^{\infty} \sum_{i=-\infty}^{\infty} \tilde{a}_2(x-u,\, m\Delta y - i\Delta y)\tilde{f}_2(u, i\Delta y)\,du\,\Delta y \tag{3}$$

or

$$\tilde{f}_3 = \tilde{a}_2 \tilde{*} \tilde{f}_2.$$

From Eq. (3), the impulse response of a post-filter which processes continuously in only one dimension is immediately defined when

$$\tilde{a}_2(x, m\Delta y) = \begin{cases} \hat{a}_2(x) \text{ if } m = 0, \\ 0 \text{ if } m \neq 0. \end{cases} \tag{4}$$

The circumflex on right-hand side of Eq. (4) indicates a one-dimensional function.

It is readily apparent that the manipulation of Eqs. (1) and (3) is greatly simplified by the use of Fourier transforms. For example, if continuous spatial frequency functions are defined as

$$F(k_1, k_2) \equiv \iint_{-\infty}^{\infty} f(x,y) \exp\,[-2\pi j(k_1 x + k_2 y)]\,dx\,dy, \tag{5}$$

where k_1 and k_2 are wave numbers or spatial frequencies, then the inversion formula is

$$f(x,y) = \iint_{-\infty}^{\infty} F(k_1, k_2) \exp\,[2\pi j(k_1 + k_2 y)]\,dk_1 dk_2. \tag{6}$$

By the convolution theorem, Eq. (1) may be expressed simply as

$$F_2(k_1, k_2) = F(k_1, k_2) A_1(k_1, k_2), \tag{7}$$

where F_2, F_1, A_1 represent the Fourier transforms of f_2, f_1, and a_1, respectively.

Similarly, if semidiscrete frequency functions are defined as

$$\tilde{F}(k_1, k_2) \equiv \int_{-\infty}^{\infty} \sum_{m=-\infty}^{\infty} \tilde{f}(x, m\Delta y) \exp\,[-j2\pi(k_1 x + k_2 m\Delta y)]\,dx\,\Delta y, \tag{8}$$

their inversion formula can be shown to be

$$\tilde{f}(x, m\Delta y) = \int_{-\infty}^{\infty}\int_{-1/2\Delta y}^{1/2\Delta y} F(k_1, k_2) \exp\,[j2\pi(k_1 x + k_2 m\Delta y)]\, dk_2 dk_1 \quad (9)$$

and Eq. (3) may be expressed simply as

$$\tilde{F}_3(k_1, k_2) = \tilde{F}_2(k_1, k_2)\tilde{A}_2(k_1, k_2), \quad (10)$$

where $\tilde{F}_3$, $\tilde{F}_2$, and $\tilde{A}_2$ are the semidiscrete transforms of $\tilde{f}_3$, $\tilde{f}_2$, and $\tilde{a}_2$, respectively.

Least-Square Optimization

Ensemble autocorrelation and cross-correlation functions for continuous spatially stationary signals are defined as

$$R_{f_1}(x, y) \equiv E[f_1(x + \alpha, y + \beta)f_1(\alpha, \beta)] \text{ or } R_{f_1} = E[f_1 f_2], \quad (11)$$

$$R_{f_1+f_2} \equiv E[f_1(x + \alpha, y + \beta)f_2(\alpha, \beta)] \text{ or } R_{f_1+f_2} = E[f_1 f_2], \quad (12)$$

where E denotes the ensemble expectation. Signals are spatially stationary if their statistical behavior is dependent only on the incremental distance between two points in the plane. The ensemble autocorrelation and cross-correlation functions for semidiscrete stationary signals are defined as

$$\tilde{R}_{f_1}(x, m\Delta y) \equiv E[\tilde{f}_1(x + \alpha, m\Delta y + \rho\Delta y)\tilde{f}_1(\alpha, \rho\Delta y)] \text{ or } \tilde{R}_{f_1} = E[\tilde{f}_1\tilde{f}_1], \quad (13)$$

$$\tilde{R}_{f_1+f_2}(x, m\Delta y) \equiv E[\tilde{f}_1(x + \alpha, m\Delta y + \rho\Delta y)\tilde{f}_2(\alpha, \rho\Delta y)] \text{ or } R_{f_1+f_2} = E[\tilde{f}_1\tilde{f}_2]. \quad (14)$$

Using definitions of the type indicated in Eqs. (5) and (8), Fourier transforms can be applied to both the continuous and semidiscrete auto- and cross-correlation functions to obtain power density spectra. Thus, if $G_f(k_1, k_2)$ denotes the transform of $R_f(x, y)$ from relationships of the type indicated in Eqs. (6) and (11), it is seen that

$$E[f_2^2] = R_f(0,0) = \int_{-\infty}^{\infty}\int_{-1/2\Delta y}^{1/2\Delta y} G_f(k_1, k_2)dk_2 dk_1 \quad (15)$$

by the inversion formula applied at zero.

Similarly, from Eqs. (9) and (13), the mean square error for the semidiscrete case is

$$E[\tilde{f}^2] = \tilde{R}_f(0,0) = \int_{-\infty}^{\infty}\int_{-1/2\Delta y}^{1/2\Delta y} \tilde{G}_f(k_1, k_2)dk_2 dk_1. \quad (16)$$

From Eqs. (11)–(14), it is demonstrated in ref. 4 that the relationships between the continuous and semidiscrete spectra are

$$\tilde{G}_f(k_1, k_2) = \sum_{m=-\rho}^{\infty} G_f[k_1, k_2 + (m/\Delta y)], \quad (17)$$

$$\tilde{G}_{f_1+f_2}(k_1, k_2) = \sum_{m=-\infty}^{\infty} G_{f_1+f_2}[k_1, k_2 + (m/\Delta y)]. \quad (18)$$

Input–output relationships of the type indicated in Eqs. (1) and (7) can be expressed in terms of correlation functions or their Fourier transforms as

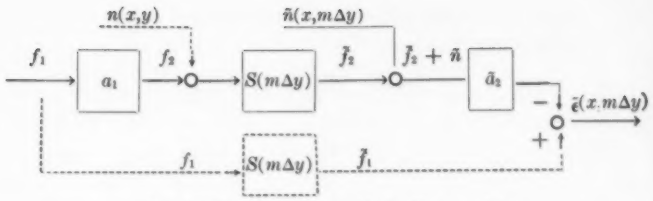

Fig. 3. Least-square optimization model.

$$R_{f_2} = R_{f_1} * a_1 * a_{1-} \text{ or } G_{f2} = G_{f_1}|A_1|^2, \quad (19)$$

$$R_{f_1 f_{2+}} = R_{f_1} * a_1 \text{ or } G_{f_1 f_{2+}} = G_{f_1}A_1, \quad (20)$$

$$R_{f_1+f_2} = R_{f_1} * a_{1-} \text{ or } G_{f_1+f_2} = G_{f_1}\bar{A}_1. \quad (21)$$

In Eqs. (19)–(21), the $a-$ represents a reflection, thus

$$a_{1-} = a_1(-x, -y). \quad (22)$$

Of course, $\bar{A}$ indicates the conjugate of A. Input–output relationships similar to Eqs. (19)–(21) apply also for semidiscrete signals and filters, and will subsequently be indicated by a tilde.

Returning to the optimization problem, Fig. 1 can be modified as depicted in Fig. 3, and a system error defined as the difference between the input and output signal on corresponding lines, or

$$\tilde{\epsilon} \equiv \tilde{f}_1 - \tilde{f}_3 = \tilde{f}_1 - (\tilde{f}_2 + n) * \tilde{a}_2. \quad (23)$$

This definition facilitates comparison of the error with one- and two-dimensional processing since the performance is measured in terms of the estimate of f_1 only on the scan lines. The philosophy of this error criterion deserves some discussion; however, such a discussion would not add to the main objectives of this paper and hence will be omitted. Suffice it to say that when the sampling rate is sufficiently high [see Eq. (47)], the criterion of estimating f_1 everywhere can be formulated and is found to lead to the same values for the mean square errors involved.

An internal additive (usually white) noise has been introduced into the system. It can account for various sources of noise such as detector noise in an infrared system, or film grain. It is shown in ref. 4 in a photographic system that a continuous two-dimensional white noise process can be made statistically equivalent to a semidiscrete noise process on corresponding sample lines if

$$G_n(k_1, k_2) = \begin{cases} \Delta y \hat{G}_n(k_1) & |k_1| < 1/2\Delta y, \\ 0 & |k_1| > 1/2\Delta y. \end{cases} \quad (24)$$

$\hat{G}_n$ is the power spectrum of the one-dimensional noise on each scan line. Independence is assumed from line to line for the noise. Thus, although the semidiscrete noise in Fig. 3 enters the system after the sampler, it is statistically equivalent to the continuous noise indicated by the dotted lines in Fig. 3.

Optimization with Two-Dimensional Post Filtering

From Eqs. (13) and (23), the autocorrelation function of the error signal is

$$\tilde{R}_\epsilon = E[\tilde{\epsilon}_+\tilde{\epsilon}] = E\ [\tilde{f}_{1+} - (\tilde{f}_2 \ast \tilde{a}_2)_+ - (\tilde{n} \ast \tilde{a}_2)_+] \\ [\tilde{f}_1 - (\tilde{f}_2 \ast \tilde{a}_2) - (\tilde{n} \ast \tilde{a}_2)]. \quad (25)$$

Expanding and assuming that the signal and noise are uncorrelated and have mean zero, Eq. (25) leads to

$$\tilde{R}_\epsilon = (\tilde{R}_{f_2} + \tilde{R}_n) \ast \tilde{a}_2 \ast \tilde{a}_{2-} - \tilde{R}_{f_1 f_{2+}} \ast \tilde{a}_2 - \tilde{R}_{f_1 + f_2} \ast \tilde{a}_2 + \tilde{R}_{f_1} \quad (26)$$

or, in the frequency domain,

$$\tilde{G}_\epsilon = (\tilde{G}_{f_2} + \tilde{G}_n)|\tilde{A}_2|^2 - \tilde{G}_{f_1+f_2}\tilde{A}_2 - \tilde{G}_{f_1 f_2}\tilde{A}_2 + \tilde{G}_{f_1}. \quad (27)$$

Completing the square, Eq. (27) may be written as

$$\tilde{G}_\epsilon = \left|(\tilde{G}_{f_2} + \tilde{G}_n)^{1/2}\tilde{A}_2 - \frac{G_{f_1+f_2}}{(\tilde{G}_{f_2} + \tilde{G}_n)^{1/2}}\right|^2 \frac{\tilde{G}_{f_1 f_2 +}\tilde{G}_{f_1+f_2}}{(\tilde{G}_{f_2} + \tilde{G}_n)} + \tilde{G}_{f_1}. \quad (28)$$

The mean square error is

$$E[\tilde{\epsilon}^2] = \int_{-\infty}^{\infty}\int_{-1/2\Delta y}^{1/2\Delta y} \tilde{G}_\epsilon(k_1, k_2)dk_2dk_1, \quad (29)$$

From Eqs. (28) and (29), it is clear that when

$$\tilde{A}_{2\ \mathrm{opt}} = \frac{\tilde{G}_{f_1+f_2}}{(\tilde{G}_{f_2} + \tilde{G}_n)} \quad (30)$$

the minimum mean square error is obtained as

$$E[\tilde{\epsilon}^2]_{\min} = \int_{-\infty}^{\infty}\int_{-1/2\Delta y}^{1/2\Delta y} \tilde{G}_f dk_2dk_1 - \int_{-\infty}^{\infty}\int_{-1/2\Delta y}^{1/2\Delta y} \frac{\tilde{G}_{f_1+f_2}\tilde{G}_{f_1 f_2 +}}{\tilde{G}_{f_2} + \tilde{G}_n} dk_2dk_1. \quad (31)$$

From Eqs. (17) and (18), Eq. (30) may be written in terms of continuous spectra as

$$\tilde{A}_{2\ \mathrm{opt}} = \frac{\sum_{m=-\infty}^{\infty} G_{f_1+f_2}(k_1, k_2 + (m/\Delta y))}{\sum_{m=-\infty}^{\infty} G_{f_2}[k_1, k_2 + (m/\Delta y)] + \tilde{G}_n(k_1, k_2)}, \quad (32)$$

continuous pre-filter and input signal spectra as

$$\tilde{A}_{2\ \mathrm{opt}} = \frac{\sum_{m=-\infty}^{\infty} \tilde{A}_1[k_1, k_2 + (m/\Delta y)]G_{f_1}[k_1, k_2 + (m/\Delta y)]}{\sum_{m=-\infty}^{\infty} |A_1[k_1, k_2 + (m/\Delta y)]|^2 G_{f_1}[k_1, k_2 + (m/\Delta y)] + \tilde{G}_n(k_1, k_2)}. \quad (33)$$

In the same manner, the least-square error with the optimum two-dimensional post-filter is

$$E[\epsilon^2] = \int_{-\infty}^{\infty}\int_{-1/2\Delta y}^{1/2\Delta y} \sum_{m=-\infty}^{\infty} G_{f_1}[k_1, k_2 + (m/\Delta y)]dk_2dk, \\ \left|\sum_m A_1[k_1, k_2 + (m/\Delta y)]G_{f_1}[k_1, k_2 + (m/\Delta y)]\right|^2 \\ - \int_{-\infty}^{\infty}\int_{-1/2\Delta y}^{1/2\Delta y} \frac{}{\sum_m |A_1[k_1, k_2 + (m/\Delta y)]|^2} dk_2dk_1. \\ \times G_{f_1}[k_1, k_2 + (m/\Delta y)] + G_n(k_1, k_2) \quad (34)$$

Optimization with Processing Only Along the Lines

From Eqs. (4), (8), (9), (13), and (14) let

$$\hat{G}_\epsilon(k_1) = \int_{-1/2\Delta y}^{1/2\Delta y} G_\epsilon(k_1, k_2)dk_2 \quad (35)$$

and replace $\tilde{A}^2$ by

$$\tilde{A}_2(k_1, k_2) = \Delta y\hat{A}_2(k_1). \quad (36)$$

The mean square error may be expressed as

$$E[\epsilon^2] = R_\epsilon(0) = \int_{-\infty}^{\infty} G_\epsilon(k_1)dk_1. \quad (37)$$

To determine the one-dimensional spectrum G_ϵ, we have from Eqs. (28), (35), and (36)

$$\hat{G}_\epsilon(k_1) = (\Delta y)^2|\hat{A}_2|^2 \int_{-1/2\Delta y}^{1/2\Delta y} (\tilde{G}_{f_2} + \tilde{G}_n)dk_2 \\ - \Delta y\hat{A}_2 \int_{-1/2\Delta y}^{1/2\Delta y} \tilde{G}_{f_1+f_2}dk_2 \quad (38) \\ - \Delta y\hat{A}_2 \int_{-1/2\Delta y}^{1/2\Delta y} \tilde{G}_{f_1+f_2} + \int_{-1/2\Delta y}^{1/2\Delta y} \tilde{G}_{f_1}dk.$$

Completing the square, Eq. (38) may be expressed in the same form as Eq. (28), or

$$\hat{G}_\epsilon(k_1) = \left|\left[(\Delta y)^2 \int_{-1/2\Delta y}^{1/2\Delta y} (\tilde{G}_{f_2} + \tilde{G}_n)dk_2\right]^{1/2} \right. \\ \left. \times \frac{\hat{A}_2 - \Delta y \int_{-1/2\Delta y}^{1/2\Delta y} \tilde{G}_{f_1+f_2}dk_2}{\left[(\Delta y)^2 \int_{-1/2\Delta y}^{1/2\Delta y} (\tilde{G}_{f_2} + \tilde{G}_n)dk_2\right]^{1/2}}\right|^2 \\ - \frac{\int_{-1/2\Delta y}^{1/2\Delta y} \tilde{G}_{f_1+f_2}dk_2 \int_{-1/2\Delta y}^{1/2\Delta y} \tilde{G}_{f_1 f_2 +}dk_2}{\int_{-1/2\Delta y}^{1/2\Delta y} (\tilde{G}_{f_2} + \tilde{G}_n)dk_2} + \int_{-1/2\Delta y}^{1/2\Delta v} \tilde{G}_{f_1}dk_2. \quad (39)$$

Again the first term on the right-hand side reduces to zero if

$$\hat{A}_2(k_1)_{\mathrm{opt}} = \frac{\int_{-1/2\Delta y}^{1/2\Delta y} G_{f_1+f_2}dk_2}{\Delta y \int_{-1/2\Delta y}^{1/2\Delta y} (\tilde{G}_{f_2} + \tilde{G}_n)dk_2} \quad (40)$$

and the least-square error for an optimum one-dimensional post-filter is

$$E[\hat{\epsilon}^2]_{\min} = \int_{-\infty}^{\infty}\int_{-1/2\Delta y}^{1/2\Delta y} \tilde{G}_{f_1} dk_1 dk_1 - \int_{-\infty}^{\infty} \frac{\int_{-1/2\Delta y}^{1/2\Delta y} \tilde{G}_{f_1+f_2} dk_2 \int_{-1/2\Delta y}^{1/2\Delta y} \tilde{G}_{f_1+f_2} dk_2}{\int_{-1/2\Delta y}^{1/2\Delta y} (\tilde{G}_{f_2} + \tilde{G}_n) dk_2} dk_1. \quad (41)$$

As previously demonstrated in Eqs. (33) and (34), the optimum one-dimensional post-filter and the corresponding least-square error can be expressed in terms of the continuous pre-filter and input signal spectra as

$$\bar{A}_1(k_1)_{\text{opt}} = \frac{\int_{-1/2\Delta y}^{1/2\Delta y} \sum_{m=-\infty}^{\infty} \bar{A}_1[k_1, k_2 + (m/\Delta y)] G_{f_1}[k_1, k_2 + (m/\Delta y)] dk_2}{\Delta y \int_{-1/2\Delta y}^{1/2\Delta y} \sum_{m=-\infty}^{\infty} \{G_{f_1}[k_1, k_2 + (m/\Delta y)] \times |A_1[k_1, k_2 + (m/\Delta y)]|^2 + G_n(k_1, k_2)\} dk_2} \quad (42)$$

and

$$E[\hat{\epsilon}^2]_{\min} = \int_{-\infty}^{\infty}\int_{-1/2\Delta y}^{1/2\Delta y} \sum_{m=-\infty}^{\infty} G_{f_1}[k_1, k_2 + (m/\Delta y)] dk_2 dk_1 - \int_{-\infty}^{\infty} \frac{\left| \int_{-1/2\Delta y}^{1/2\Delta y} \sum_{m=-\infty}^{\infty} A_1[k_1, k_2 + m/(\Delta y)] G_{f_1}[k_1, k_2 + (m/\Delta y)] dk_2 \right|^2}{\int_{-1/2\Delta y}^{1/2\Delta y} \left\{ \sum_{m=-\infty}^{\infty} G_{f_1}[k_1, k_2 + (m/\Delta y)] \times |A_1[k_1, k_2 + (m/\Delta y)]|^2 + \tilde{G}_n(k_1, k_2) \right\} dk_2} dk_1 \quad (43)$$

Applications

As an application of the theory presented above, let the pre-filter consist of a single, two-dimensional aperture limited by system self-noise generated by a continuous two-dimensional white noise process. Let the pre-filter have a top hat spatial frequency response, i.e.,

$$A_1(k_1, k_2) = \begin{cases} 1 \sqrt{k_1^2 + k_2^2} < B/2, \\ 0 \quad \text{otherwise.} \end{cases} \quad (44)$$

This response is characteristic of some types of coherent scanning systems. Let the input signal be composed of detail with a constant spectra and no background noise, i.e., let

$$G_{f_1}(k_1, k_2) = C. \quad (45)$$

If the system self-noise has a constant one-dimensional spectrum, then from Eqs. (17) and (24)

$$\tilde{G}_n(k_1, k_2) = \Delta y N. \quad (46)$$

Finally, to simplify the solution, it is assumed that

$$A_1(k_1, k_2) = 0, \ |k_2| > 1/2\Delta y,$$

and

$$G_{f_1}(k_1, k_2) = 0, \text{ whenever } A_1(k_1, k_2) = 0. \quad (47)$$

Substituting Eqs. (44)–(47) in Eq. (33), it is seen that the optimum two-dimensional post-filter is

$$\bar{A}_2(k_1, k_2)_{\text{opt}} = \frac{BC}{BC + N} \sqrt{k_1^2 + k_2^2} < B/2 \quad (48)$$

and from Eq. (42), the optimum one-dimensional filter is

$$\bar{A}_2(k_1)_{\text{opt}} = \frac{B^2 C}{BC + N} \ | k_1 | < B/2. \quad (49)$$

From Eqs. (34) and (43), the corresponding least-square errors are

$$E[\hat{\epsilon}^2]_{\min} = \frac{\pi C B^2}{4} \left(1 - \frac{C}{C - (N/B)} \right) \quad (50)$$

and

$$E[\hat{\epsilon}^2]_{\min} = CB^2 \sqrt{\frac{N}{N + BC}} \tan^{-1} \sqrt{\frac{N}{N + BC}}. \quad (51)$$

When the noise is very small, the approximate least-square errors are

$$E[\hat{\epsilon}^2]_{\min} \simeq \frac{\pi BN}{4}, \ [N \ll BC] \quad (52)$$

and

$$E[\hat{\epsilon}^2]_{\min} \simeq BN. \quad [N \ll BC] \quad (53)$$

Thus, the ratio of the least square errors is

$$\frac{E[\epsilon^2]_{\min}}{E[\epsilon^2]_{\min}} \simeq \frac{\pi}{4}. \quad (54)$$

Next a cone frequency response is considered for the pre-filter. This response has application to incoherent scanning systems when an optical aperture limits the resolution.

$$A_1(k_1, k_2) = \frac{B - \sqrt{k_1^2 + k_2^2}}{B}. \quad [\sqrt{k_1^2 + k_2^2} < B] \quad (55)$$

After some rather lengthy manipulations, the least-mean square errors are found to be

$$E[\hat{\epsilon}^2]_{\min} = \pi B \sqrt{2NBC} \tan^{-1} \sqrt{\frac{2BC}{N}} \quad (56)$$

and

$$E[\hat{\epsilon}^2]_{\min} = \frac{\pi B^2 C}{3} + \frac{8B^2 C}{3} \sqrt{\frac{N}{N + (BC/6)}} \tan^{-1} \sqrt{\frac{N}{N + (BC/6)}}. \quad (57)$$

When the noise is very small, the approximate least-square errors are

$$E[\tilde{\epsilon}^2]_{\min} \simeq \frac{\pi^2}{\sqrt{2}} B\sqrt{NBC} \left[N \ll \frac{BC}{6}\right] \tag{58}$$

and

$$E[\hat{\epsilon}^2]_{\min} \simeq \frac{\pi B^2 C}{3} + 16\,BN. \quad \left[N \ll \frac{BC}{6}\right] \tag{59}$$

Thus, the ratio of the least-square errors is

$$\frac{E[\tilde{\epsilon}^2]_{\min}}{E[\hat{\epsilon}^2]_{\min}} \simeq \frac{3\pi}{\sqrt{2}} \sqrt{\frac{N}{BC}}. \tag{60}$$

It is noted that, in the case of no noise, both the one- and two-dimensional least-square errors with the top hat pre-filter and the two-dimensional least-square error for the cone pre-filter reduce to zero. However, in the case of the one-dimensional least-square error for the cone pre-filter, there is a constant term which depends only on the signal.

Resolution and Signal-to-Noise as Criteria

In this section the response to point targets is considered. In this case it is common to evaluate the performance in terms of the peak signal-to-rms noise ratio. Also, a resolution criterion can be used. Neither of these criteria uses statistics (such as G_f) of the scene viewed, and the resolution criterion does not even use statistics of the "receiver" noise. Such criteria tend to be more useful in applications, but probably less precise as a measure of performance. The mathematics involved in the use of signal-to-noise and resolution criteria are quite similar; signal-to-noise ratios will be considered first. As before [Eq. (47)] the sampling rate will be assumed high enough that no folding need be considered.

The mean square noise out is

$$\int_{-\infty}^{\infty}\int_{-1/2\Delta y}^{1/2\Delta y} \tilde{G}_n(k_1, k_2)|\tilde{A}_2(k_1, k_2)|^2 dk_1 dk_2. \tag{61}$$

If the input is a point target at (0,0), the signal out is the following (f_1 is taken as a δ-function):

$$\int_{-\infty}^{\infty}\int_{-1/2\Delta y}^{1/2\Delta y} \exp\left[jk_1 x + jk_2 m\Delta y\right] A_1(k_1, k_2)\tilde{A}_2(k_1, k_2) dk_1 dk_2. \tag{62}$$

The peak signal response can be made to occur anywhere, $x=0$, $m=0$ is taken to be specific. If arbitrary two-dimensional processing is permitted, then the problem is to maximize the following over all possible $\tilde{A}_2(k_2, k_2)$:

$$\frac{S}{N} = \frac{\left|\int_{-\infty}^{\infty}\int_{-1/2\Delta y}^{1/2\Delta y} A_1(k_1, k_2)\tilde{A}_2(k_1, k_2) dk_1 dk_2\right|^2}{\int_{-\infty}^{\infty}\int_{-1/2\Delta y}^{1/2\Delta y} |\tilde{A}_2(k_1, k_2)|^2 \tilde{G}_n(k_1, k_2) dk_1 dk_2}. \tag{63}$$

The Swartz inequality is applied to the numerator to obtain the following ($\tilde{G}_n$ is introduced in the numerator as a weight function):

$$\left|\iint \frac{A_1}{\tilde{G}_n} A_2 \tilde{G}_n\right|^2 \le \left(\iint \left|\frac{A_1}{\tilde{G}_n}\right|^2 \tilde{G}_n\right)\left(\iint |A_2|^2 \tilde{G}_n\right) \tag{64}$$

with equality if and only if $\tilde{A}_2 = CA_1/\tilde{G}_n$ where C is any (nonzero) constant. Thus if arbitrary processing is permitted, the maximum peak signal-to-rms-noise ratio is

$$\int_{-\infty}^{\infty}\int_{-1/2\Delta y}^{1/2\Delta y} \frac{|A_1|^2}{\tilde{G}_n} dk_1 dk_2. \tag{65}$$

If the processing is constrained to be only along the scan lines, then as before replace $\tilde{A}_2(k_1, k_2)$ with $\Delta y \tilde{A}_2(k)$. Now in Eqs. (61) and (62) the integration of k_2 can be carried out. This gives

$$\frac{S}{N} = \frac{\left|\int_{-\infty}^{\infty} \tilde{A}_2(k_1)\left(\int_{-1/2\Delta y}^{1/2\Delta y} A_1(k_1, k_2) dk_2\right) dk_1\right|^2}{\int_{-\infty}^{\infty} |\tilde{A}_2(k_1)|^2 \left(\int_{-1/2\Delta y}^{1/2\Delta y} \tilde{G}_n(k_1, k_2) dk_2\right) dk_1}. \tag{66}$$

The maximum follows from (66) by Swartz, inequality:

$$\tilde{A}_2(k_1) = \frac{\int_{-1/2\Delta\epsilon}^{1/2\Delta y} \tilde{A}_1(k_1, k_2) dk_2}{\int_{-1/2\Delta y}^{1/2\Delta y} \tilde{G}(k_1, k_2) dk_2}$$

and the maximum signal to noise is

$$\int_{-\infty}^{\infty} \left[\frac{\left|\int_{-1/2\Delta y}^{1/2\Delta y} A_1(k_1, k_2) dk_2\right|^2}{\int_{-1/2\Delta y}^{1/2\Delta y} \tilde{G}_n(k_1, k_2) dk_2}\right] dk_1. \tag{67}$$

The loss in performance as measured in terms of signal-to-noise ratio can now be determined if specific A_1 and $\tilde{G}_n$ are considered. The results for a top hat and for a cone pre-filter (A_1) are as follows:

$$\frac{(S/N)_{2d}}{(S/N)_{1d}} = \frac{3\pi}{8}$$

for the top hat case; and by numerical integration, 1.3 in the case of a cone response.

Turning to the resolution criterion, an equivalent "rectangle" measure of resolution will be used (cf. ref. 3, chap. 5). If $\tilde{f}_2(x, m\Delta y)$ is the response of the system to a point target and if $\tilde{f}_2$ has its maximum value at (0,0), then the measure of resolution is taken as

$$\rho = \frac{\int_{-\infty}^{\infty} \sum_{m=-\infty}^{\infty} |f_2(x, m\Delta y)|^2 dx\,\Delta y}{|f_2(0, 0)|^2}. \tag{68}$$

This quantity provides an estimate of the number of point targets which can be placed in a region of area R with the individual target responses remaining discernible; of course the estimate is $R \div \rho$.

With a point target input the semidiscrete transform of f_2 is A_1A_2 and in turn (if the sampling rate is high enough):

$$\rho = \frac{\int_{-\infty}^{\infty}\int_{-1/2\Delta y}^{1/2\Delta y} |A_1A_2|^2\, dk_1dk_2}{\left|\int_{-\infty}^{\infty}\int_{-1/2\Delta y}^{1/2\Delta y} A_1A_2dk_1dk_2\right|^2}, \tag{69}$$

where Parseval's theorem was used in the numerator. Suppose $A_1(k_1, k_2) \neq 0$ for $\sqrt{k_1^2 + k_2^2} \leq B \leq 1/2\Delta y$ and $A_1 = 0$ for other (k_1, k_2). Then if arbitrary two-dimensional processing is permitted, A_1 and A_2 can be made to take on arbitrary values inside said circle. In this case let $A = A_1A_2$ and the integrals are taken over the circle. The minimum ρ is found by applying the Swartz inequality to the denominator with 1 playing the role of one of the two functions thus:

$$\left|\iint 1\, A dk_1dk_2\right|^2 \leq \left(\iint 1\, dk_1dk_2\right)\left(\iint |A|^2 dk_1dk_2\right)$$

with equality if and only if $A =$ constant on the circle. In this case,

$$\rho = \frac{1}{\pi B^2} \text{ and } A_2 = \frac{1}{A_1}, \text{ where } A_1 \neq 0. \tag{70}$$

Under the constraint that only processing along the lines is used, one has the following:

$$\rho = \frac{\int_{-B}^{B} |\hat{A}_2(k_1)|^2 \left\{\int_{-B}^{B} |A_1(k_1, k_2)|^2 dk_2\right\} dk_1}{\left|\int_{-B}^{B} A_2(k_1)\left\{\int_{-B}^{B} A_1(k_1, k_2)dk_2\right\} dk_1\right|^2}. \tag{71}$$

Set

$$W(k_1) = \int_{-B}^{B} |A_1(k_1, k_2)|^2 dk_2.$$

This function is used as the weight function in the following application of the Swartz inequality to the denominator:

$$\left|\int_{-B}^{B} \hat{A}_2(k_1)\left(\frac{\int_{-B}^{B} A_1(k_1,k_2)dk_2}{W(k_1)}\right) W_1(k_1)dk_1\right| \leq$$

$$\left(\int_{-B}^{B} |\hat{A}_2(k_1)|^2 W_1(k_1)dk_1\right)\left(\int_{-B}^{B} \frac{\left|\int_{-B}^{B} A_1(k_1, k_2)dk_2\right|^2}{W(k_1)}\, dk_1\right).$$

Now the minimum resolution is given by

$$\frac{1}{\rho} = \int_{-B}^{B} \frac{\left|\int_{-B}^{B} A_1(k_1, k_2)dk_2\right|^2}{\int_{-B}^{B} |A_1(k_1, k_2)|^2 dk_2}\, dk_1.$$

In the case of a top hat A_1, $\int[A_1]^2 = (\int A_1)^2$ and hence $1/\rho = \pi B^2$—the area over which the integrand is not zero. Thus for a top hat pre-filter, one-dimensional processing is adequate as far as resolution is concerned.

For the cone pre-filter, one obtains

$$\rho = \frac{3}{2}(\pi B^2)$$

which is a degradation by a factor of 3/2 when compared to two-dimensional processing.

References

1. M. Born and E. Wolfe, *Principles of Optics*, 1st ed. (Pergamon Press, New York, 1959).
2. William M. Brown, "Analysis and optimization of coherent high resolution radars by circuit theory concepts," Report Number 2900-144-T, Willow Run Laboratories, The University of Michigan, Ann Arbor, Michigan (May 1960).
3. William M. Brown, *Analysis of Linear Time Invariant Systems* (McGraw-Hill, New York, in press).
4. Leslie G. Callahan, Jr., "Optimum linear filtering for line scan imaging systems," Ph. D. Dissertation, The University of Pennsylvania, Philadelphia, Pennsylvania (1961).
5. T. P. Cheatham, Jr., and A. Kohlenberg, "Analysis and synthesis of optical systems," Boston University, Physics Research Laboratory, Technical Note 84, Part I (March 1952).
6. T. P. Cheatham and A. Kohlenberg, IRE Natl. Conv. Record, pp. 6–12 (1954).
7. L. J. Cutrona, E. N. Leith, C. J. Palermo, and L. J. Percello, IRE Trans. on Information Theory **IT-6,** 386 (1960).
8. P. Elias, J. Opt. Soc. Am. **43,** 229 (1953).
9. P. Elias, "Optical systems as communication channels," Symposium on Info. Networks, Brooklyn Poly. Inst., April 12–14, 1954.
10. P. Elias, D. Grey, and D. Robinson, J. Opt. Soc. Am. **42,** 127 (1952).
11. R. Clark Jones, J. Opt. Soc. Am. **45,** 799 (1955).
12. R. Clark Jones, Proc. Inst. Radio Engrs. **47,** No. 9, Infrared Issue (1959).
13. R. Clark Jones, "The study of IR backgrounds by the Wiener spectrum method," Polaroid Corporation, Cambridge, Mass., unpublished report prepared and edited by Infrared Laboratory, Willow Run Laboratories, The University of Michigan, Ann Arbor, Michigan (December 1959).
14. P. Mertz and F. Gray, Bell System Tech. J. **13,** 464 (1934).
15. E. O'Neill, "Selected topics in optics and communication theory," Boston Univ., Tech. Note 133 (October 1957).
16. E. O'Neill, IRE Trans. on Information Theory **IT-2,** 56 (1956).
17. E. O'Neill, "The analysis and synthesis of linear coherent and incoherent imaging system," Boston Univ., Physics Research Lab., Tech. Note 122 (September 1955).
18. E. O'Neill, "The modulation function in optics," Boston Univ., Opt. Res. Lab., Tech. Note 110 (January 1954).
19. J. Otterman, "Aperture correction for instrumentation systems," Ph.D. Dissertation, Univ. of Michigan (1956).
20. George B. Parrent, Jr., J. Opt. Soc. Am. **51,** 143 (1961).
21. O. Schade, J. Soc. Motion Picture and Television Engrs. **56,** 131 (1951); **58,** 181 (1952); **61,** 97 (1953); **64,** 593 (1955).
22. H. Wessley, Proc. IRIS, Institute of Science and Technology, University of Michigan, Ann Arbor, Michigan, **3** No. 2, 135 (1958).

Applied Optics — Optical Activities in Industry

reported by FRANK COOKE, 66 Summer Street, North Brookfield, Mass.
Mr. Cooke welcomes news and comments for this column which should be sent to him at the above address

The Diamond Band Saw is one of the more interesting uses of diamonds in the optical industry. For many years the optical worker used a wire band arranged on a saw, and charged with abrasive slurry, to cut a curved piece from flat glass. This took much time, and what a mess it made! Your reporter could not force himself to return to the old method after having installed this newer version with an 18-ft (5.49-m) blade.

The blades in heavy version cost $36.00 per foot (91.4 cm). A careless workman can ruin one if the work is pushed into the blade so that the normal easy cutting rate is exceeded. But if used sensibly, the blade will last a long time and prove profitable. 2.54-cm thick Crown disks 61 cm in diameter can be cut in less than ½ hr. A 6.4-mm thick plate cuts safely at 91.4 cm/sec. Three oval mirrors of pyrex 3.81 cm thick, 45.7 cm long, and 30.5 cm wide were cut in one day without damage. So great was the time saved, we thought the cost of the blade was saved in that one job.

Close-up showing blade in glass. Note the leading diamond edge.

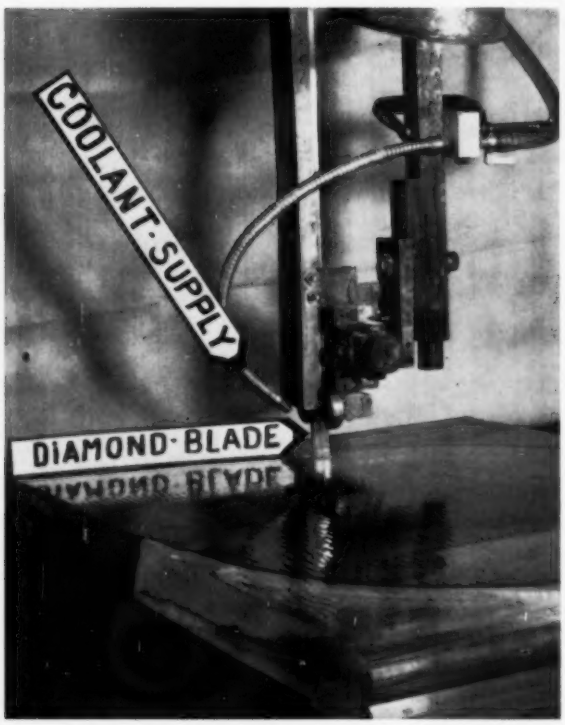

Diamond blade partially around on a 61-cm diameter. Thickness 5.08 cm.

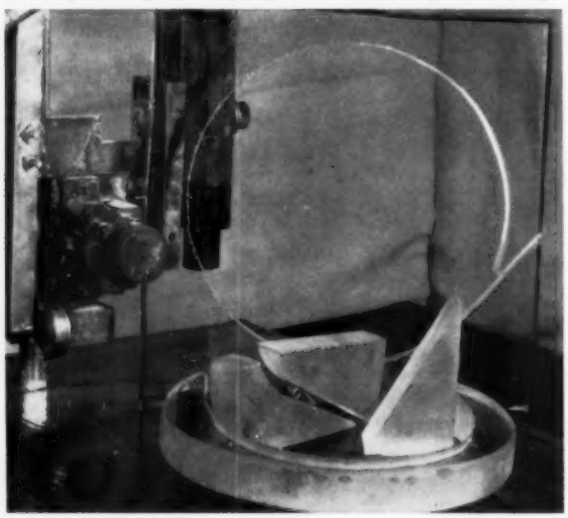

Various shapes cut on the diamond band saw. All the cuttings were made in a few hours.

Three-Dimensional Wavefront Reconstruction

Jurgen R. Meyer-Arendt

Wavefront reconstruction is a process by which a diffraction pattern can be restored into an image of the primary scatterer This process is being used to visualize the molecular structure of matter. Three-dimensional reconstruction is possible by means of a synthesizer which has two optic axes. The light in one arm of the synthesizer need not be coherent with respect to the light in the other arm.

Wavefront reconstruction is the process by which a recorded diffraction pattern, called a hologram, is reconverted into an image of the primary diffracting object. The fundamental principles of wavefront reconstruction have been elaborated in much detail by Gabor,[1] Kirkpatrick and El-Sum,[2] and others.

Thus far, the wavefront technique of producing the hologram and restoring it into an image has been limited to the two-dimensional case, although Lipson and Taylor[3] and Cowley[4] have stressed the need for an analog three-dimensional process. A two-beam synthesizer designed by Gabor[5] is used merely to eliminate the conjugate image or "ghost" that otherwise accompanies the reconstruction, rather than for stereoscopic reconstruction.

Stereo reconstruction has been carried out in the experiments reported here. Following Rogers' technique,[6] artificial holograms were prepared in the form of black-and-white line drawings. These holograms were drawn in such a way as to represent simple, three-dimensional, geometric and crystallographic figures. The simplest of them was a system of three axes intersecting each other at one point and at right angles.

Three-dimensional line drawings are made in order to prepare two drawings that are slightly different. This difference is to resemble the difference in views seen by the left and by the right eye. For crystallographic line drawings, the difference applies only to the front-to-back or α-axis. All corresponding points in the two drawings lie on the same horizontal line. The only difference between the two is in the slope of the α-axis. The slope of the α-axis for the left projection, or $\tan\alpha_L$, is 0.75 (four divisions on quadrille ruled paper to the right and three divisions up; $\alpha_L = 36.9°$) and $\tan\alpha_R = 0.667$ for the right projection (three divisions to the right and two divisions up; $\alpha_R = 33.7°$).

It is essential that the (here fictional) original object obscure a rather small fraction of the cross section of the light beam. Only in this manner can the space between the object details be fully utilized for the display of the diffraction fringes and a sufficiently intense coherent background be assured. Since the oblique, or α-axis is different in the component holograms, this axis has been emphasized by drawing fringes on *both sides* of it; the horizontal and vertical axes, as shown, are accompanied by only one set of parallel lines each.

The stereo holograms, separated by about 56 mm, were mounted in cardboard frames. The exact positioning is not critical as long as the holograms are inside the lens apertures: lateral or longitudinal displacement, in principle, is immaterial. It has been found that positive holograms gave better reconstructions than the original negatives; this is probably due to the fact that the positives were contact prints made on high-gamma Kodalith film.

The mounted stereograms were then inserted into the stereoscopic synthesizer shown in Fig. 1 which is essentially a double Fraunhofer diffraction apparatus. It consists of a xenon lamp (not shown), a beam splitter, two identical optical systems, each consisting of a pinhole, collimating, and objective lenses (f = 52 mm), and magnifiers for visual observation. The pinholes are used to assure sufficient coherency and to eliminate blurring which might arise from the occasional shifting of the xenon arc. The diameter a of the pinholes is of the order of a few microns so that Pohl's coherence condition[7]

$$a \sin\beta \ll \frac{\lambda}{2}$$

The author is at the Physics Department, Utah State University, Logan, Utah.

Received 8 May 1962.

This work was supported by a research grant from the National Institutes of Health.

This paper is based on a talk given at the 46th Meeting of the Optical Society in Los Angeles, October 1961.

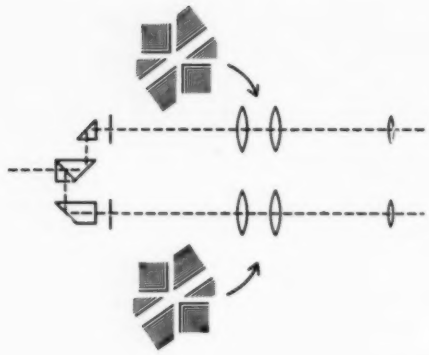

Fig. 1. Stereoscopic synthesizer for wavefront reconstruction. Inserts show two, slightly different, artificial holograms.

holds where β is one-half the vertex angle of the light cone emerging from the pinhole and λ is the wavelength. Since the fusion process in stereoscopic vision is a perceptual process rather than one based on optical interference, the light carried in one arm of the synthesizer need not be coherent with the light in the other arm. On looking into the synthesizer one sees the holograms being reconstructed into true images. The two reconstructions then fuse together and produce a three-dimensional reconstructed image.

References

1. D. Gabor, Proc. Roy. Soc. London **A 197,** 454 (1949).
2. P. Kirkpatrick and H. M. A. El-Sum, J. Opt. Soc. Am. **46,** 825 (1956).
3. H. Lipson and C. A. Taylor, Acta Cryst. **4,** 458 (1951).
4. J. M. Cowley, Acta Cryst. **9,** 399 (1956).
5. D. Gabor, U. S. Pat. 2,770,166 (1956).
6. G. L. Rogers, Proc. Roy. Soc. Edinburgh **63,** 313 (1951–52).
7. R. W. Pohl, *Einführung in die Optik* (Springer, Berlin, 1943), p. 66.

Meeting Reports

Ninth Annual East Coast Conference on Aerospace and Navigational Electronics, Baltimore, October 22–24, 1962

Reported by D. F. Nelson, Bell Telephone Laboratories

The ECCANE meeting, which contained a session of five invited papers on lasers, was opened with a review paper by P. P. Sorokin, IBM Research Center, on solid optical masers. He compared the present state of optically pumped solid optical masers with an idealized model. Crystalline imperfections that raise the threshold for maser action and distort the output wave form, wide fluorescence lines that make discrimination against unwanted axial modes difficult, and persistent relaxation oscillations are a few of the problems limiting solid optical-maser usefulness. Dr. Sorokin went on to discuss the effect of the crystalline environment on a rare-earth ion, giving particular attention to a comparison of the $SrF_2:Sm^{2+}$ and the $CaF_2:Sm^{2+}$ systems. He concluded with a discussion of exploding wire sources for ultraviolet pumping of optical masers.

C. G. Young reviewed the recent accomplishments of American Optical's researchers in the neodymium glass laser system. Energy outputs up to 113 J per pulse and conversion efficiencies up to 2.2% have been obtained using barium crown glass. A flint-glass fiber laser with an 8-μ neodymium-doped core has been operated. Semicontinuous operation at room temperature has been obtained, using a clad rod with a Nd-doped flint-glass core and an ac-excited PEK type A mercury arc lamp run at 2 kW. A completely self-contained subounce laser system using an aluminum-filled flashbulb and a battery has also been operated.

J. P. Gordon, Bell Telephone Laboratories, followed with a paper on the communications potential of coherent light. He pointed out that, though it is too early to describe what form a laser communication system will take, a number of things can be said about its information-handling rate, its noise, and the transmission portion of the system. The limit on the information capacity of light is imposed primarily by the finite size of the quantum. If an information rate comparable to the channel bandwidth is desired, then the system must satisfy the requirement that the received signal power (S) must be greater than the bandwidth (B) times the photon energy ($h\nu$). If the receiver incorporates a linear amplifier at the carrier frequency, then $S/h\nu B$ is the best possible signal-to-noise ratio at the amplifier output. He also pointed out that a transmission system having no significant diffraction loss seems feasible.

The fast-moving field of gaseous optical masers was reviewed by W. R. Bennett, Yale. The recent search for new gaseous optical masers has been greatly facilitated by the use of a confocal resonator with external mirrors and Brewster angle windows. Not only is such a system very easy to align, but its low diffraction loss allows the use of long tubes to obtain greater gain per pass and small-diameter tubes to reduce second-order collision processes. Dr. Bennett then described the He–Ne system (14 oscillating wavelengths), which uses resonant atomic-collision pumping; the Cs vapor system (2 wavelengths), which uses optical pumping; the Ne– or A–O_2 system (1 wavelength), which uses disassociative-collision pumping; and the noble gas systems (15 wavelengths), which use electron-impact pumping. He pointed out that the prospects for additional systems are quite good.

The final paper, by J. E. Geusic, Bell Telephone Laboratories, concerned optical-maser amplifiers. He described a ruby optical maser that has given 20-dB gain when operated at room temperature. It consists of three ruby amplifying sections separated by Faraday rotation isolators to prevent the amplifier from oscillating. Pulse narrowing due to upper-state population depletion during the pulse amplification has been observed. Since the ruby diameter is large compared to the amplifying wavelength, the device has a large spatial bandwidth allowing image amplification. This has been demonstrated. The large spatial bandwidth in conjunction with the frequency bandwidth leads theoretically to a channel capacity of 10^{17} cps!

Meeting Reports *continued on page 430*

Faraday Rotation in FeNi Films

H. H. Wieder and D. A. Collins

The rotation of the plane of polarization in films of a 35% nickel in iron alloy was determined as a function of the quasi-static magnetization reversal process related to the angle of incidence and azimuth of the transmitted plane polarized white light. The magnetooptic hysteresis loops determined in this manner offer direct information on the coercivity, magnetization, susceptibility, and anisotropy of ferromagnetic films. It is shown that a modified form of Kundt's empirical law can account for the experimentally measured Faraday rotation by introducing the dependence of the rotation upon the optical properties of the films, the azimuth, and the angle of incidence of the light.

Introduction

The Faraday and Kerr effects[1,2] are the principal magnetooptic phenomena associated with thin ferromagnetic films. Both are useful as tools for the investigation of the orientation, distribution, and dynamics of ferromagnetic domains and their relation to the magnetization reversal process. A number of papers have also considered the practical application[3,4] of magnetooptic phenomena to information storage and information processing devices.

The magnetooptic Faraday and Kerr effects depend upon the interaction of a plane polarized electromagnetic wave with the magnetization vector of a material medium. By virtue of this interaction, reflected and transmitted waves experience a rotation of the plane of polarization. The rotation associated with the reflected wave is the ferromagnetic Kerr effect. The Kerr effect also includes a change in the ellipticity usually associated with metallic reflection.

Faraday rotation is related to the transmitted beam and its magnitude depends upon the path length of the wave through the film. The Faraday rotation may, therefore, be considerably, but not arbitrarily, greater than the corresponding Kerr rotation since, in metallic media, a strong absorption accompanies transmission of radiant energy.

For films thicker than 10^3 Å, transmission of the visible portion of the electromagnetic spectrum drops below 1% of the incident intensity. For thicker films, the Faraday effect offers a lesser practical advantage than the Kerr effect. However, since reflection from a film involves only a few atomic layers below its surface, the Kerr effect is not suited for probing a volume dispersion of the magnetization such as might occur, for example, in layered film structures.[5] For films less than one thousand angstroms in thickness, the Faraday effect offers some advantages, especially if independent measurements are also available of the magnetization intensity, effective film thickness, and chemical composition of the ferromagnetic film constituents. In order to use the Faraday effect as a tool for investigating the magnetization process, the relation between primary magnetic parameters, such as the magnetization intensity, coercivity, and anisotropy, and optical parameters such as the angle of incidence and the azimuth of the incident plane polarized light, as well as optical properties of the film, must be determined. Some of these relations were the subject of the studies presented here.

The authors are in the U.S. Naval Ordnance Laboratory Corona, California.

Received 24 March 1962.

Theory of Measurement

Most of the literature devoted to Faraday rotation[1] in thin ferromagnetic films deals with the rotation of a plane polarized beam of light passing through the films at normal incidence. If a residual magnetization exists, then a strong demagnetizing effect forces the magnetization vector to lie in the plane of the film. A component of magnetization in the direction normal to the film is obtained only if an applied magnetic field H is large enough to overcome the demagnetizing field which is proportional to the induced magnetization M. Let χ be the magnetic susceptibility, then:

$$M = \chi(H - NM) \qquad (1)$$

with N the demagnetizing factor of the film which may be taken as $N \simeq 4\pi$. In accordance with (1), therefore:

$$M = \chi H/(1 + 4\pi\chi) \tag{2}$$

which, for $4\pi\chi \gg 1$, leads to the simple relation $4\pi M = H$ up to the saturation value M_s.

Kundt's empirical law[1] relates the angle of rotation, ρ, of the incident plane polarized light to the magnetization M of a ferromagnetic film of thickness d by means of a material dependent parameter k, identified as Kundt's constant:

$$\rho = kMd. \tag{3}$$

Therefore with reference to Eq. (2), the angle of rotation is linear in H at normal incidence, rising by a slope $(kd/4\pi)$ with the applied field, up to the saturation value ρ_T, as the magnetic flux density B approaches asymptotically the value $B_s = 4\pi M_s$.

Let the electric vector of an incident plane polarized but incoherent electromagnetic wave be transmitted through the film. Let an induced or residual magnetization vector be present in the film, directed along the path of propagation of the incident light. The cross product of the incident electric field and magnetization is an electric field in a mutually orthogonal direction to both of the original vectors. The vector sum of the original electric vector and the induced component results, upon emergence from the film, into an electric vector rotated with respect to the incident plane of polarization. In general, the light is no longer plane, but elliptically polarized, and the film is also magnetically birefringent.

This model is deceptively similar to the classical description of the Hall effect. The Faraday effect in ferromagnetics appears, however, to be due to the quantum mechanical exchange force and the electron spin-orbit interaction which produce the experimentally observed large angular rotations and the circular dichroism found in ferromagnetic films.

For the Faraday effect at normal incidence, the magnetooptic interaction does not represent phenomena associated with switching, hysteresis, domain wall motion, or other details of the magnetization reversal process because the component of the residual magnetization is zero in the direction of propagation. In order to observe these phenomena in ferromagnetic films, an angle of incidence other than normal must be used so that the magnetooptic rotation derived from the Faraday effect will respond to the changes in the remanent magnetization and Eq. (3) will still be maintained.

Fowler and Fryer[6] used an angle of incidence of 45° to photograph static domain structures in NiFe films and Reimer[7] used the same angle for illustrating a quasi-static magnetooptic hysteresis loop by plotting the photoelectric signal induced by Faraday rotation in a nickel film. Dynamic hysteresis loops were obtained by Moore[8] on FeNi films using a similar method.

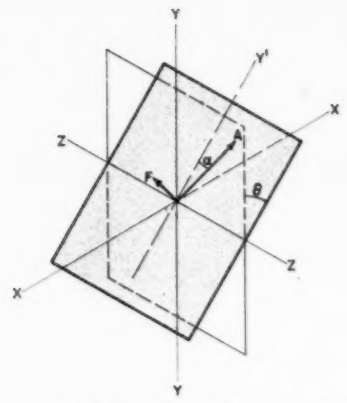

Fig. 1. A magnetic film in the $y'z$ plane having a residual magnetization M_s directed along y' interacts with a plane polarized electromagnetic wave A, traveling in the $+x$ direction at an angle of incidence θ and azimuthal angle α.

A simplified theory for Faraday rotation measurements will now be developed in close analogy to the theoretical treatment Lissberger[9] related to the Kerr effect. Consider a ferromagnetic film in a cartesian coordinate system with the plane of the film at an angle θ with respect to the yz plane as shown in Fig. 1. Let the film be placed between a polarizer and an analyzer prism whose planes of maximum transmittance are oriented at some angle ϕ with respect to each other. A source of incoherent white light is used to illuminate the film. The polarizer converts the light into a plane polarized beam A which falls upon the film at the azimuthal angle α. The direction of propagation of the light is the positive x axis. Let the film have a saturated residual magnetization vector $\mathbf{M}_s$ in the plane of the film. The magnetization component ($\mathbf{M}_s \sin\theta$) will induce a Faraday component F in the film. The analytical problem is to obtain a solution for the Faraday rotation of the transmitted beam relative to the incident plane of polarization as a function of the optical parameters of the film, the angle of incidence, and the azimuth.

Let the intensity of the incident light be taken as unity and the transmittance of the polarizer and analyzer in the plane of maximum transmittance be equally defined by the amplitude T. The vectors associated with the usual metallic transmittance, τ, and those induced by the Faraday effect, F, will be considered for an azimuth $\alpha = 0$ and $\alpha = \pi/2$ in accordance with Fig. 2. The amplitude transmittance through the analyzer is, respectively, T_p parallel to and T_s perpendicular to the plane of incidence:

$$\begin{aligned} T_p &= T(\tau_p e^{i\beta}\, T\cos\phi - F_p e^{i\gamma}\, T\sin\phi), \\ T_s &= T(\tau_s e^{i\delta}\, T\cos\phi + F_s e^{i\eta} T\sin\phi). \end{aligned} \tag{4}$$

To obtain I, the transmitted flux per unit area, the

complex quantities in (4) are multiplied by their corresponding complex conjugates. Thus:

$$I_p = T^4[\tau_p^2 \cos^2\phi + F_p^2 \sin^2\phi - 2\tau_p F_p \sin\phi \cos\phi \cos\Delta_p],$$
$$I_s = T^4[\tau_s^2 \cos^2\phi + F_s^2 \sin^2\phi + 2\tau_s F_s \sin\phi \cos\phi \cos\Delta_s], \quad (5)$$

where $\Delta_p = (\beta - \gamma)$ and $\Delta_s = (\delta - \eta)$. Since, in practice, ϕ is chosen so that $\phi = [(\pi/2) \pm \epsilon]$ and, as a first-order approximation, $\cos\phi \simeq \epsilon$ and $\sin\phi \simeq [1 - (\epsilon^2/2)]$, Eq. (5) may then be written as:

$$I_p = T^4\{(\tau_p^2\epsilon^2) + F_p^2[1 - (\epsilon^2/2)]^2 - 2\tau_p F_p \epsilon [1 - (\epsilon^2/2)] \cos\Delta_p\},$$
$$I_s = T^4\{(\tau_s^2\epsilon^2) + F_s^2[1 - (\epsilon^2/2)]^2 + 2\tau_s F_s \epsilon [1 - (\epsilon^2/2)] \cos\Delta_s\}. \quad (6)$$

Having assumed that ϵ is a small quantity, terms of higher than quadratic order in ϵ will be neglected. Also, since the Faraday component is small, all except linear quantities in F will be neglected in Eq. (6) which may then be approximated by:

$$I_p \simeq T^4 \cdot (\tau_p^2\epsilon^2 - 2\tau_p F_p \epsilon \cos\Delta_p),$$
$$I_s \simeq T^4 \cdot (\tau_s^2\epsilon^2 + 2\tau_s F_s \epsilon \cos\Delta_s). \quad (7)$$

For an azimuth of $\alpha = \pi/4$ the intensity output from the analyzer is approximately the mean value of the sum of I_p and I_s:

$$I \simeq (T^4/2)[(\tau_s^2 + \tau_p)^2\epsilon^2 + 2\epsilon \cdot (\tau_s F_s \cos\Delta_s - \tau_p F_p \cos\Delta_p)]. \quad (8)$$

In the absence of any magnetization, the intensity perpendicular to the plane of incidence is, from (7): $I_s = T^4\tau_s^2\epsilon^2$. Let the magnetization be driven by a periodic applied field from $+M_s$ to $-M_s$. This brings about a change in intensity $\Delta I_s = 4T^4\epsilon\tau_s F_s \cos\Delta_s$ and, therefore,

$$\frac{I_s}{\Delta I_s} = \frac{\tau_s \epsilon}{4F_s \cos\Delta_s}. \quad (9)$$

The tangent of the angle ρ, relating the vectors, $\mathbf{F}_s$ and τ_s, defines the Faraday rotation* as $\rho_s \simeq (\mathbf{F}_s/\tau_s)$.

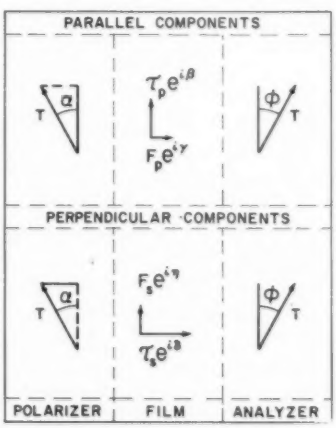

Fig. 2. Schematic showing the amplitude and phase components of the transmittance and induced magnetooptic vectors for an arbitrary azimuth.

$\cos\Delta_s$ and Eq. (9) becomes:

$$\frac{I_s}{\Delta I_s} = \frac{|\epsilon - \epsilon_0|}{4\rho_s}. \quad (10)$$

Thus, if the angular position of the analyzer relative to the polarizer is known, and the intensity transmittance as well as the change in intensity may be ascertained from experiment, then Eq. (10) yields a method for determining ρ_s. In a similar fashion one obtains for ρ_p the linear relationship:

$$\frac{I_p}{\Delta I_p} = -\frac{\tau_p \epsilon}{4F_p \cos\Delta_p} = -\frac{|\epsilon - \epsilon_0|}{4\rho_p}. \quad (11)$$

From Eq. (8) the rotation of the plane of polarization for an azimuth of 45° may be determined in a similar manner:

$$\frac{I}{\Delta I} = \left(\frac{\epsilon - \epsilon_0}{4}\right) \cdot \frac{\tau_s^2 + \tau_p^2}{\tau_s F_s \cos\Delta_s - \tau_p F_p \cos\Delta_p}. \quad (12)$$

If the intensity transmittance parallel and perpendicular to the plane of incidence of the film is known or may be measured, then Eq. (12) may be simplified by introducing the ratio $R = (\tau_p/\tau_s)^2$:

$$\frac{I}{\Delta I} = \left(\frac{\epsilon - \epsilon_0}{4}\right) \cdot \frac{R + 1}{\rho_s + R\rho_p} = \frac{\epsilon - \epsilon_0}{4\rho'}, \quad (13)$$

where ρ' is the Faraday rotation for an azimuthal angle of 45°. Thus, from experimentally measured values of ρ_s, ρ_p, and R, the calculated value of ρ at 45° may be compared against direct experimental measurements of Faraday rotation as a function of the angle of incidence θ.

Experimental

The magnetic films used in these investigations were prepared by the evaporation in vacuum of a nominally 35% nickel-iron alloy upon a heated microscope cover glass substrate in the presence of an orienting dc magnetic field.[10] The magnetooptic properties of two representative films having this composition will be illustrated here. The average physical thickness of these films was measured by means of an interferometric technique[11] as 0.06 μ and 0.02 μ, respectively. A discrepancy of $\pm 8\%$ was found between these measurements and thickness estimates based on volume, weight, and density determinations. This discrepancy decreases for thicker films, but appears to increase rapidly for films less than 0.01 μ thick. The saturation induction B_s was obtained for each of the films by means of ferromagnetic resonance measurements in the X-band microwave region[12] for a dc magnetic field parallel to the plane of the film using a g-value of 2.1. For the 0.06 μ film, $B_s \simeq 1.26 \times 10^4$ G and for the 0.02 μ film, $B_s \simeq 1.24 \times 10^4$ G. No significant dispersion of the transmitted light intensity was found in

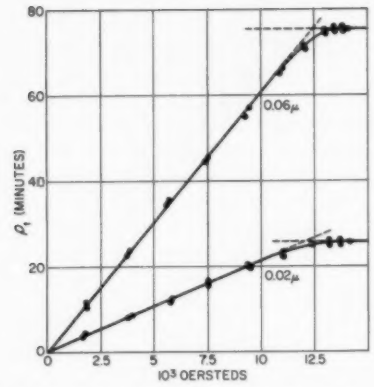

Fig. 3. Faraday rotation at normal incidence for two FeNi films, nominally of identical composition but different physical thickness.

the 400 mμ to 700 mμ spectral region for either film as determined by spectrophotometric measurements. The transmitted intensity at normal incidence was found to be 5% for the 0.02 μ and 1% for the 0.06 μ film.

In order to observe Faraday rotation at normal incidence, including saturation effects, fields greater than 1.2×10^4 Oe are necessary. The films were, therefore, mounted between the pole pieces of a 30-cm Varian electromagnet on a small platform which also contained two nonmagnetic front surface mirrors parallel to each other and at an angle of 45° with respect to the magnetic field. White light emitted by a tungsten filament powered from a stabilized 28-V dc source was collimated by a lens system and passed through a Glan-Thompson polarizing prism. The plane of polarization of the incident light was maintained normal to the plane of incidence of the mirrors. The polarized beam reflected from the first mirror passed through the film, was reflected by the second mirror, and then fell upon another Glan-Thompson prism serving as an analyzer. The light intensity output was detected by a 1P21 photomultiplier having a dc stabilized anode supply and a load impedance of 10^5 Ω. The potential difference generated by the changing light intensity measured across the load was applied to a dc amplifier and thence to a recorder.

Both the polarizer and the analyzer prisms could be rotated about their axes and the analyzer was also provided with a vernier wormgear drive calibrated in units of six seconds of arc. The over-all accuracy of the apparatus, including mechanical and electrical settings, was estimated at ±2% for a rotation greater than 1 min of arc. The magnetic field was measured by means of a Hall probe with an accuracy better than 2% between 10 and 10^4 Oe and 3% between 10^4 and 2×10^4 Oe.

Preliminary measurements upon ordinary microscope cover glass slides were made in order to determine Faraday rotation in the glass as a function of thickness. This represents a correction factor which is significant only in the Faraday rotations of the films at normal incidence, and has been properly accounted for in the subsequent measurements. The correction due to the reflection from the mirrors is less than 1% and hence will be neglected.

The rotation of the plane of polarization was determined as a function of the amplitude and polarity of an applied magnetic field by means of the compensatory angular rotation ρ of the analyzer prism. The experimental results obtained on the two films described earlier are shown in Fig. 3. Clearly both films have a linear dependence of the angle of Faraday rotations in agreement with theory and a saturation rotation which appears, at $H \simeq B_s$, in fair agreement with the measured value of B_s. The slope $(\Delta\rho/\Delta H)$ for the 0.06 μ film is 6.12×10^{-3} min/Oe. The corresponding slope for the 0.02 film is 2.14×10^{-3} min/Oe. From the discussion presented earlier, $(\Delta\rho/\Delta H) = k(d/4\pi)$, where k is a material parameter proportional to the saturation induction. The discrepancy between B_s of the two films is of the order of 1.6%. If other systematic errors are neglected, the ratio of the slopes from Fig. 3 should be proportional to the ratio of the film thicknesses and to the ratio of the saturation rotations to within 1.6%. The ratio of the two slopes from Fig. 3 is 2.86. The ratio of the nominal thickness of the films is 3, and since the respective saturation rotations are 76 min and 26 min, their ratio is 2.92. The mean ratio of 2.93 ± 2.4% thus appears quite reasonable especially in view of the lack of precision in the thickness determination of the films. An average value of k is thus of the order of 10^3 min (G, cm)$^{-1}$. Faraday rotation at normal incidence and at magnetic saturation had been reported at 3.83×10^5 deg/cm for iron films.[13] We performed similar measurements on iron films nominally of 0.05 μ thickness and, for white light, obtained a saturation rotation of 3.5×10^5 deg/cm. The FeNi

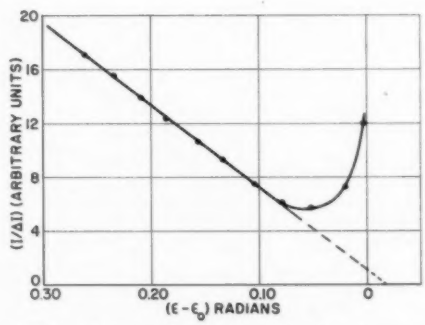

Fig. 4. Ratio of transmitted intensity to change in light intensity induced by reversal of the residual magnetization versus analyzer setting; for the 0.06 μ film at $\theta = 30°$ and for $\alpha = \pi/4$.

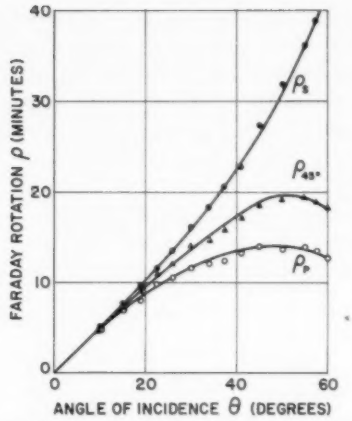

Fig. 5. Angle of saturation of Faraday rotation as a function of the angle of incidence for the 0.06 μ film. Azimuth fixed at $\alpha = 0, \pi/2$, and $\pi/4$, respectively.

films described in detail in the present experiments have a saturation rotation of 2.1×10^5 deg/cm. This is about 40% smaller than the saturation rotation of pure iron and appears to be reasonable in view of the decrease in the magnetization induction which follows the alloying of nickel and iron.

Variable Azimuth and Oblique Angle of Incidence

In order to observe Faraday rotation as a function of various angles of incidence and azimuth, the FeNi films were placed at the center of an air core Helmholtz coil. This coil, as well as the previously described polarizer, analyzer, light source, and photomultiplier, were mounted on an optical bench, also provided with a micromanipulator, which enabled the calibrated angular positioning of the film with respect to the plane of incidence of the light, the selection of the magnetic anisotropy axis of the film, and the selection of a particular azimuthal angle α. The magnetic field in the plane of the film was always ($H \sin\theta$) with H the axial driving field at the center of the Helmholtz coil. Driving power was derived from an 0.1 cps square wave generator. Magnetization reversal thus took place in an essentially quasi-static field allowing adequate time for recording magnetooptic switching, saturation, and hysteresis.

A differential amplifier interposed between the photomultiplier output and recorder was used for the determination of the photomultiplier signal due to the transmitted steady-state light intensity I, as well as the magnetooptically induced change in intensity ΔI, as a function of the analyzer setting ϵ. Figure 4 shows a plot of $(I/\Delta I)$ as a function of ϵ for $\theta = 30°$ and $\alpha = \pi/4$. Similar plots were prepared for other angles of azimuth and incidence. For each, the Faraday saturation rotation was determined in accordance with the theory presented in the preceding section using the appropriate equations: Eq. (10) for $\alpha = \pi/2$; Eq. (11) for $\alpha = 0$; and Eq. (13) for $\alpha = \pi/4$.

The rotation for these azimuthal angles is plotted in Fig. 5 as a function of θ. These results have been obtained on the 0.06 μ film and qualitatively similar data were obtained for the 0.02 μ film. Conventional Faraday rotation measurements were also performed at $\alpha = 0$ and $\alpha = \pi/2$; with the analyzer set at $\pm 5°$ from the extinction position, the displacement of the minimum intensity setting of the analyzer, brought about by the reversal of the residual magnetization, was also determined. The average discrepancy between the two sets of measurements at $\alpha = \pi/2$ was of the order of 2% for the 0.06-μ film and of the order of 5% for the 0.02-μ film. For $\alpha = 0$, this value rose to 3% for the 0.06-μ film and 6% for the 0.02-μ film. Figure 6 shows a qualitative comparison between the data obtained on a conventional 10^3 cps hysteresis loop tracer and the magnetooptic loops traced for the same 0.06-μ film. The coercivity evaluated as $H_c = 8.1$ Oe agrees to within 10% for both methods. For the 0.02 μ-film, $H_c \simeq 12$ Oe but the discrepancy between the two methods of measurement rose to 15%.

Of greater significance, however, is the variation in coercivity from the center of the film toward its edges. The cross-sectional area of the light beam was reduced by decreasing the diameter of a circular iris from 1 cm

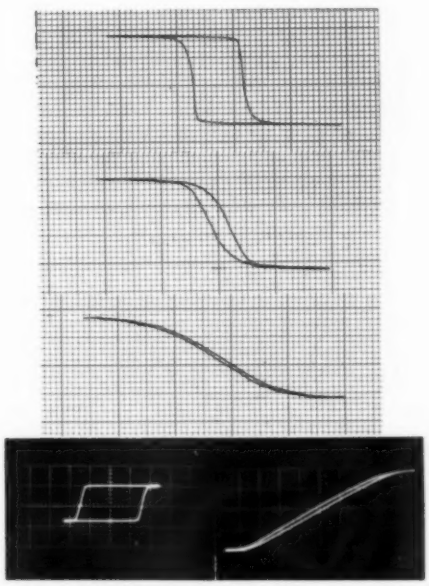

Fig. 6. A qualitative comparison between magnetooptic, quasi-static hysteresis loops, at $\theta = 30°$ and $\alpha = \pi/2$ for the 0.06 μ film (top three) and conventional magnetodynamic hysteresis loops obtained at 1 kc/sec. Magnetooptic loops taken along magnetic easy-axis, hard axis, and midway between. Magnetodynamic loop taken along easy-axis and hard axis.

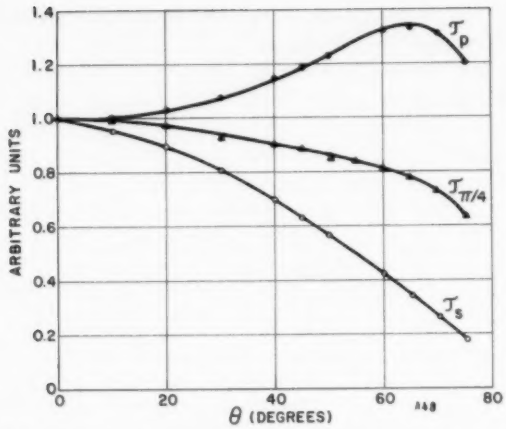

Fig. 7. Transmitted intensity as a function of θ and α for the 0.06-μ film–glass substrate measured for zero net magnetization relative to the transmitted intensity at normal incidence.

to 0.05 cm so that a series of hysteresis loops could be obtained for discrete areas of the film. It was found that while the saturation rotation is essentially independent of position, the coercivity increases from the center of the film outward as $H_c \simeq 11$ Oe $\pm 20\%$. It has not been established as yet whether this is due to a variation in thickness, composition, or a dispersion of the magnetic anisotropy axis within the films. It is clear however that, without auxiliary optical devices, a light beam 0.02 cm in diameter is still adequate for probing Faraday rotation in films up to 0.06-μ thick. The simple apparatus described above is therefore extremely useful for determining the dispersion of magnetic properties within a film, a process not feasible by means of the conventional hysteresis loop tracer.

Transmitted Intensity

The usual magnetooptic effects disappear if the orientation of domains within the film is random. Experimentally, this was brought about by applying a 60 cps current to the Helmholtz coils and observing the magnetooptic hysteresis loop on an oscilloscope while the field amplitude is gradually brought to zero.

The transmitted flux per unit area of the FeNi films was then measured relative to the same quantity determined at normal incidence. These measurements* are shown in Fig. 7 as a function of θ and α, for the 0.06-μ film. By means of Eq. (13) and the ratio $R = (\tau_p/\tau_s)^2$ obtained from Fig. 7, the slope of the theoretical curve $(I/\Delta I)$ vs $(\epsilon - \epsilon_0)$ at $\alpha = 45°$ may be compared against the direct measurement of this quantity from plots such as shown in Fig. 4. The slope of the latter curve is 61.6 rad^{-1} while the theoretically calculated slope is 63.1; hence the discrepancy of the order of 2.4% appears to be quite reasonable. An average discrepancy of 4% was found between values of ρ' determined directly and those calculated using Eq. (13) for angles of incidence between 0° and 60°. In view of the probable error of 8%, which includes the individual measurements of ρ_s, ρ_p, τ_s^2, and τ_p^2, this discrepancy appears to be justified.

If it is assumed that Kundt's expression in (3) is still valid at oblique incidence, but the rotation is inversely proportional to the transmissivity, then:

$$\rho_s \simeq K\,|M_s \sin\theta|\, s/\tau_s^2,\ \rho_p \simeq K\,|M_s \sin\theta|\, s/\tau_p^2, \qquad (14)$$

where K is a constant and s is the effective light path within the film which may be shown to be†:

$$s = d(1 + \sin^2\theta/p^2)^{1/2}. \qquad (15)$$

From (14) the ratio (ρ_s/ρ_p) is:

$$\frac{\rho_s}{\rho_p} = \left(\frac{\tau_p}{\tau_s}\right)^2. \qquad (16)$$

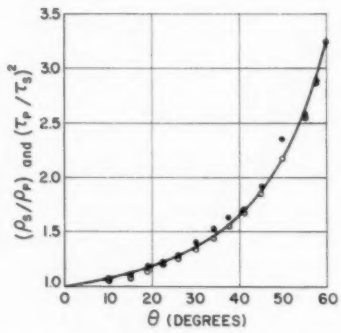

Fig. 8. Ratio of Faraday rotation normal and parallel to the plane of incidence (filled dots) has the identical dependence upon the angle of incidence as the ratio of the parallel to the perpendicular transmitted intensity (open circles) in accordance with (16).

Figure 8 illustrates the validity of these assumptions by showing that (ρ_s/ρ_p) is collinear with $(\tau_p/\tau_s)^2$, as stated in Eq. (16). Also, since the saturation rotation ρ_T at normal incidence is $\rho_T = kM_sd$, then, from Eqs. (14) and (15)

$$\frac{\rho_s}{\rho_T} = \frac{K}{k\tau_s^2}\sin\theta\cdot\left(1 + \frac{\sin^2\theta}{p^2}\right)^{1/2}, \qquad (17)$$

$$\frac{\rho_p}{\rho_T} = \frac{K}{k\tau_p^2}\sin\theta\cdot\left(1 + \frac{\sin^2\theta}{p^2}\right)^{1/2}.$$

If the path length s is essentially the thickness d of the film, then a plot of $(\rho_s/\rho_T)\tau_s^2$ vs $\sin\theta$ should, to a first approximation, be a straight line, and the same considerations ought to apply for the polarization parallel

* See Appendix III for a theoretical calculation of $\mathfrak{I}_s$ and $\mathfrak{I}_p$.

† See Appendix I.

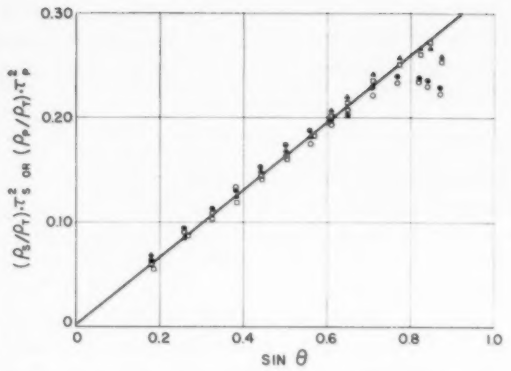

Fig. 9. A plot illustrating Eq. (17). Filled dots and open circles refer to $(\rho_s/\rho_T)\tau_s^2$ and $(\rho_p/\rho_T)\tau_p^2$ for the 0.06-μ film; triangles and squares refer to the same corresponding parameters for the 0.02-μ film.

to the plane of incidence. Figure 9 shows that for $\theta \leq \pi/4$ this is indeed the case for either film. One would have to conclude, therefore, that no significant error is introduced by neglecting the correction in path length of Eq. (15) for the films described here.* The angle of saturation of the Faraday rotation is thus related to the azimuth and the angle of incidence primarily through the dependence of the film transmissivity upon these parameters. From the slope of Fig. 9, $(K/k) = 0.32$; hence the parameter $K = 3.2 \times 10^2$ min (G, cm)$^{-1}$, a value only about one third of k, Kundt's constant for normal incidence.

Upon substituting Eq. (16) into (13):

$$\rho' = 2(\rho_s\rho_p)(\rho_s + \rho_p)^{-1}. \tag{18}$$

Thus the Faraday rotation for an azimuth of $\pi/4$ and for an arbitrary angle of incidence is determined by ρ_p shunted across ρ_s. By inspection, the maximum value of ρ_p in Fig. 5 is 13.5 min and the corresponding value of ρ_s is 32 min. Consequently from (18) ρ'_{max} = 19 min which is seen to be in very good agreement with the experimental data.

Summary and Conclusions

The experimental data presented herewith shows that Faraday rotation in ferromagnetic films may be used as a tool for the qualitative and quantitative study of the static and dynamic magnetization process.

1. From the angle of rotation of the plane of polarization at normal incidence, the magnetic saturation induction was determined and compared against the same quantity calculated from ferromagnetic resonance experiments. They appear to be in fair agreement.

2. The rotation of the plane of polarization is directly proportional to the magnetization at normal incidence. For an oblique incidence and arbitrary azimuth, due account must be taken of the corresponding dependence of the optical parameters of the film which determine its transmissivity.

3. The product of the angular Faraday rotation and the transmitted intensity for a fixed azimuth is directly proportional to the magnetization component chosen at any arbitrary angle of incidence $\theta \leq \pi/4$. The constant of proportionality K is not identical however to "Kundt's constant" k, measured at normal incidence. For the film composition reported in the present experiments $(K/k) = 0.32$.

4. Since the transmitted intensity depends critically upon the index of refraction and the extinction coefficient of the film, and they in turn depend upon the state of oxidation, its density, and stoichiometry, it is difficult to obtain, *a priori*, an analytical solution for Faraday rotation since the magnetic saturation induction may also depend on some, or all, of these parameters.

5. The qualitative correspondence between magnetodynamic and magnetooptic hysteresis loops do allow a precise determination of the coercivity and the magneto crystalline-anisotropy field. If the magnetization induction is known, then the incremental permeability may also be determined. For very thin films, Faraday rotation may indeed be superior to other methods used for determining these parameters, although this has not been completely ascertained as yet.

6. Because of the strong absorption of light in the visible part of the spectrum, the wavelength dispersion of Faraday rotation may, to a first approximation, be ignored for films thicker than 0.02 μ. This is in contrast to the ferromagnetic Kerr effect where this dispersion is large and significant.[9] The light absorption upon transmittance precludes, however, the use of films thicker than 0.1 μ.

7. No method for enhancing Faraday rotation appears feasible as yet, such as the dielectric overcoating of the films applied successfully for increasing the apparent Kerr rotation.[14,15]

8. For a film index of refraction $n = 2$ and an extinction coefficient maximum of $k = 2$, the correction in path length due to refraction may be neglected for $\theta \leqq (\pi/4)$ since the path length is essentially the physical thickness within the present error of measurement.

9. From the experimental data it appears that best results and the largest Faraday rotations are obtained for large angles of incidence and with the plane of polarization perpendicular to the plane of incidence. The definite maximum in the curve of Faraday rotation versus angle of incidence (Fig. 5) for the plane of polarization parallel to the plane of incidence is qualitatively explained by the corresponding behavior of the transmitted intensity shown in Fig. 7 and Eq. (17).

10. For an azimuth $\alpha = \pi/4$ the elliptic polarization

* See Appendix II.

of the emergent light complicates the measurement of Faraday rotation and accounts for the greater scatter of the data.

11. For a particular ferromagnetic film, the best signal-to-noise discrimination depends upon the quality of the polarizers, the type of detector used, and the degree of depolarization brought about by any auxiliary optics. Studies of this type were carried forth on the Kerr effect by Miyata,[3] Lissberger,[9] and Callaby and Lynch.[16] Similar calculations were also made by Smaller[17] for the Faraday effect. These considerations are particularly important in determining potential magnetooptic device applications.

The extent to which the relations discussed above apply in general to all ferromagnetic films remains as yet to be determined. The accuracy as well as the precision of Faraday rotation needs to be improved by refining the experimental apparatus and, whenever possible, using monochromatic light. Further work, especially on thin ferromagnetic metal and oxide films, appears justified, using the Faraday effect as a tool for the study of the magnetization process and for investigating the nature of its dependence upon the optical parameters of these films.

We are indebted to P. H. Lissberger, Assoc. Electr. Industries (Manchester) for his critical reading of the manuscript and his many useful and constructive suggestions.

Appendix I

With respect to the coordinate systems of Fig. 1, let the incident plane polarized beam of light with $\alpha = \pi/2$ have unit amplitude. Let the usual metallic amplitude transmittance τ_s and the induced Faraday component F be related by:

$$T_s = \tau_s e^{i\beta} \cos\phi + F_s e^{i\gamma} \sin\phi. \quad (19)$$

The flux transmitted per unit area $T_s^2 = I$ is obtained by multiplying Eq. (19) by its complex conjugate:

$$I = \tau_s^2 \cos^2\phi + F_s^2 \sin^2\phi + 2F\tau_s \sin\phi \cos\phi \cos(\beta - \gamma). \quad (20)$$

The maximum change in intensity with magnetic field occurs for $\phi = \rho_s$, i.e., for saturation of the Faraday rotation, therefore:

$$dI/d\phi = 0$$
$$= 2\sin\phi\cos\phi\,(F^2 - \tau_s^2) + 2F\tau_s \cos\Delta\,(\cos^2\phi - \sin^2\phi), \quad (21)$$

where $\Delta = \beta - \gamma$. It is obvious therefore that:

$$\tan 2\rho_s = 2F_s\tau_s \cos\Delta/(\tau_s^2 - F^2). \quad (22)$$

Since F is generally of the order of 1% of τ_s, the angle of saturation of the Faraday rotation is small and (22) becomes:

$$\rho_s = F_s \cos\Delta/\tau_s. \quad (23)$$

Similar considerations apply, of course, for deriving the rotation ρ_p for the plane of polarization parallel to the plane of incidence. Clearly, these derivations are the analog of the expressions obtained by Lissberger[9] for the Kerr effect.

Appendix II

The problem of the change in the path length of the light within the film as a function of the angle of incidence may be treated subject to a simplified statement of the boundary conditions such as introduced, for example, by von Hippel[18]:

Assume a plane, monochromatic wave traveling through a lossless medium with permittivity and permeability of unity, impinging upon a "thick," homogenous and isotropic film having a complex index of refraction and a sufficiently large extinction coefficient so that multiple internal reflections may be ignored. The behavior of the refracted ray will still be described by the generalized form of Snell's law and with the coordinate system of Fig. 1:

$$\sin\theta = \hat{n} \sin\hat{\theta} \quad (24)$$

where $\hat{n}$ is the complex index of refraction and $\hat{\theta}$ the imaginary angle of refraction of the film. Let

$$\hat{n}\cos\hat{\theta} = n(1 - \sin^2\theta)^{1/2} = p + i\zeta. \quad (25)$$

The time and space parameters of the transmitted wave E_t for a zx plane of incidence is then:

$$E_t = E_0\{\exp(\omega x\zeta/c)\cdot\exp\,(i\omega)\cdot t] - (px + z\sin\theta/c)]\} \quad (26)$$

in terms of Eq. (25). The surface, $x\zeta$ = constant, is parallel to the plane of the film and represents a surface of constant amplitude for the transmitted wave. The surface defined by $px + z\sin\theta$ = constant is a surface of constant phase. The direction of propagation of the wave within the film is perpendicular to this surface of constant phase and makes an angle ψ with respect to the film normal, hence:

$$\tan\psi = (\sin\theta)/p. \quad (27)$$

Squaring (27), we obtain by a trigonometric relation:

$$\cos\psi = p[\sin^2\theta + p^2]^{-1/2}. \quad (28)$$

By squaring Eqs. (24) and (25) and adding them, one obtains:

$$n^2 = p^2 + 2ip\zeta - \zeta^2 + \sin^2\theta \quad (29)$$

and since $\hat{n}^2 = [n(1 - ik)]^2$ Eq. (29) becomes, upon equating reals and imaginaries:

$$n^2 - k^2n^2 = p^2 - \zeta^2 + \sin^2\theta$$
$$-2kn^2 = 2p\zeta. \quad (30)$$

The simultaneous solution of the equations in (30) is that of a biquadratic equation in p of the form:

$$p^4 + p^2[\sin^2\theta + n^2(k^2 - 1)] - n^4k^2 = 0. \quad (31)$$

Letting $x = n^2(k^2 - 1) + \sin^2\theta$, the solution to (31) may be written as:

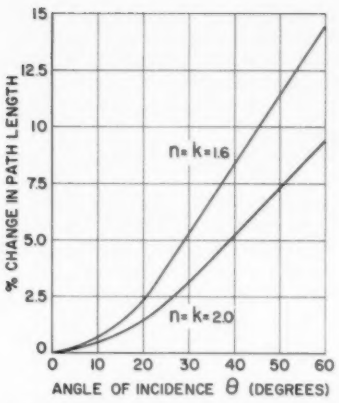

Fig. 10. A plot of $[1 + (\sin \theta/p)^2]^{1/2}$ from Eq. (33) Appendix II vs angle of incidence shows the correction in the path length of light due to refraction effects in the film.

$$2p^2 = -x + (x^2 + 4n^4k^2)^{1/2}. \tag{32}$$

The path length s of the wave through the film is $s = d/\cos\psi$, where d is the effective physical thickness of the film; the path length may therefore be written:

$$s = d[1 + (\sin \theta/p)^2]^{1/2}, \tag{33}$$

where p is defined by Eq. (32). Hence s is seen to be a function of the angle of incidence, the index of refraction, and the extinction coefficient of the film.

An estimate of n and k for iron and nickel alloys, based on published values of these parameters[19] for the individual elements in the visible region of the spectrum, leads to a mean value of $n = k = 1.6$ and probable extremes of $n = k = 2$. By means of Eq. (33) the percent change in d as a function of the angle of incidence was calculated for these parameters and is presented in Fig. 10. For metallic films having a large extinction coefficient, the planes of constant phase are nearly parallel to the planes of constant amplitudes. Hence, as seen from Fig. 10, the error is relatively small if s is taken to be $s \simeq d$ for $\theta < \pi/4$.

Appendix III

The transmissivity as a function of the angles of incidence and azimuth may be calculated by introducing a number of theoretical simplifications.[20] It will be assumed that:

(a) The boundary value problem may be solved in terms of the interaction of a plane polarized wave with the film at the air–film boundary and subsequently after passage through the film, at the film–glass–substrate boundary.

(b) The light incident upon the film is monochromatic with a wavelength $\lambda = 500$ mμ.

(c) The index of refraction of the film n is complex, $\hat{n} = n(1 - ik)$ with n and k being the real index and the extinction coefficients, respectively. Let $\hat{n}\cos\hat{\theta}_2 = (u - iv)$ and the glass substrate be considered nonabsorbing and its index of refraction $n \simeq 1.5$ as real.

(d) Absorption within the film will be large so that interference effects may be neglected and the film considered as effectively "thick."

By these means, the problem is reduced in complexity and, while tedious, is readily solved. Consider first an azimuth of $\alpha = \pi/2$, then:

$$\tau_{12}^2 = \frac{(2\cos\theta)^2}{(\cos\theta + u)^2 + v^2}, \qquad \tau_{23}^2 = \frac{4(u^2 + v^2)}{(n\cos\theta + u)^2 + v^2}, \tag{34}$$

where τ_{12} is the amplitude transmittance at the air–film boundary and τ_{23} is the corresponding transmittance at the film–glass boundary and the parameters u and v are defined by:

$$2u^2 = B + (B^2 + 4n^2k^2)^{1/2}, \tag{35}$$

$$2v^2 = -B + (B^2 + 4n^4k^2)^{1/2},$$

with $B = n^2(1 - k^2) - \sin^2\theta$ and the angle of refraction in the glass, θ', defined by $n' \sin\theta' = \sin\theta$.

For an azimuth $\alpha = 0$, the transmittance at the respective boundaries are:

$$\tau_{12}^2 = \frac{4n^4(1 + k^2)^2\cos^2\theta}{[n^2(1 - k^2)\cos\theta + u]^2 + [2n^2k\cos\theta + v]^2}, \tag{36}$$

$$\tau_{23}^2 = \frac{(2n')^2(u^2 + v^2)}{[n'u + n^2(1 - k^2)\cos\theta']^2 + [n'v + 2n^2k\cos\theta']^2}. \tag{37}$$

The transmissivity $\mathfrak{I}$ is given by:

$$\mathfrak{I} \cong \left(\frac{l\cos\theta'}{\cos\theta}\right)\tau_{12}^2 \cdot \tau_{23}^2 \exp\left(-\frac{4\pi}{\lambda}vd\right), \tag{38}$$

where $l = n'$ or $(1/n')$ depending upon whether the transmissivity perpendicular or parallel to the plane of incidence is being calculated, and the appropriate boundary transmittances τ_{12} and τ_{23} are chosen for the purpose; the parameter s is the path length of the wave in the film.

Using the measured value of d and $n = k = 1.65$, a very good fit was obtained for the curves of $\mathfrak{I}_s$ vs θ and $\mathfrak{I}_p$ vs θ shown in Fig. 7. It appears, therefore, that the gross simplifications introduced here do have some merit in allowing a simplified analytical representation for the dependence of the transmissivity upon the angle of incidence.

References

1. W. Schutz, *Magnetooptik* (Akademische Verlag, M.B.H. Leipzig, 1936), Part I, Vol. 16, part of Handb. der Experimentalphysik.
2. W. Voigt, *Magneto-und Electrooptik* (Teubner Verlag, Leipzig, 1908).
3. J. J. Miyata, "Optical readout of digital magnetic recording," Proc. Non-Linear Magnetics and Magnetic Amplifiers Conference, Philadelphia, Pa., October 1960.

4. R. L. Conger and J. L. Tomlinson, J. Appl. Phys. **33** (Suppl.), 1059 (1962).
5. R. J. Prosen, J. O. Holmen, B. E. Gran, and T. J. Cebula, J. Appl. Phys. **33** (Suppl.), 1150 (1962).
6. C. A. Fowler and E. M. Fryer, Phys. Rev. **104,** 552 (1956).
7. L. Reimer, Z. Naturforsch. **11a,** 611 (1956).
8. G. H. Moore, Naval Ordnance Laboratory Tech. Memo 42-5 (1957).
9. P. H. Lissberger, J. Opt. Soc. Am. **51,** 957 (1961).
10. M. S. Blois, Jr., J. Appl. Phys. **26,** 975 (1955).
11. S. Tolansky, *Multiple Beam Interferometry of Surfaces and Films* (Clarendon Press, Oxford, 1948).
12. M. H. Seavey and P. E. Tannenwald, J. Appl. Phys. **29,** 292 (1958).
13. H. Konig, Optik **3,** 101 (1948).
14. J. Kranz and W. Drechsel, Z. Physik **150,** 632 (1958).
15. W. Heinrich, Sitzber. math.-naturw. Kl. bayer. Akad. Wiss. München **1955,** 133 (1956).
16. E. W. Lee, D. R. Callaby, and A. C. Lynch, Proc. Phys. Soc. **72,** 233 (1958).
17. P. Smaller, Ampex Corp., Redwood City, Calif. (private communication).
18. A. R. von Hippel, *Dielectrics and Waves* (Wiley, New York, 1954).
19. *Handbook of Chemistry and Physics* (Chemical Rubber Publ. Co., Cleveland, Ohio, 1954), 36th Ed.
20. M. Born and E. Wolf, *Principles of Optics* (Pergamon Press, London, 1959).

From the Editor

In considering matters such as the metric system, it is necessary to remember that the opinions of a scientist may be sought on such technical matters as determining standards, but neither governments nor the general public are going to change established habits because of logical arguments or scientific persuasion. Gene al changes are only instituted when there is a business or economic reason to do so. At the time of the French Revolution, there was considerable demand for uniform public weights and measures to put an end to clever practices of merchants who had one weight for buying and another for selling. The National Convention appointed a commission that included such scientists as Laplace and Lagrange to devise the system of weights and measures that we call the metric system. This system was imposed on France by fiat of Napoleon, who had proclaimed himself First Consul in 1799. Napoleon, who had excelled in mathematics, prided himself on his orderly mind. "As a boy," he once wrote, "I knew the logarithms of thirty or forty numbers." But his chief reason for adopting the system was not a love of science but rather to improve tax collection on goods and materials that had to be measured or weighed. The metric system quickly established itself among scientists, and it is sad to note that it was probably anti-Napoleonic sentiment that prevented England from accepting the metric system at that time.

Let us consider some other standardizations that were adopted for business rather than scientific reasons. Time zones were introduced into the United States by the railroads, who found that local time made it difficult to compute schedules for trains. The convention that maps should show the zero meridian through the Royal Observatory at Greenwich was imposed not by scientists but by the maritime industry, which was at the time (1875) dominated by Britain. Prior to that time it was conventional for each country to draw the zero meridian through its own capital: Paris, Berlin, or Washington. Astronomers and other scientists saw no particular reason to fix the zero meridian; it was easy enough to add or subtract the position of the observer from the zero of the map or table. Those scientists who saw an advantage in fixing the zero meridian felt it should go through the Canary Islands, so that the Old World and the New would be more clearly separated.

The map-makers recently added another convert to the metric system: the Army Map Service has adopted the scales of 1:1,000,000; 1:100,000; etc., which are metric (i.e., mm or cm can be converted directly to km) rather than the English scales of miles per inch. The military now specify the bore of guns and cannons in millimeters instead of inches and caliber: it came as rather a shock to the military during World War II to discover that the French resistance movement could not use 30-caliber shells in 9-mm machine guns. Again this change was due to practical, or economic, rather than scientific reasons.

The Space Age is forcing another metric change on us. The success of the Tiros weather satellite in obtaining world-wide weather data made it suddenly desirable to be able to correlate quickly our weather maps with those of the rest of the world, most of which are in metric measure. The Air Weather Service issued a regulation on 10 October 1962 that effective 1 January 1963 height values of radiosonde, rawinsonde, and dropsonde reports will be reported in geopotential meters instead of geopotential feet. Intervals of absolute and relative topography will be 120 m (approximately 400 ft) or 60 and 30 m (approximately 200 and 100 ft). Isotherms intervals will be either 5°C (10°C and 2½°C when appropriate) or 2°C (1°C when appropriate). Isotach intervals will be 10 m/s (approximately 20 knots); 20 m/s or 5 m/s (approximately 40 and 10 knots) intervals may be used.

Although this regulation does not apply to purely domestic uses, where English (customary) units can continue to be employed, all training publications and aids must be amended to include both systems, and meteorological equipments will be planned and engineered for readout in elements of the metric system or in both customary and metric units.

The average American is not going to change his customs because scientists urge it, but the metric system is encroaching relentlessly on him. There have even been advocates of the metric system in the comic strips of his newspaper. Dean Athelstan Spilhaus of the University of Minnesota, who authors a feature in the Sunday comic pages called "Our New Age" devoted a recent issue (7 October 1962) to a graphic discussion of the confusion of liquid quarts, dry quarts, grains, drams, and ounces, with a plea that scientists everywhere and all people in 100 countries use the metric system. Could not Britain and the United States get in step?

J. N. Howard

Photographic Emulsions as Computer Storage Media—Especially with CRT Readout

Leo Levi

When long term storage is desired, photographic films are attractive storage media for electronic computers. Their storage capacity is limited primarily by granularity and turbidity of the emulsion and the spot size of a practical readout device. The relations between the element size and the number of resolvable density steps are derived as a function of the emulsion granularity and point-spread function and the light distribution in the scanning spot. Simplifications for special limiting cases of interest are derived and one such case is worked out numerically.

I. Introduction

As computer technology advances, more information storage devices compatible with high-speed computers are required. When permanent storage is required, photographic films with cathode-ray tube scanners are among the most promising. It should therefore be of some interest to evaluate the storage capabilities of actual photographic emulsions from the point of view of such a computer application. A general analysis in terms of information capacity was made in an excellent paper by Jones,[1] but his results are not readily applied to the present problem.

In the system envisioned, the information to be stored is expressed in terms of optical density and position, so that a given quantity of information corresponds to a unique density pattern. This density pattern is impressed on the photographic emulsion by appropriately exposing each area element. The information is then read out by striking the appropriate element with a constant spot of light from a cathode-ray tube* and receiving the transmitted light on a phototube.

The limitations inherent in this system are primarily due to the following factors:

1. It is impossible to impress a given density on a given film element by exposure and processing control alone. The resulting density is determined by the chance concentration of developable grains in addition to the exposure and processing. The random fluctuations occurring around the average density are called "granularity".

2. It is impossible to limit the exposing light to a given area element. Refractive nonuniformities in the emulsion, generally termed "turbidity", will scatter it into neighboring areas, whose density is thus affected by irrelevant information.

3. The readout scanning spot will cover an area much larger than the area element of interest, due primarily to reflections inside the CRT face plate, and to the finite electron beam size. Although the brightness of the spot may fall off almost completely over a very small area, there may be still significant contributions from points far removed from the bright spot center.

4. The scanning spot intensity itself may be modulated in a random manner by the chance distribution of grains in the phosphor screen.

The implication of all these factors is simply that the area element on the photographic film corresponding to one item of information must be made large enough to make these effects negligible. In other words, if one specifies a certain number of discernible density levels for the system, one has implicitly specified the maximum number of information items that can be accommodated on a given piece of photographic film (using a given CRT).

It is the purpose of this paper to analyze the basic relationships governing area element, size, and number of discernible information levels as a function of film and CRT parameters. A similar analysis, considering only granularity, has been made earlier.[2] The first step is, of course, to translate the system requirements

The author is a consulting physicist, New York, N.Y.

Received 12 March 1962.

* Clearly other readout spot images may be used and the following work can readily be applied to them when their point-spread function is known.

into a tolerance on the density. This translation will generally be a function of the specific system, but the average tolerance can never be more than

$$\overline{2\delta D} = (D_{\max} - D_0)/N, \tag{1}$$

where $D_{\max, 0}$ are the maximum and minimum usable density values, respectively, and N is the number of information levels which must be discernible.

We shall now determine what the minimum area element must be so that granularity effects permit us to maintain the $\pm\delta D$ tolerance.

II. Granularity

Granularity is a statistical phenomenon so that requirements on it can properly be expressed only in terms of probability. In other words, we cannot require that the density fluctuations *never* exceed D, only that the probability of their exceeding D be less than some small number $(1 - P)$.

On the basis of theoretical considerations, Selwyn[2] found that the density fluctuations were normally distributed and that their standard deviation varied with the square root of the area element a. He gives for the probability of finding a density deviation in the interval $u, u + du$:

$$P(u, du) = \sqrt{\frac{a}{G^2\pi}}\, e^{-u^2a/G^2}\, du, \tag{2}$$

where G is a granularity constant of the emulsion. (G is effectively the standard deviation of density observed when an area element of area one-half is viewed at a time.) G is found to be constant over wide ranges of area,[4] and is therefore a useful parameter in our investigation. It does vary with density.[1,3]

We can now write immediately the expression for the probability of finding at any spot a density within the tolerance range $D_1 \pm \delta D$ when the emulsion is exposed to the average density D_1. It is

$$P(D_1, \delta D) = \operatorname{erf}\left[\frac{\sqrt{a}\,\delta D}{G(D_1)}\right], \tag{3}$$

where

$$\operatorname{erf}(x) = \frac{1}{\sqrt{\pi}} \int_{-x}^{x} e^{-u^2} du. \tag{4}$$

Solving for a we find explicitly:

$$a = \left[\frac{G}{\delta D} \operatorname{erf}^{-1}(P)\right]^2, \tag{5}$$

where G is the known granularity of the material, δD the tolerance on density, and P the specified probability of remaining within this tolerance.

The above expression specifies the area element that must be viewed at once and presupposes that all parts of this element are illuminated equally. On the other hand, in the system under consideration the illumination distribution is that of the CRT spot image and is, therefore, far from uniform. It can be shown (see Appendix) that the effective area of the CRT spot is given by:

$$a = \frac{\left[\int_A\int B(x, y)dx\, dy\right]^2}{\int_A\int B^2(x, y)dx\, dy}, \tag{6}$$

where $B(x, y)$ represents the brightness of the CRT spot image at point (x, y), and the integration is performed over the whole effective CRT face (or all portions of significant brightness of the image). For instance, if the brightness of the scanning spot has the form:

$$B(r) = \frac{B_0}{2\pi s^2}\, e^{-r^2/2s^2} \tag{7}$$

then the effective area is

$$a_e = 4\pi s^2. \tag{8}$$

Equation (5) then specifies the minimum *scanning spot* size, if density fluctuations are to be kept below D.

If phosphor grain is to be taken into account, the distribution of fluctuations in phosphor efficiency must be known for the given spot size. Unfortunately, it was impossible to obtain these data.

Assuming (1) that this distribution, too, is Gaussian, and (2) that its variance varies inversely with the spot area, we may combine phosphor grain effects with those of the photographic emulsion by using a combined granularity constant

$$G = \sqrt{G_E^2 + G_P^2}, \tag{9}$$

where G_E is the granularity constant of the emulsion and G_P is the standard deviation of the logarithm of brightness when the phosphor is scanned with a spot of effective area one-half.

III. Turbidity

The amount of error introduced into the record due to internal scattering of light is far more difficult to evaluate due to the nonlinear character of the H and D curve: $D = f(E)$, where E is the logarithm of exposure. We assume that the point spread function of the light in the emulsion is known to be of the form $S(r)$, where $S(r)$ represents the amount of exposure at a point a distance r from a point on the emulsion having received unit exposure.

We simplify the algebraic work by writing directly the transmissivity as a function of the exposure:

$$T = g(e), \tag{10}$$

where

$$T = 10^{-D} \tag{11}$$

Then the exposure e at any point will be, in terms of the impressed exposure e^*,

$$e(x, y) = \int_A\int e^*(x', y')S[(x - x')^2 + (y - y')^2]^{1/2}dx'\,dy' \tag{12}$$

and the amount of light transmitted with the scanning spot at (x_0, y_0)

$$L(x_0, y_0) = \int_A\int T(x, y)B[(x - x_0), (y - y_0)]dx\,dy$$
$$= \int_A\int g\{\int\int e^*(x', y')S[(x - x')^2 + (y - y')^2]^{1/2}dx'\,dy'\}B[(x - x_0), (y - y_0)]dx\,dy. \tag{13}$$

On the other hand, the amount of light that would be transmitted in the absence of turbidity effects, and with the total spot luminosity $B_0 \equiv \int BdA$ concentrated in a point, would be

$$L^*(x_0, y_0) = B_0\, g[e^*(x_0, y_0)]. \tag{14}$$

When the exposure e^* in the region surrounding x_0, y_0 is given a constant value, say e, L will approach L^* as this region is increased in area, a. The value of a for which $10^{-\delta D} < L/L^* < 10^{+\delta D}$ represents the minimum element area sought.

In general it will be neither practical nor necessary to evaluate the convolution integral (12) for the exposure at point (x, y). It will suffice to take the most severe situation of an element with minimum exposure e_1 surrounded by a region with maximum exposure e_2. By breaking up the integral (12) into two regions, e^* may be treated as a constant and taken out of the integral, yielding, for A exceeding the region of significant S,

$$e(x, y) = e_2\int_A\int S[(x - x')^2 + (y - y')^2]^{1/2}dx'\,dy'$$
$$+ (e_1 - e_2)\int_a\int S[(x - x')^2 + (y - y')^2]^{1/2}dx'\,dy'$$
$$= e_2 + (e_1 - e_2)U(a, \sqrt{x^2 + y^2});$$

or

$$e(r) = e_2 + (e_1 - e_2)\,U\,(a, r), \tag{15}$$

where $U\,(a, r)$ represents the integral over a region a, situated a distance r from the center of the point-spread function. The resulting expression for the transmission ratio is, when the origin is taken at the center of the scanning spot ($x_0 = y_0 = 0$) and using Eqs. (10) and (15) in the second member of Eq. (13):

$$\lambda = \frac{L}{L^*} = \frac{1}{B_0\, g(e_1)}\int_A\int B(x, y)\, g[e_2 + (e_1 - e_2)U(a, \sqrt{x^2 + y^2})]dx\,dy. \tag{16}$$

If B, too, has circular symmetry and becomes negligible before the edge of the CRT is reached, this may be written:

$$\lambda = \frac{2\pi\left\{\int_0^\infty r\, B(r)\, g[e_2 + (e_1 - e_2)\,U\,(a, r)]dr\right\}}{B_0\, g(e_1)} \tag{17}$$

At this point it becomes necessary to introduce some specialization. We shall assume that the area element is a square $2b \times 2b$. (The alternative, a hexagonal area element, would result in a slightly smaller resolution element, but the resultive increased difficulty in the numerical analysis appears unwarranted, especially in view of the approximate nature of the other assumptions.) Realistic approximations for the other parameters are somewhat more difficult to make. The form of the effective point-spread function is complicated by adjacency effects in processing and that of the CRT spot by reflections from the face plate surface. The following assumptions should therefore be taken as illustrations rather than recommendations:

If $S\,(r)$ is taken to be Gaussian

$$S(r) = \frac{1}{2\pi\sigma^2}\, e^{-r^2/2\sigma^2}, \tag{18}$$

we find that

$$U(r, b) = {}^1\!/_2\,\mathrm{erf}\left(\frac{b}{\sqrt{2}\sigma}\right)\left[\mathrm{erf}\left(\frac{r + b}{\sqrt{2}\sigma}\right) - \mathrm{erf}\left(\frac{r - b}{\sqrt{2}\sigma}\right)\right]. \tag{19}$$

$B(r)$ is usually taken as

$$B(r) = \frac{B_0}{2\pi s^2}\, e^{-r^2/2s^2} \tag{20}$$

and, in the linear portion of the H and D curve, we may take

$$T = g(e) = T_0\left(\frac{e_0}{e}\right)^\gamma,\ e > e_0. \tag{21}$$

With these assumptions, λ becomes:

$$\lambda = \frac{e_1}{s^2}^\gamma\int_0^\infty re^{-r^2/2s^2}\left\{e_2 + \frac{(e_1 - e_2)}{2}\,\mathrm{erf}\left(\frac{b}{\sqrt{2}\sigma}\right)\left[\mathrm{erf}\left(\frac{r + b}{\sqrt{2}\sigma}\right) - \mathrm{erf}\left(\frac{r - b}{\sqrt{2}\sigma}\right)\right]\right\}^{-\gamma}dr. \tag{22}$$

λ may now be evaluated as a function of b, and that value of b for which $\lambda = 10^{-\delta D}$ gives the minimum element size. If conditions are such that $s << \sigma$, we may set $r = 0$ in the factor in braces and take this factor out of the integral. This yields

$$\lambda = \left(\frac{e_1}{e_2 + (e_1 - e_2)\,\mathrm{erf}^2\,(b/\sqrt{2}\sigma)}\right)^\gamma = 10^{-\delta D} \tag{23}$$

or, letting $e_2/e_1 = R$,

$$b = \sqrt{2}\,\sigma\,\mathrm{erf}^{-1}\left(\frac{R - 10^{\delta D/\gamma}}{R - 1}\right)^{1/2}, \qquad (24)$$

again giving the size of the area element in closed form.

IV. Numerical Results

We shall now apply the above results to an actual emulsion. Higgins and Stultz[4] give the Selwyn granularity of Kodak Plus-X film at a density of 0.13 and scanning aperture diameter 24 μ as $G = 0.66$.

Zweig *et al.*[5] give the line-spread function of Plus-X film and Jones[6] both line and point-spread functions of other films. From these two papers it is possible to estimate the value of σ of Plus-X film as 7 μ. (Since the shape of the point-spread function is not truly Gaussian, it is here approximated by a Gaussian curve whose 2.5% points coincide with those of the actual point-spread function. This is the lowest point that could be read off the curve.)

Assuming that it is required that twenty signal levels be distinguishable over a density range $D_1 = 0.2$, $D_2 = 2.2$ and that $\gamma = 1$ ($R = 100$), we find that $\overline{\delta D} = 0.05$. For the present approximation we shall take this* as our operating $\overline{\delta D}$ and require that the probability of exceeding this tolerance be less than 0.034. We have then

$$\mathrm{erf}^{-1}(P) = 1.5,$$

and using Eqs. (5) and (8):

$$a = 400 \text{ sq. } \mu, \qquad s = 5.65\ \mu.$$

Noting that $[(R - 10^{\delta D/\gamma})/(R - 1)]^{1/2} = 0.99939$ and $\mathrm{erf}^{-1}(0.99939) = 2.423$, we find, using Eq. (24): $b = 24\ \mu$. Thus, the resolution element should not be made smaller than 48 μ square.

Working out the case where only two levels (black and white) are to be recorded, we use $G = 1.21$ (corresponding to an operating density 0.96) and $\sigma = 4.6\ \mu$ (corresponding to the 10% point on the point-spread function). We may take δD here as 1. This calls for $b = 9\ \mu$ so that 18-μ elements are possible. This corresponds to 350,000 elements per square cm. Obviously, higher resolution films will yield correspondingly greater storage capacity.

Conclusions

The relationship between the number of spatial resolution elements and the number of discernible levels of gray has been worked out in terms of emulsion granularity and point-spread function and CRT spot parameters. The resulting expressions lend themselves to evaluation by numerical integration methods [Eq. (17) and (22)]. With certain simplifying assumptions, expressions in closed form can be obtained [Eq. (24)]. A numerical example showed that with all the above limitations, the photographic emulsion is a highly efficient information storage medium. Not too much weight should be attached to the numerical examples worked out because of the discrepancy between fact and assumption.

Appendix. The Effective Area of a Nonuniformly Illuminated Scanning Spot in Determining Granularity Effects

Let the standard deviation (s.d.) of the transmissivity be given by $t/\sqrt{a_e}$, where a_e is the equivalent area, and let the s.d. of an elementary area α be given by $\tau = t/\sqrt{\alpha}$.

The s.d. of the average transmissivity equals the s.d of the transmitted light over the area covered divided by the incident light.

Clearly, with a scanning spot of a brightness/unit area distribution $B(x, y)$, the s.d. of the transmitted light is the root-sum-square of the s.d.'s of all the elementary area segments α (even though the distribution of the transmissivity fluctuations is *not* normal). That is,

$$\sigma(L) = \sqrt{\sum_N (\alpha B \tau)^2} = \sqrt{\sum_N \alpha^2 B^2 t^2/\alpha} = t\sqrt{\sum_N B^2\,\alpha} \doteq t\sqrt{\int B^2\,da},$$

where αB is the light incident on each area element. Similarly, the incident light is given by

$$L_0 = \int B da.$$

We have therefore for the s.d. of the transmissivity:

$$\sigma(T) = \frac{t\sqrt{\int B^2\,da}}{\int B\,da} = t/\sqrt{a_e}.$$

We conclude that the equivalent area of the above situation is:

$$a_e = [\int B da]^2/\int B^2\,da.$$

References

1. R. C. Jones, J. Opt. Soc. Am. **51,** 1159 (1961).
2. L. Levi, J. Opt. Soc. Am. **48,** 9 (1958).
3. E. W. H. Selwyn, Phot. J. Sec. B **75,** 571 (1935).
4. G. C. Higgins and K. F. Stultz, J. Opt. Soc. Am. **49,** 925 (1959).
5. H. J. Zweig, G. C. Higgins, and D. L. MacAdam, J. Opt. Soc. Am. **48,** 926 (1958).
6. R. C. Jones, J. Opt. Soc. Am. **48,** 934 (1958).

* The actual δD should be a function of the density. Specifically it should be $\delta D(D_1) = C/G(D_1)$ where

$$C = \frac{(D_{\max} - D_0)}{2}\left[\sum_{i=1}^{N} \frac{1}{G(D_i)}\right]^{-1}.$$

Photorefractometer I. Extension of Sensitivity and Range

N. S. Kapany and D. A. Pontarelli

The fractional sensitivity and operational refractive index range of the rod photorefractometer have been extended by physical modifications of axially symmetric refracting elements and the mode of illumination. Optical systems using conical and cylindrical rod elements with flat or spherical entrance ends illuminated by an axial light cone or a hollow annular light cone have been studied. Expressions describing the sensitivity of these configurations are presented, and typical numerical cases are computed on an IBM 650 computer. Extension of range to specimen index close to 1.0 permits the photorefractometer to detect index changes of low refractive index media. Experimental verification of the theory is achieved.

I. Introduction

The basic theory of a dielectric rod photorefractometer and experimental results have been described by Kapany and Pike.[1,2] The optical system of a photorefractometer consists of a long dielectric cylinder with its entrance end illuminated by an axial cone of monochromatic radiation, a photoelectric detector located at the exit end, and the specimen medium surrounding the rod. If the specimen medium surrounding the rod has a refractive index substantially lower than that of the rod, and the interface is of high optical quality, the incident radiation is transmitted along the rod directly and by multiple total internal reflections. However, when the two indexes are close, the total flux reaching the detector is, of course, a function of the critical angle at the rod–specimen interface which is related to the refractive index changes occurring in the surround. This change in refractive index of the medium can be simply related to its various other physical constants such as temperature, pressure, composition, and concentration, etc.

A detailed theoretical investigation of a dielectric-rod-type and cone-type photorefractometer and its application to problems in process control refractometry, concentration determination, etc., has been undertaken. It is shown that both the range and the sensitivity of a photorefractometer can be increased substantially by modifying the rod and cone elements and using an incident hollow cone illumination. Thus, a substantial improvement over the straight rod-type element is achieved.

The authors were both at the Physics Division, Armour Research Foundation, Chicago, Illinois. N. S. Kapany is now at Optics Technology, Inc., 248 Harbor Blvd., Belmont, California.

Received 13 January 1962.

This work was sponsored by Chicago Aerial Industries, Chicago, Illinois.

This paper was presented in the Forty-Third Annual Meeting of the Optical Society of America, October 1958, Detroit, Michigan.

II. General Theory

The optical arrangement of a basic rod refractometer system is illustrated diagrammatically in Fig. 1. A point source is imaged on the axis of the cylinder; therefore, all rays in the light cone can be treated as meridional. After refraction at the entrance end of the rod, radiation contained in the shaded region (solid lines) is totally reflected and hence conducted along the rod to the detector, while rays outside this cone are refracted out of the rod into the surrounding medium after a certain number of reflections and, therefore, are lost to the detector. Changes in refractive index of the surrounding medium affect the critical angle at the rod–medium interface, thereby producing a variation in the angle of the totally reflected light cone which in turn results in the variation of total flux received by the detector. Expressions in the elementary theory relating index changes of the surrounding medium to the flux reaching the detector have been modified[1] to take account of absorption losses in the rod, reflection losses at the rod ends, and Fresnel reflection at the cylindrical walls. Multiple internal reflections within the rod are of importance, for they provide excellent rejection of nontotally reflected radiation after ten or more reflections and thus render the system highly sensitive when the refractive index of the rod and the surround are close. However, reflection losses at the ends combined

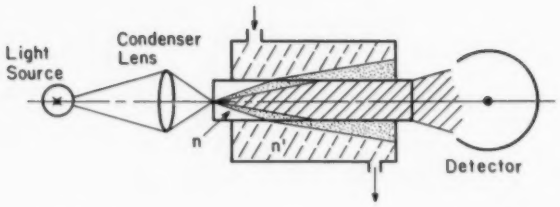

Fig. 1. Illustrating the basic photorefractometer design.

with refraction of the incident light cone cause the simple rod photorefractometer to be less sensitive for large refractive index differences between the rod and the surround.

The elementary theory describing the photorefractometer operation uses the quantities: the emergent flux E' calculated from geometric considerations, the sensitivity S' taken as the first derivative of the flux with respect to n', the index of the surround, and the fractional sensitivity S/E. These quantities are functions of the illumination system, refracting element geometry, index of the element n, and index of the surround n'. The minimum detectable change in n' is given by

$$|(\Delta n')|_{\min} = \frac{dE/E}{S/E}, \tag{1}$$

where dE/E is the sensitivity of the detection system.

The emergent flux E is given by the expression

$$E = K_1 \int_{\theta_2}^{\theta_1} [1 - R(\theta)]^s \cdot \exp(-\alpha L \sec\theta') \cdot \sin\theta' d\theta. \tag{2}$$

In this expression, the term $[1-R(\theta)]^s$ represents the Fresnel reflection losses at the rod ends and K is a constant. The quantity s has the value 1 or 2, depending on the shape of the rod ends and the type (air spaced or immersed) of detector used. The incident and refracted angles θ and θ' are as shown in Fig. 2. The term $\exp(-\alpha L \sec\theta')$ accounts for absorption losses in the rod of axial length L. The Fresnel reflection coefficient $R(\theta)$ for unpolarized light is calculated from the well-known expression

$$R(\theta) = {}^1/_2(\rho_{\|} + \rho_{\perp}),$$

where

$$\rho_{\|} = \left[\frac{\cos\theta - (n^2 - \sin^2\theta)^{1/2}}{\cos\theta + (n^2 - \sin^2\theta)^{1/2}}\right]^2,$$
$$\rho_{\perp} = \left[\frac{n^2\cos\theta - (n^2 - \sin^2\theta)^{1/2}}{n^2\cos\theta + (n^2 - \sin^2\theta)^{1/2}}\right]^2. \tag{3}$$

The exact sensitivity term S is given by

$$S = (1 - R)^s S'. \tag{4}$$

A. Illumination and Rod Configurations

For the simple configuration illustrated in Fig. 1, it can be shown that

$$E'(n, n') = 2\pi I(\theta)[1 - (1 - n^2 + n'^2)^{1/2}] \tag{5}$$

and

$$S' = 2\pi I(\theta)\left[\frac{n'}{(1 - n^2 + n'^2)^{1/2}}\right], \tag{6}$$

where $I(\theta) = I(0)$ if the angular energy distribution in the incident light cone is uniform. Expressions describing the general configuration of hollow cone illumination incident upon a flat ended rod with an air-spaced detector are presented in Appendix A. Values of S/E were computed on an IBM 650 computer for a simple rod configuration having $n = 1.5$ and $1.12 < n' < 1.5$, and are plotted in Fig. 3(a). The high fractional sensitivity attainable when the index of the specimen medium is only slightly lower than the rod index is clearly demonstrated, and it is seen that increasing difference between the two indexes results in a decrease in fractional sensitivity.

Fresnel reflection losses for oblique rays at the entrance end are significantly reduced by making the end surface concave or convex and centered upon the focal point of the illumination system. Changing the air-spaced detector to a detector immersed on the rod end eliminates the Fresnel reflection loss at the exit end. A ground rod end accomplishes somewhat the same purpose for an air-spaced detector, but at the cost of a considerable loss of flux. Two of these design changes are incorporated in the refractometer shown in Fig. 3(b). Where the operational index range was previously between $(n^2 - 1)^{1/2} = n' < n$, it is now enhanced to $1.000 \leq n' < n$. Thus an extension of the fractional sensitivity to large index differences has been accomplished by modification of the rod end, illumination configuration, detector position, and finally by the use of a conical element. This extension of operation range to lower surround refractive index values and larger differences of refractive index is desirable because of the possibility of using a single rod to cover a wide range and because of the lack of availability of optical rod materials with refractive indices between 1.00 and 1.45.

The E versus n' curve shows that high fractional sensitivity exists when most of the flux is incident at an angle close to critical. By providing a hollow cone illumination as shown in Fig. 3(c), the above condition for index values of $n' < n$ is established. A centrally

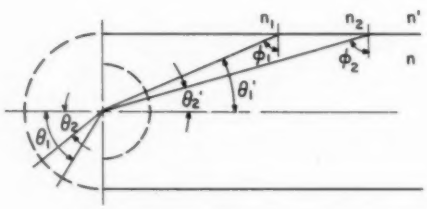

Fig. 2. Rod entrance end geometry.

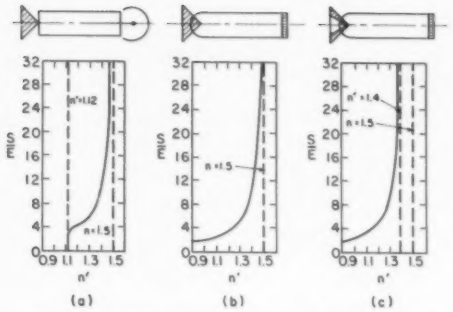

Fig. 3. Fractional sensitivity of various cylindrical rod systems.

located disk obscuring the inner portion of the high numerical aperture light cone shifts the region of high fractional sensitivity. Furthermore, combining the hollow cone radiation, the spherical ended rod, and the optically immersed detector results in a system having a controllable fractional sensitivity and a large range: the range of operation is $1.00 \leq n' \leq n_1$, where $n_1 < n$.

The results of calculations of fractional sensitivity for three rod configurations illustrated in Fig. 3 are for the physical constants $n = 1.5$, $n_1 = 1.40$, $L = 10.2$ cm, $\alpha = 0.002$/cm, and $0.9 < n' < 1.5$. In Fig. 3(a), the typical high sensitivity at $n' = 1.50$ and the sharp cutoff at $n' = 1.12$ is observed. Hollow cone illumination shown in Fig. 3(c) causes the fractional sensitivity maximum to shift to a lower index value $n' = 1.4$. A spherical entrance rod end, as shown in Fig. 3(b) and (c), changes the form of the curve for low n' values, but leaves the maximum and minimum values unaltered. The spherical rod end and immersed detector extend the region of fractional sensitivity to specimen index values below 1.00. The combination of hollow cone illumination and modified rod ends shown in Fig. 3(c) theoretically permits the photorefractometer to operate in the refractive index range $0.9 \leq n' \leq 1.4$ with maxmum fractional sensitivity at $n' = 1.4$.

III. Cone Geometry

Before discussing the application of a refracting conical element to the photorefractometer, let us consider the geometrical optics of a refracting cone. To facilitate tracing a meridional ray through the cone, the reflected cone images in Fig. 4 are drawn, whereby the totally reflected ray may be treated as a straight line.[2] Totally reflected rays subtend a decreasing angle of incidence at the (n,n') interface at each reflection until the critical angle is no longer exceeded and the ray escapes from the cone wall. The condition for total reflection at the ηth reflection is expressed as:

$$\theta' = \pi/2 - \phi_c - (2\eta - 1)a, \tag{7}$$

where a is the semiangle of the conical element, θ' the angle of the ray with the cone axis, and ϕ_c the critical angle given by $\phi_c = \sin^{-1}(n'/n)$. This expression describes the behavior of the ray as it proceeds along the cone; however, for the flux to emerge from the other end of the cone, the angle of incidence at the rear surface must be less than the critical angle $\gamma_c = \sin^{-1}(n_3/n)$. The angle of incidence γ' at the exit end is given by

$$\gamma' = \pi/2 + a - \phi_c. \tag{8}$$

The condition for emergence of a ray from this end of the cone can be shown to be:

$$a \leq \sin^{-1}\left(\frac{n_3}{n}\right) + \sin^{-1}\left(\frac{n'}{n}\right) - \frac{\pi}{2}, \tag{9}$$

where $n_3 = 1$ for an air-spaced detector. Equations (7), (8), and (9) permit the calculation of the maximum cone apex angle commensurate with the number of internal reflections, the indices of the rod, the specimen, and the medium external to the cone end.

Consideration of reflection losses at both entrance and exit ends, the cone angle, and the number of total internal reflections results in a modified total transmitted flux integral of the form:

$$E = K_2 \int_{\theta_2}^{\theta_1} [1 - R(\theta)][1 - R(\gamma')] \cdot \exp(-\alpha L \sec\theta') \cdot \sin\theta' \, d\theta. \tag{10}$$

Computation of reflection losses at the cone ends involves separate evaluation of $R(\theta)$ at the entrance and exit surfaces. At the entrance surface, R is computed for the angle θ', while at the exit surface, the angle γ' is used. Equations for fractional sensitivity of a conical element are included in Appendix B, and the values computed on an IBM 650 computer are plotted as solid curves in Fig. 5. The data do not show high fractional sensitivity for low index because the entrance angle of rays making six internal reflections is very small. The six total reflections used in the present calculations were chosen arbitrarily. The dotted curves show the effect of reflection losses at a flat cone end. More than two or three total reflections of rays outside of the critical cone are necessary because energy is not lost completely by a single refraction at the (n,n') interface.

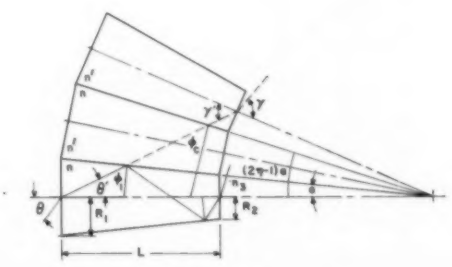

Fig. 4. Cone geometry.

The elementary theory equations give a fair representation of the performance of the cone, although the normal incidence Fresnel reflection losses and absorption within the conical rod are neglected. The curves shown in Fig. 5(a)–(d) remain unchanged when an immersed detector is used. It can be seen that the values of fractional sensitivity for the conical rod photorefractometers are higher than that for the corresponding cylindrical rod refractometer. This comparison is presented numerically in Table I. Considering the values of fractional sensitivity corresponding to a $n' = 1.30$, the cone is seen to be three times as sensitive as a rod when used with full cone illumination and an immersed detector. The cone and rod elements when illuminated with hollow cone illumination exhibit similar fractional sensitivity curves, and for all values of surround refractive index the cone has a higher sensitivity. Table I also illustrates the shift of maximum sensitivity to lower index values and the significant extension of the region of good fractional sensitivity to lower specimen medium refractive index values and, therefore, to a range of large medium-rod refractive index differences.

IV. Cone Photorefractometer Experiment

Verification of the theory was achieved using a flat entrance end glass cone, full cone illumination, and an air-spaced detector. A cone formed from optical glass of refractive index $N_d = 1.7552$ (SF-4) was designed to measure refractive index changes resulting from temperature changes in an immersion oil having a refractive index of 1.5150 (±0.0002) at 25°C and a temperature coefficient of 0.00035/°C. Graphical solutions of the equations of Section III and optical fabrication limitations dictated the cone design. A cone

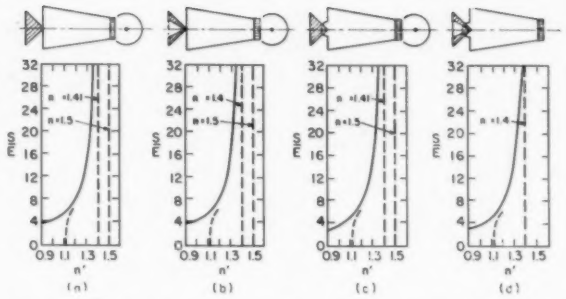

Fig. 5. Fractional sensitivity of various conical rod systems. $n = 1.5$, $n' = 1.4$ [in the notation in (a)–(d) the upper value should read n'], $a = 1.82°$, $\eta = 6$ reflections.

68.33 mm in length, with a total apex angle of 6° and an exit end 2 mm in diameter, was constructed. The arrangements shown in Fig. 6 permit this cone to be surrounded by the specimen oil. The cone was cemented to a window on the cylindrical tank, and an aluminized rod of larger diameter than the small cone end was cemented thereon in order to conduct the emergent flux to the detector. The rod end adjacent to the detector was fine-ground to direct some of the highly divergent radiation into the detector. This is not necessary provided the sensitive surface of the detector is in contact with the rod end.

The illumination system (full cone) for this experiment required a convergence angle of 11.2° at the cone entrance end. To obtain this angle, the filament of a tungsten lamp was imaged on a circular aperture of 0.051-cm diameter. The radiation from the aperture was first collimated and then brought to a focus on the axis at the entrance end of the cone using a 50 mm focal length $f/2.8$ lens system. To insure the correct

Table I. Comparison of S/E vs n' for Photorefractometer Geometries
Design Constants: $n = 1.5$, $n_1 = 1.4$, $\eta = 6$, $a = 1.82°$

	S/E				
Photorefractometer element	Rod	Rod	Cone	Rod	Cone
Entrance end	Spherical	Spherical	Spherical	Spherical	Spherical
Illumination	Full	Full	Full	Hollow	Hollow
Detector	Air-spaced	Immersed	Immersed	Immersed	Immersed
n'	...	...	...	...	...
1.5	...	...	...	...	...
1.45	13.60	20.0	...	...	...
1.41	...	...	...	...	...
1.40	6.80	10.0	76.0	...	...
1.35	5.02	6.67	30.3	20.0	34.3
1.30	3.37	5.00	15.5	10.0	16.1
1.25	2.66	4.00	...	6.67	...
1.20	2.14	3.33	7.53	5.00	7.63
1.15	1.61	2.86	5.92	4.00	5.98
1.12	0.00	...	...	...	...
1.10	...	2.50	4.87	3.33	4.91
1.05	...	2.22	4.12	2.86	4.15
1.00	...	2.00	3.44	2.50	3.46

incident angle at the glass–liquid interface, careful centering of the image on the cone end is necessary. The chamber around the cone was filled by the immersion oil heated to 35°C. As the oil cooled, simultaneous measurements of oil temperature and transmitted flux were taken, and the temperature data permitted the calculation of the refractive index change of the oil. A Cr–Al thermocouple was used for the temperature measurements.

Total flux versus refractive index change of the oil is plotted in Fig. 7. Also, results of theoretical calculations for the conditions of this experiment are shown. The change of flux associated with index change of the experimental cone indicated by the data is many times greater than that predicted by theory. Such a large discrepancy between theory and experiment is attributed to nonuniform angular flux distribution in the illumination cone. A large flux density in the periphery of the incident light cone is capable of creating this high sensitivity. Consideration of the equations describing

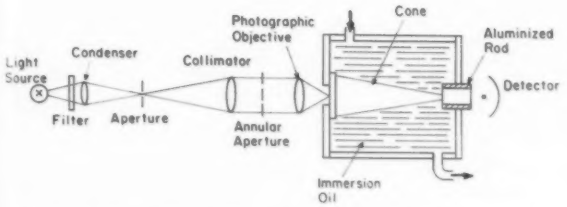

Fig. 6. Cone photorefractometer—experimental arrangement.

flux transmission in the case of hollow cone illumination reveals the possibility of extremely high sensitivity (a) when the hollow cone illumination beam is narrow and (b) when the beam is incident upon the oil–glass interface at critical angle for one of the internal reflections. Photometric measurements on the nonuniformity of illumination showed this to be the case: the variation in flux results from the aberrations in the condensing lens. This caused the radiation transmitted by the central cone to be very low in comparison with that transmitted at the periphery, thus approximating a hollow cone illumination condition.

The above experiment confirms the theoretically expected increase in sensitivity and operating range of a photorefractometer when an appropriately designed conical element is used in conjunction with appropriate illumination conditions.

V. Conclusion

Elementary considerations show that the rod photorefractometer is capable of detecting a minimum change in the surround index $|(\Delta n')_{\min}| = K\delta$ or $K/(S/E)$ where K is the receptor sensitivity and $\delta = n - n'$. This illustrates the high sensitivity achievable, but only over small δ values; therefore the value of the simple photorefractometer is limited as a measuring and process control instrument. This paper shows that high sensitivity and longer range are achievable by (a) modifying the entrance end of the element to a spherical form, (b) using hollow cone illumination, (c) employing a conical element of appropriate design, and (d) employing an immersed detector. Theoretical and experimental investigations show that an $|(\Delta n')_{\min}|$ of 0.0006 is achievable at δ values as large as 0.20. It is therefore expected that high precision refractometers with large operation range will evolve using these techniques.

Appendix A

Rod Photorefractometer Equations

The variables shown in Fig. 2 are used in the analysis of a rod refractometer employing hollow-cone illumination incident on a flat entrance end and an air-spaced detector. In the elementary theory, the transmitted flux E' and the sensitivity S' are given by:

$$E'(n'_1, n'_2, n) = 2\pi I(0)[(1 - n^2 + n_2^2)^{1/2} - (1 - n^2 + n_1^2)^{1/2}]$$

and

$$S'(n'_1, n'_2, n) = 2\pi I(0)\left[\frac{n_1}{(1 - n^2 + n_1^2)^{1/2}}\right].$$

In the extended theory, the transmitted flux is given by:

$$E = K\int_{\theta_2}^{\theta_1} [1 - R(\theta)]^s \exp(-\alpha L \sec\theta') \sin\theta' d\theta$$

where $\theta_1 = \sin^{-1}(n^2 - n_1^2)^{1/2}$, $\theta_2 = \sin^{-1}(n^2 - n_2^2)^{1/2}$, and $s = 2$. The sensitivity is given by:

$$S = [1 - R(\theta)]^s S'.$$

For the same illumination system, a spherical entrance end and an immersed detector,

$$E' = 2\pi I(0)\left(\frac{n_2 - n_1}{n}\right)$$

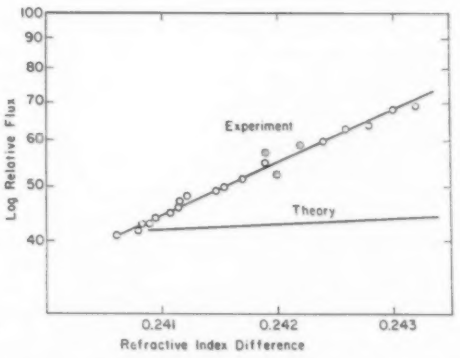

Fig. 7. Cone photorefractometer—experimental results compared with theory.

and

$$S' = 2\pi I(0)\left(\frac{1}{n}\right).$$

Appendix B

Cone Photorefractometer Equations

The variables shown in Fig. 4 are used in the analysis of a cone refractometer employing hollow-cone illumination incident on a flat entrance end and an air-spaced detector. In the elementary theory, the transmitted flux E' and the sensitivity S' are given by:

$$E'(n'_1, n'_2, n) = 2\pi I(0)\{[1 - n^2\cos^2(\beta + \phi_2)]^{1/2} - [1 - n^2\cos^2(\beta + \phi_1)]^{1/2}\}$$

and

$$S' = 2\pi I(0)\left[\frac{n^2\cos(\beta + \phi_1)\sin(\beta + \phi_1)/(n^2 - n_1^2)^{1/2}}{[1 - n^2\cos^2(\beta + \phi_1)]^{1/2}}\right].$$

In the extended theory

$$E = K\int_{\theta_2}^{\theta_1}[1 - R(\theta)]\{1 - R[\gamma'(\theta)]\}\exp(-\alpha L\sec\theta')\cdot\sin\theta'\,d\theta,$$

where

$$\theta_1 = \cos^{-1}[1 - n^2\cos^2(\beta + \phi_1)]^{1/2},$$

$$\theta_2 = \cos^{-1}[1 - n^2\cos^2(\beta + \phi_2)]^{1/2},$$

$$\phi_1 = \sin^{-1}\left(\frac{n_1}{n}\right),$$

$$\phi_2 = \sin^{-1}\left(\frac{n_2}{n}\right),$$

and

$$\gamma' = \left(\frac{\pi}{2}\right) + a - \phi_1,$$

$$\gamma' = \left(\frac{\pi}{2}\right) + a - \phi_2.$$

For the above illumination system, when a spherical entrance end and an immersed detector are used E' and S' are given by

$$E'(n, n'_1, n'_2) = 2\pi I(0)\,[\sin(\beta + \phi_2) - \sin(\beta + \phi_1)],$$

$$S' = 2\pi I(0)\left[\frac{\cos(\beta + \phi)}{n\cos\phi}\right],$$

where

$$\theta_1 = \left(\frac{\pi}{2}\right) - \beta + \phi_1,$$

$$\theta_2 = \left(\frac{\pi}{2}\right) - \beta + \phi_2,$$

$$\gamma'_1 = \left(\frac{\pi}{2}\right) + a - \phi_1,$$

and

$$\gamma'_2 = \left(\frac{2}{\pi}\right) + a - \phi_2.$$

References

1. N. S. Kapany and J. N. Pike, J. Opt. Soc. Am. **47**, 1109–1117 (1957).
2. N. S. Kapany, J. Opt. Soc. Am. **47**, 413 (1957).

Meeting Reports *continued from page 410*

Technical and Military Application of Lasers Symposium, s'Gravenhage, The Netherlands, April 3–5, 1962

Reported by B. H. Billings, Baird-Atomic

The North Atlantic Treaty Organization (NATO) and the Supreme Headquarters Allied Powers Europe (SHAPE) were joint sponsors of a conference on optical masers that had been conceived and was organized by Max Nagel and E. C. Williams of the SHAPE Air Defense Technical Center in the Hague. The title of the conference, "Technical and Military Applications of Laser Technology," was somewhat pleasantly misleading; the conference actually covered laser physics and technology and did this to a detail that is difficult to achieve in an American meeting. To an eager student of Dutch whose only sentence is a phrase from an American Army Handbook, "Hoe laat beginnt de Bioscoop?" (When do the movies start?), the prospect of an international symposium in the Hague was overwhelming. However, all hopes of linguistic progress were speedily dashed: First, the small Dutch contingent apparently spoke all languages fluently; second, the girl assigned to this reporter at a local cabaret was from Worms and knew not one word of Dutch. Fortunately, the excitement of the technical material more than compensated for the philological disappointment. It is believed that this symposium was the first purely scientific meeting to use simultaneous translation. The official languages were English, French, and German, and there were headphones at each chair with switches to get either the amplified voice of the speaker or a translation. The translators did a magnificient job and were particularly blessed by some of the American contingent whose languages were a bit rusty.

Dr. Nagel, in his introduction, demonstrated the enormous rise in activity in the optical maser field by describing the different companies in the United States that are based on masers. Some companies provide complete optical masers; some provide crystals; some provide scientific manpower; and some, investment opportunities. In every case, a large part of the business of these corporations is based almost exclusively on the maser.

The purpose of the symposium was to review for scientists in the NATO community the present state of optical maser technology. Certain of the Americans benefited enormously by the review. Dr. Townes, in his lead paper, summarized the basic mathematical relationships that lead to optical maser operations and described the various masers that have been developed. Each succeeding speaker felt that Dr. Townes had laid a framework that made his own topic easier to present. It was particularly interesting to this reporter to listen to a series of papers in which each piece of work was presented in the context of other work by the speaker and by other researchers.

Meeting Reports *continued on page 440*

High-Index-of-Refraction Spherical Sheath Composite-Rod Optical Masers

O. Svelto and M. Di Domenico, Jr.

The focusing of pumping light by high-index-of-refraction spherical and cylindrical sheaths covering a ruby-rod maser material has been studied both theoretically and experimentally. In the experimental work, the reduction in threshold pumping energy and the increase in optical output energy for the same ruby rod have been measured as a function of the index of refraction of the sheath by using spherical and cylindrical sheaths of water and benzyl benzoate, which have indices of refraction of 1.33 and 1.57, respectively. The results of the measurements clearly show that the spherical sheath is better than the cylindrical sheath. In the theoretical work, a thermodynamical method of analysis has been used to develop an approximate three-dimensional theory for the power absorbed per unit volume at each point in the rod. This theory treats the spherical and cylindrical sheath composite-rod structures in a unified way. The theoretical results are in fair agreement with the experimental ones. Moreover, the theory shows that the spherical sheath of sapphire is an optimum composite-rod optical-maser configuration. In fact, the theory predicts that in this case the threshold pumping energy for maser oscillation should be reduced by a factor of 4, whereas the cylindrical sheath of sapphire should only give an improvement by a factor of 2.4.

Introduction

The performance of pulsed optical masers is usually measured in terms of the amount of the electrical input energy necessary to start maser oscillation and the amount of optical output energy for a given input energy above threshold. The threshold and output energies depend upon both the properties of the maser material and the ability to concentrate or focus pumping radiation from the flashtube into the active material. Devlin *et al.*,[1] have studied the properties of composite-rod structures, wherein a ruby rod is covered by a cylindrical sheath of sapphire. It was shown in this case that the focusing action of the sheath caused the threshold energy for maser oscillation to be lowered.

One may now ask whether there is a still better method for focusing the pumping radiation from the flashtube into the ruby rod. In this paper, we will show that more pumping energy can be concentrated into the ruby rod by surrounding the rod with a spherical sheath of sapphire. The improvement in performance of the spherical sheath composite-rod structure over the cylindrical sheath structure can be understood qualitatively by noting that, while the cylindrical sheath acts like a cylindrical lens that magnifies the diameter of the ruby rod,[1] the spherical sheath acts like a spherical lens that magnifies not only the diameter but also the length of the rod. Consequently, more pumping energy can be concentrated into the composite-rod structure composed of the spherical sheath than into the structure composed of the cylindrical sheath.

In order to demonstrate that these statements are correct, we report in this paper the experimental results obtained by surrounding a ruby rod with clear liquids of high index of refraction in spherical and cylindrical glass enclosures. The use of liquid sheaths has the obvious advantage that they can be readily removed from the rod. Therefore, by using the same rod under identical conditions, it is possible to study the effects of the focusing action of the sheath as a function of geometry and the refractive index of the sheath. Moreover, by performing the experiment in this way, we have been able to obtain a better understanding of the experiment referred to above.[1]

Experimental Arrangement and Results

The apparatus used in this experiment is shown schematically in Fig. 1. The ruby rod shown here was

At the time of the writing of this paper, the authors were with Microwave Laboratory, W. W. Hansen Laboratories of Physics, Stanford University, Stanford, California. O. Svelto is now with Instituto di Fisico del Politecnico, Milan, Italy. M. Di Domenico, Jr., is now with Bell Telephone Laboratories, Murray Hill, New Jersey.

Received 29 October 1962.

The research reported in this paper was sponsored by the National Science Foundation under Grant 22929.

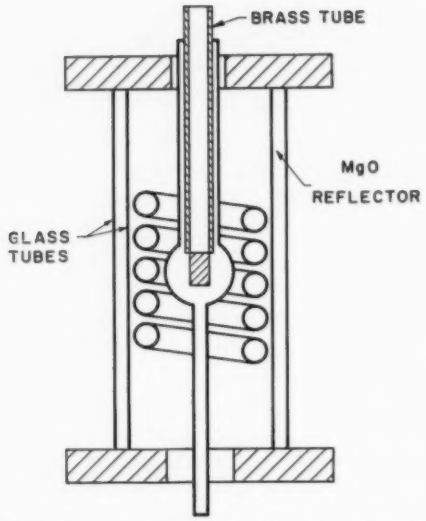

Fig. 1. Experimental arrangement of the ruby rod and spherical glass enclosure at the center of the spiral flashtube.

1 cm long and 6 mm in diameter and had a concentration of 0.05% of Cr^{3+} ions. The *c*-axis was oriented at 90° to the axis of the rod. The ends of the rod were polished flat and parallel and were silver coated; one end was totally reflecting while the other was ~4% transmitting. The ruby rod was supported at the center of a G.E. type FT 524 xenon spiral flashtube. Electrical energy was supplied to the flashtube by discharging a 200-μF bank of capacitors and was varied by changing the charging potential. For the experiment performed with the cylindrical sheaths, the spherical enclosure illustrated in Fig. 1 was replaced by a cylindrical tube. Both the spherical and cylindrical enclosures had a diameter of about 2.2 cm and were made of pyrex glass. A small glass tube was affixed to the bottom portion of each sheath in the manner shown in Fig. 1. The liquids used in the experiment were fed into the sheath enclosures via this tube. In this way it was possible to fill and empty the sheaths with different liquids without changing the position of the ruby rod.

The liquids employed were distilled water (index of refraction $n = 1.33$) and benzyl benzoate ($n = 1.57$). The choice of benzyl benzoate was dictated by the fact that, among all of the transparent liquids tested with high index of refraction, benzyl benzoate was found to be the most stable under the intense radiation from the flashtube. Each of the liquids tested became opaque when the electrical input energy to the flashtube was increased beyond a certain threshold value, which differed from liquid to liquid. This phenomenon was probably due to molecular decomposition of the liquid. Water was found to be completely stable.

The pulse of coherent radiation from the laser was detected by an RCA type 925 phototube. The laser output was attenuated by a sufficient number of neutral density filters to insure a linear response of the phototube. A red interference filter with a bandwidth of 100 Å centered at the output wavelength of the laser was also used to eliminate the detection of light from the flashtube. In order to measure the total energy of the output pulse of the laser, the phototube current was integrated by an RC circuit with a time constant of approximately 2.5 msec (the total duration of the laser action was about 250 μsec).

The output energy due to stimulated emission is shown in Figs. 2 and 3 as a function of electrical input energy supplied to the flashtube. The data given in Fig. 2 apply for the spherical sheath, and the data in Fig. 3 are for the cylindrical sheath. The curve for benzyl benzoate is not shown in Fig. 3 since it was found to be almost identical to the curve given for water.

It is important to emphasize at this point that particular care was taken throughout the course of the experiment to keep the temperature of the ruby as constant as possible. Thus, for the experiments run with the ruby rod in air, we cooled the rod and the flashtube with forced air and waited long enough (~5 min) between successive runs to allow the rod to reach thermal equilibrium with the circulating air. In the experiments performed with the liquids, we changed the liquid contained in the sheath enclosure for each run and cooled the flashtube with forced air as before. The forced air as well as the liquids was at room temperature. These precautionary measures were thought to be necessary since it is known that the threshold and, to a greater extent, the slope of the curves of the energy output versus energy input depend upon the temperature of the rod.[2–5]

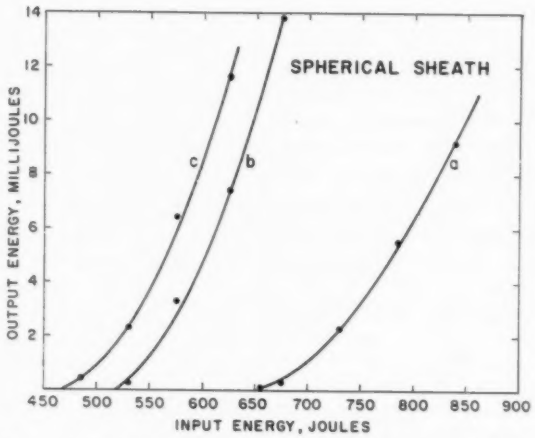

Fig. 2. Optical energy output vs electrical energy to the flashtube in the case of a spherical sheath: (a) air, (b) water, and (c) benzyl benzoate.

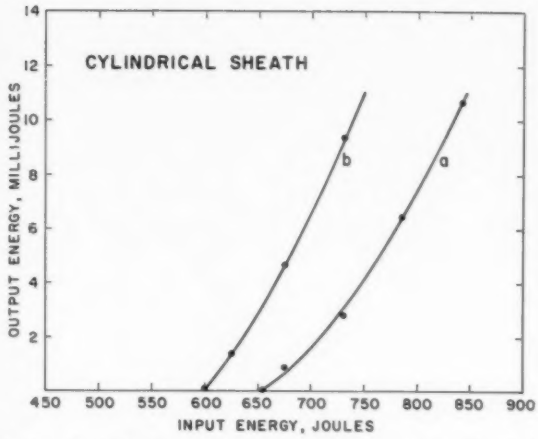

Fig. 3. Optical energy output vs electrical energy to the flashtube in the case of a cylindrical sheath: (a) air and (b) water. The curve for benzyl benzoate is not shown since it was found to be almost identical to that of water.

From the curves given in Figs. 2 and 3, it is possible to compare the threshold and the slopes of the various curves. In order to make this comparison, the curves obtained for the ruby in air (curves *a* in Figs. 2 and 3) have been taken as a reference. For the case of the spherical sheath (Fig. 2), curves *b* and *c* are both compared with curve *a;* and for the case of the cylindrical sheath (Fig. 3), the comparison is made between curves *a* and *b*. Table I summarizes the results of the comparison. The ratio of the slopes listed in Table I has been obtained by calculating the slopes from the linear part of each curve. It should be noticed that there is a slight difference between curves *a* shown in Figs. 2 and 3. This is because these curves were obtained with different experimental arrangements; i.e., for the curve given in Fig. 2 the rod was placed in the center of the spherical-sheath enclosure, and for the curve given in Fig. 3 it was aligned with the axis of the cylindrical sheath. In this way it was possible to run curves with air and then with the liquids while having the rod see identical geometrical configurations at the same time. Since it was found by inspection that the optical quality of the spherical enclosure was considerably poorer than that of the cylindrical enclosure, it is not surprising that curves *a* in Figs. 2 and 3 differ. However, it must be emphasized that this in no way affects the *relative* comparison listed in Table I. From the results summarized in Table I, it is evident that the spherical sheath gives better performance than the cylindrical sheath. It is, however, particularly surprising that in the case of the cylindrical sheath the curves for water and benzyl benzoate, which have an appreciable difference in refractive index, were practically the same.

Table I. Comparison of Improvement in Threshold to Improvement in Slope

		Threshold	Slope
Sphere	Water	1.27	1.80
	Benzyl benzoate	1.40	1.70
Cylinder	Water and benzyl benzoate	1.11	1.12

In order to obtain a better understanding of the previous results, we have taken photographs of the near-field patterns at the transmitting end of the ruby rod. Some of these photographs for the case of the cylindrical sheath filled with air and water are shown in Fig. 4. Figures 4(a) and 4(c) were taken at the respective thresholds, while Figs. 4(b) and 4(d) were taken at the same electrical input energy. By comparing Figs. 4(a) and 4(c) it can be seen that, although the two threshold energies are different, the near-field patterns are practically the same and essentially consist of three bright spots that are off-center with the axis of the rod. It is therefore possible to conclude that the cylindrical sheath of water must increase the energy density in the three spots in which the rod first

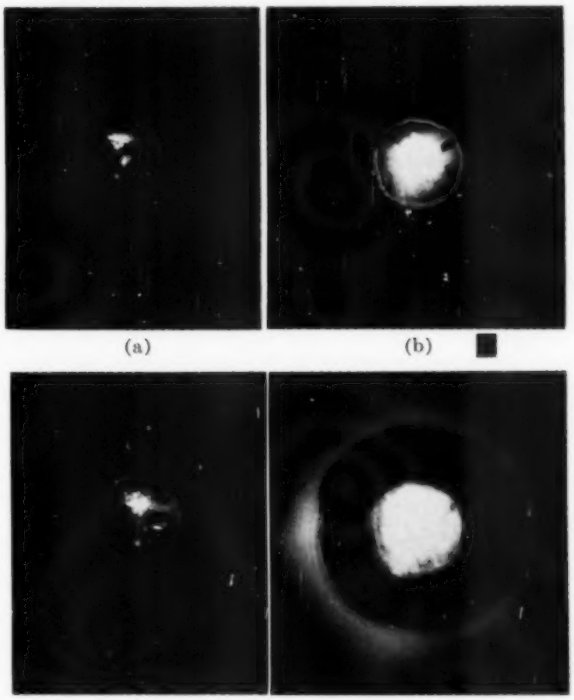

Fig. 4. Near-field patterns of the transmitting end of the ruby rod in the case of air (a) and (b) and in the case of a cylindrical sheath of water (c) and (d). Photographs (a) and (c) were taken at the respective thresholds, while photographs (b) and (d) were taken at the same electrical energy to the flashtube [780 J].

lases. Another interesting result can be observed from Fig. 4(d). From this photograph, it is apparent that above threshold the cylindrical sheath causes the entire end surface of the ruby rod to lase. For comparison, Fig. 4(b) shows that an unclad rod lases only in its central core, as already observed by previous researchers.[6,7] Note that the electrical input energy to the flashtube is the same for Figs. 4(b) and 4(d).

The photographs taken with benzyl benzoate in the cylindrical enclosure and with water and benzyl benzoate in the spherical enclosure are very similar to those shown in Figs. 4(c) and 4(d). In fact, at the respective thresholds the near-field pattern in all the cases consisted of the three spots shown in Fig. 4(c), and immediately beyond threshold the laser action was observed to extend over the whole surface of the rod as in Fig. 4(d). Each of the photographs was taken many times, and the results were found to be consistent.

Calculation of the Pump Power Absorbed at Each Point in the Ruby Rod

To explain more fully the experimental results obtained in the foregoing section, we now calculate the amount of pump power absorbed at each point within the ruby rod. In making this calculation, we must bear in mind that for the value of the diameter of the rod considered here (6 mm) and for the concentration of Cr^{3+} ions in our rod (0.05%), which is rather typical, the absorption in the rod is not small.[8] Moreover, for the case of the spherical sheath composite rod, it is essential to make a three-dimensional analysis of the pumping light absorbed in the rod. The two-dimensional theory developed by Devlin *et al.*,[1] therefore cannot be used for our case. A three-dimensional theory has already been developed by McKenna[9] for a rod clad with a cylindrical sheath of sapphire. His analysis is somewhat complicated, however, and cannot be simply extended to the case of a rod clad by a spherical sheath. By using some of the concepts discussed in a previous paper,[10] we will develop an approximate and rather simple three-dimensional theory.

Theory

In the treatment presented here, we combine a thermodynamical method of analysis with an analysis based upon geometrical optics. The flashtube is considered to be a blackbody[11] at temperature T. Since the absorption for our rod is large, we will neglect the effect of the successive reflections of the light after the first passage through the rod. The liquids surrounding the rod are assumed to be transparent (i.e., absorptionless); and the ruby is assumed, for simplicity, to have only an absorption band for the pumping radiation, which we describe by a power absorption coefficient α.

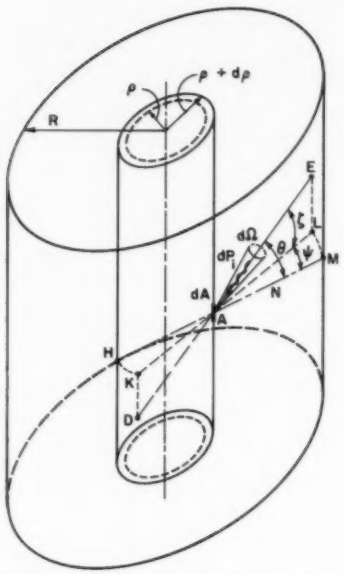

Fig. 5. Calculation of the power absorbed between radii ρ and $\rho + d\rho$ within the rod of radius R due to the power dP_i incident on dA.

We now propose to calculate the power absorbed per unit volume by the ruby rod between radii ρ and $\rho + d\rho$ (see Fig. 5). The calculation performed here applies for a simple rod as well as for a rod covered by a spherical or cylindrical sheath, where the sheath can have an index of refraction that is different from that of the ruby rod. Accordingly, the sheath is not specified in Fig. 5. Consider all of the rays in the solid angle $d\Omega$ that come directly from the flashtube and that are incident on the elemental area dA of the cylinder of radius $\rho + d\rho$ (within the ruby rod of radius R). Assuming that these rays carry power dP_i and form an angle θ with the normal N to the area dA, the power dP_a absorbed by the rod between radii ρ and $\rho + d\rho$ due to dP_i is given by

$$dP_a = \eta\alpha\, ds'\, (1 + e^{-\alpha x'})\, dP_i, \qquad (1)$$

where η is the fraction of the total radiation from the flashtube effective in pumping the ruby[8,12] and x' is the length of the segment BD in Fig. 6(a). The factor $(1 + e^{-\alpha x'})$ in Eq. (1) accounts for the absorption in the two equal infinitesimal segments AB and CD referred to as ds' in Fig. 6(a). The power dP_i can now be expressed in terms of the power dP_{io} that would have been incident on dA if the rod had been absorptionless:

$$dP_i = e^{-\alpha s'} dP_{io}, \qquad (2)$$

where s' is the length of the segment EA in Fig. 6(a). It is now a relatively simple matter to calculate dP_{io} from a thermodynamical point of view. From the discussion given in ref. 10, we have

$$dP_{io} = (n^2\sigma T^4/\pi)\cos\theta\, dA\, d\Omega\,(1 - r), \tag{3}$$

where σ is the Stefan's constant, n is the index of refraction of ruby ($n = 1.76$), and T is the temperature of the flashtube. Here, r is a power-reflection coefficient defined in the following way: Consider the fictitious case where a ray carrying power dP_{io} is emitted by the elementary surface dA into the solid angle $d\Omega$ with the same direction as the ray dP_i incident on dA in Fig. 5. Then, due to the discontinuities in the refractive index between the rod and the sheath and between the sheath and the air, a certain fraction r of the power dP_{io} emitted by dA will be reflected back into the cylinder of radius $\rho + d\rho$. The coefficient r so defined is a complicated function of the ratio ρ/R, the angles ψ and ζ in Fig. 5 and the geometry and index of refraction of the sheath. At this point, it is necessary to emphasize that Eq. (3) only applies for problems having cylindrical symmetry[10]; however, it is possible to show that the same equation applies in the case of a spherical sheath, provided that the diameter of the sphere is much greater than the product of the index of refraction of the sheath and the length of the rod.

The power dP_{io} can be expressed in terms of the angular coordinates ψ and ζ by noting, with the aid of Fig. 5, that

$$d\Omega = \cos\zeta d\zeta\, d\psi, \tag{4a}$$

$$\cos\theta = \cos\zeta\cos\psi. \tag{4b}$$

Moreover, from Figs. 6(a) and 6(b) we obtain

$$ds' = (ds/\cos\zeta) = (d\rho/\cos\zeta\cos\psi), \tag{4c}$$

where ds is the projection of ds' on the plane $HKLM$ orthogonal to the axis of the rod. By combining Eqs. (1), (2), and (3) and by using the relations expressed in Eqs. (4a) and (4b), we find that

$$dP_a = (\eta\alpha\sigma T^4 dA d\rho/\pi)\, n^2(1 - r)\, e^{-\alpha s'}(1 + e^{-\alpha x'})\cos\zeta d\psi d\zeta. \tag{5}$$

The power absorbed per unit volume p_a is obtained by dividing Eq. (5) by the elementary volume $dV = dA d\rho$ and integrating over the angles ψ and ζ;

$$p_a = [\eta\alpha\sigma T^4]\,(n^2/\pi) \int (1 - r)\, e^{-\alpha s'}(1 + e^{-\alpha x'})\cos\zeta d\psi d\zeta, \tag{6}$$

where the integral must be calculated for $-\pi/2 \leqq (\psi,\zeta) \leqq \pi/2$. To simplify Eq. (6) it is useful to remember that when reflections occur at the boundary between a dense and a rare medium (from the side of the dense one) the power-reflection coefficient has an almost constant value until the angle of incidence reaches the critical angle, i.e., the angle of total reflection.[12] At this angle, the reflection coefficient rises sharply to the value 1.* The value of the reflection coefficient below the critical angle is approximately equal to the value for normal incidence. This value is very low in each of our cases. For example, for normal incidence between water ($n = 1.33$) and ruby ($n = 1.76$), it is only 0.02. Indeed our case is even more complicated, for r must take into account 2 reflections: (a) the reflection at the surface separating the ruby rod from the sheath and (b) the reflection at the surface separating the sheath from the air. However, since both of these reflections occur from the side of the dense medium, it is clear that the behavior of r should be similar to that described in the above-mentioned case. Therefore, we will approximate the expression $(1-r)$ in Eq. (6) by 1 for all those angles ψ and ζ smaller than the limit angles. Thus Eq. (6) becomes

$$p_a = [\eta\alpha\sigma T^4]\,(n^2/\pi) \int_{-\psi}^{\psi_0} d\psi \int_{-\zeta_0}^{\zeta_0} e^{-\alpha s'}(1 + e^{-\alpha x'})\cos\zeta d\zeta, \tag{7}$$

where ψ_0 and ζ_0 are the limit angles.

In order to evaluate the double integral appearing in Eq. (7), it is necessary to determine the limit angles ψ_0 and ζ_0 for the 2 sheath configurations under consideration here. For this purpose, let us first consider a plane containing the axis of the rod, as illustrated in Figs. 7 and 8 for the cylindrical and spherical sheath, respectively. The ray dP_{io} in Fig. 7 is totally reflected at the point Y when $\sin\beta_0 = (1/n_s)$, where n_s is the index of refraction of the sheath. The angle β_0 at the surface of the sheath corresponds to the angle ζ_0 at the surface of the cylinder of radius ρ within the rod. Then, by using Snell's law we have

$$\sin\zeta_0 = (1/n). \tag{8}$$

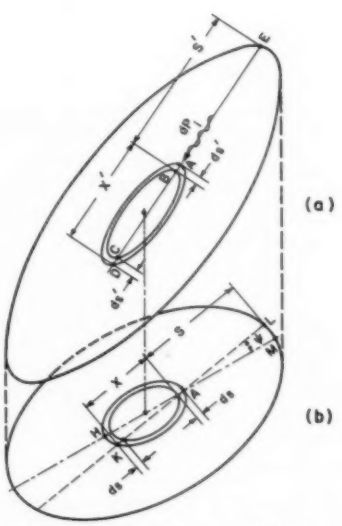

Fig. 6. (a) Plane containing the ray dPi and inclined of ζ over the plane $HKLM$ of Fig. 5. (b) Plane $HKLM$ of Fig. 5 which is orthogonal to the axis of the rod.

* Our reflection coefficient r can be thought of as the average between the reflection coefficients for the electric field in the plane of incidence and normal to the plane of incidence.

There is still another way of having total reflection, which occurs at the surface separating the rod and the sheath. From Fig. 7 we see that this happens for the angle ζ_0', for which $\sin\zeta_0' = (n_s/n)$. But since $n_s > 1$, it follows that Eq. (8) determines the limit angle. In contrast to this case, in the case of the spherical sheath (Fig. 8), if the diameter of the sphere $(2R_s)$ is much bigger than the length of the rod, the angle β at the point Y is always smaller than the limit angle β_0 given by $\sin\beta_0 = (1/n_s)$. Therefore, in this case ζ_0 is determined by the reflection occurring between the ruby rod and the sheath, i.e., at the point X in Fig. 8, and we have

$$\sin\zeta_0 = (n_s/n). \tag{9}$$

It has to be noticed now that the limit angles for ζ_0 expressed by Eqs. (8) and (9) are only valid for a plane containing the axis of the rod, i.e., when $\psi = 0$. When $\psi \neq 0$, the calculation is more complicated, and ζ_0 results as a function of the angle ψ. As shown in the Appendix, if the radius of the cylindrical sheath is much greater than the radius of the rod and if the diameter of the spherical sheath is at least equal to $n_s(l^2 + R^2)^{1/2}$, where $2l$ is the length of the rod, the results are

$$\sin\zeta_0 = \min\left\{1, \frac{n_s}{n}\left[\frac{1 - (n\rho/n_sR)^2\sin^2\psi}{1 - (\rho/R)^2\sin^2\psi}\right]^{1/2}\right\}, \tag{8a}$$

$$\sin\zeta_0 = \frac{n_s}{n}\left[\frac{1 - (n\rho/n_sR)^2\sin^2\psi}{1 - (\rho/R)^2\sin^2\psi}\right]^{1/2}, \tag{9a}$$

for the case of the cylindrical and spherical sheaths, respectively. As expected, Eqs. (8a) and (9a) simplify to Eqs. (8) and (9) for $\psi = 0$.

The limit angle ψ_0 entering in Eq. (7) can be found by applying a set of arguments similar to the prior ones to a plane orthogonal to the axis of the rod.[10] However, the angle ψ_0 can be obtained in a more direct way from Eqs. (8a) and (9a) by noting that the expression under the square root, which appears in both equations, has to be positive. Hence,

$$\sin\psi_0 = \min(1, n_sR/n\rho). \tag{10}$$

This relation holds for both the spherical and cylindrical sheath under the same approximations in which Eqs. (8a) and (9a) were obtained.

In conclusion, we have now derived a rather simple formula for the power absorbed per unit volume in the rod [Eq. (7)], and we have obtained expressions for the limits of integration [Eqs. (8a), (9a), and (10)] for the various cases of interest. In obtaining the preceding formulas, we have made use of two approximations: (a) we have approximated $1 - r$ in Eq. (6) as 1 for all the angles ψ and ζ smaller than the limit angles, and (b) we have assumed that the radius of the cylindrical sheath is much bigger than the radius of the rod. However, provided that the radius of the cylindrical sheath is at least n times bigger than the radius of the rod, we have estimated that the error for these approximations is only a few percent.

At this point, it is worthwhile to mention that the thermodynamical method used here and in ref. 10 differs in a certain respect from the more common method in which we consider the power carried by rays entering the sheath and then calculate the power absorbed at each point in the rod due to these rays.[1,9] It can be shown, as might be expected, that the two methods are equivalent. However, the advantage of our method is that the analysis and, hence, the final formula are the same for every sheath configuration. The index of refraction and geometry of the sheath only enter in determining the value of $1 - r$ in Eq. (6) and,

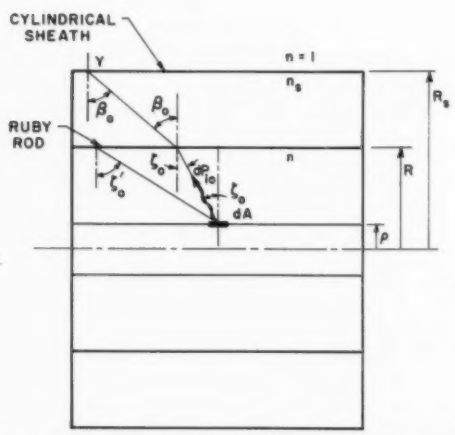

Fig. 7. Ruby rod covered by a cylindrical sheath of dielectric material. The plane contains the axis of the rod.

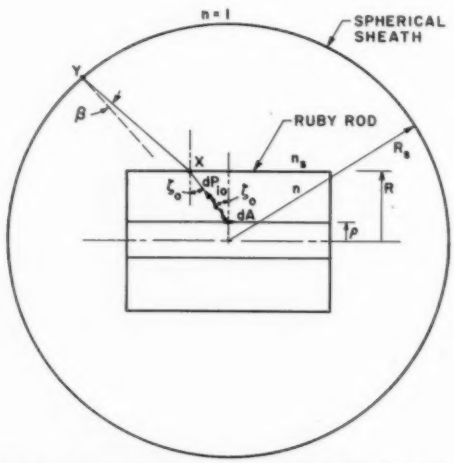

Fig. 8. Ruby rod covered by a spherical sheath of dielectric material. The plane contains the axis of the rod.

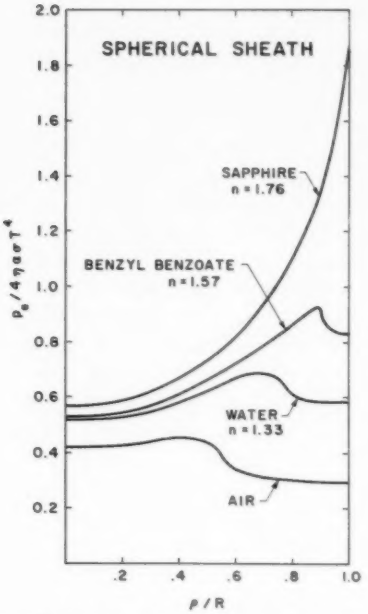

Fig. 9. Dimensionless plot of the power p_a absorbed per unit volume between radii ρ and $\rho + d\rho$ within the ruby rod of radius R. Case of a spherical sheath.

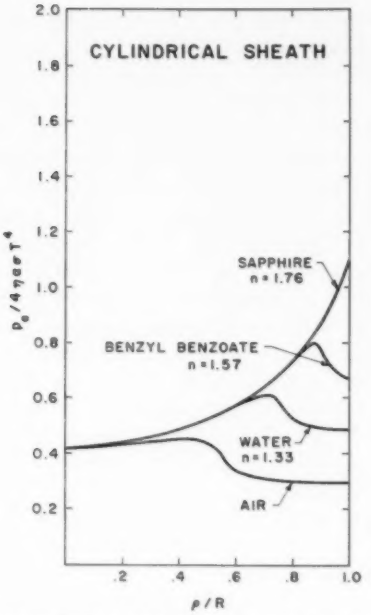

Fig. 10. Dimensionless plot of the power p_a absorbed per unit volume between radii ρ and $\rho + d\rho$ within the ruby rod of radius R. Case of a cylindrical sheath.

consequently, the limits of integration ψ_0 and ζ_0 in Eq. (7). It is now a simple matter to compare the spherical to the cylindrical sheath. By comparing Eqs. (8a) and (9a) we see that the effect of the spherical sheath is to cause the limit angle ζ_0 to be increased.

Numerical Evaluation and Discussion

Equation (7) has been numerically evaluated with the help of Eqs. (8a), (9a), and (10) for the cases of interest in this paper. Figures 9 and 10 give plots of the dimensionless ratio $p_a/(4n\alpha\sigma T^4)$ as a function of (ρ/R) for the case of the spherical and cylindrical sheath, respectively. In making these computations, the distances x' and s' appearing in Eq. (7) have been expressed as

$$s' = (s/\cos\zeta) = (R/\cos\zeta)\{[1 - (\rho/R)^2 \sin^2\psi]^{1/2} - (\rho/R)\cos\psi\} \tag{11}$$

and

$$x' = (x/\cos\zeta) = 2\rho\cos\psi/\cos\zeta, \tag{12}$$

where x is the length of the segment AK and s is the length of AL in Fig. 6(b). Each of the curves shown in Figs. 9 and 10 exhibits a maximum for a critical value of ρ/R [the curves for sapphire have no maxima due to the approximations made in evaluating the factor $1-r$ in Eq. (6)]. This behavior can be understood qualitatively as follows: As the light enters the rod, it is simultaneously attenuated owing to the absorption by the quantum system and intensified due to the focusing action of the sheath. (In the case of the simple rod, the rod itself provides for the focusing.) It is therefore apparent that, as the light penetrates into the rod, it is initially intensified more than it is attenuated since the distance traversed is small. However, as the distance into the rod increases, the concentration of light due to focusing reaches a plateau, but the light continues to be attenuated. As a consequence, it is certainly not surprising that the power absorbed per unit volume should at first increase, reach a maximum, and then decrease, as is shown graphically in Figs. 9 and 10. With the aid of the same two figures, it is noteworthy to mention that the focusing action of the spherical sheath is far more intense than that due to the cylindrical sheath.

The experimental results given in Figs. 2, 3, and 4 can now be interpreted on the basis of the theoretical curves of Figs. 9 and 10. For an ideal rod (i.e., one having no scattering losses due to crystalline imperfections), we would expect that laser action should initially take place in a ring concentric with the axis of the rod and at that value of the radius ρ for which the power absorbed in the rod is a maximum. The reduction in threshold for the various sheath configurations should therefore be given by the ratio of the maxima of the curves in Figs. 9 and 10. The conditions for laser action in our rod are much more complicated due to the presence of scattering losses owing

to strains and inhomogeneities which differ from point to point in the rod material.[14,15] In fact, as observed in connection with the photographs of Fig. 4, our rod, with any of the sheaths used, always first lased in the three spots shown in Figs. 4(a) and 4(c), which are believed to correspond to filamentary regions of low scattering losses in the rod. Now it can be seen from Figs. 5(a) and 5(c) that the average distance of the three spots from the center of the rod gives a value of ρ/R approximately equal to 0.4. Therefore, for each of the sheath configurations, the threshold should be proportional to the ordinate of the corresponding curve in Figs. 9 or 10 for $\rho/R = 0.4$. However, to interpret in a correct way the experimental results, the coefficient $(1 - r)$ of Eq. (6) approximated as 1 in Eq. (7) is now taken into account as $(1 - r_0)$, where r_0 is the value of the reflection for normal incidence. Now, if the index of refraction of glass is assumed to be $n = 1.5$, the single reflections at the interfaces are the following:

Air–glass–air–ruby	$r_{01} = 15.6\%$
Air–glass–water–ruby	$r_{02} = 6.3\%$
Air–glass–benzyl benzoate–ruby	$r_{03} = 4.4\%$

Therefore, each of the curves in Figs. 9 and 10 must be multiplied by the respective value of $(1 - r_0)$. Once this is done, Figs. 9 and 10 give the following theoretical improvements in threshold for $\rho/R = 0.4$:

Water or benzyl benzoate in the cylinder	1.17
Water in the sphere	1.38
Benzyl benzoate in the sphere	1.49

These are in fair agreement with the experimental ones listed in Table I. Moreover, the theoretical curves of Figs. 9 and 10 can obviously be used to explain why the simple rod lased over its central core whereas the composite rod lased over its entire cross section for the same energy input. The same theoretical curves could be used to calculate the optical energy output for a given energy input above threshold and, therefore, the slopes of the curves in Figs. 2 and 3. However, the problem is much more complicated from the scattering losses that differ from point to point, and therefore it is only possible to use Figs. 9 and 10 to obtain a qualitative understanding of the slopes in Figs. 2 and 3.

Finally, it is interesting to observe that our theory proves that a spherical sheath of sapphire is the best system for concentrating the pumping radiation from the flashtube into the ruby rod. In fact, since $n_s = n$ in this case, we see from Eqs. (9a) and (10) that the limits of integration reach their maximum value, which is given by $\zeta_0 = \psi_0 = \pi/2$. Since Eq. (7) depends on the characteristics of the sheath only through the limits of integration, it follows that the spherical sheath of sapphire gives the maximum value absorbed per unit volume at each point into the rod.

Conclusions

We have studied the focusing effects of water and benzyl benzoate in spherical and cylindrical sheath composite-rod lasers and have proved experimentally that the spherical sheath gives a better performance than the cylindrical sheath. Experimentally, we have compared the effects of the two sheath geometries by measuring the reduction in threshold and improvement in output energy from a ruby rod covered by these sheaths as a function of the index of refraction of the sheaths. The results of the experiment are shown in Figs. 2 and 3 and are summarized in Table I. It is worth mentioning that even a sheath of water gives an improvement in threshold and output energy, which may offer some advantages when operating near room temperature. Photographs of the near-field patterns of the laser output (Fig. 4) were also taken in order to obtain a better understanding of the way in which the composite rod lases.

In the theoretical treatment, a rather simple three-dimensional theory for the power absorbed per unit volume in the rod has been developed [Eq. (7)]. Although the theory is approximate, the errors involved are only of the order of a few percent. The significant feature of our theory is that it treats in a unified way the cases of interest in this paper. By numerically evaluating Eq. (7), we have obtained theoretical curves for the power absorbed per unit volume at each point in the rod (Figs. 9 and 10). These curves can be used to determine the reduction in threshold and general shape of the energy output versus energy input curves for the different sheath configurations. Moreover, they can be used to explain qualitatively the experimental results when the effects of scattering losses in the rod are taken into account, as discussed previously.

We have also proved that the composite rod with a spherical sheath of sapphire is an optimum configuration provided that the radius R_s of the sphere is at least equal to $n(l^2 + R^2)^{1/2}$, where $2l$ and R are the length and the radius of the rod, respectively, and n is the index of refraction of the ruby. Generally, the reduction in threshold and improvement in output energy for such a composite rod depend on (a) the radius of the rod, (b) the concentration of Cr^{3+} ions, and (c) the crystalline imperfections of the rod. For the rod used in our experiments (6 mm in diameter and 0.05% of Cr^{3+} ions), we would expect from Fig. 9 that for uniform scattering losses through the rod the threshold level should be reduced by a factor of 4 and that the output energy should improve by an even more dramatic factor. This should be compared with the case where the rod is clad by a cylindrical sheath of sapphire; here we obtain a reduction in threshold of a factor of only 2.4.

We should note that the spherical sheath composite-

rod laser has a number of advantages. For example, it provides a larger surface area for the transfer of heat. This fact, together with the fact that the threshold pumping energy necessary for laser action is reduced considerably, is of importance for cw laser operation. Finally, we should emphasize that, although the discussion presented here has been limited to ruby as an active material, the same considerations apply to any optical maser material.

The authors are indebted to Mrs. Cora H. Barry for computing the curves of Figs. 9 and 10 and to S. B. Sears, J. Weaver, and P. Duran for technical assistance during the course of the experiment.

Appendix. Calculation of the Limits of Integrations Given by Eqs. (8a) and (9a)

A. Cylindrical Sheath

Let us consider the ray dP_i in the direction EA as shown in Fig. 5. As explained in the paper, the angles ζ and ψ in Fig. 5 will be the limit angles if a ray emitted by the elemental surface dA in the direction AE is totally reflected back into the cylinder of radius ρ. Now there are 2 possible ways of total reflection: (1) at the surface separating the rod and the cylindrical sheath, i.e., at the point E in Fig. 5, and (2) at the external surface of the sheath, which is not shown in Fig. 5. If we call Γ_1 the angle between EA and the normal to the rod at the point E, the angle Γ_1 will be the angle of incidence at the surface separating the rod and the sheath. In addition, let us call Γ_2 the angle of incidence of the ray emitted by dA at the external surface of the sheath. The ray emitted by dA will be totally reflected at the point E if

$$\sin\Gamma_1 = n_s/n. \tag{A1}$$

The ray will be totally reflected at the external surface of the sheath if

$$\sin\Gamma_2 = 1/n_s. \tag{A2}$$

With simple geometrical considerations (see Appendix B in ref. 10), the angle Γ_1 can be expressed as a function of the angles ζ and ψ of Fig. 5, and Eq. (A1) transforms into

$$\sin\zeta = \frac{n_s}{n}\left[\frac{1-(n\rho/n_sR)^2\sin^2\psi}{1-(\rho/R)^2\sin^2\psi}\right]^{1/2}. \tag{A3}$$

In a similar way, the angle Γ_2 can be expressed as a function of the angles ζ and ψ, and Eq. (A2) transforms into

$$\sin\zeta = \frac{1}{n}\left[\frac{1-(n\rho/R_s)^2\sin^2\psi}{1-(\rho/R_s)^2\sin^2\psi}\right]^{1/2}, \tag{A4}$$

where R_s is the radius of the sheath.

For each value of the angle ψ the limit angle ζ_0 will be given by the minimum between the two values of ζ given by Eqs. (A3) and (A4). If $R_s \gg R$, Eq. (A4) can be approximated as

$$\sin\zeta = 1/n, \tag{A5}$$

and the combination of Eqs. (A5) and (A3) leads to Eq. (8a). We have estimated that the preceding approximation leads to an error for p_a in Eq. (7) of only a few percent if R_s is at least equal to nR, where n is the index of refraction of ruby.

B. Spherical Sheath

As with the cylindrical sheath, in this case there may be two ways of total reflection: (1) at the surface separating the rod and the spherical sheath and (2) at the external surface of the sheath. However, if the radius R_s of the sphere is at least equal to $n_s[l^2 + R^2]^{1/2} = n_sR^*$, where $2l$ and R are the length and the radius of the rod, respectively, it can be easily shown that a total reflection at the external surface of the sheath cannot occur. In fact, as the ruby rod is internal to the sphere of radius R^*, a ray emitted by an elemental area dA of the rod can be considered as emitted from the corresponding point of the sphere of radius R^*. If the radius R_s of the spherical sheath is at least n_s times bigger than R^*, any ray emitted by the sphere of radius R^* will be incident at the external surface of the sphere of radius R_s with an angle less than the limit angle.

Therefore the limit of integration ζ_0 is, in this case, only determined by the total reflection at the surface separating the rod and the sheath, and it is given by Eq. (A3), which is the same as Eq. (9a).

References

1. G. E. Devlin, J. McKenna, A. D. May, and A. L. Schawlow, Appl. Opt. **1**, 11 (1962).
2. A. L. Schawlow, Solid State **2**, 21 (1961).
3. A. L. Schawlow, *Advances in Quantum Electronics*, ed. J. R. Singer (Columbia University Press, New York, 1961), p. 50.
4. J. P. Wilke, J. Appl. Phys. **33**, 2333 (1962).
5. J. D'Haenens and C. K. Asawa, J. Appl. Phys. **33**, 3201 (1962).
6. T. Li and S. D. Sims, Proc. Inst. Radio Engrs. **50**, 464 (1962).
7. R. L. Aagard D. L. Hardwich, and J. F. Ready, Appl. Opt. **1**, 537 (1962)
8. T. H. Maiman, R. H. Hoskins, I. J. D'Haenens, C. K. Asawa, and V. Evtuhov, Phys. Rev. **123**, 1151 (1961).
9. J. McKenna, Bell Telephone Laboratories Memorandum Case 20878-4 (May 21, 1962).
10. O. Svelto, Appl. Opt. **1**, 745 (1962).
11. H. E. Edgerton, *Advances in Quantum Electronics*, ed. J. R. Singer (Columbia University Press, New York, 1961), p. 276.
12. M. L. Stitch, J. Appl. Phys. **32**, 1994 (1961).
13. F. A. Jenkins and H. E. White, *Fundamentals of Optics* (McGraw-Hill, New York, 1950), 2nd ed., p. 565.
14. W. Kaiser and M. J. Keck, J. Appl. Phys. **33**, 762 (1962).
15. M. Hercher, Appl. Opt. **1**, 655 (1962).

Meeting Reports *continued from page 430*

A series of papers from Hughes Aircraft covered work from Maiman's discovery of optical maser action to a Kerr cell Q-spoiler. George Smith of Hughes gave a general view of the whole program in which he summarized the work by presenting a table of typical ruby laser characteristics:

Peak power output	14 MW
Energy output	20 J
Efficiency	0.25%
Spectral bandwidth	<0.01 Å
Beamwidth (without optics)	1 mrad

These various numbers had not been achieved simultaneously with the same ruby. The 20 J was obtained from a ruby approximately 20 cm long. He then discussed a series of basic experiments or applications, most of which were confined to ruby. Maser action was obtained at the R-2 line of ruby by coating the ends of a rod with dielectric layers that had high reflectivity at the R-2 line at 6929 Å and low reflectivity at the R-1 line at 6943 Å.

Smith also discussed various modulation techniques such as hair trigger modulation, in which two pumping sources are used with the ruby. The first provides enough energy to bring half the ground-state population to the excited state, so that the maser is just in the point of oscillation. The second source can then, with a short intense flash, trigger the ruby and produce an extremely high peak-power pulse at a controlled time. "Colidar," or "coherent light detection and ranging," was also discussed by Smith. He described the first experiment carried out at Hughes in January, 1961; later experiments gave daytime ranges of 11 km.

A second Hughes paper by Hellwarth, McClung, and Smith presented the 14-MW, 35-nsec, Q-spoiling experiment. They showed that, if a ruby were pumped in a high-threshold condition, a sudden lowering of the threshold would produce a single giant pulse of energy. The ruby threshold is maintained at a high level by inserting it in a system with external mirrors. Between the ruby and one of the mirrors is placed a shutter that can be opened suddenly after a sufficient pumping time. In the Hughes experiment, a Kerr cell was placed between the ruby and one end reflector. In one situation, the ruby was cut so that the optic axis was inclined to the axis of the rod; and, because of the natural linear dichroism of the material, polarized light was emitted. With the Kerr cell excited to give one-quarter wave retardation, regeneration could not take place until the light had been reflected twice through the system. Sudden removal of the Kerr cell voltage produced the giant maser pulse. In the second situation, a polarizer was placed between the Kerr cell and the ruby. In this case, a Z-cut rod could be used.

A second paper on Q-spoiling was presented by M. Mayer of the Compagnie Generale de Telegraphie sans Fils. He also used a Kerr cell, but in combination with a quarter-wave plate. Accordingly, his giant pulse was obtained when voltage was applied to the cell rather than when it was removed, as in the Hughes experiment. M. Mayer did not report the power value for his giant pulse. Dr. Katzman of the U. S. Army Signal Laboratories at Fort Monmouth discussed experiments in which two ruby rods were operated in series in a cavity which consisted of two concentric spherical mirrors. The mirrors were placed 4 m apart; the rods were each 44 mm long. Since X-cut rods would not oscillate when their axes were crossed, there seemed to be coupling between the two ruby sections.

Dr. Früngel of Impulsphysik/GmbH of Germany presented two papers which covered his "spark light" and its application to optical radar and optical maser pumping. The spark light is one of a series of flash lamps made by Dr. Früngel. They are filled with a gas such as xenon or krypton and can be pulsed up to 500,000 times per second for a period of the order of 0.01 sec. At 1000 flashes per second, the lamp can run continuously. The conversion efficiency from electrical to optical energy is 10–15%. The flash energies can be 4 J. One interesting application was for the measurement of cloud heights. He also presented the hair-trigger operation of a ruby maser, in which conventional pumping brought the maser-stored energy to a level just below threshold. The spark-light directed at the end of the rod could then trigger oscillations. He also showed the use of the spark-light alone as a pump. The light was placed in the center of a hollow ruby rod, the interior of which was coated with a phosphor. This phosphor converted some of the ultraviolet from the flash lamp into light at the ruby-pumping acceptance band.

Although we were all somewhat weary by the end of the conference we felt it had been one of the most efficiently conducted sessions we had ever attended. Our hosts modestly explained that they were responsible for similar sessions every week. Perhaps in this expanding field of optical masers there is room for this group to leave NATO and set up a new commercial company devoted to the running of scientific conferences in optical masers.

OSU Symposium on Lasers and Applications, Columbus, November 7-8, 1962

Reported by Edward K. Damon, OSU

The capacity audience of 350 represented more than 150 industrial, governmental, and educational organizations and included guests from France, Japan, Israel, Canada, and the United States at this Ohio State University meeting. The keynote address by John E. Keto, Chief Scientist of the Aeronautical Systems Division, USAF, stressed the importance to modern research efforts of good experimental facilities, cited the value to the space program of several large installations, and described a proposed multimillion dollar coherent radiation research facility planned for ASD.

The newly discovered laser action in junction diodes formed a stimulating topic for discussion. Following an invited paper by Keyes and Quist *Lincoln Laboratory*, on spontaneous emission from gallium–arsenide junction diodes, J. D. Kingsley *General Electric Research Laboratory*, described the shift to laser action in properly prepared diodes as the injection current is increased, with a decrease in emission line-width of less than 0.6 Å and the narrowing of the isotropic output to a 1° plane-polarized beam. Lincoln Laboratory reported measured efficiencies of 100% for photon production from injected electrons in a lasing diode, and IBM Watson Laboratories announced the observation of laser action with thresholds as low as several hundred milliamperes.

Alfred Kastler *Université de Paris*, presented an invited paper which discussed a double-resonance experiment performed by Margerie and him to probe the fine structure of optical absorption bands. The proper choice of laser materials received further attention in an invited paper by Z. J. Kiss *RCA*, which discussed the divalent rare earths and in one by R. F. Rowntree and W. S. C. Chang *Ohio State University*, who have measured some possible host materials for use in the very far infrared. The present status of gaseous optical masers was described in an invited paper by C. Patel *Bell Laboratories;* T. S. Jaseja and A. Javan *MIT*, described some meticulous experiments wherein stabilities of three parts in 10^{13} were obtained. Absorption and

Meeting Reports *continued on page 444*

Exploding Wire Blast Shutter

W. G. Chace and C. V. Fish

A capping shutter actuated by an electrically exploded copper ribbon is described. It is suitable for use with very high-speed rotating mirror devices, since it has a closing time of < 5 μsec. Usable pictures may be taken even when the light intensity increases by 1000 between image repeats.

A capping shutter is required whenever a rotating mirror device such as a framing camera, streak camera, or time-resolved spectrograph is used to study phenomena that last longer than the "repeat time" of the device (time for mirror to revolve and to form the next image on the film). This may be mechanical, electro-optical, magnetic, or "blast," i.e., explosive.

A conventional between-the-lens type shutter is usually not fast enough, and it suffers from the considerable difficulty of synchronization with the mirror.

Rotating mechanical shutters are fast enough, but there is even greater difficulty in synchronizing two rotating systems. A rotating shutter is described by Wiese[1]; however, he does not use it with a rotating mirror.

Electro-optical shutters, Kerr cells, and Faraday magnetooptical shutters have been extensively described in the literature and are available commercially. They are easily synchronized and are probably not more generally used because of the difficulty of construction, the consequent expense, and the low optical aperture. Quite recently, it has been suggested that a tube of thin aluminum foil might be collapsed by a strong magnet and shut off the light beam.

The most commonly recommended method of preventing rewrite is a blast shutter. Here, an explosion interrupts the optical path after the picture has been taken. Four types of blast shutters have been described: flap, lead wire, mirror, and shatter.

The flap type was described by Wurster.[2] It consists of a flap of black electrical-type Scotch tape which is blown into the optical path by an exploding lead wire. The author claims a closing time of 5 μsec.

The authors are with Air Force Cambridge Research Laboratories, Bedford, Massachusetts.

Received 9 October 1962.

The Edgerton lead-wire shutter[3] consists of a grid of lead wires between two sheets of glass. A surge of current evaporates the lead uniformly over the glass plates, producing in about 30 μsec a screen of optical density 3.

In the mirror type, the image is brought into the camera by reflection from a mirror surface. The shutter is closed by destroying either the reflecting surface or the whole mirror.

A more commonly recommended type of blast shutter is, however, the shatter type. As described by Brixner,[4] it consists of a small sheet of 12-mm ($^1/_2$-in.) thick plate glass enclosed in a strong steel holder along with a blasting squib. When the squib, placed along one or two edges of the glass, is exploded, the glass is shattered; although not wholly opaque, it no longer transmits an image; hence, rewrite is prevented.

Exploding Wire Blast Shutter

It has been found in this laboratory that an electrically exploded copper ribbon could be substituted for the high explosive squib to operate a shutter similar to Brixner's. Experiments to develop such a shutter brought out certain requirements:

1. The shattered or crazed glass must be held together by some method; heavy black plastic electrical tape wrapped completely around the glass does this very well. A 3.5-cm hole allows the light to pass.

2. A metal ribbon gave a better result than any wire. Copper ribbon 0.005-cm thick, 0.55-cm wide, with length adapted to fit the holder, is satisfactory for 6-mm ($^1/_4$-in.) plate glass.

3. By placing a micarta "anvil" behind the copper ribbon, the shock is more efficiently driven through the glass, and a much more complete shattering occurs.

4. For best shuttering action, the glass must be broken into very fine pieces. Uniformly fine breakup can be assured by grinding each edge of the glass on a

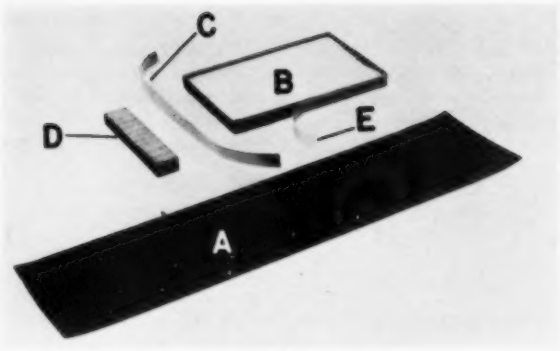

(a)

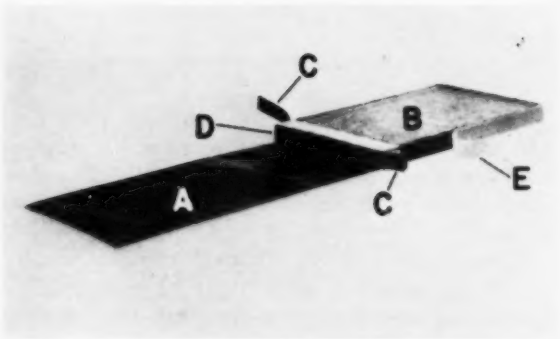

(b)

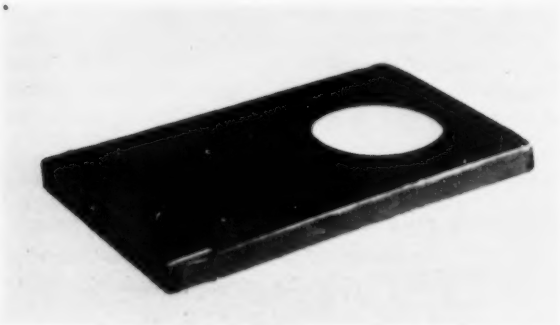

(c)

Fig. 1. Assembly of shutter element. (a) Parts arranged for assembly; (b) partially assembled; (c) completed shutter element. A—plastic tape binding, B—glass, C—copper ribbon, D—micarta anvil, E—retainer tape [$^1/_4$-in. (6-mm) masking tape].

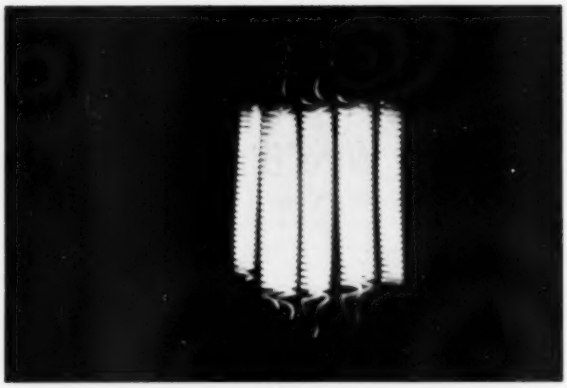

(a)

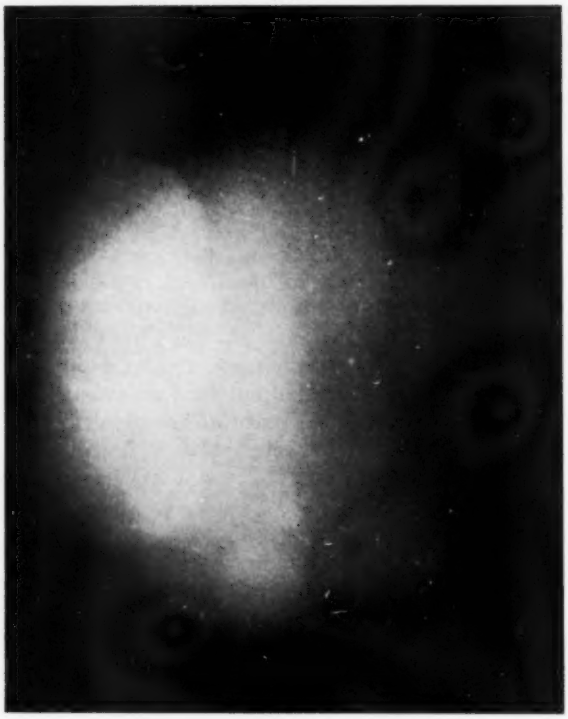

(b)

Fig. 2. Effectiveness of exploding wire blast shutter. (a) lamp filament, exposure 1/50 sec, *f*/22, through clear shutter glass and Wratten No. 96 ND-3 filter, Polaroid P/N-55 film. (b) lamp filament, exposure 1/50 sec, *f*/22, through exploded shutter glass, Polaroid F/N-55 film.

coarse (60-grit J8) grinding wheel. This gives a multitude of scratches from which the breakup can start.

5. The flash from the exploding wire must be kept out of the camera. Direct transmission through the shutter glass is prevented by blacking the ground edges with a heavy coating of black paint. A carefully planned holder will confine the rest of the flash. Figure 1 shows the glass shutter—exploded view, partially assembled, and ready for use. The glass is ordinary 6-mm ($^1/_4$-in.) plate cut into 5 × 7.5 cm (2 × 3 in.) pieces.

Results

A piece of shattered glass is surprisingly opaque, but its effectiveness as a capping shutter lies principally in its ability to prevent image formation.

Although accurate optical measurements were not made on the shutter, its usefulness may be indicated

by the tests shown in Figs. 2 and 3. Figure 2 (a) is a photograph of a lamp filament taken through an unexploded blast shutter and a neutral density filter (density 3.0). In Fig. 2 (b), a similar picture was taken under identical conditions, except that the unexploded filter was replaced with an exploded one, and the 3.0 ND filter was removed. This approximates the condition where the rewrite situation occurs when the light intensity has increased by 1000 over that in the original exposure. For example, when a picture is taken of the early stages of a wire explosion, the rewrite occurs when the light is at its peak. It may be from 100 to 1000 times as intense as that used to make the image, a severe test of a capping shutter. In Fig. 3, the same two exposures were made on one piece of film. The image is still wholly usable, although surrounded by fog. If the light does not increase between the original picture and the rewrite, the fog is imperceptible.

Fig. 3. Simulated rewrite. First exposure—lamp filament, exposure 1/50 sec, $f/22$ through clear glass shutter and Wratten No. 96 ND-3 filter. Second exposure—lamp filament, exposure 1/50 sec, f-22, through exploded glass shutter, Polaroid P/N-55 film.

Fig. 4. Closing action of exploding wire blast shutter. Framing camera. Framing rate, 1 μsec.

To determine the time required for the shutter to close, a framing camera sequence was taken of the process of shattering. This is shown in Fig. 4. In the first frame, the shattering has not yet started; the shattering progresses through frames 2, 3, and 4 and is complete on frame 5. The framing rate is 1 μsec per frame; hence, the shutter closing process requires less than 5 μsec.

Another time of interest is that between the application of the trigger to the switch in the discharge circuit and the closing of the shutter. This requires 18 μsec in the arrangement used in this laboratory. Most of this time is consumed in shock-wave travel through the glass. The wire explosion is accomplished in less than 2 μsec after the application of the trigger.

Little need be said about the holder except that it must be strong. Exploding wires produce surprisingly destructive shock waves.

The condenser bank and switch are also not critical. Voltages around 10 kV work well; 6 kV is too low. Capacitor banks of 24 μF and 36 μF have been used successfully; 12 μF was tried, but proved inadequate.

References

1. W. L. Wiese, Rev. Sci. Instr. **31,** 943 (1960).
2. W. H. Wurster, Rev. Sci. Instr. **28,** 1093 (1957).
3. H. E. Edgerton and F. J. Strabala, Rev. Sci. Instr. **27,** 162 (1956).
4. B. Brixner, J. Soc. Motion Picture and Television Engrs. **59,** 503 (1952).

John E. Keto, Chief Scientist, ASD; Robert A. Fouty, Symposium Coordinator, OSU; Raymond J. Nordlund, Technical Director of Avionics, ASD; and A. Kastler, Université de Paris, who presented an invited paper, during The Ohio State University's Symposium on Lasers, November 1962 (see report on page 440).

pressure-broadening measurements on water vapor at various concentrations were reported by R. K. Long and T. H. Lewis *Ohio State*, using the infrared 11,522.82 Å line of a He-Ne laser.

The subject of nonlinear optical properties was introduced by an invited theoretical paper by P. S. Pershan *Harvard*, and P. D. Maker *Ford Motor Company*, who reported that their group has achieved third harmonic generation and 20% efficiency in generating the second harmonic of the ruby laser. H. Hsu interpreted nonlinear effects in terms of parametric photon interactions, of which harmonic generation is a special case; P. J. Price *IBM*, presented equivalences between nonlinear polarization phenomena and classical principles. The observation of nonlinear ionization of gases in a laser beam was reported by E. K. Damon and R. G. Tomlinson *Ohio State*.

Considerations of pumping and material choice were treated in several papers. The energy output of several materials was compared by W. Ruderman *Isomet;* J. H. Wensel *GE* discussed performance prediction, including a proposed 1000 J laser; and R. L. Aagard *Honeywell* reported observing some anomalous effects when part of the laser rod was shielded from the pumping radiation. The use of exploding wires and the use of plasma-impingement as pumping sources were presented by C. H. Church *Westinghouse*, and G. Fonda-Bonardi *Litton*, respectively.

Improvements in microwave modulation of laser beams were discussed in an invited paper by I. Kaminow *Bell*, where substantially lower power requirements were achieved. The selection of a single laser mode by the use of a secondary etalon within the laser cavity was described by S. A. Collins *Sperry;* and C. M. Stickley *AFCRL*, had some interesting results on the axial frequency switching patterns in ruby lasers. A. Okaya *IBM*, showed some experimental evidence of phase uniformity at the laser end surface, and P. S. McDermott *IBM*, discussed laser action in rectangular dielectric waveguides. The use of a *Q*-switched ruby laser system for tracking satellites was described by T. S. Johnson *NASA*.

Arranged by The Ohio State University Antenna Laboratory, the symposium included an open house inspection of laser and related facilities and opportunities for many informal discussions. The technical program was arranged by W. S. C. Chang, with C. B. G. Garrett *Bell*, D. E. Lewis *ASD*, G. Parrent *Tech. Ops.*, and R. W. Terhune *Ford* serving as the papers review committee. The general excellence of the papers presented deserve special recognition. C. A. Levis was symposium chairman, and R. A. Fouty acted as coordinator. Professor Chang is also the editor of the *Proceedings*.

1962 International Symposium on Information Theory, Brussels, Belgium, September 3–7, 1962

Reported by Nelson M. Blachman, Sylvania Electronic Systems

The International Symposium on Information Theory, held at the Free University of Brussels, registered about three hundred people; half that number were in attendance during each of the ten half-day sessions, which took place in the Paul Emile Janson Auditorium of the University.

The 48 papers presented dealt with a wide range of topics: coding theory, adaptive systems, pattern recognition, signal processing and detection, human psychological and nervous activity, entropy and channel capacity, speech and music, signal and channel analysis, modulation systems, and threshold effects in signal detection. Their authors came from ten countries—well over half of them from the U.S.—with about a tenth from Great Britain and another tenth from the Soviet Union, although none of the latter authors came to the meeting. Instead, a delegation of five people attended; one of them, Aleksandr Mikhailovich Petrovsky of the Institute of Automatics and Telemechanics, read Basharinov's paper and also presented an unscheduled paper of his own on "Some Problems in the Analysis of a Closed-Loop System Influenced by Noise." This paper involved controlling a system described by a multidimensional binary vector in the shortest possible time. Two computers are required, one to keep track of the past and the other to control the first one. The case of ternary vector components has also been investigated. Although Petrovsky's paper was not distributed at the symposium, as were the majority of the others (IRE Trans. on Information Theory, September 1962) that of B. S. Fleishman of the U.S.S.R. Academy of Sciences' Institute of Radio Engineering and Electronics, which was evidently received too late for inclusion in the *Transactions*, was available in English although it was not presented. This 25-page paper, "Basic Theorems of the Constructive Information Theory," deals with the probability of obtaining a good code for a constant, discrete, memoryless channel by random selection, summarizing work presented by the author at radio and mathematical meetings in the U.S.S.R. between 1959 and 1961. His principal result is that the probability of obtaining a good code by random selection tends to unity with increasing word length more rapidly than the probability of correct decoding.

Other papers presented and distributed but not included in the *Transactions* are: "Human Search Characteristics in the Space and Time Domains," by Norman S. Potter, RCA/Moorestown, in which a theory of perception performance with changing relative geometry is developed that leads to a functional relationship between the probability of perception of an approaching object and the relative velocity and separation of the observer at perception; "On the Use of Boolean Functions in Pattern Recognition," by S. R. Petrick, AFCRL, who used minimum Boolean forms giving correct decisions for previously identified patterns in the study of automatic speech recognition by means of quantized short-term spectra at a sequence of instants of time; "The Independent Specification of the Modulus of a Function and the Modulus of its Fourier Transform," (i.e., of the power spectrum and the envelope of a waveform) by Evert N. Fowle of the Mitre Corp., who shows that, as long as the time-bandwidth product is at least 10 and the prescribed functions are both smooth, phase functions can be found which, when associated with the two moduli, make an approximate Fourier pair, but, when *both* moduli vanish outside a certain interval, a time-bandwidth product of 100 or more is required to give good accuracy in the approximate Fourier pair; and "The Logic and Behaviour of Self-Organizing Systems as Illustrated by the Interaction between Men and Adaptive Machines," by Gordon Pask, System Research Ltd., Richmond, England, who devoted particular attention to the case of teaching machines.

Among the papers published in the *Transactions* a number were excellent, of which space permits mentioning only a few: David Huffman, MIT, discussed the generation of pulse trains with as-nearly-as-is-theoretically-possible the same autocorrelation function as a single pulse. Peter Neumann, BTL, presented a class of variable-length codes which resynchronize themselves quickly after an error and are, furthermore, efficient. David Slepian, also of BTL, dealt with the signal-to-noise ratio required for a given bandwidth-expansion factor (or memory requirement, measured in Nyquist intervals), information rate, and error probability, and he applied his results in a remarkably simple manner to voice and television transmission. A BTL team headed by E. E. David presented their "voice-excited vocoder," which uses 1145 cps of bandwidth and produces speech that is often almost undistinguishable from the input by generating the excitation from a 250- to 970-cps portion of the input speech. L. H. Zetterberg,

continued on page 447

Multilayer Reflection Coatings on a Metal Mirror

Leo Young

The design of a thin-film dielectric multilayer on a metal surface to enhance its reflectance is discussed. A numerical example is solved in detail.

Introduction

It is well known that the reflectance of metal mirrors can be enhanced appreciably by depositing several quarter-wave layers of dielectric,[1-4] whose refractive indices alternate (starting at the metal surface) low-high-low-high .... The reflectance of such a system is frequency-dependent, thus resulting in filter properties. The present application called for the highest possible reflection at certain specified wavelengths, but did not require any filter action. The system was to be used as a mirror for a laser cavity, and high reflectance was desired at the ruby line (0.7 μ) and the neodymium line (1.06 μ).

The Problem

The uncoated metal mirror had been used to close a laser cavity. The mirror had been rotated at several thousand revolutions per second, its speed and the geometry determining the length of the output pulse. The mirror surface had been damaged by the heat generated at the imperfectly reflecting surface, and it was now required to improve the reflectance of this rotating mirror, especially at the ruby line of 0.7 μ and the neodymium line of 1.06 μ.

It was decided to use a gold film as the metal mirror and to coat it with quarter-wave layers of cryolite (refractive index $n = 1.32$) and ZnS ($n = 2.2$). The reflectance of gold[5] at 0.7 μ is 97%, and at 1.06 μ it is 98.2%. The questions which had to be answered were these: How many layers should be used? With the number of layers decided, at what wavelength should each layer be one-quarter wavelength thick?

Maximum Reflectance

The reflectance R_m of a metal surface in vacuum is related to its complex refractive index $n - ik$ by

$$R_m = 1 - \frac{4n}{(1+n)^2 + k^2}. \tag{1}$$

When a stack of $2N$ nonabsorbing quarter-wave layers of refractive indexes $n_2, n_1, n_2, n_1 \ldots$ (Fig. 1) is deposited on the metal surface, it can be shown that its reflectance is increased to

$$R = 1 - \frac{4xn}{(x+n)^2 + k^2} \tag{2}$$

$$= 1 - \frac{4x}{\left(\frac{4}{1-R_m}\right) - 2(1-x) - \left(\frac{1-x^2}{n}\right)}, \tag{3}$$

where

$$x = \left(\frac{n_2}{n_1}\right)^{2N}. \tag{4}$$

The quantity x will, in practice, always be less than unity. If the real part n of the complex refractive index $n - ik$ is large compared to $1 - R_m$, that is,

$$n \gg 1 - R_m, \tag{5}$$

then the expression for R reduces to

$$R \approx 1 - x(1 - R_m). \tag{6}$$

In the case of a gold film,[6] n is about 0.3, while $(1 - R_m)$ is less than 0.03, at wavelengths around 1 μ, so that Eq. (5) may be considered satisfied. The maximum reflectance is then a function of x and of R_m only, by Eq. (6), and hardly depends on n and k separately.

The effect of small absorption losses in the dielectric layers on a mirror has been treated by Young,[7] but will not be considered here.

Computed Reflectance Curves

It was pointed out above that the maximum reflectance in the present case is determined almost by R_m alone and not by n and k separately. The maximum reflectance is thus very nearly equal to that produced by a hypothetical mirror or medium with

The author is with Stanford Research Institute, Menlo Park, California.

Received 6 August 1962.

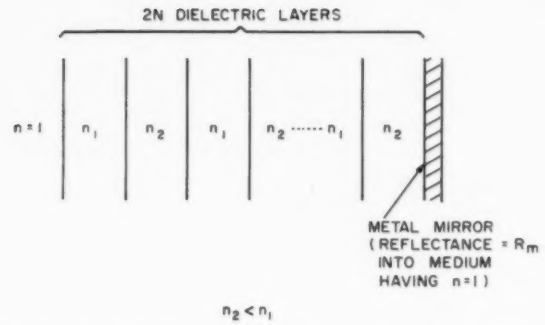

Fig. 1. Stack of $2N$ dielectric quarter-wave layers on a metal mirror to enhance its reflectance.

$$n = \frac{1 + \sqrt{R_m}}{1 - \sqrt{R_m}} = \frac{1.985}{0.015} = 132 \tag{7}$$

and with $k = 0$. The reflectance in the vicinity of the maximum may likewise be expected to be very close to that obtained by substituting a fictitious medium of refractive index $n = 132$ for the gold mirror.

A digital-computer program was available on the Burroughs Electro-Data 220 at SRI for microwave quarter-wave transformers. This is analytically the same problem as the one posed above. The computed curves (Fig. 2) show the frequency variation of the reflectance for three cases, namely with 2, 4, and 6 layers, on the same metal surface. The computations assumed the dielectrics to be without absorption and supposed a metal film reflectance of 97%. However, the curves can be used for other high metal reflectances also, as will be shown presently. (As has already been pointed out, the reflectance of gold changes appreciably between the two wavelengths of interest.)

The computed curves are symmetrical about the band-center ($f/f_0 = 1$) on a frequency scale. The actual performance may be expected to be unsymmetrical because k is not zero, as assumed in the computations. However, the general appearance of the response curve, particularly in the region near the maximum reflectance, should be given closely by the curves in Fig. 2.

For large R_m we see from Eq. (6) that

$$(1 - R) \propto (1 - R_m). \tag{8}$$

Since Fig. 2 has been plotted on a logarithmic scale for $(1 - R)$, and since both $(1 - R_m)$ and $(1 - R)$ are small, we can obtain the reflectance of the multilayer system with a different metal reflectance R_m, such as $R_m = 0.982$, by sliding the ordinate scale on the left in Fig. 2 until the number 0.982 appears opposite the center horizontal line, which previously corresponded to 0.97.

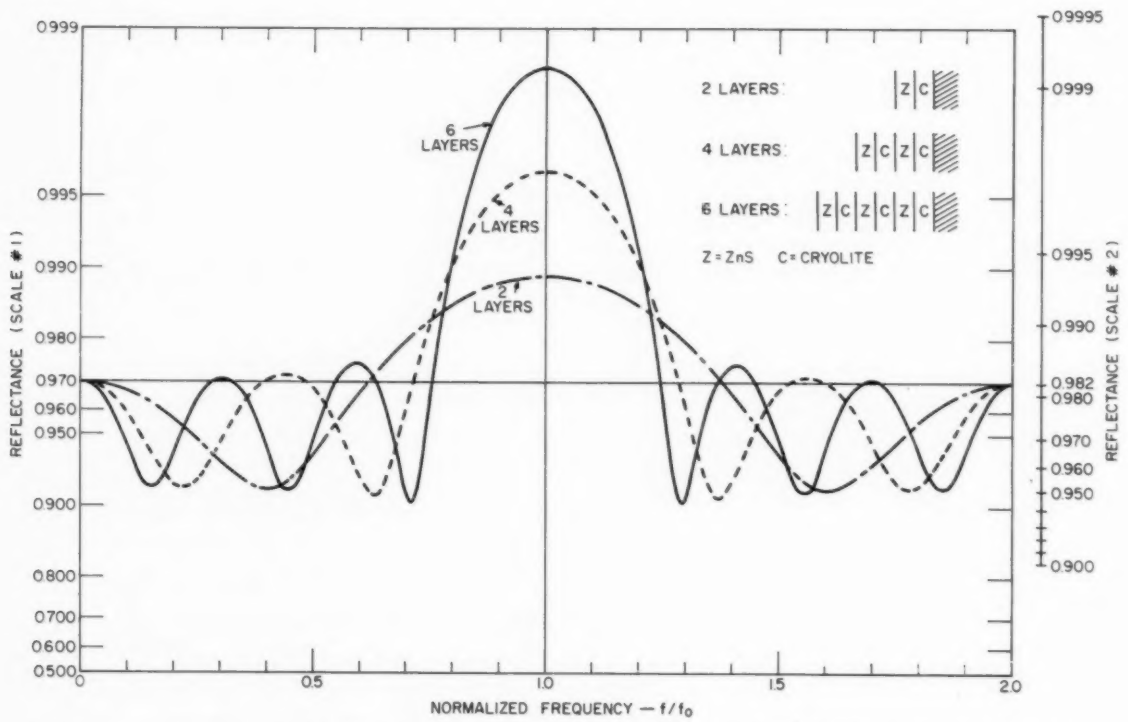

Fig. 2. Computed reflectance characteristics of three metal mirrors with 2, 4, and 6 dielectric quarter-wave layers, respectively.

Solution of the Problem

The metal reflectances R_m of 0.97 and 0.982, which give the left-hand and right-hand scales in Fig. 2, correspond to the reflectance of gold at the two wavelengths 0.7 μ and 1.06 μ in the problem under consideration. The two wavelengths (and therefore frequencies) are in the ratio of 1.06:0.7. It is then necessary to find two normalized frequencies in this ratio, for which the system reflectance is the same when the two different scales are used.

Consider first the case of two dielectric layers. As a first guess we try $f = 0.7$ and $f = 1.06$, which are in the desired ratio. We see at $f = 1.06$ on the left-hand scale (Scale 1) the reflectance is 0.988, while at $f = 0.7$ the reflectance is 0.989 on the right-hand scale (Scale 2). This is close enough, and we need go no further. The band-center should therefore be a free-space wavelength of $0.7 \times 1.06 = 0.742$ μ.

Consider next the case of four layers. By inspection, the normalized frequencies $f = 0.77$ (on Scale 2) and $f = 1.156$ (on Scale 1) yield a reflectance 0.9925. The band-center wavelength is then $0.7 \times 1.156 = 0.8092$ μ.

For the six-layer mirror the normalized frequencies are $f = 0.785$ and $f = 1.19$. They yield only about the same reflectance (0.9925), and the six layers would be more critical to fabricate.

The choice then lies between a two-dielectric-layer system of reflectance 98.8% and a four-dielectric-layer system of reflectance 99.25%. The improvement due to the extra two layers will be slightly less than the calculated 0.45% because of absorption losses[7] and because it is harder to hold the tolerances required for four dielectric layers than for two. Had the two wavelengths been further apart, the two dielectric layers would have made the best mirror even before considering dielectric absorption losses and tolerances; if the two lines had been closer together, six or more dielectric layers might have reflected better.

Conclusion

The design of dielectric coatings to enhance the reflection from metal surfaces has been briefly discussed. An example was treated numerically, but the method illustrates the general procedure.

The help and advice of J. R. Jennings and the interest of R. C. Honey are gratefully acknowledged. The author also wishes to acknowledge the many helpful comments made by the reviewers of this journal.

References

1. A. F. Turner, J. phys. radium **11**, 444 (1950).
2. A. F. Turner, U.S. Patent 2,519,722, 22 August 1950.
3. F. A. Jenkins, J. phys. radium **19**, 301 (1958).
4. O. S. Heavens, *Optical Properties of Thin Solid Films* (Academic Press, New York, 1955), pp. 221–224.
5. *American Institute of Physics Handbook* (McGraw-Hill, New York, 1957), Sec. 6, p. 108.
6. *American Institute of Physics Handbook* (McGraw-Hill, New York, 1957), Sec. 6, p. 105.
7. L. Young, J. Opt. Soc. Am. **52**, 753 (1962).

Meeting Reports *continued from page 444*

SAAB, analyzed a communication game in which one player chooses the spectrum of a portion of the interfering noise, the other selects a filter for the receiver, and the resulting signal-to-noise ratio is the pay-off. N. M. Blachman presented new results concerning the capacity of a channel perturbed by interference whose form can depend on the signal being transmitted and on the forms of all of the other signals that might have been sent instead. The talk that provoked the most heated discussion was that of Wilhelm Fucks, T. H./Aachen, who analyzed the statistics of tone duration, pitch, and intervals in the music of the last five centuries and found certain similarities in the statistics of Bach's and Weber's music not shared by Beethoven's.

Thanks are due F. L. H. M. Stumpers, chairman of the organizing committee of the meeting, and to the sponsor, the IRE Professional Group on Information Theory, as well as to the Benelux Section of the Institute of Radio Engineers, the Société Belge des Ingenieurs des Télécommunications et d'Electronique, and the Université Libre de Bruxelles, for arranging this meeting, which provided a useful picture of the current work in communication theory and related fields. It is unfortunate, however, that some important groups were not represented; although the Institute for Information Theory and Automatization in Prague is very active and sponsored the third of a triennial series of meetings in June 1962, that group did not participate in the Brussels meeting. This meeting would probably have been more lively, too, if there had been more than four British papers; some of the most eminent communication theoreticians in the U.K. did not attend. The judicious invitation of speakers and other participants, as the case of the London symposia, might have been beneficial.

P.I.B. Symposium on Optical Masers to be Held in New York City April 16–18, 1963

Optical Masers is the topic of the thirteenth Polytechnic Annual Symposium to be held at the Waldorf-Astoria Hotel in New York City on April 16, 17, and 18, 1963, organized by the Microwave Research Institute of the Polytechnic Institute of Brooklyn in cooperation with the Optical Society of America and the Professional Technical Groups on Microwave Theory and Techniques and Electron Devices of the Institute of Electrical and Electronics Engineers, and cosponsored by the Air Force Office of Scientific Research, the Office of Naval Research and the Army Research Office. The symposium will attempt a comprehensive integration of the physics and technology bearing directly on the discovery, theory, and application of maser phenomena at optical and infrared frequencies. In keeping with tradition, the symposium will endeavor to serve the twofold purpose of providing both a review of the present state of research in the field and a forum for discussion of recent outstanding advances of interest to engineers, chemists, and physicists involved in laser research and development.

For further information, call Jerome Fox, Polytechnic Institute of Brooklyn, 212-ULster 5-2414.

Applied Optics

Letters to the Editor

Letters to the Editor should be addressed to the Editor, APPLIED OPTICS, 1155 16th St., N.W., Washington 6, D.C.

Appearance Criteria for Uncolored Anodized Aluminum Surfaces

Roger L. Saur

Research Laboratories, General Motors Corporation, Warren, Michigan

Received 31 October 1962.

A program was undertaken to determine the criteria people use in their judgment of appearance of anodized aluminum surfaces. Although this was reported at the National Meeting of the American Electroplaters' Society in June, 1962, at Milwaukee, Wisconsin (it will be included in the Technical Proceedings to be sent to each AES member), it was felt that those in other fields would also find the program interesting. Reprints of the original report can be obtained from the author.

Twelve aluminum panels which had been buffed, polished, and anodized in a commercial process, and which ranged from worst to best of industrial practice, were ranked by each of 24 people in his order of preference for automative trim. Image resolution loss and haze for each panel were then measured, each by a subjective visual technique, and by a more nearly objective instrumental technique. Plotted results gave similarly shaped curves for haze and for resolution loss, thus implying that the instrumental technique measured that which was being assessed by the corresponding visual technique. Results of these techniques were plotted against the visual ranking order; correlation of data was inferred by a smooth unidirectional progression of the curve from the best to the worst panel appearance. Using this rule, the data showed that 22 of the 24 people tested used either haze, resolution loss, or both, in their appearance judgment. The sixteen who preferred that the surface be a perfect mirror (as judged by the data) visually integrated the haze and resolution loss criteria. Of the four who preferred matte surfaces, three based their judgment on resolution loss alone and one based it on haze alone. The remaining two people whose ranking orders were accounted for by these criteria preferred either perfectly matte or perfect mirror surfaces.

The program demonstrated that (1) appearance of uncolored anodized aluminum can be measured and (2) different people may have differing visual standards (some prefer mirrors, others prefer matte surfaces), but they almost always use the same criteria (haze and resolution loss) in their appearance judgment.

Interferometer Laser Mode Selector

S. A. Collins and G. R. White

Sperry Gyroscope Company, Division of Sperry Rand Corporation, Great Neck, New York.

Received 14 November 1962.

This letter discusses a new type of laser mode selector, composed of tilted Fabry-Perot etalons placed internal to the laser. This mode selector is unique in that it simultaneously performs two functions: it limits the frequency spectrum radiated and it narrows the beam angle. The mode selectors discussed heretofore have either affected the spectrum without changing the beam angle[1] or have narrowed the beam angle[2,3] without eliminating any of the axial mode frequencies.

As shown in Fig. 1, the selector consists of one or more Fabry-Perot etalons placed within the laser cavity, and tipped with respect to the axis of the laser. Frequency selection and beam angle narrowing are both achieved by rejecting from the laser cavity all light which does not satisfy the conditions for maximum transmission through the etalon. The modes of highest Q are those which most closely satisfy the resonance condition of the laser end mirrors and simultaneously have maximum transmission through the mode selector etalon. The mode selector is designed so that the frequency bandwidth is wide enough to transmit at least one frequency acceptable to the laser end mirrors.

Beam angle narrowing occurs because of the angular bandpass characteristics of the etalon. The point of interest is the bandwidth about the angles of maximum transmission of the etalon. If the angular passband is narrower than the beam spread angle of the laser, then the beam angle will be decreased. Further, the angular bandwidth decreases as the angle of tilt of the mode selector becomes greater. Since a given etalon will narrow the beam in one direction only, two etalons are required tilted to provide both vertical and horizontal narrowing.

The analysis of the mode selector is based on its effects on plane waves assuming that the effects will be approximately the same on the laser fields. The physical situation analyzed consists of plane light waves impinging on a Fabry-Perot etalon of mirror spacing d, cocked at an angle θ to the rays. The light from unwanted modes is reflected out of the laser cavity.

It can be shown that the angles of maximum transmission $\theta(p, \nu)$ satisfy the dependence on frequency ν_1, and order number, p, given in Eq. (1).

$$\theta^2(p, \nu_1) = \frac{c}{d\nu_1}\left[(p-1) + \frac{\nu_1 - \nu_0}{\Delta\nu}\right]. \qquad (1)$$

There ν_0 is a frequency for which there is just an integral number of half-waves at normal incidence and $\Delta\nu$ is the spectral free range[4] $c/2d$.

Equation (2) presents the transmitted light as a function of

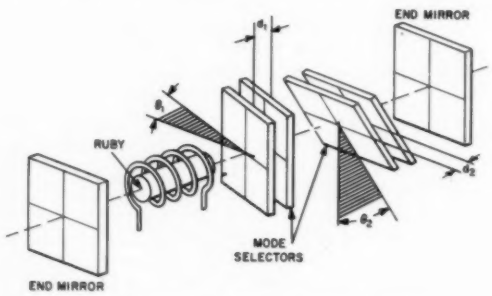

Fig. 1. Laser with mode selectors inserted.

Fig. 2. Photograph of Fabry-Perot rings taken without the mode selector in the laser.

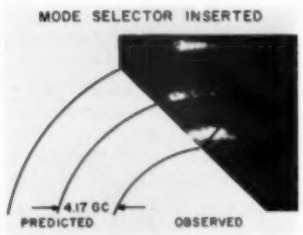

Fig. 3. Photograph of Fabry-Perot rings taken with the mode selector inserted in the laser.

frequency ν and angle θ; ν_1 and $\theta(p, \nu_1)$ denote a point lying on the maximum transmission curves. $(\delta\nu)$ is the frequency bandwidth between half-power points, defined in Eqs. (3a) and (3b) in terms of the finesse $\mathfrak{F}$, and mirror reflectivity, R.

$$\frac{I_t}{I_0} = \frac{1}{1 + \left[\dfrac{\nu - \nu_1}{(\delta\nu)/2} + \dfrac{\theta - \theta(p, \nu_1)}{(\delta\theta)/2}\right]^2}, \tag{2}$$

$$\delta\nu = \frac{\Delta\nu}{\mathfrak{F}}, \tag{3a}$$

$$\mathfrak{F} = \frac{\pi\sqrt{R}}{1 - R}. \tag{3b}$$

$$\delta\theta = \frac{\Delta\nu}{\mathfrak{F}\nu_1\theta(p, \nu_1)}. \tag{4}$$

$(\delta\theta)$ is the angular bandwidth at constant frequency. It is defined in Eq. (4). This expression shows, as indicated earlier, that the angular bandwidth is inversely proportional to the angle of tilt. With the equations derived it is possible to design a mode selector with predetermined characteristics.

The expected operation of such a mode selector has been demonstrated. A ruby laser was used which had mirrors external to the ruby and had provisions to mount two Fabry-Perot etalon mode selectors. The spectral free range of the laser itself is 319 Mc/sec.

Mode selector etalons were made from 28.6 mm by 3.2 mm thirtieth wave quartz flats, with reflective coatings on front and back. The coatings of the three mode selectors tested had a reflectivity of 70, 85, and 93%, respectively, allowing 12, 5, and $2^1/_2$ laser modes in the selector passbands.

The frequency rejection characteristics of a single mode selector, of 70% reflectivity, are shown by means of photographs taken with the external analyzing Fabry-Perot interferometer and a 7.55-m telephoto camera. A set of ring patterns, taken without the mode selector, is shown in Fig. 2. The profuseness of overlapping rings indicates many laser frequencies. With the insertion of the mode selector, we obtain the photograph shown in Fig. 3. The black spaces indicate the rejection of oscillation at certain frequencies. Both photographs were taken about 50% above threshold voltage. The spacing of the rings corresponds to 4.17 Gc/sec. The ring fine structure corresponds to the spectral free range of the lasers.

Beam angle narrowing is demonstrated by a series of far-field photographs. Figure 4 shows such a photograph taken with the same mode selector canted approximately 45 mrad. A subsidiary mode selector passband is also seen. The far field photograph in Fig. 5 vividly shows the small beam angle. It is approximately 1.5×10^{-4} rad wide. This value is essentially the diffraction limit for the ruby, oscillating over its entire cross section.

In this letter we have described a mode selector, which not only limits the number of axial modes, but also limits the beam angle and is applicable to any laser. Simple analysis has been used to determine design parameters. The mode selector tested indeed did demonstrate the frequency rejection and beam narrowing expected. Single etalon mode selectors can be designed to give single frequency output and beam angle at the diffraction limit.

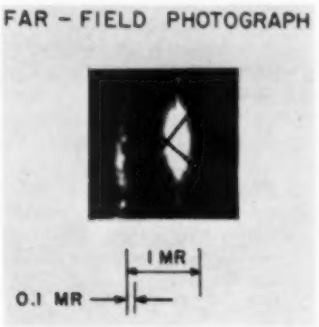

Fig. 4. Far-field photograph taken with the mode selector in the laser. The large spot is the laser beam. The other line is a subsidiary mode selector angular passband.

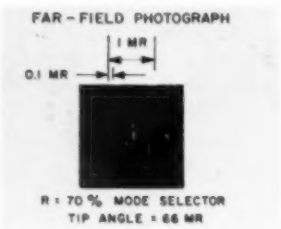

Fig. 5. Far-field photograph showing extreme beam narrowing.

The authors wish to thank W. Kalfur for assisting with the design, construction of the apparatus, and with performance of experiments.

References

1. D. A. Kleinman and P. P. Kisliuk, Bell System Tech. J. **41**, 453 (1962).
2. J. A. Baker and C. W. Peters, Appl. Opt. **1**, 674 (1962).
3. J. G. Skinner and J. E. Geusic, Contributed Paper, Optical Society Meeting, October 4, 1962, Rochester, New York.
4. M. Born and E. Wolf, *Principles of Optics* (Pergamon Press, New York, 1959), pp. 326 ff.

Use of Platinum or Gold Grating Surface at Grazing Incidence

D. O. Landon

Spex Industries, Inc., Metuchen, New Jersey.
Received 26 November 1962.

In selecting a coating material for a concave diffraction grating to be used at grazing incidence, one must take account of the relation between the glancing angle (θ) and the shortest wavelength that will be totally reflected.

Since astigmatism (and other aberrations) increase rapidly with decreasing θ, while the slit to grating distance becomes progressively shorter, it is desirable to have θ as large as possible, commensurate with the shortest wavelength of interest.

From the formula for critical angle,[1]

$$\sin\theta_c = \lambda c^{-1} (n/\pi m)^{1/2},$$

The only variables are θ, λ, and n, where θ is the glancing angle (complement of the incident angle), e and m are, respectively, the charge and mass of the electron, c is the velocity of light, n is the number of electrons per unit volume, and λ is the shortest wavelength to be totally reflected. This formula for critical angle is based on formal diffraction and simplified dispersion theory.[2] As the glancing angle increases the reflectance decreases gradually until, at the critical angle, it drops rapidly. The angle at which this drop occurs is determined mainly by the real index of refraction μ; and the rapidity of the drop is determined by the absorption index β.[3] In the present treatment the absorption effects will be ignored.

Now, assuming that one is interested in some specific wavelength, only θ and n remain as variables, and $\sin\theta$ is proportional to the square root of n. With this in mind the comparisons listed in Table I were made for various materials of interest in connection with diffraction gratings.

The n tabulated in Table I includes all of the electrons ($K,L,M, \ldots$) per atom or molecule, which is the usual approach taken in dealing with x-rays. At the longer wavelengths in the XUV it is doubtful whether all electrons take part in the dispersion process to the same extent, and one should probably use a smaller value for n in the calculation of critical angle. One suggestion has been to consider only the electrons in the last complete shell and in the unfilled shells. The effect of this would be to reduce the $n^{1/2}$ values somewhat. For example, the value for Al_2O_3 would decrease from 10.7 to 9.6, and that for platinum from 22.7 to 18.2.

The gratings most frequently used at grazing incidence are either ruled directly on glass, or are aluminized replicas. Since the aluminum is rapidly converted to Al_2O_3 at the surface, aluminized gratings should be slightly superior to gratings ruled on glass with respect to reaching the shortest wavelength possible at any given glancing angle. Gratings ruled in or coated with either platinum or gold (available from Bausch & Lomb, Inc.) should be superior to others in this sense, since their $n^{1/2}$ values are approximately double those for the usual gratings.

Sprague *et al.*,[4] and Hendrick[3] have dealt with various aspects of grating performance and reflectivity for soft x rays at grazing incidence. Their results and the theoretical treatments thereof appear to be in accord with the relatively simple approach taken here.

The effect of thin films of organic material (diffusion pump oil) can be deduced from the calculated value of $n^{1/2}$ for pentadecane; the cutoff wavelength would probably be shifted to higher values. Recently, Holliday[5] reported measuring to 13.3 Å—Cu L—using a Bausch & Lomb aluminized replica grating at an angle of $\theta = 2°$. Holliday went to considerable pains to avoid contaminating his system with organic vapors, using a liquid-nitrogen-trapped diffusion pump to evacuate his spectrometer. Others using less elaborate vacuum systems—such as untrapped oil diffusion pumps—have reported wavelength cutoffs of approximately 120 Å at $\theta = 8°$. Calculating from Holliday's data that a clean Al_2O_3 surface would show a wavelength cutoff at approximately 55 Å at this angle, the 120 Å cutoff possibly indicates a layer of hydrocarbon material on the grating surface.

The importance of cleanliness of the vacuum system in attaining the shortest wavelengths possible at reasonable angles of incidence is apparent. Consideration should be given to the use of dry vacuum pumps as well as mercury pumps.

The new turbomolecular pumps, and new diffusion pump fluids, such as Convalex-10, should be of considerable interest.

References

1. R. A. Sawyer, *Experimental Spectroscopy* (Prentice Hall, New York, 1951), 2nd ed., p. 311.
2. G. L. Clark, *Applied X-rays* (McGraw-Hill, New York, 1955), p. 103.
3. R. W. Hendrick, J. Opt. Soc. Am. **47,** 165 (1957).
4. G. Sprague, D. H. Tomboulian, and D. E. Bede, J. Opt. Soc. Am. **45,** 756 (1955).
5. J. E. Holliday, "Soft X-Ray Emission Spectroscopy in the 13 Å to 44 Å Region," J. Appl. Phys. (to be published).

Table I. n, the Number of Electrons per Cubic Centimeter, Calculated For Various Materials

Material	Total no. of electrons per atom or molecule	Atomic wt. (molecular)	Density	Atoms cc (molecules)	n	$n^{1/2}$
C	6	12.0	1.9	9.5×10^{22}	57×10^{22}	7.5×10^{11}
Al	13	27.0	2.7	6.0	78	8.8
Ge	32	73.0	5.3	4.4	141	11.9
Pt	78	195	21.4	6.6	514	22.7
Au	79	197	19.3	5.9	466	21.6
U	92	238	19.0	4.8	442	21.0
Al_2O_3	50	102	3.9	2.3	115	10.7
SiO_2 (glass)	30	60	2.6	2.6	78	8.8
U_3O_8	340	842	8.3	0.59	201	14.2
Pentadecane $CH_3(CH_2)_{13}CH_3$	122	212	0.77	0.22	27	5.2

Construction and Calibration of a Bass-Kessler Grating Spectrograph

Theodore Baurer

Research Department, Grumman Aircraft Engineering Corporation, Bethpage, New York.
Received 31 December 1962.

A portable large-aperture grating spectrograph suitable for survey work in the visible range has been built from a National Bureau of Standards design[1] with some modifications, at a cost of less than $1600 for purchased components. Performance of this spectrograph has been thoroughly satisfactory. Its dispersion is approximately 210 Å/mm, but this can be improved by enlargement from the 35-mm film used. The relative aperture is $f/4.5$.

In order to accommodate anyone interested in duplicating this design and building such an instrument, a Grumman Research Department Memorandum has been written.[2] This includes a complete set of engineering drawings and an exploded-view diagram of the assembly. It contains descriptive material pertaining to particular features of the construction and calibration. A copy may be had by writing to the author.

References

1. A. M. Bass and K. G. Kessler, J. Opt. Soc. Am. **49**, 1223 (1959).
2. T. Baurer, Grumman Research Department Memorandum RM–212 (September 1962).

Optical Pumping of Lasers Using Exploding Wires

Charles H. Church, R. D. Haun, Jr., T. A. Osial, and E. V. Somers

Westinghouse Research Laboratories, Beulah Road, Churchill Borough, Pittsburgh 35, Pennsylvania.
Received 4 October 1962.

In many laser systems, it is desirable to have a high pumping rate, particularly if the laser material possesses a short metastable lifetime. Exploding wires would appear attractive as a source of this high pumping-rate excitation. A major problem in this application of exploding wires is to determine what conditions give a high radiant efficiency, particularly at very high energy levels. The exploding wires have a saturation or limiting brightness similar to that encountered in the gas-filled flashtubes.[1]

The rapidly expanding plasma from the exploding wire both increases the size of the source and tends to absorb light generated in the interior of the plasma column. The limit in brightness may be attributed in part to this absorption by the plasma.[2,3] The entire question of high-brightness discharges either from exploding wires or from gases warrants much more extensive investigation.

Marshak,[4] for energy inputs of approximately 1000 J, quotes a light yield of 14 lm-sec/J for tungsten vapor. This is a factor of two to three times lower than the 25–45 lm-sec/J that is the range usually quoted by Marshak and others for the xenon-filled tubes. Oster and Marcus[5] measured efficiencies comparable to the xenon-filled tubes for the ultraviolet wavelengths (2000–3300 Å) for nichrome wire but unfortunately gave no information on light in the visible or ruby-pumping wavelengths.

A large capacitor bank made by Westinghouse was used for the experiments. The bank consisted of fourteen 12-μF capacitors rated for 20 kV, which had a total energy storage of 33,600 J, with individually triggered spark gaps on each capacitor. The ringing frequency of the bank and spark gaps was about 140 kc/sec, but when connected with the laser–exploding-wire termination, the ringing frequency was 30 kc/sec. This meant that the current reached a maximum in about 8 μsec with a low resistance load.

An elliptic-cylinder reflector[6,7] of polished 304 stainless steel with a major axis of 8.03 cm and a minor axis of 7.62 cm with the foci 2.54 cm apart was used. The wire in its holders was along one focus, the laser rod with its protection tubes was along one focus, the laser rod with its protection tubes was along the other. The scheme adopted for protecting the laser rod consisted of a pyrex outer tube and a plexiglass inner tube surrounding the laser rod. These served to cushion the shock wave, to withstand the heat of the flash, and to filter out deleterious short-wavelength radiation. The pyrex tube was usually shattered after each shot. Further filtering of the radiation incident upon the laser rod within the protection tubes was attempted using a Wratten 2B filter cutting off below 4100 Å; it was thermally damaged by the flash even though it was within the pyrex and plexiglass tubes.

In these experiments, fluorescence and laser output were determined by means of a Polaroid film pack located about 18 cm from the end of the laser rod and shielded from the direct flash of the exploding wire. Suitable filters were used to remove undesired pump light and to attenuate the laser-output radiation. Phototubes with similar filters were used to record the time development of the pump light and laser-output pulses.

A series of fluorescence measurements were made using ruby rods. The fluorescence from the ruby was measured using aluminum, copper, nichrome, and tungsten wires varying from 0.01 cm to 0.16 cm in diameter, at voltages ranging from 6 kV to 20 kV, with energies up to 16,000 J. Saturation effects were noted for the smaller wires (i.e., increasing voltage did not significantly change the ruby fluorescence output below laser threshold). The larger wires gave more light, but the shock-wave intensity increased in proportion. The larger wires, particularly the copper ones, deposited almost opaque coatings on the protection tubes and on the walls of the reflector. The tungsten wires yielded the greatest fluorescent emission, though the arc from the tungsten wires pitted the walls of the reflector quite badly. The deposition and pitting effects tended to inhibit laser action for subsequent shots.

Using a 7.6-cm long, 0.64-cm diam Linde 0.05% ruby with silvered ends, operated at room temperature, and a 0.038-cm tungsten wire, 5.0-cm long, exploded at 14 kV and 168 μF, 16,500 J excitation, the output of the ruby was measured to be

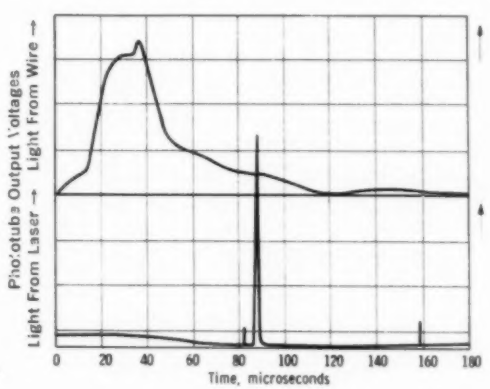

Fig. 1. Time development of the light output from the exploding wire and from the laser. The wire, which was tungsten, 0.02-cm diameter and 5-cm long, was exploded at 13 kV, 168 μF.

0.4 J. A copper-wire calorimeter provided by R. M. Baker* was used to measure the energy.

For 13,000-J excitation, the laser output was about 0.2 J. Figure 1 shows the time development of the light from the exploding wire and from the laser. The duration of the main laser pulse was on the order of 4 μsec. The time resolution of the laser-output measuring circuit was not high enough to resolve any individual spikes. The small burst just prior to the main burst indicates when inversion was achieved; the small burst occurring much later probably resulted from further low-level pumping by the plasma. The relatively short time delay between the light emission by the exploding wire and the laser outputs is due to the high pumping rate.

In order to determine the size of the light-emitting portion of the wire plasma, the integrated light emission from this core for the wire, fired under about the same conditions (12 kV, 168 μF), was measured using a camera focused upon the wire, with filters to select the range 4000–6000 Å. The core proved to be uniformly luminous and was about 2 cm in radius. The large size of this core reduced considerably the efficiency of the elliptical reflector.[6] The total light emitted by the plasma in the range 4000–6000 Å was determined using a film pack to be approximately equal to that of the FT-524** flash lamp at 4 kV and 400 μF (3200 J), though the spectra may be considerably different.

The exploding wire does allow much higher pumping rates than flash lamps. As a source of light, in the visible it appears to be less efficient. Its efficiency for pumping lasers could be enhanced appreciably by a better choice of laser conditions together with improved coupling to the laser rod of the light emitted by the plasma.

References

1. M. P. Vanyukov and A. A. Mak, Soviet Phys.-Uspekhi **66,** 137 (1958).
2. F. H. Webb, N. Chase, M. Ernstene, and A. Tollestrup, *Exploding Wires*, W. G. Chase and H. K. Moore, eds. (Plenum Press, New York, 1959).
3. W. Lochte-Holtgreven, Rept. Progr. Phys. **21,** 312 (1958).
4. I. S. Marshak, Opt. i Spektroskopiya **10,** 801 (1961), Opt. Spectr. **10,** 424 (1961).
5. G. K. Oster and R. A. Marcus, J. Chem. Phys. **27,** 189 (1957).
6. W. R. Busing, J. Opt. Soc. Am. **42,** 774 (1952).
7. M. Cliftan, C. F. Luck, G. G. Shafer, and H. Statz, Proc. Inst. Radio Engrs. **49,** 960 (1961).

* Electronics Division, Westinghouse Electric Corporation, Baltimore, Maryland.

** Made by Photo Lamp Department, General Electric Company, Cleveland 12, Ohio.

photo D. L. MacAdam

Norma Miller *Ohio State Vision Lab*, Louise Sloan *Johns Hopkins*, and R. C. Jones *Polaroid* during the OSA 1962 Rochester Meeting.

Information for Contributors

Scope: Papers are welcomed in the broad areas of applied optics, in disciplines related to optics and employing optical techniques. Papers should be sent to *The Editor, APPLIED OPTICS, 1155 Sixteenth St., N.W., Washington 6, D.C.* Manuscripts may be submitted in English, French, German, or Russian, and the presentation should be as succinct as comprehension will permit. In general, the metric system of units is preferred. One original and one carbon copy of the manuscript, with two sets of all illustrations, must be sent in. Manuscripts should be typed double or triple spaced on one side of 22 × 28 cm (8½ × 11 in.) paper, leaving a 3.8 cm (1½ in.) margin all around. Equations must be typed not hand written wherever possible. Papers on the more fundamental aspects of experimental and theoretical optics should be sent to *The Editor, JOURNAL OF THE OPTICAL SOCIETY OF AMERICA, National Bureau of Standards, Washington 25, D.C.*

An **abstract,** adequate as an index and a summary, of not more than 100 words should appear at the beginning of the paper after the *title, author's name, affiliation, and address.* In the case of papers in a non-English language, they must be accompanied by an abstract in English as well as an abstract in the language of the paper. It should be borne in mind that this abstract may be used in toto by the abstracting journals, therefore it should be self-contained.

Figures suitable for printer's use should be sent. Bear in mind that illustrations will normally be reduced to column width (8.4 cm—3⅜ in.—20 picas). *Halftones:* two sets of glossy prints are needed, which should be mailed flat, with any proportion or framing indicated on a working copy. *Line drawings* should be suitable for reproduction and be not larger than 22 × 28 cm (8½ × 11 in.). *Captions* should be listed on a separate sheet in addition to each caption appearing on each illustration.

Tables should be typed on separate sheets and the data therein be intelligible, by title, without reference to the text. Tables should include a minimum of vertical ruling.

References must be typed on a separate sheet, be numbered consecutively in the order of their appearance in the text, and follow this form:

1. F. C. Brown, Phys. Rev. **12,** 345 (1821).
2. J. Culpeper, *Space Optics* (Georgetown Institute of Technology Press, Washington, D.C., 1861), pp. 12, 345.

A list of abbreviations for the names of journals is published in *Chem. Abstr. List of Periodicals 1961.* To make for uniformity of presentation generally, the American Institute of Physics *Style Manual,* second edition, should be used. In general, *APPLIED OPTICS* differs from the *Style Manual* only inasmuch as footnotes appear at the bottom of the page of text, while references are listed numerically at the end of the paper.

There will be no **page charge** for publishing in *APPLIED OPTICS* for the time being.

Letters to the Editor should follow the above suggestions, but no abstract is required.

Applied Optics

Of Optics and Opticists

This column is compiled partly from information sent by our Reporters in various centers of optics across the continent, but the Managing Editor welcomes news from any source

Sir Humphry Davy
Abominated gravy.
He lived in the odium
Of having discovered sodium. *E. C. Bentley*

Opticists in the news this month include: **Gilbert W. King,** former research director of IBM, has become vice-president and director of research of Itek. . . . **Dwain B. Bowen** has moved from Autonetics to Electro-Optical Systems where he will be Manager, Laser Applications. . . . **Robert P. Mason** and **Paul T. Kaestner,** who are two of the three newly appointed vice-presidents of Photomechanisms. . . . **Robert M. Hexter** has returned from Israel to the Mellon Institute. . . . **Howard Coleman,** former vice-president in charge of research and engineering at Bausch & Lomb, has accepted appointment as head of physics research at Melpar. . . . and **Robert Laughlin** will head the newly established electro-optical laboratory at HRB-Singer.

The 1962 Los Angeles November Junior Science Symposium, part of the **Army's** established Junior Science and Humanities Symposia Program, had a new feature. Seven young California students, five of whom read papers at the symposium, were given $200 summer research grants plus the opportunity of working on their projects under the supervision of professional scientists drawn from universities and industry in the Los Angeles area. This symposium was held at the California Museum of Science and Industry and cosponsored by International Business Machines Corporation. IBM as part of its support is providing the grants for the young researchers. A key aspect of the JSS conferences held under the Army's program is the presentation of scientific papers by leading high school science students. 1962, however, was the first time that the program had reached out to aid and stimulate the young research workers in advance of the symposia they will address. Administrative people as well as educators and scientists involved in planning these symposia and in following the over-all progress of the program, are keenly interested in the results of last summer's experiment. It was approved primarily as a means of providing the individuals selected with the opportunity of working with adult scientists under excellent laboratory conditions. It seemed clear also that the summer grants would do a great deal to intensify the prestige that the Army's JSS meetings have generated across the country since their inception in North Carolina in 1958. Among students given grants, and their research projects, are Paul B. Ohannesian (Los Angeles), research on division of bacteria using microphotography, supervisor: James Bartholemew, USC; Stanley Furmanski (Los Angeles), analytical research using the spectroscope, supervisor: Gerhard E. Weissler, USC; Mark Evan Albert (Covina), photography of the moons of Jupiter: a new way of calculating the speed of light.

Masers. . . .TRG, Inc., has recently completed an interim report on its optical heterodyne development program. One important result is the experimental demonstration that heterodyne amplification preserves signal-to-noise ratio in the presence of incoherent noise. The report discusses the uses of heterodyne detection in broad-band optical communication, demodulation of FM and AM, demultiplexing of channels, Doppler and displacement measurements, and the stabilization of lasers. The elements of an optical communications link are discussed: lasers, modulators, transmission path, and detectors. Recommendations are made for future work. This work has been partially supported by Rome Air Development Command, and RADC Technical Documentary Report TDR-62-491 is available through ASTIA. . . . **Maser Optics, Inc.,** announces that ruby crystals with their premeasured outputs and thresholds will be available. This company has designed special equipment that defines these specific characteristics. Until now, the variances caused at ambient temperatures by optical quality, strains, polishing, coatings, and so on, left the crystals without their specific identifying measurements.

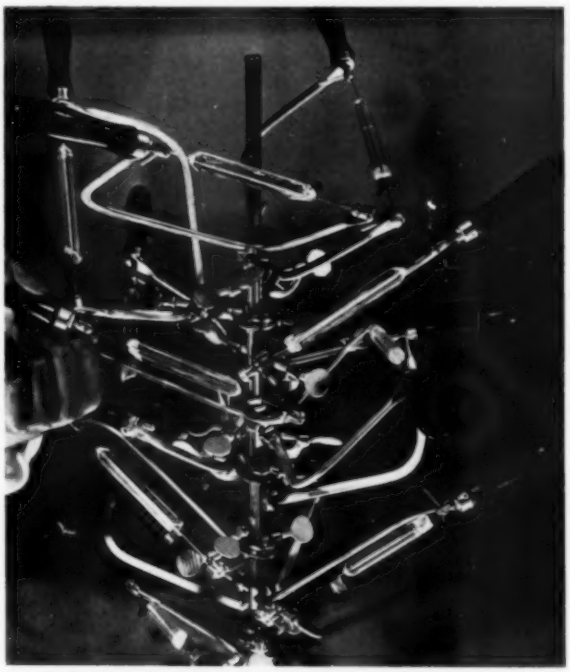

Laser rods grow on man-made tree at Electro-Optical Systems, Inc. . . . Taut wires through hardening plastic cylinders form straight holes that are later filled with experimental laser material. The result is a thin laser rod with a thick plastic cladding that gives it proper dimensions for end polishing, pumping, and flashing in standard test equipment, and reduces the amount of expensive compounds and doping materials needed for experiments.

Readers' attention is drawn to three reports available from the Office of Technical Services, Washington 25, D.C. Conversion of sunlight into energy is practical, and "the time when mankind will turn to the primary source of energy on the earth—the sun—is not far off," Russian scientist V. B. Veinberg predicts in **Optics in Equipment for the Utilization of Solar Energy,** translated for the U.S. Atomic Energy Commission (published by State Publishing House of Defense Industry, Moscow, 1959) AEC-tr-4471, 257 pp., $3.50. . . . Inorganic materials that change color when exposed to light and return to a colorless state when the light is removed may someday be the means of providing giant computers with better brains. Because this reaction takes place at microsecond speed, U.S. Air Force researchers believe that they may eventually be able to use some of these so-called phototropic materials as memory devices for the high-density storage of computer data. A report of their work thus far has been released in **Investigations of Inorganic Phototropic Materials as a Bi-Optic Element Applicable in High Density Storage Computer Memories,** Polacoat, Inc., for the U.S. Air Force, April 1962, AD 277 793, 59 pp., $1.50. . . . A literature review of near-infrared attenuating media is the subject of another report now available from the Office of Technical Services: **Literature Review of Near Infrared Attenuating Media,** R. A. Coleman and H. C. Donoian, American Cyanamid Company, for the U.S. Air Force, May 1962, AD 283 443, 30 pp., 75¢. This literature review emphasizes those symptoms that allow transmission of visible wavelengths. The spectral range of interest, according to the report, is between 0.4 and 0.5 μ. Types of infrared attenuating systems investigated in this research include organic and inorganic compounds and such other optical methods as interference and Christiansen filters.

More infrared news. . . . A line of off-the-shelf **infrared refractive optical systems,** made commercially available by the Servo Corporation of America. The optical systems cover the broad spectrum of frequently used infrared wavelengths through 15 μ and also include the ultraviolet. . . . A memo is available from Infrared Industries, Inc., on **lead sulfide detector recovery from intense radiation,** which concludes that results indicate that the recovery of the ac signal is rapid after exposure to the sun and that accidental prolonged exposure to equivalent radiant power in an uncooled condition will not harm the detector. Inquiries should be addressed to J. Bisbee.

Glass. . . . Bausch & Lomb now offers on a custom basis its precisely controlled glass-melting facilities, developed under Norbert J. Kreidl for the demanding needs of sophisticated instrumentation. . . . A new development in the preparation of optical elements is a method of slicing quartz, glass, silicon, germanium, sapphire and similar glass-like materials recently announced by **Precision Lapping Company.** This company can now furnish spherical (concave) sections in large production runs at much lower cost than was previously possible. . . . **Schott** has made some changes in the chemical stability of some of its optical glasses to give better resistance to acid and weather. The change does not appear to have appreciably altered the optical properties but has made small differences in some other properties, including thermal expansion and density. Inquiries should be addressed to the Fish-Schurman Corporation, Schott's representative in this country. . . . A catalog entitled *Coloured Optical Glass* recently came to us via the **Soviet Embassy** listing over 100 colored glasses. The properties described include spectral transmittances on different thicknesses, absorption coefficients, and optical densities, all given for the wavelength range from 240 to 3000 mμ; the color coordinates for two sources, having color temperatures of 2848° and 4800°K, respectively: specific gravity; refractive index for the sodium D line; and chemical resistance. It would appear from this catalog that a wide variety of colored glasses are available for many technical purposes. Many more glasses are listed than in either the Schott catalog or the Corning catalog.

R. E. Hopkins *Rochester* in the Herrenchiemsee during the ICO Munich Meeting last year.

ANNUAL SUBSCRIPTIONS

OSA members	$ 6.00
Other AIP societies' members	$ 8.00
Non-members and libraries	$10.00
Single copies	$ 2.00

Subscriptions should be addressed to APPLIED OPTICS **Subscription Handling, American Institute of Physics, 335 East Forty-Fifth Street, New York 17, New York. Eight weeks should be allowed for order processing.**

ADVERTISING

Advertising inquiries, orders, plates, and correspondence should be addressed to the APPLIED OPTICS Advertising Office, 1155 Sixteenth Street, N.W., Washington 6, D.C. 202-DI 7-4131. Mrs. Boraks.

Diffraction Limited

...MEANS

Fine Custom Optics

FOR

☐ INDUSTRY
☐ EDUCATION
☐ DEFENSE

DL has the senior scientists and craftsmen to follow through from—— planning . . . design fabrication . . . and testing.

REMEMBER THE NAME . . .

Tel: 275-8212
Area Code: 617

Diffraction Limited INC.
OPTICS

MIDDLESEX TURNPIKE • BEDFORD, MASS.

FS TM. REG.

"ZIRCONARC"

PHOTOMICROGRAPHIC LAMP

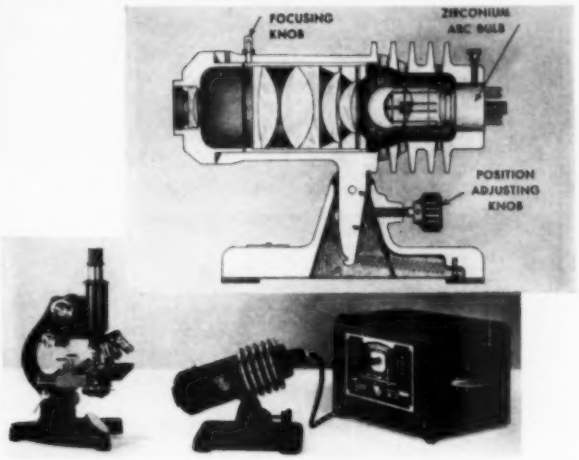

For better results in microscopy, macrophotography, photomicrography and microprojection

The "Zirconarc" not only saves time and effort in microscopy, but also contributes importantly to the quality of photomicrographs—whether in color or black-and-white.

It is basically an arc lamp, but its electrodes are fixed and sealed within a glass bulb containing an inert atmosphere. Activity is concentrated upon a very small portion of the electrode, producing a circular spot of light of high intensity and only 0.037″ (less than 1 mm) in diameter—closest approach to a point source of light. Center of illumination is fixed in position, sharply defined and uniformly brilliant. The color temperature of its 40-watt bulb (3200° Kelvin) is ideal for color photography; the character of the light is such that no color correction filters are required. Lamp spectrum extends into both the ultraviolet and infrared wavelengths. Laboratory tests show that the "Zirconarc" is less harmful to living cultures than carbon or tungsten arcs.

The condenser system of 7 optical elements is of extremely short focal length—only 16.5 mm—essential to use the point source of light to fullest advantage. Lenses are coated to minimize loss of light by stray reflection.

The optical system is mounted in a barrel which slides back and forth for focusing within the external housing—ventilated for heat dissipation. A detachable lens for high-power microscopy increases focal length, concentrating the light into a long, narrow beam. Light beam is aimed upon the microscope mirror by means of a non-slip adjusting screw, which controls angle of beam with the horizontal.

Uses regular 110 V alternating current through its power supply unit. "Amperite" regulator minimizes current fluctuation. Entire apparatus meets rigid safety specifications. Over-all length of lamp 10″, height $6\frac{1}{2}$″. Base 5 × 7″.

Price, including power supply unit for 110–120 V, 50–60 cycles ac, $325. Extra bulb, type 321-7 (40 watt) $44 plus $2.64 Federal Excise Tax. Prices f.o.b. New Rochelle.

FISH-SCHURMAN CORPORATION
90 Portman Road, New Rochelle, N. Y.

Supervisor Experimental Optical Group

You will be expected to develop an experimental support activity of exceptional superiority to support the work of our numerous research teams, as well as carry on optical engineering on R & D-supported contracts. Ideally, you will cultivate the potential of our less experienced optical engineers, so that they will gain the necessary experience to work within Itek's systems groups.

Senior Reconnaissance Engineers

Responsible for the design and development of aerial photographic reconnaissance system technical leadership from proposal and conceptual phase through customer acceptance. Work requires: good knowledge of military and intelligence requirements—through experience with system hardware—original thinking in seeing both the problems involved and the ingenious solutions. Background should include a degree in physics, engineering or mathematics and 10 years' experience.

Optical Engineers

B.S. required, M.S. desired in Physics or Optics. Must be experienced in precision optical procedures for assembly, testing and evaluation of high acuity systems. To work in conjunction with project teams in the development of precision automated optical-mechanical equipment.

Interested candidates may arrange for an interview by sending their resume to:

Mr. Louis D. Rudzinsky
Personnel Manager

Itek Corporation
10 MAGUIRE ROAD, LEXINGTON 73, MASSACHUSETTS

An equal opportunity employer

Future Issues

Each issue will specially feature one area of applied optics in addition to the usual contributed papers, shop and technical notes, reports of meetings, Letters to the Editor, book reviews, Meetings Calendar, and special columns. The feature subject of each issue is the responsibility of the named editor.

1963		
May	**Interferometry**	R. A. Woodson
June	**Super Achromats**	—
July	**Spectroscopy**	Mary E. Warga
August	**Masers**	—
September	**Lens Design and Computers**	D. P. Feder
October	**Bubble Chamber Optics**	S. Rosin
November	**Coblentz Commemoration**	E. K. Plyler
December	**Chemical Optics**	M. Kent Wilson
1964		
January	**Photographic Optics**	George C. Higgins
February	**Atmospheric Optics**	D. Q. Wark
March	**Spectroscopic Instrumentation**	—
April	**Visibility**	S. Q. Duntley
May	**Microscopy**	J. R. Benford
June	**Fiber Optics**	C. W. Peters
July	**Optics in Japan**	R. A. Oetjen
November	**High Speed Photography**	—
December	**Solar Optics**	G. Newkirk Jr.
1965		
February	**Plasma Radiation**	L. M. Branscomb

D. Nickerson *Dept. of Agriculture*, H. R. Condit *Eastman Kodak*, I. Balinkin *Cincinnati*, G. Wyszecki *National Research Council—Ottawa*, D. B. Judd *NBS*, members of the CIE Technical Committee on Colorimetry and Daylight.

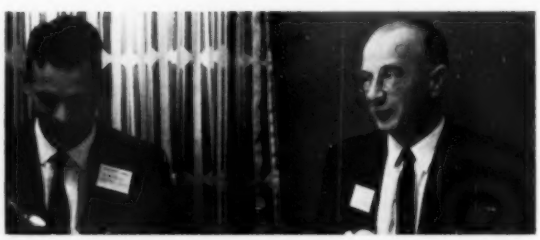

Sumner Davis *Berkeley* and F. W. Lucy *G. E. Valley Forge*, during OSA Rochester Meeting last October.

A NEW Catalog

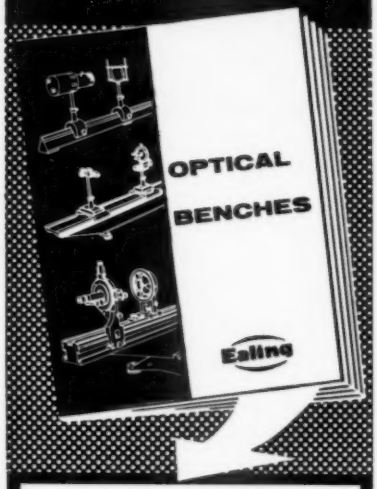

Introduction page

" This, we believe, is the most comprehensive range of Optical Benches and Accessories offered.

There are five basic benches for different applications with varying accuracies, each with its appropriate carriers. There are sixty different accessories.

This range meets every requirement from simple alignment to the precise investigation of any optical system.

A unique feature of this range of Optical Benches is its flexibility.

The first three benches all take accessories mounted on 13·5 mm. stems and therefore all 40 accessories listed — can be used interchangeably on these three benches.

The last three benches take the research accessories listed.

The middle bench, that is the Precision Lathe Bed Optical Bench — has the special advantage of taking both the standard accessories — and the research accessories listed."

WANT TO READ FURTHER?
This Catalog is FREE on request from

THE **Ealing** CORPORATION

2225 Massachusetts Ave.
Cambridge 40, Massachusetts
Telephone: (617) 547-5760

EC|44

WAVE LENGTHS, TO ORDER

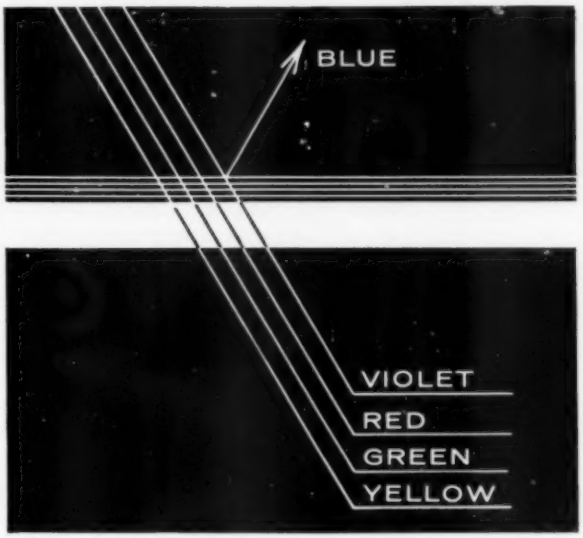

Multilayer vacuum-deposited coatings can put light to work in several ways

These coatings, applied in separate layers to glass or plastic, allow you to split light beams in many ways on a single application. Multilayer coatings can be applied to produce a specific beam-splitting result.

Liberty Mirror engineers can do all the design and development work on any potential use for this technique, or help solve application problems.

Vacuum-deposited coatings of various metals are used to make front-surface mirrors, neutral filters, transparent mirrors, high-efficiency beam splitters, beam-splitting dichroic mirrors and filters. Metallic and transparent electrically conducting coatings are available for resistance heating. Static-dissipating and high-frequency shielding coatings are also available.

Applied to all types of glass, metal or plastic, the coatings are used in such varied products as scientific and optical instruments, cameras, toys, pin setters, wheel-aligning equipment, aircraft and missiles. Free data sheets are available on all coatings.

Write L·O·F, Liberty Mirror Division, 5543 Libbey·Owens·Ford Building, Toledo 2, Ohio.

LIBERTY
MIRROR DIVISION
LIBBEY·OWENS·FORD

MADE IN U.S.A.
LOF GLASS

OSA Group Flight to Europe

JULY 1963

The revised schedule for the OSA 1963 Group Flight will enable members to attend some of the following July meetings in Europe. (This schedule has had to be revised because, under the new charter agreements, no group flights may take place during the period 24th June/7th July.)

July 1–Aug 23	Summer School of Theoretical Physics, Grenoble, France
1–14	Application of quantum mechanical methods to the study of molecular properties Symposium, Paris, France
8–13	Ionization Phenomena in Gases Symposium, Orsay, France
10–17	IUPAC Congress, London, England
15–19	IUPAP Second International Conference on Nuclidic Masses, Vienna, Austria
17–19	SAC Microchemical meeting, London, England
22–26	Physics of Electronic and Atomic Collisions, London, England
22–26	Symposium on Microscopy, Brighton, England
22–27	7th European Congress on Molecular Spectroscopy, Budapest, Hungary

The probable flight schedule is as follows:

7.9.63	Lv New York	SWISSAIR	20:30	7.20.63	Lv Amsterdam*	
7.10.63	Arr Geneva, Switzerland		10:45	7.20.63	Arr Budapest, Hungary*	
7.10.63	Lv Geneva	BEA	12:45	7.28.63	Lv Budapest	MALEV*
7.10.63	Arr London, England		14:10	7.28.63	Arr Zurich, Switzerland*	
7.20.63	Lv London Airport*			7.29.63	Lv Zurich (Ft #800)	SWISSAIR*
7.20.63	Arr Amsterdam, Holland*			7.29.63	Arr New York.	

* Details to be announced

Because there is no same day connection Budapest—Zurich—New York, SWISSAIR will absorb hotel and meal expenses for one day.

Such a round-trip group fare would cost $416 + $4 handling charge, **i.e., $420,** assuming a minimum of 25 participants. This fare includes internal European travel only if the members travel as a group, i.e., the ticket cannot be used for other planes. Forty seats have been tentatively reserved, and we need your deposit ($50 per seat) as soon as possible; the balance of the fare ($370) must be paid by **30th April.**

THIS GROUP FLIGHT WILL BE ON A SWISSAIR REGULARLY SCHEDULED JET AIRCRAFT.

There are three other meetings in Europe in 1963 of particular interest to opticists:

6–10 May	2nd Hungarian Optical Conference, Budapest, Hungary
24–26 June	12th Liège Astrophysical Symposium, Cointe-Sclessin, Belgium
8–15 September	ICO Symposium on Thin Films, Marseille, France

If sufficient members (minimum of 25 per meeting) are interested, the Assistant Secretary will endeavor to arrange group transportation for these too.

Assistant Secretary, OSA, Room 101,
1155 Sixteenth Street, N.W.
Washington 6, D.C.

REPLY

( ) I wish to reserve .... seats on the OSA GROUP FLIGHT N.Y.-Geneva-London-Amsterdam-Budapest-Zurich-N.Y. 9 July through 29 July.

( ) I enclose my check for a deposit of $... (.... seats)

( ) I am an OSA Member and will be accompanied by .... my wife
.... children (how many?)

( ) I am interested in principle in attending the May ☐ June ☐ September ☐ meeting and wish to hear whether group transportation can be arranged.

ONLY OSA MEMBERS THEIR WIVES AND THEIR CHILDREN MAY PARTICIPATE IN THE GROUP FLIGHT

Name.....OSA Membership No.....

Address.....

.....

HIGH QUALITY STANDARDS

. . . in Optical Crystal Blanks

Calcium Fluoride	Sodium Chloride
Barium Fluoride	Potassium Chloride
Lithium Fluoride	Potassium Bromide

• *Prompt Delivery* • *Large Size Availability*
• *Precision Cutting* • *Scattering Free*
• *Impurity Absorption Free* • *Strain Free*

. . . in Optical Maser Crystals

$U^{+3} \cdot CaF_2$	$Dy^{+2} \cdot CaF_2$	$Nd^{+3} \cdot CaF_2$
$U^{+3} \cdot BaF_2$	$Sm^{+2} \cdot CaF_2$	$Nd^{+3} \cdot BaF_2$
$U^{+3} \cdot SrF_2$	$Sm^{+2} \cdot SrF_2$	$Nd^{+3} \cdot SrF_2$
$Tm^{+3} \cdot SrF_2$	$Tm^{+2} \cdot CaF_2$	$Ho^{+3} \cdot CaF_2$

Also, all other trivalent rare earths in CaF_2, BaF_2 and SrF_2.
Indicative of our quality, most of the above were first mased in Optovac grown crystals.

OPTOVAC

OPTOVAC, INC.
NORTH BROOKFIELD, MASSACHUSETTS

Mr. and Mrs. D. J. Lovell *Mich.* and Dr. L. G. Mundie *Lockheed*, on a Bavarian island. Mr. Lovell was recently appointed chairman of a DOD committee to study re-entry problems jointly between U.S., Canada, & U.K.

David Wright *Imperial College* and P. Mollet *Belgium*, respectively Secretary and one of the Vice Presidents of the International Commission for Optics.

IF YOU USE GLASS BEAM SPLITTERS

MIRRORS • FILTERS • PRISMS

in apparatus you are designing, manufacturing or using

THIS FREE BOOKLET IS FOR YOU.

Thin film pellicles introduce neither refractive error nor ghost images, can be had flat to $1/20$ wave, and offer full coating selection including dichroics. This booklet tells you how and when to specify thin film pellicles.

NATIONAL PHOTOCOLOR CORP.
225 EAST 44TH STREET NEW YORK 17, NEW YORK

Ask for "*Application and Specification of Pellicles*"

ENVIRONMENTAL MEASURING

Optical instrumentation with unlimited potential signify the obtainable abilities of Gaertner Scientific. Shown are examples of environmental test measuring instruments that can be applied or tailored to your requirements.

EXTENSOMETERS – For measuring dimensional changes of specimens due to creep, thermal expansion, strain and other environmental conditions. Filar micrometer readings on some instruments can be made to 0.000010″ over a range of 0.040″ **Send for Bulletin 162-62.**

DILATOMETERS AND INTERFEROMETERS—For determining with high precision the coefficient of thermal expansion of small metallic, ceramic or plastic samples at temperatures up to 1000°C. **Send for Bulletin 140-62.** GSC-3-213

Gaertner
SCIENTIFIC CORPORATION
1294 Wrightwood Ave., Chicago 14, Ill.
Area Code 312, BUckingham 1-5335

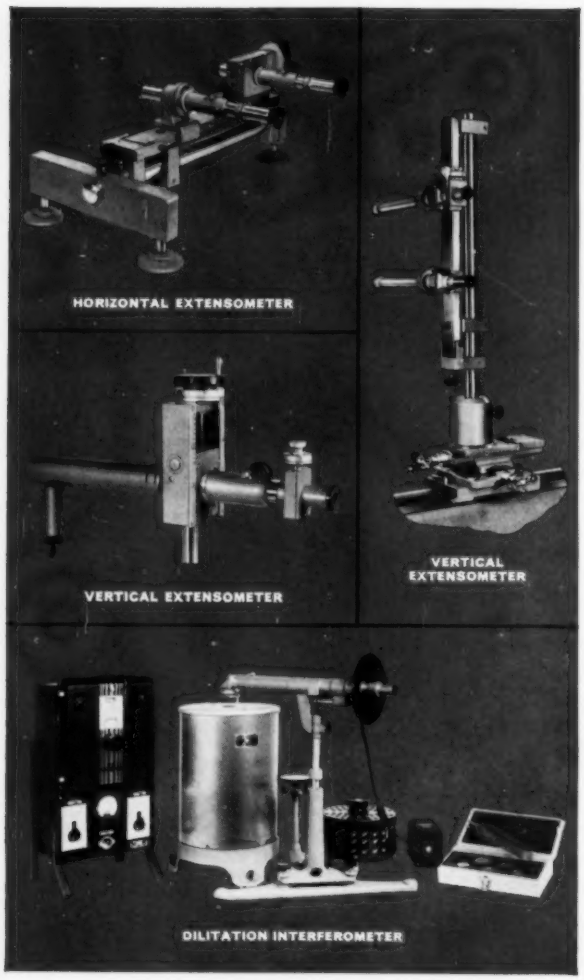

"OFF THE SHELF" LENSES

MAMMOTH ON-HAND SELECTION

Whatever your lens need ... B & J can provide you instant action! Large "Room Size" Vaults that hold thousands of Photo Optics and include famous brands of the world's finest domestic and foreign manufacturers are *at your immediate disposal!!!* ... Here are lenses of every conceivable speed and size, from ¼″ to 80″ big Berthas. An inventory second to none! All Lenses sold on *15-Day Free Trial* and **UNCONDITIONALLY GUARANTEED!**

RESEARCH OPTICAL ASSEMBLY LAB—for your special custom lens problem! In our modern fully equipped lab; precision grinding, rigid testing, custom mounting, and lens coating are speedily done by *expert craftsmen* to meet the specific requirements of such companies as Ford, R.C.A., G.E., Atomic Energy Comm., etc. ***You benefit from the priceless ingredient of 66 years experience.***

Precision PROTOTYPE OPTICS From Stock . . .

Whatever your LENS requirements ... be it new optical systems or replacements for the most simple or most complex precision work ... *B & J can SAVE YOU TIME AND MONEY,* and still offer you a choice from stock of over 2,000 of the finest LENS Prototype optical systems from world markets.

BURKE & JAMES has the most complete LENS service. Quality-control Instrument Shop, LENSKOTING dept., and your choice of Special Mountings.

REMEMBER—when planning a project where LENS elements are specified ... or for any photographic purpose let Burke & James advise and supply you.

HIGH SPEED OPTICS

For Image Amplifiers—
Speeds Equal to F/0.5

- Designed for use with RCA—Phillips—Bendix—Friez—Westinghouse and cascading image amplifiers. One-to-one systems of extreme speed—short focal lengths.
- ***New Optical Systems available for prompt delivery from stock.*** State full data for quotation. Ideal for X-Ray—Radiation research and astronomic telescopes.
- Other optics, photo and recording equipment available from world's largest "LENS BANK"

FREE 66th Anniversary CATALOG

148 Pages Of Photo Equipment— • Greatest Lens Offerings! • Cameras—Regular, Industrial & Scientific! • Enlargers—Solar, Etc.! • Lighting—Professional—Strobe, Etc.! • Accessories! Write Dept. A.O. 363

1892 **Burke & James, Inc.**
321 S. WABASH, CHICAGO 4, ILL.

The Optical Society of America

Officers of the Society

President STANLEY S. BALLARD, Department of Physics, University of Florida, Gainesville, Fla.
President-Elect RICHARD C. LORD, Spectroscopy Laboratory, MIT, Cambridge 39, Mass.
Past President DAVID L. MACADAM, Research Laboratories, Eastman Kodak Company, Rochester 4, N.Y.
Executive Secretary MARY E. WARGA, OSA, 1155 16th Street N.W., Washington 6, D.C.
Treasurer ARCHIE I. MAHAN, Applied Physics Laboratory, 8621 Georgia Avenue, Silver Spring, Md.
Editor of the Journal of the Optical Society of America DEANE B. JUDD, National Bureau of Standards, Washington 25, D.C.
Editor of Applied Optics JOHN N. HOWARD, AFCRL, Bedford, Mass.

Directors-at-Large

** Term expires December 31 of the indicated year.*

RUDOLF KINGSLAKE (63)* Eastman Kodak Company, Rochester 4, N.Y.
EARLE K. PLYLER (63)* Department of Chemistry, Florida State University, Tallahassee, Fla.
DAVID RICHARDSON (63)* Bausch & Lomb, Inc., Rochester 2, N.Y.
GEORG H. HASS (64)* ERDL, Fort Belvoir, Va.
R. CLARK JONES (64)* Polaroid Corp., Cambridge, Mass.
E. D. MCALISTER (64)* Scripps Institution of Oceanography, La Jolla, Calif.
W. LEWIS HYDE (65)* J. W. Fecker, Inc., 4709 Baum Boulevard, Pittsburgh, Pa.
JOHN A. SANDERSON (65)* Naval Research Laboratory, Washington 25, D.C.
GEORGE WALD (65)* Biological Laboratories, Harvard University, Cambridge 38, Mass.

Local Sections

Rochester
JOHN L. TUPPER *President*
JOSEPH L. ROOD *President-Elect*
SHELDON PHILLIPS *Secretary*
Eastman Kodak Co.
Rochester 4, N.Y.
MANUEL KINER *Treasurer*

Detroit
RICHARD MAJKOWSKI *President*
CARL LEISTNER *President-Elect*
DANIEL L. HARMON *Secretary*
16152 Parkside, Detroit 21, Mich.
SAMUEL COHEN *Treasurer*

Niagara Frontier
E. SCHUSTIK *President*
THOMAS FROST *President-Elect*
CALVIN W. YOUNG *Secretary*
Carborundum Metals Co.
Box 32, Akron, N.Y.
RAY ANNINO *Treasurer*

New England
DAVID S. GRAY *President*
CHARLES KOESTER *Vice-President*
GEOFFREY HARVEY *Secretary*
Itek Corporation
10 Maguire Rd.
Lexington, Mass.
WILLIAM J. DAVIS *Treasurer*

Texas
CHARLES S. WILLIAMS *President*
P. O'B. MONTGOMERY *Vice-President*
HARRY J. AUVERMANN *Secretary-Treasurer*
LTV Research Center
P.O. Box 5003
Dallas 22, Tex.

Delaware Valley
F. J. WARZAK *President*
J. E. TUDOR *Secretary*
General Electric Company MSVD
3316 Spring Garden Street
Philadelphia, Pa.
M. CONSHERRY *Treasurer*

Chicago
FRED CLARKE *President*
DONALD PONTARELLI *Vice-President*
RICHARD STECK *Secretary*
4556 North Oakview
Chicago 31, Ill.
HOWARD PADGITT *Treasurer*

Southwestern Connecticut
LEONARD EISNER *President*
ROBERT C. GORE *Vice-President*
MARTIN ROME *Secretary*
Machlett Laboratories, Inc.
1063 Hope Street
Springdale, Connecticut
EDWARD SPEYER *Treasurer*

Southern California
R. HENRY FRELS *President*
ERNEST DAVIDSON *Vice-President*
CLIFFORD O. THOMAS *Secretary*
10 Miramonte Drive
Fullerton, Calif.
W. S. GALLAWAY *Treasurer*

Northern California
ANDREW L. JORGENSEN *President*
CLYDE C. SHAW *Vice-President*
HARVEY MORTON *Secretary-Treasurer*
Tinsley Laboratories
2448 Sixth Street
Berkeley, Calif.

National Capital
RICHARD TOUSEY *President*
FREDERICK W. PAUL *First Vice-President*
HARRY K. HAMMOND, III *Secretary*
National Bureau of Standards
Washington 25, D.C.
RICHARD S. HUNTER *Treasurer*

San Diego
JOHN E. TYLER *President*
JOHN H. TAYLOR *Vice-President*
JOHN M. HOOD *Secretary-Treasurer*
Bldg. 4, U.S. Navy Electronics Laboratory
San Diego 52, Calif.

The Optical Society of America was organized in 1916 **"to increase and diffuse the knowledge of optics in all its branches, pure and applied, to promote the mutual interests of investigators of optical problems, of designers, manufacturers and users of optical instruments and apparatus of all kinds and to encourage cooperation among them."** The Society invites to membership all who are interested in any branch of optics, either in research, in instruction, in optical or illuminating engineering, in the manufacture and distribution of optical goods of all kinds, or in physiological and medical optics. Further information may be obtained from the Executive Secretary of the Society. **Annual Dues:** Regular members and Fellows, $17.00; Associate members, $13.00; Corporate members, $125.00. These dues include subscription to the Society's official journal, the **Journal of the Optical Society of America,** but not to its other publications.

Significant new titles from Spartan . . .

PROCEEDINGS OF THE Xth COLLOQUIUM SPECTROSCOPICUM INTERNATIONALE

Edited by
ELLIS R. LIPPINCOTT,
University of Maryland
and
MARVIN MARGOSHES,
National Bureau of Standards

816 pages Illustrated $20.00

Contents include: The role of spectroscopy in astrophysics. Present status of our knowledge of atomic transition probabilities; Recent developments in infrared atomic emission spectroscopy in the 1- to 4-micron region; Isotopic shifts in the spectra of dysprosium and samarium; Absorption spectra of gaseous atoms forced at flash-heated tungsten surfaces; Critical review of the methods and results of time-resolved spectroscopy; Atomic absorption spectroscopy; Excitation and related phenomena in flames; New sources for flame spectrophotometry; Extreme ultraviolet spectra; A pulsed light source for the extreme ultraviolet; Sur quelques methodes de spectrometrie X; X-ray emission spectra and the chemical bond; Spectroscopie X d'elements radioactifs; X-ray emission spectrography at long wavelengths; Scanning techniques in electron probe microanalysis, with some applications in mineralogy and biology; Quantitative electron microprobe analysis of radioactive and irradiated materials; High precision microprobe analysis by thin metallic film calibration; On the application of optical masers to spectroscopic studies; The optical emission mode patterns of ruby lasers; Recent developments in infrared reflection spectroscopy; attenuated total reflection; Comparative studies of infrared and Raman group frequencies and their applications; The origins of group frequency shifts. Part II: The influence of inductive effects and of non-bonded interactions on infrared group frequencies; Substituent effects on the infrared and electronic absorption spectra of organic molecules; The donor characteristics of the carbonyl group. III. BF_3 complexes; High resolution studies in the near infrared; Infrared dispersion studies; Infrared studies in liquid bromine; Recording the infrared spectra of gas chromatography fractions; Optical spectra of gaseous free radicals; Features and regularities in research of diatomic molecular spectra; The methodology of the measurement and representation of fluorescence spectra; Total luminescence of organic molecules of petrochemical interest. I. Naphthalene, and 1, 2, 4, 5-tetramethylbenzene; Chemical applications of nuclear magnetic resonance; Recent applications of high resolution nuclear magnetic resonance to chemical problems; Spin density distributions in conjugated molecules by NMR contact shifts; Unsteady modes of the spin generator; The application of electron magnetic resonance techniques to the study of the phosphorescence of organic molecules; High resolution electron spin resonance; Electron spin resonance in oriented radicals; Low frequency to near microwave electron spin resonance spectroscopy; Correlation of mass spectra with molecular structure; Vacuum spark mass spectrographic analysis of solids and liquids; The teaching of spectroscopy.

OPTICAL CHARACTER RECOGNITION

Edited by George L. Fischer, Donald K. Pollock, Bernard Radack, and Mary Elizabeth Stevens.

416 pages Illustrated $10.00

This is the proceedings of the Symposium on Optical Character Recognition which was co-sponsored by the Information Systems Branch of the Office of Naval Research and Research Information Center of the National Bureau of Standards. The volume explores the present state of the art, operational requirements and the implications of current research.

Contents include: The RCA Multi-Font Reading Machine; Some Elements of Optical Scanning; Character Recognition Techniques for Address Reading; Reading Russian Scientific Literature; An Evaluation of Vidicon Scanning Techniques Coupled with Area Analysis Recognition; A Typed Page Reader for Elite Type; Wide Tolerance Optical Character Recognition for Existing Printing Mechanisms; Design Consideration for A Stylized Font Character Reader; Some Important Factors in the Practical Utilization of Optical Character Readers; Character Recognition as Signal Detection in Noise; Automatic Reading of Cursive Script; Digital Pattern Recognition by Moments; Analytic Approximation and Invariance in Character Recognition; Weighted Area Scanning Techniques for Character Recognition; Recognition of Mixed Font, Imperfect Alpha-Numeric Characters; A Scheme for Recognizing Patters From an Unspecified Class; Linear Decision Functions with Application to Pattern Recognition; Multi-Font Print Recognition; Use of Autocorrelation for Character Recognition; The Search to Recognize.

OPTICAL PROCESSING OF INFORMATION

Edited by: Donald K. Pollock, Charles T. Koester and James T. Tippett.

Based on the symposium on Optical Processing of Information, which was held during October 1962.

288 pages Illustrated $7.50

Contents include: Parallel Organized Optical Computers; Elementary Derivation of Wave Shape and Coherence Properties of Natural Light Using the Tools of Communication Theory; A High Speed Large Capacity Fixed Store for a Digital Computer; Linear Discrimination Optical-Electronic Implementation Techniques; Visual Information Processing in the Beetle Lixus; Vibrating Optic Fibers—A New Concept for Audio Frequency Information Processing and Pattern Recognition; Considerations in Optoelectronic Logic and Memory Arrays; Information Retrieval from Phase Modulating Media; A Natural Image Computer; Broadband Demodulators for Microwave-Modulated Light; Some Properties of Fiber Optics and Lasers; Feasibility of Neuristor Laser Computers; Optical Filtering by Double Diffraction; Selected Aspects of Optical Processing Problems; Light Induces Processes in Cuprous Oxide; The Problem of Light Beam Deflection at High Frequencies; Theory and Applications of the Single Side-Band Suppressed-Carrier Optical Modulation; Storage and Logic in an Optical Digital Computer.

SPARTAN BOOKS

6411 CHILLUM PLACE, N. W. • WASHINGTON 12, D. C.